# Thermodynamics and fluctuations of small machines

Hadrien Vroylandt

## ▶ To cite this version:

## HAL Id: tel-01968075
## https://theses.hal.science/tel-01968075

# Thermodynamique et fluctuations des petites machines

Thèse de doctorat de l'Université Paris-Saclay
préparée à l'Université Paris-Sud

Ecole doctorale n°564 Physique en Île de France (EDPIF)
Spécialité de doctorat : Physique

Thèse présentée et soutenue à Orsay, le 4 septembre 2018, par

## Hadrien Vroylandt

Composition du Jury :

Cécile Monthus
DR (CEA Saclay)                                        Présidente du jury

Christian Van den Broeck
Professeur (Hasselt University)                        Rapporteur

Sergio Ciliberto
DR (ENS Lyon)                                          Rapporteur

Raphaël Chetrite
CR (Université de Nice Sophia-Antipolis)               Examinateur

Freddy Bouchet
DR (ENS Lyon)                                          Examinateur

Hendrik-Jan Hilhorst
Professeur (Université Paris-Sud)                      Directeur de thèse

Gatien Verley
MCF (Université Paris-Sud)                             Co-encadrant de thèse

# Abstract

Small machines – like molecular motors or active particles – operate in highly fluctuating environments that affect their efficiency and power. This thesis aims at describing small machines using stochastic thermodynamics and large deviation theory. By relating mean currents to thermodynamic forces, locally first and then at the global level, we introduce the non-equilibrium conductance matrix that generalizes the Onsager matrix for stationary non-equilibrium systems. We use it to bound machine efficiency by a universal function depending only on the degree of coupling between input and output currents and to find new general power-efficiency trade-offs. On the fluctuations side, the non-equilibrium conductance matrix can be used to find a quadratic bound on the large deviation function of currents. This enables to revisit the fluctuation-dissipation theorem as an inequality when dealing with far-from-equilibrium systems, but also to derive bounds on the efficiency large deviation function. Finally, we study the effects of ergodicity breaking on the fluctuations of observables like activity, currents or efficiency. In particular, we derive the efficiency large deviation function for a model of interacting nanomachines, for which tight coupling and ergodicity breaking emerge in the thermodynamic limit.

**Keywords:** Stochastic thermodynamics, Large deviations theory, Efficiency, Thermodynamic machines, Fluctuations

# Résumé

Les petites machines, comme les moteurs moléculaires ou les particules actives, fonctionnent dans un environnement fortement fluctuant qui affecte leur efficacité ou leur puissance. L'objectif de cette thèse est de décrire les petites machines à l'aide de la thermodynamique stochastique et de la théorie des grandes déviations. En reliant localement puis globalement les courants aux forces thermodynamiques, on introduit une matrice de conductance hors d'équilibre, qui généralise la matrice d'Onsager pour un système stationnaire hors d'équilibre. Cela permet de majorer l'efficacité des machines par une fonction universelle qui ne dépend que du degré de couplage entre les courants d'entrée et de sortie. On obtient aussi de nouvelles relations générales entre puissance et efficacité. Du point de vue des fluctuations, la matrice de conductance hors d'équilibre est reliée à une borne quadratique pour les fonctions de grande déviation des courants. Cette borne permet d'obtenir des bornes pour les fonctions de grande déviation de l'efficacité, mais aussi de revisiter le théorème de fluctuation-dissipation comme une inégalité dans le cas des systèmes loin de l'équilibre. Pour terminer, on étudie l'effet d'une brisure d'ergodicité sur les fluctuations d'observables comme l'activité, les courants ou l'efficacité. En particulier, on calcule la fonction de grande déviation de l'efficacité pour un ensemble de nanomachines en interaction pour lesquelles un couplage fort et une brisure d'ergodicité apparaissent à la limite thermodynamique.

**Mots-clefs:** Thermodynamique Stochastique, Théorie des grandes déviations, Efficacité, Machines thermodynamique, Fluctuations

# Remerciements

Pour commencer, je souhaiterais remercier chacune des personnes qui m'ont aidées, accompagnées ou soutenues durant ma thèse.

Tout d'abord, merci à Gatien pour avoir eu l'idée de cette thèse et l'avoir encadré au jour le jour. Nous ne sommes peut-être pas allés là où nous pensions au début mais le chemin fût intéressant et instructif. Merci également à Henk pour avoir permis la réalisation de cette thèse, et pour tous les précieux conseils donnés.

Merci à mes collaborateurs, David et Massimiliano, ce fût un plaisir de travailler avec vous, et j'espère que je pourrai continuer à le faire. Merci David, aussi pour ton implication dans l'amélioration de mes prises de paroles.

Merci beaucoup aux membres de mon jury, notamment aux deux rapporteurs Christian Van den Broeck et Sergio Ciliberto pour votre lecture attentive de mon manuscrit, et à Cécile Monthus, Freddy Bouchet et Raphaël Chétrite pour m'avoir permis de soutenir.

Je souhaiterais également remercier l'ensemble des membres du Laboratoire de Physique Théorique, et en particulier les membres de l'équipe de physique statistique, Cécile, Françoise, Jean-Michel, Martial et Dominique, ainsi que le directeur du laboratoire Sébastien Descotes-Genon pour m'avoir permis de participer à des séminaires et conférences aux quatres coins de l'Europe ainsi que pour son écoute attentive. Merci également à Damir mon parrain de thèse, aux autres thésards du labo, en particulier Mathias, Antoine et Timothée, ainsi qu'à l'équipe administrative. Merci également à Marie pour son aide dans toutes les innombrables tâches du quotidien. Lydia, bon courage pour la relève.

Je remercie également toutes les personnes qui ont contribué à m'inclure dans un environnement scientifique riche, que ce soit de par l'organisation d'école d'été et de conférences ou simplement par l'accueil qui m'a été fait dans divers laboratoires. Merci à Pascal Viot d'avoir accepté d'être mon tuteur scientifique. Thank you in particular to the members of the luxembourg team, it was always a great pleasure to visit you.

Au delà de mon domaine scientifique, j'ai également eu la chance d'interagir avec nombres de doctorants, que se soit par l'organisation des RJP (Rencontres des Jeunes Physiciens et physiciennes), les conférences, l'aventure lemp (dont

j'espère qu'elle va continuer) ou plus simplement pour boire un verre (les quatre n'étant pas incompatibles).

Merci également à mes amis, Aurélien, Clément et Jean pour votre soutien pendant ces trois années, et en particulier pour nos nombreuses soirées et sorties au restaurant. Paul, Rémi, Lola et Laure, merci également pour m'avoir fait lever la tête et fait faire autre chose que de la physique !

Merci à Catherine et Flor de m'avoir écouté parler de mon sujet de thèse sans rien y comprendre. Merci pour l'aide apportée pour la préparation de mon pot de thèse. Bien entendu merci à ma famille, mes frères et soeurs, en particulier Thomas d'avoir relu et corrigé des parties de cette thèse et mes parents pour l'excellente éducation qu'ils m'ont donnée.

Enfin, Pauline, je ne pourrais lister ici tout ce que tu m'as apporté, en tout cas merci de m'avoir supporté durant ces trois années de thèse.

# Notations

## Linear algebra and graph theory

We denote vectors with a bold notation $\boldsymbol{u}$ and linear forms as transposed vectors $\boldsymbol{w}^{\mathrm{T}}$. Subscripts indicate the space of the vector or linear form. When looking at components of the vectors, by abuse of notation, the label are removed and the index indicate the space of origin.

| | | | |
|---|---|---|---|
| $\boldsymbol{u}_{\mathrm{v}}$ | Vertex vector | $u_x$ | Element for state $x$ |
| $\boldsymbol{u}_{\mathrm{e}}$ | Edge vector | $u_{(x,y)}$ | Element for edge $(x,y)$ |
| $\boldsymbol{u}_{\mathrm{c}}$ | Cycle vector | $u_{c_1}$ | Element for cycle $c_1$ |
| $\boldsymbol{u}_{\mathrm{r}}$ | Reservoir vector | $u_{r_1}$ | Element for reservoir $r_1$ |
| $\boldsymbol{u}$ | Physical vector | $u_X$ | Element for physical quantity $x$ |

| | | | |
|---|---|---|---|
| $Ns$ | Number of states | $Rev$ | Number of reservoirs |
| $Ed$ | Number of edges | $Ph$ | Number of physical quantities |
| $Cy$ | Number of cycles | $Lc$ | Number of conservation laws |

| | | |
|---|---|---|
| $\mathbf{Id}$ | Identity matrix | |
| $\boldsymbol{D}$ | Incidence matrix ($Ns \times Ed$) | Eq. (1.1) |
| $\boldsymbol{C}$ | Cycle matrix ($Ed \times Cy$) | Eq. (1.3) |
| $\boldsymbol{R}$ | Reservoir matrix ($Rev \times Ed$) | Eq. (1.42) |
| $\boldsymbol{V}$ | Selection matrix ($Rev \times Ph$) | Eq. (2.40) |
| $\boldsymbol{P}$ | Physical matrix ($Ph \times Cy$) | Eq. (2.43) |
| $\boldsymbol{\ell}$ | Vector of a conservation law | Eq. (2.38) |

## Probability and random variables

Random variables are almost always represented by uppercase letters, while the specific outcomes of these random variables are denoted by lowercase letters. The probability of outcome $o$ for random variable $O$ is denoted $\Pr(O = o)$. The expectation of a random variable $O$ is denoted $\mathbf{E}[O]$ and its most probable value $\bar{o}$.

| | | |
|---|---|---|
| $\boldsymbol{\pi}_{\mathrm{v}}$ | Stationary probability | Eq. (1.36) |
| $\omega_{(x,y)}$ | Transition rate from $y$ to $x$ | Eq. (1.18) |
| $\boldsymbol{K}$ | Transition matrix | Eq. (1.20) |
| $\gamma, \kappa$ | Counting fields | Eq. (2.12) |
| $\boldsymbol{K}^{\gamma}$ | Tilted matrix | Eq. (2.18) |
| $G(x^{\mathrm{f}}, x^{\mathrm{i}}, \gamma)$ | Propagator of the generating function | Eq. (6.14) |
| $I(o)$ | Large deviation function (LDF) | Eq. (2.7) |
| $\phi(\gamma)$ | Cumulant generating function (CGF) | Eq. (2.12) |

## Units and physical quantities

We work in natural units, *i.e.* the Bolztmann's constant $k_\mathrm{B}$ is set to 1. The typical energy fluctuation of one of the reservoir set the energy scale, *i.e.* one of the inverse temperature is set to 1. The typical time constant of one of the reservoir set the time scale, *i.e.* one of the coupling constant is set to 1.

| | | |
|---|---|---|
| $\mathcal{L}$ | Onsager matrix | Eq. (3.4) |
| $\mathcal{G}$ | Non-equilibrium conductance matrix | Eq. (4.1) |
| $\mathcal{R}$ | Non-equilibrium resistance matrix | Eq. (4.29) |
| $\mathbf{Cov}$ | Covariance matrix | Eq. (3.8) |
| $\sigma$ | Entropy production rate | Eq. (1.49) |
| $\eta$ | Efficiency | Eq. (3.2) |
| $\xi$ | Degree of coupling | Eq. (4.61) |

# Publications

The results presented in this manuscript were reported in the following publications

**A.1** H. Vroylandt, A. Bonfils, and G. Verley, "Efficiency fluctuations of small machines with unknown losses", Phys. Rev. E **93**, 052123 (2016) [190]

**A.2** H. Vroylandt, M. Esposito, and G. Verley, "Collective effects enhancing power and efficiency", EPL (Europhysics Letters) **120**, 30009 (2017) [191]

**A.3** H. Vroylandt, D. Lacoste, and G. Verley, "Degree of coupling and efficiency of energy converters far-from-equilibrium", Journal of Statistical Mechanics: Theory and Experiment **2018**, 023205 (2018) [192]

**A.4** H. Vroylandt and G. Verley, "Non equivalence of dynamical ensembles and emergent non ergodicity", Journal of Statistical Physics (2018) `10.1007/s10955-018-2186-7` [193]

Another article is in preparation. The scientific results it will report are presented in the last chapter:

**A.5** H. Vroylandt, M. Esposito, and G. Verley, "Efficiency fluctuations of a non-ergodic brownian machine", (in preparation), 2018

# Softwares

The author of this manuscript is grateful to free software movement that lead to the release of various software whose use contribute to this thesis.

In particular, this manuscript was typeset with LaTeX on a Debian computer. The bibliographic management was done with JabRef and figures made with Gnuplot[1] The program used for numerical computation was written using Python3 and Fortran and uses the algorithms implemented in the Scipy library[2]. GNU parallel [3] helped to manage the launch in parallel of the computations.

[1]E. A. Merritt et al., *Gnuplot 5.0 an interactive plotting program*, edited by T. W. Č. Kelley, 2018

[2]E. Jones, T. Oliphant, P. Peterson, et al., *SciPy: open source scientific tools for Python*, 2001–

[3]O. Tange, "Gnu parallel - the command-line power tool", ;login: The USENIX Magazine **36**, 42–47 (2011)

# Contents

Contents

# Introduction

**Foundations of thermodynamics** 1769: James Watts patented his version of a steam engine, whose rising use contributed to the industrial revolution. This invention and its further developments have raised new fundamental questions about the physical description of engines and the improvement of their efficiency. Answers to these questions have emerged gradually as a new branch of physics called thermodynamics [5]. Thermodynamics is, as stated by Lord Kelvin in 1882, "the subject of the relation of heat to forces acting between contiguous parts of bodies, and the relation of heat to electrical agency" [17].

Thermodynamics was formalized through the definition of the laws of thermodynamics. The first law follows from the experiment of Joule, who showed that heat and mechanical work were both a form of energy transfer.

The second law originates in work on thermal machines by Carnot, who stated the impossibility for a machine to have an efficiency in energy conversion greater than the Carnot efficiency, the latter efficiency depending only on the temperatures of the exterior heat baths. The second law was later formulated by Clausius, who introduced entropy as a quantity that describes the direction, thermodynamically, in which a system can evolve . Based on entropy, one can quantify the useful work that can be extracted from a system.

These two laws have been widely used as guiding principles for the improvement of heat engines.

Entropy remained a mysterious quantity until an interpretation was given by Boltzmann through the development of equilibrium statistical mechanics. Equilibrium statistical mechanics connects thermodynamic quantities (such as temperature, pressure, ...) to microscopic behavior of systems. Within this framework, entropy is related to the number of microscopic configurations that are consistent with the macroscopic quantities characterizing the system.

Thermodynamics and statistical physics are now an important part of the description of many macroscopic systems, ranging from chemical to astrophysical systems. They feature the thermodynamic limit , *i.e.* a large system limit, as a key ingredient. This limit allows us to characterize macroscopic systems by few degree of freedom upon averaging on most of the microscopic degrees of freedom.

**Brownian motion**   In contrast to systems with a thermodynamic limit, studying "small" systems reveals huge fluctuations that influence the behavior of the systems. These fluctuations were discovered by Brown, who observed the erratic trajectory of particles inside a grain of pollen suspended in water. This Brownian motion was studied intensively in the 19th century (Gouy, Perrin, Langevin, Einstein, ...) and several properties were established :

- The Brownian motion is fully erratic and never stops.

- The nature of the particle does not matter, but its size matters, and for a big enough particle, the motion is unobservable.

- The viscosity and the temperature of the surrounding fluid affect the motion.

The Brownian motion originates in the collision of the particle with the fast-moving molecules in the fluid. Due to the high complexity of the many-body dynamics that governs the molecular motion, these collisions appear as random. As a consequence only probabilistic models can be employed to describe the surrounding fluid, in conjunction with the molecular chaos hypothesis. These probabilistic models are parametrized by the temperature of the fluid, which sets the typical energy scale of the interaction between the fluid molecules and the particle. When the particle is big enough the energy changes due to the collisions with the fluid molecules become negligible compared with the typical kinetic energy of the particle, and the effect of the fluctuating environment is unobservable.

**Stochastic thermodynamics**   Over the last two decades, stochastic thermodynamics has emerged as a comprehensive framework for the description of "small" systems in contact with a fluctuating environment. We consider here that a "small" system is a system on which the effect of the environmental fluctuations are perceptible, unlike the classical thermodynamics where these fluctuations are absent. Examples range from colloids in solution [180] to the complex machinery of life [156, 165].

Stochastic thermodynamics is rooted on one hand, in the development of non-equilibrium statistical mechanics, on the other hand in the mathematical theory of stochastic processes. Non-equilibrium statistical physics was initially developed in the close-to-equilibrium regime. The concept of Onsager matrix, fluctuation-dissipation theorem or Green-Kubo relations have emerged within the framework of linear response theory [10, 113, 131, 132]. Some of these results can now be understood through extremization principles for entropy production used to predict non-equilibrium currents or steady-states [130, 135, 20]. On the mathematical side, Markov processes have been introduced to describe formally the random evolutions of small systems [13]. The elaboration of large deviation theory has improved the mathematical foundation of equilibrium statistical physics and suggested directions for its out-of-equilibrium generalization [43, 73–76, 78, 14, 25].

Stochastic thermodynamics has led to important results based on a precise framework:

- Thermodynamic quantities are defined at the level of a single trajectory, *e.g.* energy [168, 24] or entropy [167], and the connection with large deviation theory are clearly stated [133, 136].

- A symmetry of the probability distribution of entropy production exists and is called the 'fluctuation theorem' (or 'relations'). This symmetry was first observed in numerical simulations of sheared fluids [88], and has been generalized to numerous cases [86, 104, 114, 117]

- There has been experimental validation of stochastic thermodynamics using modern experimental techniques in single-molecule pulling, optical trapping of colloidal particles, and single-electron counting in mesoscopic electronic devices, among many others [62]. Let us cite the measurement of free energy difference for various systems, from a torsion pendulum [77] to DNA folding/unfolding [68, 120], the determination of the probability distribution of entropy production for a single electron box [111], or various realizations about the connection between information and stochastic thermodynamics [47, 180].

Nowadays, stochastic thermodynamics aims at answering new questions, among which:

- The study of specific systems: biological and chemical systems [21, 158], systems with time-dependent driving [52] , quantum systems [58, 174] or connection with the information theory [134]

- The definition of dynamical ensembles to generalize the notion of microcanonical and canonical ensemble of equilibrium statistical physics [60].

- The study of dynamical phase transitions found in various systems [36], such as glassy systems [92] or simple models of lattice gases [11, 18].

- The connection between mean values of observables and their fluctuations [39, 40], aiming in particular at infering hidden properties of a system [31, 94].

Energy conversion by machines is still today intensively studied in the framework of stochastic thermodynamics:

The impossibility of extracting power from the fluctuations of the environment has been revisited. This question was studied through the design of *gedanken* experiments [66, 67, 137, 161, 183], the analysis of biological molecular motors [55, 106, 115] and the realization of artificial stochastic machines [49, 125, 153, 159, 169].

As an extension of the work of Carnot, general laws and constraints of machines operation have been considered, *e.g.* the condition of operation of machines at Carnot efficiency is a widely debated subject [51, 53, 57, 81, 148, 154, 160, 171], and general power-efficiency relations have been derived using the close-to-equilibrium framework [109, 152].

Small machines operate in the presence of highly fluctuating input and output energy fluxes associated with large efficiency fluctuations. The study of efficiency probabilities at large time have revealed surprising results, with the Carnot efficiency being the least likely efficiency of stationary machines [186, 189].

In this manuscript, we focus on the study of small machines within the large deviation framework, with the following questions in mind:

- What is the appropriate description of small machines?

- In view of the description of machines in the close-to-equilibrium regime [109], can we extend based on Refs. [40, 141, 149] this remarkable theory to far-from-equilibrium machines?

- In Ref. [189], general results were established about efficiency fluctuations after a very long time. What happens for machines with losses or ergodicity breaking in the thermodynamic limit?

# Outline and contributions of this manuscript

This manuscript can be divided into three parts:

- The first part is composed of the chapters 1, 2 and 3. It consists of a detailed introduction. Ch. 1 introduces first the description of stochastic processes and stochastic thermodynamics in the framework of graph theory; Ch. 2 develops the large deviation theory that is used to describe fluctuations of observables such as heat fluxes and defines the notion of dynamical ensembles; Ch. 3 focuses on thermodynamic machines both at the average and fluctuating level.

- The second part is composed of the chapters 4 and 5. Ch. 4 defines the non-equilibrium conductance matrix used to describe average behavior of machines and approximate the fluctuations. Ch. 5 uses the non-equilibrium conductance matrix to bound efficiency fluctuations. We also study there efficiency fluctuations in the presence of losses.

- The third part is composed of the chapters 6 and 7. Ch. 6 studies when the equivalence between dynamical ensembles defined in sec. 2.1 is broken. Ch. 7 introduces a model derived from the fully-connected Ising model to study how of the non-equivalence of dynamical ensembles impacts efficiency fluctuations.

**Main results** The contributions of the first part are mainly of pedagogical value and the author hopes that this part may be useful to introduce future students to stochastic thermodynamics. The second and the third part includes some original results (at least to a certain degree, and up to our knowledge):

- The introduction of the non-equilibrium matrix for physical currents as a generalization of the Onsager matrix, sec. 4.1 [**A.3**].

- Various bounds on the non-equilibrium conductance matrix (sec. 4.2) and its connection with the thermodynamic uncertainty relations, sec. 4.2.3[**A.3**].

- The generalization of the notion of degree of coupling to far-from-equilibrium machines, Eq. (4.61)[**A.3**].

- A formula for the maximum efficiency of any machine based solely on the degree of coupling, Eq. (4.68)[**A.3**].

- The definition of a power-efficiency trade-off from the non-equilibrium conductance matrix and its connection with previously established power-efficiency trade-off, sec. 4.4.3[**A.3**].

- The derivation of a bound on the scale of efficiency large deviation function from total entropy production rate, Eq. (5.5).

- The derivation of a bound on the efficiency large deviation function from the non-equilibrium conductance matrix, Eq. (5.7).

- The study of efficiency fluctuations for machines with three fluxes, sec. 5.2.3 [**A.1**].

- The consistency between efficiency fluctuations of machines with losses and "ideal" machines of Ref. [189], sec. 5.2.4 [**A.1**].

- The computation of non-convex large deviations functions from the propagator of the generating function, sec. 6.1.2 [**A.4**].

- The study of fluctuations of dynamical observables for the fully-connected Ising model in presence of ergodicity-breaking, sec. 6.2 [**A.4**].

- The link between mixing time and non-convex large deviations functions, sec. 6.3 [**A.4**].

- The emergence of a tight coupling in the thermodynamic limit for some models and its interpretation as an emergent conservation laws, sec. 7.2 [**A.2**].

- The efficiency large deviation function in the presence of ergodicity breaking for the Brownian Donkey, sec. 7.3.3 [**A.5**].

# Stochastic thermodynamics

This first chapter introduces the mathematical tools used to describe non-equilibrium processes, starting with graph theory. Next we switch to the dynamical evolution of systems, in particular in presence of an external environment. Finally, we study the stochastic behavior of our system by introducing the observables we will use throughout the manuscript.

The material presented in this chapter mainly comes from the current literature. Readers can refers to the following publications for more details:

- The book of N. Biggs [3] and the thesis manuscript of M. Polettini [19] present many interesting aspects of algebraic graph theory.

- The thesis manuscript of B. Wynants [30] contains a very nice introduction to Markov stochastic processes and their use for non-equilibrium physics.

- On the connection with an external environment, we base our explanations on two articles by Bulnes-Cutera, Polettini, Rao and Esposito [147, 157]. The review by U. Seifert [23] is also a central reference.

**State space**   A system is described by its states or configurations. These are the values of the variables used for modeling the system under consideration. For example, the system state may be the vector of the positions and momenta of the atoms of a gas, the set of spin configurations for a magnet or just the position for a colloidal particle in a viscous fluid. The set of states or configurations, denoted $\Omega$, can be continuous or discrete, bounded, compact or finite.

We assume in this manuscript that $\Omega$ is a discrete and finite space of size $Ns$. Such state space are well described by graph theory, the state space being set as the vertex of a graph. We concentrate on the algebraic graph theory where graph elements are considered as vectors and manipulated through algebraic relations. This algebraic formulation of graph theory allows for a simple description and manipulation of the various concepts used in stochastic thermodynamics.

# 1.1 Algebraic graph theory

A graph $\mathscr{G}$ is a set of vertices $x$ that are connected by edges. We denote $Ns$ the number of vertices and $Ed$ the number of edges. Each vertex represents a possible state of the system and each edge a possible transition between states. We also introduce an arbitrary orientation on the graph, for each couple of states $(x, y)$ (we choose arbitrarily an orientation $(y \to x)$) such that $y$ is the origin of the edge and $x$ its end. We define $(y, x)$ as the oriented edge with the reverse orientation $(x \to y)$.

In this thesis, we focus on multigraphs without loops, that is to say that it is possible to have several edges between two vertices, but no edges connecting a vertex to itself.
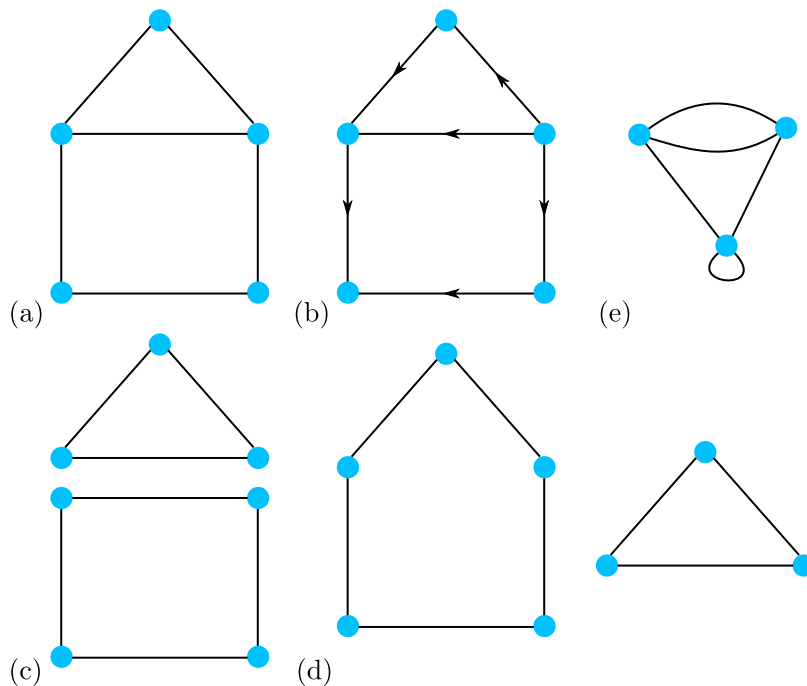


Figure 1.1: (a) Example of graph with 5 vertices and (b) an arbitrary orientation. (c) A possible choice for the fundamental cycle basis and (d) another possible choice. (e) An example of multigraphe with three vertex and a loop.

## 1.1.1 Properties of graphs: connected graphs and cycles

**Connected graphs** We say that a graph is connected if there is a path of edges connecting any pair of vertices in the graph. A graph is decomposable into a set of connected components, and $Kc$ is the number of these components. We shall consider, with some exceptions, only connected graphs. If a graph is not connected, then it suffices to consider separately each of its connected components as an independent graph.

**Cycles** A cycle is a set of consecutive edges that form a closed paths on the graph. A simple cycle is a cycle with no edge repetition. We define a cycle by the successive list of edges belonging to the cycle. A graph without a cycle is called a tree. Given two cycles $c_1$ and $c_2$, that share at least one edge, we construct a third cycle by considering the set of edges that belong to $c_1$ or $c_2$ but not to both, see Fig. 1.1.

Then there exists a basis of cycles such that any cycle is decomposable as a sum of cycles of the basis. Such a basis is called a fundamental cycle basis. The number of fundamental cycles $Cy$ is given by the Euler formula $Cy = Ed - Ns + Kc$. Like for edges, we orient arbitrarily the fundamental cycles.

A graph with a unique cycle, like the three state model of Fig. 1.2 is called a unicyclic system. Due to their simplicity, unicyclic systems are quite popular as model example, but they have drawbacks for modeling of machines that we discuss in sec. 3.1.3.



(a)                              (b)
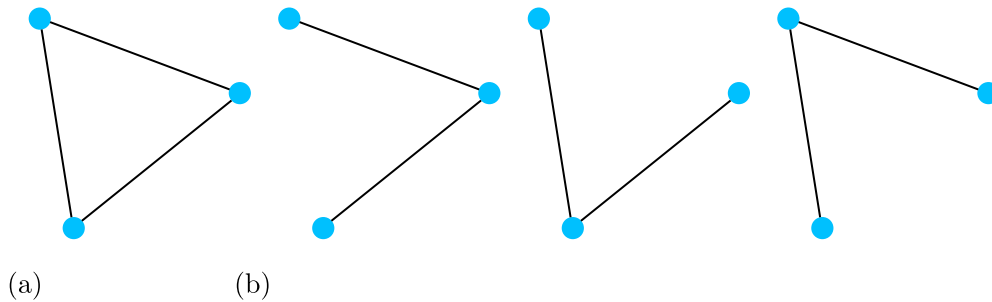
Figure 1.2: (a) Unicyclic three state graph and (b) its three spanning trees

**Spanning trees** There is a simple procedure to obtain a fundamental cycle basis for connected graphs. Consider a spanning tree $\mathscr{T}$, that is, a subgraph of $\mathscr{G}$ connecting all the vertices of $\mathscr{G}$ but without cycle. By Euler formula, it is thus a graph with $Ns - 1$ edges. The edges that do not belong to $\mathscr{T}$ are called chords, so there are $Cy$ chords. To obtain a cycle of the fundamental cycle base, we choose one of the chords of the graph and add it to $\mathscr{T}$, to produce exactly one cycle. We then remove all the edges not belonging to the cycle and we orient the cycle in the direction of the chord. Doing this for all chords, we obtain a basis of fundamental cycles. This basis is not unique, by choosing another spanning tree, we can obtain another basis of fundamental cycles, as shown on Fig. 1.1c-d.

## 1.1.2  Incidence matrix

The algebraic graph theory uses algebraic theory to study graphs. Many approaches are possibles, for instance using group theory [3], but we concentrate on the use of linear algebra to extract graph properties from particular matrices.

We define the incidence matrix $\boldsymbol{D}$ that contains all the information on graph topology and edge orientation. Its elements are

$$D_{z,(x,y)} = \begin{cases} -1 & \text{if } z = y \\ +1 & \text{if } z = x \\ 0 & \text{else} \end{cases} . \tag{1.1}$$

where $y$ is the origin of the oriented edge $(x, y)$.

**Connected components**  As a first property of $\boldsymbol{D}$, let's show that for each connected component $\mathscr{G}_k$, the sum on the vertex belonging to the component is zero, *i.e.* $\sum_{z \in \mathscr{G}_k} D_{z,(x,y)} = 0$. Indeed for each edge, the sum over the vertices give $-1 + 1$ since we count the starting vertex as $-1$ and the final vertex as $+1$. Therefore the vector $(1, \ldots, 1, 0, \ldots, 0)^{\mathrm{T}}$, with 1 for the vertex member of one connected components and 0 for the other components, is a member of the kernel of $D^{\mathrm{T}}$. The rank of the incidence matrix is then $Ns - Kc$. For a connected graph $(1, \ldots, 1)^{\mathrm{T}}$ is the only member of the kernel of $D^{\mathrm{T}}$.

**Cycles**  The kernel of $D$ also informs on the graph properties: an element $c$ of the kernel is a combination of edges such that

$$\forall z \in \mathscr{G}, \sum_{(x,y)} D_{z,(x,y)} c_{(x,y)} = 0 \tag{1.2}$$

that is the definition of cycles. Indeed, for a cycle $c$, let's consider the vector $\boldsymbol{c}$ such that for each edge $e$

$$c_{(x,y)} \begin{cases} +1, & \text{if } (x,y) \uparrow c, \\ -1 & \text{if } (x,y) \downarrow c, \\ 0 & \text{else} , \end{cases} \tag{1.3}$$

where $(x,y) \uparrow c$ means that edge $(x, y)$ belong to the cycle $c$ with an orientation similar to the one of the cycle and $(x,y) \downarrow c$ the orientation is opposite. At each vertex $\sum_{(x,y)} D_{z,(x,y)} c_{(x,y)}$ is zero. The kernel of $\boldsymbol{D}$ is then the cycle space of the graph. Hence a basis of the kernel is a basis of fundamental cycles. We denote by $\boldsymbol{C}$ the $Ed \times Cy$ matrix composed of the vector forming a basis of ker $\boldsymbol{D}$.

We remark that the Euler formula is recovered from the fundamental theorem of linear algebra. Indeed, we have

$$\mathbb{R}^{Ed} = \ker \boldsymbol{D} \oplus \operatorname{im} \boldsymbol{D}^{\mathrm{T}} \Rightarrow Ed = \dim \ker \boldsymbol{D} + \dim \operatorname{im} \boldsymbol{D} \tag{1.4}$$

that gives again the Euler formula $Ed = Cy + Ns - Kc$.

**Laplacian matrix**  From the incidence matrix, we build the Laplacian matrix $\boldsymbol{\Delta} = -\boldsymbol{D}\boldsymbol{D}^{\mathrm{T}}$, this is the matrix

$$\Delta_{x,y} = \begin{cases} 1 & \text{if } x \text{ and } y \text{ are connected by an edge,} \\ -\deg x & \text{if } x = y, \\ 0 & \text{else} , \end{cases} \tag{1.5}$$

where $\deg x$ is the degree of the vertex, that is the number of edges connected to the vertex. Notice that the Laplacian matrix is independent of the chosen orientation.

The matrix-tree theorem is an important result of algebraic graph theory. The number of spanning trees of the graph is given by any minor of the Laplacian matrix, that is the determinant of the Laplacian matrix with row and column corresponding to one state removed.

### 1.1.3 Vectors and linear forms

We consider now functions on the edges of the graph $\mathscr{G}$. Such function $u$ assigns a value for each edge $(x, y)$ of the graph that could depend on the edge orientation $u_{(x,y)} \neq u_{(y,x)}$. We decompose edge functions between the symmetric $(u_{(x,y)} + u_{(y,x)})/2$ and the antisymmetric part $(u_{(x,y)} - u_{(y,x)})/2$.

**Vertex, edge and cycle space as vector space** Let's consider the vector with elements being the value on edge of the antisymmetric part of any function. This vector is then a member of the edge space $\mathbb{R}^{Ed}$. The edge space $\mathbb{R}^{Ed}$ can be considered as real vector space and its elements are called the edge vectors.

Similarly, we consider the linear forms that are elements of the dual of the vector space $\mathbb{R}^{Ed}$. They are called the edge linear forms.

We generalize these interpretations of edge space as a vector space to vertex and cycle space. We therefore define elements of $\mathbb{AR}^{Ns-1}$ as vertex vector and element of $\mathbb{R}^{Cy}$ as cycle vector, and similarly for the dual vector space. $\mathbb{AR}^{Ns-1}$ being the affine space of dimension $Ns - 1$ that is $\mathbb{R}^{Ns}$ with an additional constraint between coordinates.

We denote vectors with a bold notation $\boldsymbol{u}$ and linear forms as transposed vectors $\boldsymbol{w}^{\mathrm{T}}$. Subscripts indicate the space of the vector or linear form: edge quantities are denoted with e subscript as $\boldsymbol{u}_{\mathrm{e}}$, cycle quantities with c as $\boldsymbol{u}_{\mathrm{c}}$ and vertex quantities with v as $\boldsymbol{u}_{\mathrm{v}}$. When looking at components of the vectors, by abuse of notation, the label v, e and c are removed and the index indicate the space of origin, $u_x$, $u_{(x,y)}$ and $u_{c_1}$ are respectively elements of the vectors $\boldsymbol{u}_{\mathrm{v}}$, $\boldsymbol{u}_{\mathrm{e}}$ and $\boldsymbol{u}_{\mathrm{c}}$.

The vectors and linear forms can be related one to another, but this requires to define an inner product, or a metric. This question relies on the definition of a dynamics on the graph and is treated in sec 1.2.

**Decomposition of vectors and linear forms** The incidence matrix and the cycle matrix are now considered as linear maps between vector spaces. They relate edge vectors to cycle vectors or vertex vectors. For instance a cycle vector $\boldsymbol{u}_{\mathrm{c}}$ generates an edge vector $\boldsymbol{u}_{\mathrm{e}}$ such that $\boldsymbol{u}_{\mathrm{e}} = \boldsymbol{C} \cdot \boldsymbol{u}_{\mathrm{c}}$, and a vertex linear form $\boldsymbol{w}_{\mathrm{v}}^{\mathrm{T}}$ generates an edge linear form $\boldsymbol{w}_{\mathrm{e}}^{\mathrm{T}} = \boldsymbol{w}_{\mathrm{v}}^{\mathrm{T}} \cdot \boldsymbol{D}$.

As $\operatorname{im} C = \ker D$, we have the exact sequence[119]

$$\mathbb{AR}^{Ns-1} \xleftarrow{\boldsymbol{D}} \mathbb{R}^{Ed} \xleftarrow{\boldsymbol{C}} \mathbb{R}^{Cy}, \tag{1.6}$$

meaning that $\mathbb{R}^{Ed} = \mathbb{AR}^{Ns-1} \oplus \mathbb{R}^{Cy}$. This is another form of relation (1.4). As a consequence, for an edge vector $\boldsymbol{u}_\mathrm{e}$, there exists a cycle vector $\boldsymbol{u}_\mathrm{c}^\mathrm{d}$ and an edge vector $\boldsymbol{u}_\mathrm{e}^\mathrm{d}$ such that

$$\boldsymbol{u}_\mathrm{e} = \boldsymbol{u}_\mathrm{e}^\mathrm{d} + \boldsymbol{C} \cdot \boldsymbol{u}_\mathrm{c}^\mathrm{d} \quad \text{with} \quad \boldsymbol{D} \cdot \boldsymbol{u}_\mathrm{e}^\mathrm{d} = \boldsymbol{D} \cdot \boldsymbol{u}_\mathrm{e} = \boldsymbol{u}_\mathrm{v}. \tag{1.7}$$

The d superscript denotes the decomposition. This mean that an edge vector decomposes into a cycle part and the rest.

In the same idea, for an edge linear form $\boldsymbol{w}_\mathrm{e}^\mathrm{T}$ there exists a vertex linear form $\boldsymbol{w}_\mathrm{v}^{\mathrm{d}\mathrm{T}}$ and an edge linear form $\boldsymbol{w}_\mathrm{e}^{\mathrm{d}\mathrm{T}}$ such that

$$\boldsymbol{w}_\mathrm{e}^\mathrm{T} = \boldsymbol{w}_\mathrm{v}^{\mathrm{d}\mathrm{T}} \cdot \boldsymbol{D} + \boldsymbol{w}_\mathrm{e}^{\mathrm{d}\mathrm{T}} \quad \text{with} \quad \boldsymbol{w}_\mathrm{e}^{\mathrm{d}\mathrm{T}} \cdot \boldsymbol{C} = \boldsymbol{w}_\mathrm{e}^\mathrm{T} \cdot \boldsymbol{C} = \boldsymbol{w}_\mathrm{c}^\mathrm{T}. \tag{1.8}$$

There is a connection between these decompositions and the Helmholtz decomposition, and more generally with Hodge theory. The linear map $\boldsymbol{D}$ is a kind of divergence for vector and gradient for linear form. The cycle matrix is a kind of curl. We advise to read the introduction by Lim [119] for more details.

**Building the decomposition** The decomposition (1.7) or (1.8) can be computed as follows. We pick one of the spanning tree of the graph $\mathscr{G}$.

- For an edge vector $\boldsymbol{u}_\mathrm{e}$, we define the elements of the cycle vector $\boldsymbol{u}_\mathrm{c}^\mathrm{d}$ as the components of $\boldsymbol{u}_\mathrm{e}$ that correspond to chords, since each chord is associated to a cycle. The other part of the decomposition is simply obtained from the remaining vector $\boldsymbol{u}_\mathrm{e}^\mathrm{d} = \boldsymbol{u}_\mathrm{e} - \boldsymbol{C} \cdot \boldsymbol{u}_\mathrm{c}^\mathrm{d}$. Cycle vectors being in the kernel of the incidence matrix, we have $\boldsymbol{D} \cdot \boldsymbol{u}_\mathrm{e}^\mathrm{d} = \boldsymbol{D} \cdot \boldsymbol{u}_\mathrm{e}$. Cycle vectors will be later interpreted as flow of quantities along cycle, whereas the remaining part represents sources and sinks.

- For an edge linear form $\boldsymbol{w}_\mathrm{e}^\mathrm{T}$, we build a vertex linear form $\boldsymbol{w}_\mathrm{v}^{\mathrm{d}\mathrm{T}}$ by considering each edge $(x, y)$ belonging to the spanning tree such that

$$w_{(x,y)} = w_y^\mathrm{d} - w_x^\mathrm{d}. \tag{1.9}$$

This lead to a consistent definition of the vertex linear form as this imposes $Ns - 1$ equations for $Ns - 1$ values to be determined. The other part of the decomposition is obtained as the remaining linear form $\boldsymbol{w}_\mathrm{e}^{\mathrm{d}\mathrm{T}} = \boldsymbol{w}_\mathrm{e}^\mathrm{T} - \boldsymbol{w}_\mathrm{v}^{\mathrm{d}\mathrm{T}} \cdot \boldsymbol{D}$ and verify $\boldsymbol{w}_\mathrm{e}^{\mathrm{d}\mathrm{T}} \cdot \boldsymbol{C} = \boldsymbol{w}_\mathrm{e}^\mathrm{T} \cdot \boldsymbol{C}$ as the cycle matrix is in the kernel of the incidence matrix. Vertex linear forms are also called potential functions, and cycle linear forms are circulations around the cycle.

**Illustration of the decomposition** Let's illustrate the decomposition (1.7) with a simple example. We consider the three state unicyclic graph of Fig. 1.2 It has incidence and cycle matrices

$$\boldsymbol{D} = \begin{pmatrix} 1 & 0 & -1 \\ -1 & 1 & 0 \\ 0 & -1 & 1 \end{pmatrix}, \quad \boldsymbol{C} = \begin{pmatrix} 1 \\ 1 \\ 1 \end{pmatrix}. \tag{1.10}$$

We aim at decomposing the edge vector $\boldsymbol{u}_{\mathrm{e}}^{\mathrm{ex}} = (1,2,3)^{\mathrm{T}}$ into vertex and cycle contributions. Using the three spanning tree of the Fig. 1.2b, we obtain these three equivalent decompositions

$$\boldsymbol{u}_{\mathrm{e}}^{\mathrm{ex}} = \boldsymbol{C}\cdot(1) + \begin{pmatrix}0\\1\\2\end{pmatrix} = \boldsymbol{C}\cdot(2) + \begin{pmatrix}-1\\0\\1\end{pmatrix} = \boldsymbol{C}\cdot(3) + \begin{pmatrix}-2\\-1\\0\end{pmatrix} \qquad (1.11)$$

such that

$$\boldsymbol{D}\cdot\boldsymbol{u}_{\mathrm{e}}^{\mathrm{ex}} = \boldsymbol{D}\cdot\begin{pmatrix}0\\1\\2\end{pmatrix} = \boldsymbol{D}\cdot\begin{pmatrix}-1\\0\\1\end{pmatrix} = \boldsymbol{D}\cdot\begin{pmatrix}-2\\-1\\0\end{pmatrix} = \begin{pmatrix}-2\\1\\1\end{pmatrix}. \qquad (1.12)$$

**Non unicity of the decomposition and gauge invariance** The previous example shows that different spanning trees give different decompositions of edge vectors and linear forms. Among these decompositions we have some invariants. For an edge vector with two decompositions $\boldsymbol{u}_{\mathrm{e}} = \boldsymbol{u}_{\mathrm{e}}^{\mathrm{d1}} + \boldsymbol{C}\cdot\boldsymbol{u}_{\mathrm{c}}^{\mathrm{d1}} = \boldsymbol{u}_{\mathrm{e}}^{\mathrm{d2}} + \boldsymbol{C}\cdot\boldsymbol{u}_{\mathrm{c}}^{\mathrm{d2}}$, we always obtain the same vertex vector $\boldsymbol{u}_{\mathrm{v}} = \boldsymbol{D}\cdot\boldsymbol{u}_{\mathrm{e}}^{\mathrm{d1}} = \boldsymbol{D}\cdot\boldsymbol{u}_{\mathrm{e}}^{\mathrm{d2}} = \boldsymbol{D}\cdot\boldsymbol{u}_{\mathrm{e}}$. Therefore the vertex vector $\boldsymbol{u}_{\mathrm{v}}$ is an invariant of the decomposition. Similarly for linear forms, the cycle linear form $\boldsymbol{w}_{\mathrm{c}}^{\mathrm{T}} = \boldsymbol{w}_{\mathrm{e}}^{\mathrm{T}}\cdot\boldsymbol{C}$ is an invariant of the decomposition.

As the matrix $\boldsymbol{D}$ and $\boldsymbol{C}$ are singular, the problem of finding solutions $\boldsymbol{x}_{\mathrm{e}}$ to the inverse problem $\boldsymbol{D}\cdot\boldsymbol{x}_{\mathrm{e}} = \boldsymbol{y}_{\mathrm{v}}$ has multiple solutions. This implies the non-unicity of the decomposition, see the appendix A.1.3 for more details. This non-unicity of the decomposition can be seen as a gauge invariance, as the various decomposition can be related through local symmetry operations [144, 146].

However, if we assume that the vertex vector is zero, *i.e.* $\boldsymbol{D}\cdot\boldsymbol{u}_{\mathrm{e}} = 0$, the cycle vector is uniquely determined by

$$\boldsymbol{u}_{\mathrm{c}}^{\mathrm{d}} = \boldsymbol{C}^{+}\cdot\boldsymbol{u}_{\mathrm{e}} \qquad (1.13)$$

where $\boldsymbol{C}^{+}$ is the Moore-Penrose pseudo inverse of the matrix $\boldsymbol{C}$ (see App. A.1.3). For linear forms, the nullity of the cycle linear form, *i.e.* $\boldsymbol{w}_{\mathrm{e}}^{\mathrm{T}}\cdot\boldsymbol{C} = 0$, assures the unicity of the vertex linear form

$$\boldsymbol{w}_{\mathrm{v}}^{\mathrm{dT}} = \boldsymbol{w}_{\mathrm{e}}^{\mathrm{T}}\cdot\boldsymbol{D}^{+}. \qquad (1.14)$$

**The symmetric part** The symmetric part is also defined on the oriented graph, but its value is independent of the orientation. It is noted also with a bold notation, the context should allow to distinguish between symmetric and antisymmetric part. In general, it cannot be decomposed on cycle and vertex parts.

## 1.2 Markovian processes in continuous time

We are interested in the dynamical properties of our systems. Due to fluctuations, we use stochastic processes as a tool to explore the statistical properties of theirs evolution.

A stochastic process visits over the time various states of the system. The actual system state at time $t$ is then a random variable $X(t)$. The study of stochastic processes focuses on the computation of the probability for the system to be at $x$ at time $t$, denoted $\rho_x(t) = \Pr\left(X(t) = x\right)$. Discrete stochastic processes are also called jump processes.

### 1.2.1 Markov assumption

A Markov process is a stochastic process whose probability of finding the system at a later time step in some state, only depends on the present state, not on the former one. In a more formal way, this means that the probability $\Pr\left(X(t') = y | X(t) = x\right)$ to be in $y$ at time $t'$ knowing it was in $x$ at time $t$ respects the Markov assumption, for a sequence of times $t_1 \leqslant t_2 \leqslant \ldots \leqslant t_n \leqslant t$:

$$\Pr\left(X(t) = y | X(t_n) = x_n, \ldots, X(t_1) = x_1\right) = \Pr\left(X(t) = y | X(t_n) = x_n\right). \quad (1.15)$$

In other words, the knowledge of the state of the system at past time $t_i$ does not bring more information on its future evolution than the knowledge of its state in the present time $t_n$. In the remaining of this manuscript, we always assume our process to be Markovian.

There are two common reasons to justify such an assumption. First, Markov assumption amount to memory-less assumption. This means that the system loses at each time the memory of its past. In reality, if the system loses rapidly memory on a small timescale, one can focus on the dynamics for the bigger timescale that is Markovian. The other reason is a sort of determinism. In classical mechanics, the initial conditions allow to compute the future states. For stochastic process, the state of the system is a random variable, but its probability distribution should be obtained in a deterministic way, *i.e.* the knowledge of the probability distribution of state at actual time is sufficient to compute the future probability of each state [7, 30].

### 1.2.2 Master equation

**Transition rates** Our processes being Markovian, the transition probability respects the Chapman-Kolmogorov equation, if $t'' \geqslant t' \geqslant t$, then

$$\Pr\left(X(t'') = z | X(t) = x\right) =$$
$$\sum_y \Pr\left(X(t'') = z | X(t') = y\right) \Pr\left(X(t') = y | X(t) = x\right). \quad (1.16)$$

We assume in the following, that the process is time-homogeneous, *i.e.* there is an invariance of the transition probability with time-translation, more formally

$$\forall t, \Delta t \, \Pr\left(X(t + \Delta t) = y | X(t) = x\right) = \Pr\left(X(\Delta t) = y | X(0) = x\right). \quad (1.17)$$

We introduce the transition rate from $y$ to $x$

$$\omega_{x,y} = \lim_{\Delta t \to 0} \frac{\Pr\left(X(\Delta t) = x | X(0) = y\right)}{\Delta t}. \quad (1.18)$$

This implies that all transitions rates are non-negative. We also assume that if a transition is allowed $\omega_{x,y} > 0$ then the reverse transition is also allowed $\omega_{y,x} > 0$, sometimes called microreversibility.

**Master equation**   Eq. (1.16) allows the derivation of the master equation that rules the evolution of the probability $\boldsymbol{\rho}_{\mathrm{v}}(t)$ [28]

$$\dot{\boldsymbol{\rho}}_{\mathrm{v}}(t) = \boldsymbol{K} \cdot \boldsymbol{\rho}_{\mathrm{v}}(t), \tag{1.19}$$

where $\dot{\boldsymbol{\rho}}_{\mathrm{v}}(t)$ is the time derivative of the probability $\boldsymbol{\rho}_{\mathrm{v}}(t)$. $\boldsymbol{K}$ is the transition matrix whose elements are

$$K_{x,y} = \begin{cases} \omega_{x,y} & \text{if } x \neq y \\ -\tau_x & \text{if } x = y \end{cases} . \tag{1.20}$$

The escape rate $\tau_x$ from the state $x$ is given by the sum of rate leaving the state $x$,

$$\tau_x = \sum_z \omega_{z,x}. \tag{1.21}$$

**Probability current and activity**   To each transition matrix, we associate the graph $\mathscr{G}$ whose vertices are the state of the system. A couples of states, $x, y$ is an edge of the graph if the transition rate between both states is positive $\omega_{x,y} > 0$. For an oriented edge $(x, y)$, we use the notation $\omega_{(x,y)} = \omega_{x,y}$. The master equation is a conservation equation for the probability flow on the graph. We introduce the probability current along the edge $(x, y)$

$$j^{\rho}_{(x,y)}(t) = \omega_{(x,y)}\rho_y(t) - \omega_{(y,x)}\rho_x(t), \tag{1.22}$$

the first term is the probability per unit time that the system jumps from the origin $y$ of the edge $(x, y)$ to its end $x$, while the second term the probability per unit time for the reverse transition. We emphasize that $j^{\rho}_{(x,y)}(t)$ is a deterministic variable, the master equation being a deterministic equation for probability. The evolution of the probability distribution is then the difference between incoming and outgoing probability currents. Using the incidence matrix, this gives

$$\dot{\boldsymbol{\rho}}(t) = \boldsymbol{D} \cdot \boldsymbol{j}^{\rho}_{\mathrm{e}}(t), \tag{1.23}$$

which is why $\boldsymbol{D}$ is interpreted as a divergence when applied to an edge vector. The probability current is here an edge vector and the time derivative of the probability a vertex vector.

For latter reference, we introduce the symmetric counterpart of the probability current, that is the probability activity [30]

$$a^{\rho}_{(x,y)}(t) = \omega_{(x,y)}\rho_y(t) + \omega_{(y,x)}\rho_x(t). \tag{1.24}$$

It provides the jump frequency along an edge independently of the orientation.

**Normalization of the probability**   From the last form of the master equation (1.23), it is easy to see that the norm of the probability is conserved. Indeed, the vector $\mathbf{1}^{\mathrm{T}} = (1, \ldots, 1)$ is a left eigenvector with eigenvalue 0 of the incidence matrix $\boldsymbol{D}$. This leads to

$$\mathbf{1}^{\mathrm{T}} \cdot \boldsymbol{D} \cdot \boldsymbol{j}_{\mathrm{e}}^{\boldsymbol{\rho}} = 0 = \mathbf{1}^{\mathrm{T}} \cdot \dot{\boldsymbol{\rho}}(t). \tag{1.25}$$

Hence the norm of the probability distribution is constant.

**Decomposition of the transition rate**   The rates may also be written as

$$\omega_{(x,y)} = \sqrt{\omega_{(x,y)} \omega_{(y,x)}} \exp \left[ \frac{1}{2} \ln \frac{\omega_{(x,y)}}{\omega_{(y,x)}} \right]. \tag{1.26}$$

The probability current is then given by the relation

$$j_{(x,y)}^{\rho}(t) = g^{\rho}(t) \sinh \left[ \frac{1}{2} f_{(x,y)}^{\omega \rho}(t) \right], \tag{1.27}$$

with the geometrical activity

$$g^{\rho}(t) = 2\sqrt{\omega_{(x,y)} \omega_{(y,x)} \rho_y(t) \rho_x(t)} \tag{1.28}$$

and the edge affinity

$$f_{(x,y)}^{\omega \rho}(t) = \ln \frac{\omega_{(x,y)} \rho_y(t)}{\omega_{(y,x)} \rho_x(t)}. \tag{1.29}$$

The probability activity writes then

$$a_{(x,y)}^{\rho}(t) = g^{\rho}(t) \cosh \left[ \frac{1}{2} f_{(x,y)}^{\omega \rho}(t) \right]. \tag{1.30}$$

The edge affinity being a linear form, it can be decomposed into

$$\boldsymbol{f}_{\mathrm{e}}^{\boldsymbol{\omega \rho} \mathrm{T}} = -\boldsymbol{f}_{\mathrm{v}}^{\boldsymbol{\rho} \mathrm{T}} \cdot \boldsymbol{D} + \boldsymbol{f}_{\mathrm{e}}^{\boldsymbol{\omega} \mathrm{T}} = -\boldsymbol{f}_{\mathrm{v}}^{\boldsymbol{\rho}/\boldsymbol{q} \mathrm{T}} \cdot \boldsymbol{D} + \boldsymbol{f}_{\mathrm{e}}^{\boldsymbol{\omega q} \mathrm{T}} \tag{1.31}$$

where $\boldsymbol{q}_{\mathrm{v}}$ is any probability distribution and the vertex affinity $\boldsymbol{f}_{\mathrm{v}}^{\boldsymbol{\rho}/\boldsymbol{q} \mathrm{T}}$ is defined by

$$f_x^{\rho/q} = \ln \frac{\rho_x(t)}{q_x}. \tag{1.32}$$

When $\boldsymbol{q}_{\mathrm{v}}$ is the uniform distribution, we simply remove it from the superscript. The decomposition being non unique, we can freely choose the probability distribution $\boldsymbol{q}_{\mathrm{v}}$. The cycle affinities, that are invariant of the decomposition, are given by

$$\boldsymbol{f}_{\mathrm{c}}^{\mathrm{T}} = \boldsymbol{f}_{\mathrm{e}}^{\boldsymbol{\omega \rho} \mathrm{T}} \cdot \boldsymbol{C} = \boldsymbol{f}_{\mathrm{e}}^{\boldsymbol{\omega} \mathrm{T}} \cdot \boldsymbol{C}. \tag{1.33}$$

The last equality contains only time-independent quantities, such that the cycle affinities are also time-independent. When the cycle affinities are all zero, the system satisfies the *detailed balance*. The decomposition of the edge affinities is then uniquely determined from the Eq. (1.14). This definition of detailed balance is also call Kolmogorov's criterion.

Eq. (1.27) can be seen as a non-linear way of connecting vectors and linear forms generalizing the notion of metric that does so linearly [107, 112].

### 1.2.3 Properties of the transition matrix

**Formal solution to the master equation** The solution of the master equation is formally determined from the set of eigenvalues and eigenvectors of $\boldsymbol{K}$. We denote $\lambda_n$, $n = 0 \ldots, Ns - 1$ the eigenvalues of $\boldsymbol{K}$, $\boldsymbol{r}_{\mathrm{v}}^n$, $n = 0 \ldots, Ns - 1$ the right eigenvectors and $\boldsymbol{l}_{\mathrm{v}}^n$, $n = 0 \ldots, Ns - 1$ the left eigenvectors. Given the initial probability distribution $\boldsymbol{\rho}_{\mathrm{v}}^{\mathrm{i}}$, the probability distribution at time $t$ is

$$\boldsymbol{\rho}_{\mathrm{v}}(t) = \sum_{n=0}^{Ns-1} e^{\lambda_n t} \boldsymbol{r}_{\mathrm{v}}^n \boldsymbol{l}_{\mathrm{v}}^{n\mathrm{T}} \cdot \boldsymbol{\rho}_{\mathrm{v}}^{\mathrm{i}}. \tag{1.34}$$

**Irreducible transition matrix** Properties of the graph $\mathscr{G}$ are equivalent to those of $\boldsymbol{K}$. In particular an irreducible transition matrix is a matrix whose associated graph is connected.

**Perron-Frobenius theorem** The off-diagonal elements of the transition matrix being all non negative, the transition matrix is a Metzler matrix. Therefore when $\boldsymbol{K}$ is irreducible, the Perron-Fröbenius theorem is valid and implies the following sentences [16]

- The highest eigenvalue $\lambda_0$ is real and unique.

- $\boldsymbol{K}$ has a right and left eigenvector with eigenvalue $\lambda_0$ whose components are all positive.

- The only eigenvector whose all components are positive is the one associated with the eigenvalue $\lambda_0$.

For $\boldsymbol{K}$ defined by the Eq. (1.20), the vector $\mathbf{1}^{\mathrm{T}} = (1, \ldots, 1)$ is a left eigenvectors with eigenvalues 0. Being a vector with components all positive, this is the eigenvector with the highest eigenvalue $\lambda_0 = 0$. Then the right eigenvector $\boldsymbol{\pi}_{\mathrm{v}}$ is a stationary solution of the master equation (1.19), and all others eigenvalues have a negative real part.

The solution of the master equation then rewrite

$$\boldsymbol{\rho}_{\mathrm{v}}(t) = \boldsymbol{\pi}_{\mathrm{v}} + \sum_{n=1}^{Ns-1} e^{\lambda_n t} \boldsymbol{r}_{\mathrm{v}}^n \boldsymbol{l}_{\mathrm{v}}^{n\mathrm{T}} \cdot \boldsymbol{\rho}_{\mathrm{v}}^{\mathrm{i}}. \tag{1.35}$$

When $\boldsymbol{K}$ is an irreducible matrix, whatever the initial probability distribution is, the probability distribution $\boldsymbol{\rho}(t)$ converges towards the stationary distribution. The independence of the stationary probability distribution with the initial probability distribution highlights the ergodicity of irreducible Markov processes in continuous time [45].

**Steady state solution** We turn to the study of the stationary solution, *i.e.* the solution of

$$\boldsymbol{K} \cdot \boldsymbol{\pi}_{\mathrm{v}} = 0. \tag{1.36}$$

There exists a well-know graph theoretical expression for the steady state probability distribution. The transition matrix is the equivalent of the Laplacian matrix (1.5) for an oriented weighted graph [19]. Using the matrix-tree theorem, we obtain the steady state solution as a sum of the minor of the transition matrix. This solution has a nice interpretation in term of spanning tree of the associated graph [163]. Consider all the spanning tree of the graph. For each state $x$ we orient all spanning tree $\mathscr{T}$ towards this state, producing the rooted spanning tree $\mathscr{T}_x$. We then denote $\omega(\mathscr{T}_x)$ the spanning tree polynomial that is the product of the transition rates along all oriented edges of the spanning tree. Then the stationary probability is

$$\pi_x = \frac{\sum_{\mathscr{T}_x} \omega(\mathscr{T}_x)}{\sum_x \sum_{\mathscr{T}_x} \omega(\mathscr{T}_x)}, \tag{1.37}$$

where the sum $\sum_{\mathscr{T}_x}$ runs over all spanning trees of the graph rooted into $x$. The denominator ensures the normalization of the stationary probability.

At steady state, the conservation equation on the currents implies the nullity of the divergence of the stationary edge current $\bar{\boldsymbol{j}}_{\mathrm{e}} = \boldsymbol{j}_{\mathrm{e}}^{\boldsymbol{\pi}}$ such that

$$\boldsymbol{D} \cdot \bar{\boldsymbol{j}}_{\mathrm{e}} = 0. \tag{1.38}$$

We have introduced the notation $\bar{j}$ for stationary currents. The vertex contribution to the edge current is then null, and there exists a unique stationary cycle current $\bar{\boldsymbol{j}}_{\mathrm{c}}$ such that

$$\bar{\boldsymbol{j}}_{\mathrm{e}} = \boldsymbol{C} \cdot \bar{\boldsymbol{j}}_{\mathrm{c}}. \tag{1.39}$$

Moreover when we have detailed balance, the edge affinity is given from a vertex affinity. As for any choice of spanning tree, the decomposition (1.9) is identical, we obtain

$$\boldsymbol{f}_{\mathrm{e}}^{\boldsymbol{\omega}\boldsymbol{\rho}\mathrm{T}} = -\boldsymbol{f}_{\mathrm{v}}^{\boldsymbol{\rho}/\boldsymbol{\pi}\mathrm{T}} \cdot \boldsymbol{D} \tag{1.40}$$

resulting in the detailed balance condition

$$\frac{\omega_{(y,x)}}{\omega_{(x,y)}} = \frac{\pi_y}{\pi_x}. \tag{1.41}$$

As a consequence of detailed balance, using the Eq. (1.27) at stationary state all edge current are zero. Hence the stationary cycle current are also zero. This is what is called equilibrium stationary state.

## 1.2.4   Thermodynamics of stochastic processes in contact with reservoirs.

**State variables**   As stated before, states are the values of the collection of variables used to model the system (microstates variables). However we would like to characterize the states by a small number of thermodynamic variables (macrostates) that describe globally the system.

For example, a gas is characterized by the occupied volume, the number of particles and the sum of the energy of each of its components. We provide example

of such variable in the table 1.1. We emphasize that these macrostate variables do not substitute to the formal description of the microstate, as two microstates with the same macrostate variable are in most cases different. As an example, for a magnet there are many different microstates that leads to the same global magnetization.

The existence of such macrostate variables is derived from the Noether's theorem. The theorem states that conservation laws follow from symmetries of the dynamics. Hence, macrostates variables correspond to quantities that are conserved for an isolated system. As an example, for system that are invariant by translation in time, from the Noether's theorem, the energy is a conserved quantity and is then a state variable.

In this thesis, we consider only non-isolated systems. Thermodynamics approach consists into separating the system from its environment, system plus environment being called "universe" [5]. Our goal is to study the flux of the macrostate variables that the system exchanges with the environment.

| Extensive macrostate variables | Intensive forces |
| --- | --- |
| Energy | Inverse temperature |
| Particles number | Chemical potential |
| Charge | Electric potential |
| Displacement | Generic force |
| Angle | Torque |
| Volume | Pressure |
| Magnetization | Magnetic field |

Table 1.1: Examples of state variables with theirs conjugated intensive forces.

**Reservoirs and reservoirs matrix**  The environment could be further separated into various subsystems that we call reservoirs.

A reservoir is an equilibrium system that is assumed bigger than the system such that all exchanges with the system do not affect its macrostate. Each reservoirs is assumed to be of one type, such that it exchange only a particular state variable with the system. The reservoirs are characterized by an intensive variable conjugated to the extensive state variable. Examples are provided in the table 1.1. The number of reservoirs connected to the system is denoted $Rev$.

For a system modeled by a graph, we describe system-reservoirs interaction as follows: For each oriented edge, we have a variation of the state variables, this variation corresponds to an exchange with one of the reservoirs. We denote $M$ the macrostate variable exchanged with reservoir $r$. We introduce the $Rev \times Ed$ reservoir matrix that describe the interactions of the system with the reservoirs.

$$R_{r,(x,y)} = \begin{cases} M_x - M_y & \text{if on the edge } (x,y) \text{ } M \text{ is exchanged with the reservoir } r, \\ 0 & \text{otherwise,} \end{cases}$$

(1.42)

that is the inflow of the macrostate variable $M$ coming from the reservoir $r$ to the system. Macrostate variables are exchanged with their corresponding reservoir type only, *i.e.* particle with particle reservoirs, charge with charge reservoirs,...

The flow $\dot{\boldsymbol{M}}_{\mathrm{r}}(t)$ of macrostate quantities between the reservoirs and the system is then written from the edge probability current (1.22) as

$$\dot{\boldsymbol{M}}_{\mathrm{r}}(t) = \boldsymbol{R} \cdot \boldsymbol{j}_{\mathrm{e}}^{\boldsymbol{\rho}}(t). \tag{1.43}$$

We emphasize that the reservoirs currents are oriented towards the system.

**Remark:** In this manuscript, exchange with reservoirs only occurs during transitions. We do not consider time-dependent control parameter that would enable work exchange with a work source even when the system remains in the same state [187, 188].
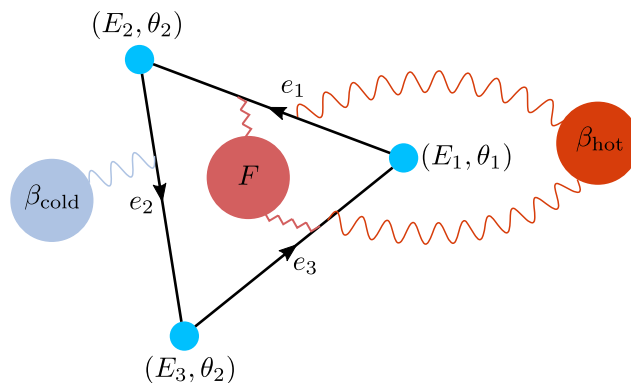


Figure 1.3: Sketch of a unicyclic system connected to two energy reservoirs at inverse temperature $\beta_{\mathrm{hot}}$ and $\beta_{\mathrm{cold}}$ and one work source associated with torque $F$.

**Example of reservoir matrix**  Let's consider as simple example the system depicted on Fig. 1.3. The state variables are $(E, \theta)$, the energy and the angle of each state, we set $\theta_3$ as $\theta_2$. It is connected to three different reservoirs, two energy reservoirs at inverse temperature $\beta_{\mathrm{hot}}$ and $\beta_{\mathrm{cold}}$ and one work source associated with torque $F$. We denote $\dot{E}_{\mathrm{hot}}$ (resp. $\dot{E}_{\mathrm{cold}}$) the energy flux from the hot (resp. cold) energy reservoirs, and $\dot{\theta}_{\mathrm{angle}}$ the angle flux. The current of the state variable with the reservoirs is

$$\begin{pmatrix} \dot{E}_{\mathrm{hot}} \\ \dot{E}_{\mathrm{cold}} \\ \dot{\theta}_{\mathrm{angle}} \end{pmatrix}(t) = \begin{pmatrix} E_2 - E_1 & 0 & E_1 - E_3 \\ 0 & E_3 - E_2 & 0 \\ \theta_2 - \theta_1 & 0 & \theta_1 - \theta_2 \end{pmatrix} \begin{pmatrix} j_{(2,1)}^{\rho} \\ j_{(3,2)}^{\rho} \\ j_{(1,3)}^{\rho} \end{pmatrix}(t). \tag{1.44}$$

The matrix connecting probability currents to the reservoir currents is then the reservoir matrix $\boldsymbol{R}$.

## 1.2.5  Entropy production

**Kullback-Leibler divergence**  An important quantity to study stochastic processes is the Kullback-Leibler divergence (KL-divergence), defined for a probability distribution $\boldsymbol{p}_{\mathrm{v}}$ and a prior distribution $\boldsymbol{q}_{\mathrm{v}}$ by

$$D(\boldsymbol{p}_{\mathrm{v}} \| \boldsymbol{q}_{\mathrm{v}}) = \sum_x p_x \ln \frac{p_x}{q_x}. \tag{1.45}$$

It is not a distance in the mathematical terms, since it is neither symmetric nor does it satisfy the triangle inequality. Nevertheless it quantifies the difference between two probability distributions, here $\boldsymbol{p}_v$ and $\boldsymbol{q}_v$. When $\boldsymbol{q}_v$ is the uniform probability distribution $\boldsymbol{1}_v$, the KL-divergence becomes minus the Shannon entropy

$$S(\boldsymbol{p}_v) = -D(\boldsymbol{p}_v \| \boldsymbol{1}_v) = -\sum_x p_x \ln p_x. \tag{1.46}$$

**Entropy production rate** The time derivative of the KL-divergence of the probability $\boldsymbol{\rho}_v(t)$ with a time-independent probability $\boldsymbol{q}_v$ is the scalar product of vertex current with vertex affinity

$$\frac{\mathrm{d}}{\mathrm{d}t} D(\boldsymbol{\rho}_v(t) \| \boldsymbol{q}_v) = \boldsymbol{f}_v^{\rho/q\mathrm{T}} \cdot \dot{\boldsymbol{\rho}}_v(t). \tag{1.47}$$

Using the master equation (1.23) and Eq. (1.31), we can go further

$$\frac{\mathrm{d}}{\mathrm{d}t} D(\boldsymbol{\rho}_v(t) \| \boldsymbol{q}_v) = \boldsymbol{f}_v^{\rho/q\mathrm{T}} \cdot \boldsymbol{D} \cdot \boldsymbol{j}_e^\rho = -\boldsymbol{f}_e^{\omega\rho\mathrm{T}} \cdot \boldsymbol{j}_e^\rho + \boldsymbol{f}_e^{\omega q\mathrm{T}} \cdot \boldsymbol{j}_e^\rho. \tag{1.48}$$

The scalar product

$$\boldsymbol{f}_e^{\omega\rho\mathrm{T}} \cdot \boldsymbol{j}_e^\rho = \sum_{(x,y)} f_{(x,y)}^{\omega\rho} j_{(x,y)}^\rho = \boldsymbol{f}_e^{\omega q\mathrm{T}} \cdot \boldsymbol{j}_e^\rho - \frac{\mathrm{d}}{\mathrm{d}t} D(\boldsymbol{\rho}_v(t) \| \boldsymbol{q}_v) \tag{1.49}$$

is called the total entropy production rate [87]. From its edge expression

$$\boldsymbol{f}_e^{\omega\rho\mathrm{T}} \cdot \boldsymbol{j}_e^\rho = \sum_{(x,y)} f_{(x,y)}^{\omega\rho} j_{(x,y)}^\rho = \sum_{(x,y)} \left( \omega_{(x,y)} \rho_y(t) - \omega_{(y,x)} \rho_x(t) \right) \ln \frac{\omega_{(x,y)} \rho_y(t)}{\omega_{(y,x)} \rho_x(t)} \geqslant 0 \tag{1.50}$$

it is a non-negative quantity, due to the non-negativity of the function $(x - y)\log(x/y)$. It is a central quantity of stochastic thermodynamics, as it characterizes the irreversibility of the evolution.

**Decomposition of the entropy production rate** From the Eq. (1.48), the entropy production rate is the sum of two terms that depends on the choice of the decomposition. We emphasize some choices of $\boldsymbol{q}_v$ that have been used

- $\boldsymbol{q}_v = \boldsymbol{1}_v$ the KL-divergence is now minus the Shannon entropy (1.46), the total entropy production is so the sum of $\dot{S}(\rho)$, the internal entropy variation and $\boldsymbol{f}_e^{\omega\mathrm{T}} \cdot \boldsymbol{j}_e^\rho$ the entropy flow.

- $\boldsymbol{q}_v = \boldsymbol{\pi}_v$ this is the adiabatic/non-adiabatic splitting of the entropy production. The adiabatic contribution is $\boldsymbol{f}_e^{\omega\pi\mathrm{T}} \cdot \boldsymbol{j}_e^\rho$, whereas $-\frac{\mathrm{d}}{\mathrm{d}t} D(\boldsymbol{\rho}_v(t) \| \boldsymbol{\pi}_v)$ is called the non-adiabatic contribution. For this splitting, both contributions are non-negative [87].

**Particular cases**   Let's now characterize two particular cases where the decomposition (1.49) is unique. At stationary state, the current decomposition is given by Eq. (1.39), then the total entropy production rate $\bar{\sigma}$ is simply given by the cycle current and affinity, as

$$\bar{\sigma} = \boldsymbol{f}_{\mathrm{e}}^{\boldsymbol{\omega\pi}\,\mathrm{T}} \cdot \bar{\boldsymbol{j}}_{\mathrm{e}} = \boldsymbol{f}_{\mathrm{e}}^{\boldsymbol{\omega\pi}\,\mathrm{T}} \cdot \boldsymbol{C} \cdot \bar{\boldsymbol{j}}_{\mathrm{c}} = \boldsymbol{f}_{\mathrm{c}}^{\mathrm{T}} \cdot \bar{\boldsymbol{j}}_{\mathrm{c}}. \tag{1.51}$$

When the system respects detailed balance, the entropy production rate is given by minus the time derivative of the KL-divergence between the probability $\boldsymbol{\rho}_{\mathrm{v}}(t)$ and the stationary probability $\boldsymbol{\pi}_{\mathrm{v}}$

$$\boldsymbol{f}_{\mathrm{e}}^{\mathrm{T}} \cdot \boldsymbol{j}_{\mathrm{e}}^{\rho} = -\frac{\mathrm{d}}{\mathrm{d}t} D(\boldsymbol{\rho}_{\mathrm{v}}(t) \| \boldsymbol{\pi}_{\mathrm{v}}). \tag{1.52}$$

It is then possible to show that the system evolves following the gradient of Shannon entropy, such that the equilibrium stationary state is the maximum of the entropy with respect to the system's constraints [33, 112]. This makes the connection with equilibrium statistical mechanics. We say that detailed balance system are *equilibrium* systems. In particular, equilibrium systems do not produce entropy in the stationary state.

## 1.2.6   Entropy exchange with reservoirs

From Eq. (1.49), the entropy production rate is the sum of two terms. Stochastic thermodynamics assumes [184, 30]:

(i) The relevant prior distribution $\boldsymbol{q}_{\mathrm{v}}$ is the uniform probability distribution $\mathbf{1}_{\mathrm{v}}$.

(ii) The entropy flow $\boldsymbol{f}_{\mathrm{e}}^{\boldsymbol{\omega}\,\mathrm{T}} \cdot \boldsymbol{j}_{\mathrm{e}}^{\rho}$ corresponds to entropy exchanged by the system with the reservoirs.

(iii) The reservoirs do not interact with each others.

(iv) The reservoirs are weakly coupled with the system such that the system does not affect the stationary (equilibrium) probability of the reservoir.

We have some heuristic arguments for theses assumptions. Assumption (i) is connected with a similar assumption for equilibrium statistical physics. If the system is let evolve alone in absence of any information about its dynamics, we expect to observe a uniform distribution. Assumption (ii) is valid if the system plus the reservoirs (the "universe") are isolated, such that entropy production of the "universe" is solely due to time variation of its entropy. For assumption (iii), if the system interacts locally in time and space with each reservoirs, one at time, the reservoirs are independent of each others [30]. The last assumption (iv) is simply the assumption that the reservoirs are big enough to exchange entropy with the system without affecting their stationary probabilities.

These assumptions give constraints on the transition rates, that will depend on the way reservoirs are connected to the system. In order to characterize these entropy fluxes, we first study a system in equilibrium with one reservoir only.

**Equilibrium dynamics with heat baths**   Let's consider a system in contact with a unique energy reservoir at inverse temperature $\beta$. Its reservoir matrix is then an $1 \times Ed$ matrix of elements

$$R_{r,(x,y)} = E_x - E_y \tag{1.53}$$

with $E_x$ the energy of the state $x$. From equilibrium statistical mechanics, the stationary probability is given by

$$\pi_x^{\text{eq}} = \frac{e^{-\beta E_x}}{Z} \tag{1.54}$$

with $Z = \sum_x e^{-\beta E_x}$. We also know that the system has no stationary currents. Using the detailed balance condition, we then have

$$f_{(x,y)}^{\omega} = \ln \frac{\omega_{(x,y)}}{\omega_{(y,x)}} = \ln \frac{\pi_x^{\text{eq}}}{\pi_y^{\text{eq}}} = -\beta(E_x - E_y). \tag{1.55}$$

Writing now the entropy balance (1.49), we have the entropy flux from the system into the environment using assumption (i) and (ii)

$$\boldsymbol{f}_{\text{e}}^{\omega\text{T}} \cdot \boldsymbol{j}_{\text{e}}^{\rho} = -\sum_{(x,y)} \beta(E_x - E_y)j_{(x,y)}^{\rho} \tag{1.56}$$

We recognize the reservoir matrix and obtain

$$\boldsymbol{f}_{\text{e}}^{\omega\text{T}} \cdot \boldsymbol{j}_{\text{e}}^{\rho} = -\beta\dot{E}. \tag{1.57}$$

Such that the entropy flux from the system into the environment is minus the product of the inverse temperature and the energy flux $\dot{E}$ into the system, *i.e.* the reservoir current. Defining $-\beta$ as the affinity $f_r$ of the energy reservoir, the entropy flux is then $f_r\dot{E}$. The minus originates in the choice of orienting reservoirs currents towards the system. The energy fluxes are also called heat fluxes, and energy reservoirs are often called heat baths or thermal baths.

**Equilibrium dynamics with others type of reservoirs**   We now connect also to the system a reservoir that is not an heat bath, but corresponds to an intensive force $F$, such reservoirs are also called non conservative work sources. When the work source exchanges a state quantity with the system during a transition between two states $x$ and $y$, this induces a work $F(M_x - M_y)$ done by the reservoirs on the system. Due to energy conservation, we must also connect an heat bath of inverse temperature $\beta$ to complete the energy balance. The energy difference between the two states being $E_x - E_y$, the heat bath gives $E_x - E_y - F(M_x - M_y)$ to the system during the transition. The entropy flux into the heat bath is then

$$-\beta\left(E_x - E_y - F(M_x - M_y)\right)j_{(x,y)}^{\rho}. \tag{1.58}$$

We decompose this entropy flux into a contribution from the heat bath $-\beta(E_x - E_y)j_{(x,y)}^{\rho}$ and a contribution from the non-conservative work source as $\beta F(M_x - M_y)j_{(x,y)}^{\rho}$, such that $\beta F$ defines the affinity of the non-conservative work source.

As an example, for chemical reservoirs, the intensive force is the chemical potential $\mu$ and the exchanged state quantity the number of particles $n_x$, such that the entropy flux is $-\beta \left(E_x - E_y - \mu(n_x - n_y)\right) j^\rho_{(x,y)}$ and the affinity of the chemical reservoir is $\beta\mu$.

**Information reservoirs**   Another category of reservoirs are the information reservoirs. These are reservoirs that only exchange entropy with the system. Introducing these reservoirs is very convenient to understand the Maxwell's demon, the Szilard engine or the Landauer's eraser [37, 46, 47, 99, 121, 138, 180]. When the system exchanges entropy with an information reservoir, we add entropy flux into the reservoir matrix $\boldsymbol{R}$, the reservoir affinity is then simply one.

Taking into consideration error rates for the transfer of entropy between the information reservoirs and the system modifies the reservoir affinities [37].

**Entropy production at reservoirs level in presence of several reservoirs**
Let's now connect several reservoirs to our system. During a transition, the system will exchange quantities with some reservoirs, if necessary we connect a heat bath to the transition to complete the energy balance. For each reservoir, we have a reservoir affinity. It is minus the inverse temperature $-\beta_r$ for heat baths, and the product of the inverse temperature of the heat bath connected to the transition with the intensive force for the work sources. The linear form of the reservoir affinities is denoted $\boldsymbol{f}_\mathrm{r}^\mathrm{T}$.

As a consequence of the assumptions (i)-(iv), the entropy flow $\sigma_\mathrm{exch}$ is the sum of all entropy exchanges with each reservoirs, such that

$$\sigma_\mathrm{exch} = \boldsymbol{f}_\mathrm{r}^\mathrm{T} \cdot \dot{\boldsymbol{M}}_\mathrm{r}. \tag{1.59}$$

**Local detailed balance**   The condition of thermodynamic consistency requires that the entropy exchange with reservoirs coincides with the entropy flow at edge level. This implies the constraint

$$\boldsymbol{f}_\mathrm{r}^\mathrm{T} \cdot \dot{\boldsymbol{M}}_\mathrm{r} = \boldsymbol{f}_\mathrm{r}^\mathrm{T} \cdot \boldsymbol{R} \cdot \boldsymbol{j}_\mathrm{e}^\rho = \boldsymbol{f}_\mathrm{e}^{\boldsymbol{\omega}\mathrm{T}} \cdot \boldsymbol{j}_\mathrm{e}^\rho \tag{1.60}$$

The thermodynamic consistency is respected when edge affinity are defined by the *local detailed balance* [108, 123, 124]

$$\boldsymbol{f}_\mathrm{e}^{\boldsymbol{\omega}\mathrm{T}} = \boldsymbol{f}_\mathrm{r}^\mathrm{T} \cdot \boldsymbol{R}. \tag{1.61}$$

Therefore the local detailed balance set constraints on the antisymmetric part of the transition rates. The symmetric part is to be determined as it describes the strength of the exchanges with the baths. Often it is set to a constant.

As shown, the local detailed balance is a direct consequence of the assumption (i)-(iv) of stochastic thermodynamics. The locality refers to the locality of interaction with reservoirs in time and space during the evolution [30].

A weaker condition can be obtained on the edge affinity, if one asks for example only the equality of the reservoir entropy exchange with cycle entropy production

rate, that is the entropy production rate at stationary state. The constraint is now

$$\boldsymbol{f}_{\mathrm{r}}^{\mathrm{T}} \cdot \boldsymbol{j}_{\mathrm{r}} = \boldsymbol{f}_{\mathrm{r}}^{\mathrm{T}} \cdot \boldsymbol{R} \cdot \boldsymbol{C} \cdot \bar{\boldsymbol{j}}_{\mathrm{c}} = \boldsymbol{f}_{\mathrm{c}}^{\mathrm{T}} \cdot \bar{\boldsymbol{j}}_{\mathrm{c}}. \tag{1.62}$$

This only gives an equation for the cycle affinities

$$\boldsymbol{f}_{\mathrm{c}}^{\mathrm{T}} = \boldsymbol{f}_{\mathrm{r}}^{\mathrm{T}} \cdot \boldsymbol{R} \cdot \boldsymbol{C}. \tag{1.63}$$

Therefore, due to the non unique solution for the definition of the edge affinity from the cycle affinity, see sec. 1.1.3, the edge affinity are non uniquely defined.

We emphasize that when the matrix $\boldsymbol{R} \cdot \boldsymbol{C}$ is zero, the cycle affinities $\boldsymbol{f}_{\mathrm{c}}^{\mathrm{T}}$ are necessary zero and the system respects then detailed balance with stationary probability given by equilibrium probability.

**Internal entropy**   States can also have internal entropy that originates in the coarse-graining of many similar microstates into a unique mesostate. When considering entropy flow we must consider this additional term. Denoting $\boldsymbol{s}_{\mathrm{v}}^{\mathrm{T}}$ the internal entropy of each mesostate, the entropy balance is modified as [82]

$$\boldsymbol{f}_{\mathrm{e}}^{\mathrm{T}} \cdot \boldsymbol{j}_{\mathrm{e}}^{\rho} = \boldsymbol{f}_{\mathrm{e}}^{\boldsymbol{\omega}\mathrm{T}} \cdot \boldsymbol{j}_{\mathrm{e}}^{\rho} + \boldsymbol{s}_{\mathrm{v}}^{\mathrm{T}} \cdot \boldsymbol{D} \cdot \boldsymbol{j}_{\mathrm{e}}^{\rho} + \frac{\mathrm{d}}{\mathrm{d}t} S(\boldsymbol{\rho}_{\mathrm{v}}(t)) \tag{1.64}$$

with $\boldsymbol{\rho}_{\mathrm{v}}(t)$ the probability of the mesostates and assuming that no jumps are allowed inside a mesostate. The second term must then be included into the exchanged entropy and modify the local detailed balance

$$\boldsymbol{f}_{\mathrm{e}}^{\boldsymbol{\omega}\mathrm{T}} = \boldsymbol{f}_{\mathrm{r}}^{\mathrm{T}} \cdot \boldsymbol{R} + \boldsymbol{s}_{\mathrm{v}}^{\mathrm{T}} \cdot \boldsymbol{D}. \tag{1.65}$$

We provide in Ch. 6 examples where the transition rates do include an internal entropy in their definition.

**Examples of local detailed balanced system**   We come back to the example of sec. 1.2.4, represented on Fig. 1.3. It is a unicyclic system connected to two heat baths. The reservoirs affinities are given by

$$\boldsymbol{f}_{\mathrm{r}}^{\mathrm{T}} = (-\beta_{\mathrm{hot}}, -\beta_{\mathrm{cold}}, \beta_{\mathrm{hot}} F). \tag{1.66}$$

Using local detailed balance, and denoting $\Gamma_i$, for $i = 1, 2, 3$ the symmetric part of the transitions rates, the transition rates are

$$\omega_{(2,1)} = \Gamma_1 e^{-\frac{\beta_{\mathrm{hot}}}{2}[E_2 - E_1 - F(\theta_2 - \theta_1)]}, \quad \omega_{(1,2)} = \Gamma_1 e^{-\frac{\beta_{\mathrm{hot}}}{2}[E_1 - E_2 - F(\theta_1 - \theta_2)]}; \tag{1.67}$$

$$\omega_{(3,2)} = \Gamma_2 e^{-\frac{\beta_{\mathrm{cold}}}{2}[E_3 - E_2]}, \qquad \omega_{(2,3)} = \Gamma_2 e^{-\frac{\beta_{\mathrm{cold}}}{2}[E_2 - E_3]}; \tag{1.68}$$

$$\omega_{(1,3)} = \Gamma_3 e^{-\frac{\beta_{\mathrm{hot}}}{2}[E_1 - E_3 - F(\theta_1 - \theta_3)]}, \quad \omega_{(3,1)} = \Gamma_3 e^{-\frac{\beta_{\mathrm{hot}}}{2}[E_3 - E_1 - F(\theta_3 - \theta_1)]}. \tag{1.69}$$

## 1.3 Trajectories and observables

A realization of a stochastic process, *i.e.* the list of states that the system visits, is called a trajectory or a path. Examples of trajectories are shown on Fig. 1.4.

We denote $\{x(t)\}_{t=0}^T$ a trajectory starting at $t = 0$ and ending at $t = T$. They are realization of the stochastic process $\{X(t)\}_{t=0}^T$. Considering the set of all possible trajectories, we can compute the path probability density function $d\mathbb{P}[\{x(t)\}_0^T]$, that is the probability of the trajectory $\{x(t)\}_{t=0}^T$. Note that the trajectory depends on its initial condition, which is drawn from the initial probability $\boldsymbol{\rho}_v^i$.



(a)  (b)
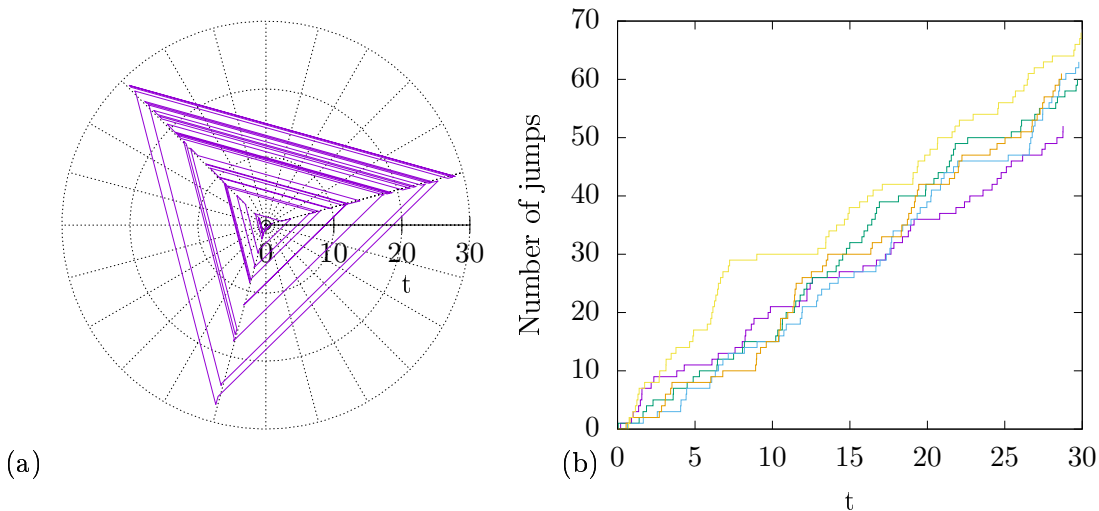
Figure 1.4: (a) Examples of a trajectory for the three state unicyclic system with rates of Eqs. (1.67–1.69). The time is the distance to the origin and the position on the graph is encoded in the angle. (b) Total number of jumps for 5 different trajectories as a function of the time. Parameters are $\Gamma_1 = \Gamma_2 = \Gamma_3 = 1$, $E_1 = 0.5$, $\theta_1 = 0.5, E_2 = 1$, $\theta_2 = 1, E_3 = 1.5$, $\beta_{\text{hot}} = 1$, $\beta_{\text{cold}} = 2$ and $F = 0.5$.

**Path probability density function** From the master equation (1.19), the probability of a path $\{x(t)\}_{t=0}^T$ can be explicitly determined. We index by $i$ the consecutive states $x_i$ (with $i = 0, \ldots, n$) the system visits and the times $t_i$ at which it jumps, such that

$$x(t) = x_i \quad \text{for} \quad t_i \leqslant t < t_{i+1}. \tag{1.70}$$

We have $t_0 = 0$ and $t_n$ the last jump time before $T$. The path probability density function is then

$$d\mathbb{P}_{\boldsymbol{K}}[\{x(t)\}_0^T] = \rho_{x_0}^i \prod_{i=0}^{n-1} \left[\omega_{x_{i+1},x_i} e^{-\tau_{x_i}(t_{i+1}-t_i)} dt_i\right] e^{-\tau_{x_n}(T-t_n)} dt_n. \tag{1.71}$$

That can be condensed in the more elegant form

$$d\mathbb{P}_{\boldsymbol{K}}[\{x(t)\}_0^T] = \rho_{x_0}^i \exp\left[\sum_{i=0}^{n-1} \ln \omega_{x_{i+1},x_i} - \int_0^T \tau_{x(t)} dt\right] \prod_{i=0}^n dt_i. \tag{1.72}$$

**Observables** When studying stochastic processes, we aim at computing some observables that contain less information that the whole set of trajectories but still enough information for being useful. A simple way of withdrawing information on the system evolution over time is to look at time average observables. To that purpose, we consider the generic random variable $O$ defined along a trajectory $\{X(t)\}_{t=0}^{t=T}$ by [60, 61]

$$O = \frac{1}{T}\int_0^T \mathfrak{f}(X_t)\mathrm{d}t + \frac{1}{T}\sum_{0\leqslant t\leqslant T:\Delta X_t\neq 0}\mathfrak{g}(X_{t^+}, X_{t^-}) \qquad (1.73)$$

where $\mathfrak{f}$ and $\mathfrak{g}$ are two arbitrary functions, and the sum is a sum over all jumps along the trajectory. For example, if we choose $\mathfrak{f} = 0$ and $\mathfrak{g} = 1$, $O$ becomes the average number of jumps over the trajectory also called activity. Another choice could be $\mathfrak{f} = \mathbf{1}_S$ the indicator function and $\mathfrak{g} = 0$, $O$ becomes the fraction of time the system spends into the set $S$.

The expectation value of observable (1.73) is then obtained from the path probability density function as

$$\mathbf{E}[O] = \int d\mathbb{P}[\{x(t)\}_0^T]O(\{x(t)\}_{t=0}^T), \qquad (1.74)$$

where the integration is done over all possible trajectories and all possible initial conditions. This formula can be futher simplified as

$$\mathbf{E}[O] = \int \mathrm{d}o\,o\int d\mathbb{P}[\{x(t)\}_0^T]\mathbf{1}_o(O(\{x(t)\}_{t=0}^T)) = \int \mathrm{d}o\,o\Pr(O = o). \qquad (1.75)$$

where $\mathbf{1}_y(x)$ is the indicator function that is one only if $y = x$.

**Empirical occupations times and jump fractions** Among the various observables, we introduce the empirical occupations times

$$R_x = \frac{1}{T}\int_0^T \mathbf{1}_x(X(t))\mathrm{d}t \qquad (1.76)$$

and the empirical jump fractions

$$Q_{x,y} = \frac{1}{T}\sum_{0\leqslant t\leqslant T:\Delta X_t\neq 0}\mathbf{1}_x(X_{t^+})\mathbf{1}_y(X_{t^-}). \qquad (1.77)$$

Both correspond to given choices of the observable $O$ (1.73), with $\mathfrak{f} = \mathbf{1}_x$ and $\mathfrak{g}(x,y) = \mathbf{1}_x\mathbf{1}_y$. Any observable given by Eq. (1.73) can be written as

$$O = \sum_x \mathfrak{f}(x)R_x + \sum_{x,y}\mathfrak{g}(x,y)Q_{x,y} \qquad (1.78)$$

if $\mathfrak{f}(x)$ and $\mathfrak{g}(x,y)$ are time-independent.

**Empirical activity and currents**   The jump fraction can be decomposed into its symmetric and antisymmetric part. For each edge $(x, y)$, we have the orientation $y \to x$. We define the empirical activity

$$A_{(x,y)} = Q_{x,y} + Q_{y,x} = \frac{1}{T} \sum_{0 \leqslant t \leqslant T : \Delta X_t \neq 0} \mathbf{1}_x(X_{t^+})\mathbf{1}_y(X_{t^-}) + \mathbf{1}_y(X_{t^+})\mathbf{1}_x(X_{t^-}) \quad (1.79)$$

and the empirical current

$$J_{(x,y)} = Q_{x,y} - Q_{y,x} = \frac{1}{T} \sum_{0 \leqslant t \leqslant T : \Delta X_t \neq 0} \mathbf{1}_x(X_{t^+})\mathbf{1}_y(X_{t^-}) - \mathbf{1}_y(X_{t^+})\mathbf{1}_x(X_{t^-}). \quad (1.80)$$

The empirical activity counts the number of jumps for edge $(x, y)$ whereas the empirical current counts the flow along edge $(x, y)$.

**Reservoir currents**   Let's look at the variation of a state variable $M$ along a trajectory, this can be computed as

$$\Delta M = \sum_{0 \leqslant t \leqslant T : \Delta X_t \neq 0} \left( M_{X_{t^+}} - M_{X_{t^-}} \right). \quad (1.81)$$

The state variable being exchanged with reservoirs, this can be rewrite as

$$\Delta M = \sum_{0 \leqslant t \leqslant T : \Delta X_t \neq 0} \sum_{r} \left( M_{X_{t^+}} - M_{X_{t^-}} \right) \delta(r, (X_{t^+}, X_{t^-})) \quad (1.82)$$

where the delta-Dirac ensures that the edge $(X_{t^+}, X_{t^-})$ is connected to the reservoir $r$. The empirical reservoir current $J_{r_1}$, that is the rate of exchange with a particular reservoir $r_1$, is then

$$J_{r_1} = \frac{1}{T} \sum_{0 \leqslant t \leqslant T : \Delta X_t \neq 0} \left( M_{X_{t^+}} - M_{X_{t^-}} \right) \delta(r_1, (X_{t^+}, X_{t^-})). \quad (1.83)$$

It could be derived also from Eq. (1.73) by taken $\mathfrak{f} = 0$, and $\mathfrak{g}$ to be the antisymmetric function $\mathfrak{g}(x, y) = R_{r_1,(x,y)}$. We emphasize that the empirical reservoirs currents are oriented towards the system.

The vector of empirical reservoir currents $\boldsymbol{J}_{\mathrm{r}}$ is the collection of all empirical reservoir currents. Like for mean currents, we can write for the empirical currents $\boldsymbol{J}_{\mathrm{e}}$

$$\boldsymbol{J}_{\mathrm{r}} = \boldsymbol{R} \cdot \boldsymbol{J}_{\mathrm{e}}. \quad (1.84)$$

**Entropy production at trajectory level**   One of the main results of recent years was the definition of the entropy production at the level of trajectories [167]. Let's consider a particular trajectory $\{x(t)\}_0^T$ and define the reversed trajectory $\{\widehat{x}(t)\}_0^T$ as

$$\widehat{x}(t) = x(T - t). \quad (1.85)$$

The reversed trajectory has for probability of its initial state, the probability of the final state of the normal trajectory $\rho^{\mathrm{f}}_{X_T}$, leading to the path probability for the reversed trajectory

$$d\mathbb{P}_{\boldsymbol{K}}[\{\hat{x}(t)\}^T_0] = \rho^{\mathrm{f}}_{X_T} \exp\left[\sum_{i=0}^{n-1} \ln \omega_{x_i,x_{i+1}} - \int_0^T \tau_{x(t)}\mathrm{d}t\right] \prod_{i=0}^n \mathrm{d}t_i. \tag{1.86}$$

The entropy production is then defined as

$$\Delta S_{\mathrm{tot}} = \ln \frac{d\mathbb{P}_{\boldsymbol{K}}[\{X(t)\}^T_0]}{d\mathbb{P}_{\boldsymbol{K}}[\{\hat{X}(t)\}^T_0]} = \ln \frac{\rho^{\mathrm{i}}_{X_0}}{\rho^{\mathrm{f}}_{X_T}} + \sum_{i=0}^{n-1} \ln \frac{\omega_{X_{i+1},X_i}}{\omega_{X_i,X_{i+1}}}. \tag{1.87}$$

It is a measure of the irreversibility as it quantifies the difference between the forward and backward evolution in time. The last equation has to be compared with the Eq. (1.49). We have

$$\mathbf{E}\left[\Delta S_{\mathrm{tot}}\right] = \int \mathrm{d}t\boldsymbol{f}^{\boldsymbol{\omega}\mathrm{T}}_{\mathrm{e}} \cdot \boldsymbol{j}^{\boldsymbol{\rho}}_{\mathrm{e}}(t) + S(\boldsymbol{\rho}_{\mathrm{v}}(T)) - S(\boldsymbol{\rho}_{\mathrm{v}}(0)). \tag{1.88}$$

Therefore, we define the empirical exchanged entropy $\Delta S_{\mathrm{exch}}$, that is also the stochastic heat, and the entropy variation $\Delta S_{\mathrm{sys}}$ of the system as

$$\Delta S_{\mathrm{exch}} = \sum_{i=0}^{n-1} \ln \frac{\omega_{X_{i+1},X_i}}{\omega_{X_i,X_{i+1}}} \quad \text{and} \quad \Delta S_{\mathrm{sys}} = \ln \frac{\rho^{\mathrm{i}}_{X_0}}{\rho^{\mathrm{f}}_{X_T}}. \tag{1.89}$$

The empirical entropy flow $\Sigma_{\mathrm{exch}} = \Delta S_{\mathrm{exch}}/T$ is then an observable of the form (1.73) with $\mathfrak{f} = 0$ and

$$\mathfrak{g}(x,y) = \ln \frac{\omega_{(x,y)}}{\omega_{(y,x)}}. \tag{1.90}$$

Using the edge affinity and the local detailed balance condition, the entropy flow is written as

$$\Sigma_{\mathrm{exch}} = \boldsymbol{f}^{\boldsymbol{\omega}\mathrm{T}}_{\mathrm{e}} \cdot \boldsymbol{J}_{\mathrm{e}} = \boldsymbol{f}_{\mathrm{r}}^{\mathrm{T}} \cdot \boldsymbol{J}_{\mathrm{r}}. \tag{1.91}$$

That is similar to Eq. (1.59) but for stochastic observable.

Using a different prior, we can also write the entropy production as

$$\Delta S_{\mathrm{tot}} = \ln \frac{\rho^{\mathrm{i}}_{X_0}}{\rho^{\mathrm{f}}_{X(T)}} + \sum_{i=0}^{n-1} \ln \frac{\pi_{X_{i+1}}}{\pi_{X_i}} + \sum_{i=0}^{n-1} \ln \frac{\omega_{X_{i+1},X_i}\pi_{X_i}}{\omega_{X_i,X_{i+1}}\pi_{X_{i+1}}}. \tag{1.92}$$

That leads to the adiabatic/non-adiabatic splitting of the entropy variation as

$$\Delta S_{\mathrm{ad}} = \sum_{i=0}^{n-1} \ln \frac{\omega_{X_{i+1},X_i}\pi_{X_i}}{\omega_{X_i,X_{i+1}}\pi_{X_{i+1}}} \quad \text{and} \quad \Delta S_{\mathrm{na}} = \ln \frac{\rho^{\mathrm{i}}_{X_0}\pi_{X(T)}}{\rho^{\mathrm{f}}_{X(T)}\pi_{X_0}}. \tag{1.93}$$

## 1.3.1 Fluctuations relations

One of the important features of the empirical entropy production is a symmetry on its probability distribution, that is the *fluctuations relation* or *fluctuations theorem.*

**Detailed fluctuation theorem**   We consider the ratio of the probability to have a given empirical entropy production over the probability to have the opposite empirical entropy production. The detailed fluctuation theorem imposes the symmetry [86]

$$\frac{\Pr\left(\Delta S_{\text{tot}} = \Delta s_{\text{tot}}\right)}{\Pr\left(\Delta S_{\text{tot}} = -\Delta s_{\text{tot}}\right)} = e^{\Delta s_{\text{tot}}} \tag{1.94}$$

for stationary systems. Many results are available about fluctuation theorem [35, 54, 86, 88–91, 114, 117, 139, 164, 194].

For Markov jump processes, the fluctuation theorem is easily proved from the path probability (1.71). Interested readers can refer to Refs [35, 86, 114, 29] and references therein.

Other relations are available for the adiabatic/non-adiabatic splitting of the entropy production [86],

$$\frac{\Pr\left(\Delta S_{\text{ad}} = \Delta s_{\text{ad}}\right)}{\Pr\left(\Delta S_{\text{ad}} = -\Delta s_{\text{ad}}\right)} = e^{\Delta s_{\text{ad}}} \quad \text{and} \quad \frac{\Pr\left(\Delta S_{\text{na}} = \Delta s_{\text{na}}\right)}{\Pr\left(\Delta S_{\text{na}} = -\Delta s_{\text{na}}\right)} = e^{\Delta s_{\text{na}}}. \tag{1.95}$$

Among particular cases of the fluctuation theorem, we have the Crooks relation [70, 71] that have be used to experimentally determine RNA folding free energies [32, 68], but also for others experimental systems [63, 77].
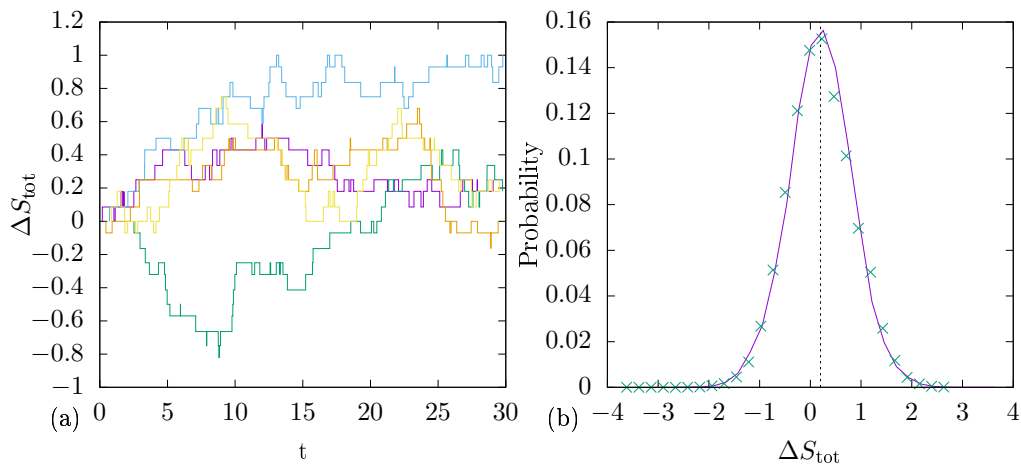


Figure 1.5: (a) Entropy production computed on trajectories of Fig. 1.4
(b) Probability distribution of the entropy production (solid line) compared with $e^{\Delta s_{\text{tot}}} \Pr\left(\Delta S_{\text{tot}} = -\Delta s_{\text{tot}}\right)$ (crosses). The probability distribution is an histogram made from $10^6$ trajectories of length $T = 30$. The vertical dashed line indicates the mean value, that is positive as expected from Eq. (1.97). Parameters are the same as in Fig. 1.4.

**Integral fluctuation theorem and the second law of thermodynamics**
Previous results are named *detailed* fluctuation theorem because they apply on the probability distribution of empirical entropy production. We can average over empirical entropy production to obtain the *integral* fluctuation theorem [103, 104,

167]

$$\mathbf{E}\left[e^{-\Delta S_{\text{tot}}}\right] = \int \mathrm{d}\Delta S_{\text{tot}} \Pr\left(\Delta S_{\text{tot}}\right) e^{-\Delta S_{\text{tot}}} = 1. \tag{1.96}$$

The integral fluctuation theorem allows connection with the second law of thermodynamics. From Jensen inequality $\mathbf{E}\left[e^x\right] \geqslant e^{\mathbf{E}[x]}$, we obtain the second law of thermodynamics

$$\mathbf{E}\left[\Delta S_{\text{tot}}\right] = \mathbf{E}\left[\Delta S_{\text{sys}}\right] + \mathbf{E}\left[\Delta S_{\text{exch}}\right] \geqslant 0. \tag{1.97}$$

Therefore the second law of thermodynamics holds on average [105].

# Dynamical fluctuations

Equilibrium and non-equilibrium systems are increasingly studied with methods borrowed from the theory of large deviations [2, 78, 15, 26]. This theory is a powerful tool developed in the 1970s by Donsker and Varadhan and Freidlin and Wentzell [73–76, 14], even if the first calculations go back to Boltzmann [79].

In this chapter, we introduce the theory of large deviations. Next we use this theory for the stochastic observables defined in the previous chapter, allowing practical computations of the dynamical fluctuations. Finally, we explicit the notion of equivalence of dynamical ensemble, that generalizes equivalence of ensemble from equilibrium statistical mechanics. This equivalence allows the characterization of the fluctuations of a stochastic process as the typical realization of another stochastic process.

- Large deviation theory: The main document that we use is the review of Hugo Touchette [25]. The book of Ellis [12] is also a good starting point.

- Equivalence of ensemble: The main source is the article by Raphaël Chetrite and Hugo Touchette [60].

## 2.1 Large deviation theory

### 2.1.1 Introductory example: the random walk

Let's begin with a simple example. Consider a single particle moving on the infinite discrete line starting at position 0. The particle can hop to left or right with rate $\omega$. This is a symmetric random walk, see Fig. 2.1a for a set of trajectories. We aim at studying the number of times the walker jumps during a trajectory of duration $T$. Denoting $X(t)$ the random position of the walker at time $t$, we look at the random variable

$$A = \sum_{0 \leqslant t \leqslant T : \Delta X_t \neq 0} 1. \tag{2.1}$$

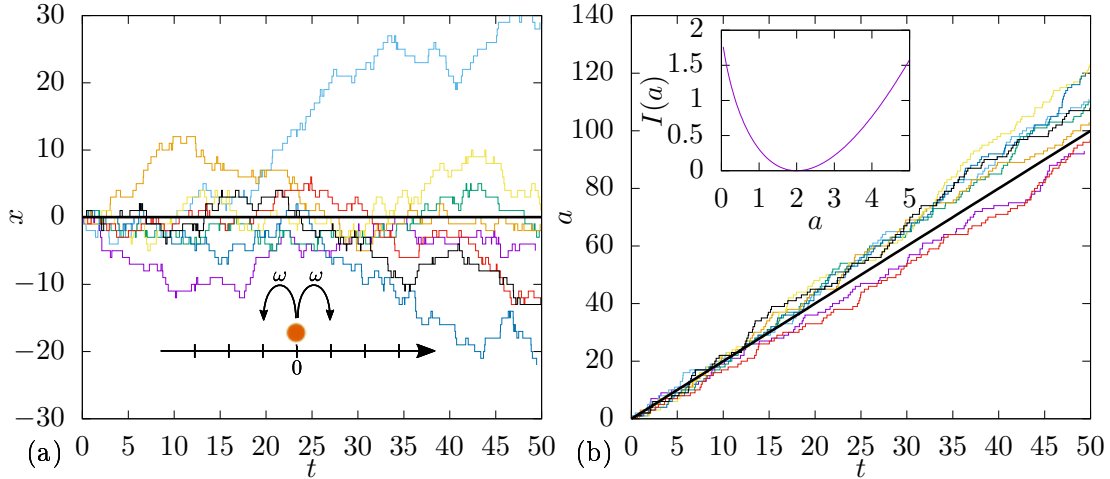Example of realizations of this stochastic process are shown on Fig. 2.1b

Figure 2.1: (a) A set of 8 trajectories for $\omega = 1$. The thick black line is the mean behavior of the position. Insert: Sketch of the random walker. (b) Activity versus time. Insert: Large deviation function of the number of jump per unit time.

**Law of large numbers**    By virtue of the law of large numbers, we expect the number of jumps $A$ at large time to be $2\omega T$. However at finite time, as shown on Fig. 2.1b, the activity fluctuates around the expected value. A finer analysis is required.

**Central limit theorem**    As a first approach of the fluctuations, we could use the central limit theorem. The central limit theorem states that the distribution probability of the number of jump will approaches a normal distribution as

$$\Pr\left(\frac{1}{\sqrt{T}}\left(A - 2\omega T\right) = u\right) \rightarrow \frac{1}{\mathcal{N}}\exp\left(\frac{u^2}{4\omega}\right) \tag{2.2}$$

with $\mathcal{N}$ a normalization factor. The theorem accounts for fluctuations around the mean value of the order of $\frac{1}{\sqrt{T}}$, that we call small fluctuations.

**Large deviations**    The simplicity of the system allows the direct computation of the probability of the number of jumps, that is given by the Poisson distribution of parameter $2\omega$

$$\Pr\left(A = aT\right) = \frac{(2\omega T)^{aT}e^{-2\omega T}}{(aT)!}. \tag{2.3}$$

For large time, we use Stirling approximation to obtain

$$\frac{1}{T}\log\Pr\left(\frac{A}{T} = a\right) \simeq -a\ln\frac{a}{2\omega} + a - 2\omega. \tag{2.4}$$

At large time, the approximation we made becomes exact, and we write the probability as

$$\Pr\left(\frac{A}{T} = a\right) \simeq e^{-TI(a)}. \tag{2.5}$$

where $I(a) = a \ln(a/2\omega) - a + 2\omega$ is a positive function, shown on insert of Fig. 2.1, that is only zero for $a = 2\omega$. Such approximation allows a finer result than the central limit theorem or the law of large number. The probability to observe a deviation from the average behavior decreases exponentially with time. The function $I(a)$ controls the rate of decay of the probability.

Such an exponential behavior is an instance of a large deviation principle that turns out to be common in statistical physics and stochastic processes [25]. We establish next the main results based on this framework.

## 2.1.2 Large deviation principle

We recall the expression of the generic observable that we introduce in the previous chapter, for a trajectory $\{X(t)\}_{t=0}^{t=T}$, our generic observable $O$ is

$$O = \frac{1}{T} \int_0^T \mathfrak{f}(X_t) \mathrm{d}t + \frac{1}{T} \sum_{0 \leqslant t \leqslant T : \Delta X_t \neq 0} \mathfrak{g}(X_{t^+}, X_{t^-}) \tag{2.6}$$

where $\mathfrak{f}$ and $\mathfrak{g}$ are two arbitrary functions. We emphasize the $1/T$ scaling. Indeed, such generic observable will grow with time.

We say that the probability $\Pr(O = o)$ satisfies a large deviation principle if there exists a function $I(o)$ such that

$$I(o) = - \lim_{T \to +\infty} \frac{1}{T} \log \Pr(O = o). \tag{2.7}$$

$I(o)$ is called the rate function or the large deviation function (LDF), and quantifies the rate of exponential decay toward a delta-dirac probability distribution at $\mathbf{E}[O]$. We have some properties of the LDF:

- LDF are non-negative: $I(o) \geqslant 0$. This prevents divergence of the probability, that is forbidden from normalization conditions.

- The limit (2.7) may not exist. This corresponds to decay of the probability distribution faster than exponentially in $T$. In this case the LDF is set to $+\infty$.

- The LDF may be zero for some values of the random variable, meaning that the probability distribution decays slower than exponentially with $T$.

The definition could be generalized to the case of multiple random variables or even random functions, in which case the LDF becomes a functional.

The formal definition of large deviation requires additional mathematical details, that we do not provide here. Moreover we do not prove the large deviation principle, assuming it holds for all our probabilities. We refer to Ref. [12] for full mathematical analysis.

We focus here on time integrated observables and their large deviations as time goes by, but it exists large deviation in system size or number of particles

also. The formal definition is similar, but deals instead with observables of the form

$$A = \frac{1}{Ns} \sum_{i=1}^{Ns} A_i. \tag{2.8}$$

Equilibrium statistical mechanics can be framed within this large deviation setup [25]. Most of the results presented here can be used also with large deviation in size.

### 2.1.3 Contraction of large deviation functions

Suppose we are given a new random variable $B$, defined trough a function of $O$ such that $B = h(O)$. The relation between $B$ and $O$ is not necessary isomorphic, and is often many-to-one. We aim at computing the LDF of the new variable from the LDF of the old one. The contraction principle states that the probability of $B$ obeys a large deviation principle and the LDF of $B$ is given by the contraction of the LDF $I(o)$

$$J(b) = \inf_{o|h(o)=b} I(o). \tag{2.9}$$

This can be justified heuristically as follows: the probability distribution of $B$ is

$$\Pr(B = b) = \int_{o|h(o)=b} \mathrm{d}o \, \Pr(O = o) \simeq \int_{o|h(o)=b} \mathrm{d}o \, e^{-TI(o)}, \tag{2.10}$$

where the approximation uses the large deviation principle for $O$. We then use the saddle point method or Laplace approximation to derive the limit

$$-\lim_{T \to +\infty} \frac{1}{T} \log \int_{o|h(o)=b} \mathrm{d}o \, e^{-TI(o)} = \inf_{o|h(o)=b} I(o) = J(b). \tag{2.11}$$

### 2.1.4 Gärtner-Ellis theorem

**Cumulant generating function**  The scaled cumulant generating function (CGF) is defined as

$$\phi(\gamma) = \lim_{T \to +\infty} \frac{1}{T} \log \mathbf{E} \left[ e^{T\gamma O} \right]. \tag{2.12}$$

This is the dominant behavior of the generating function $\mathbf{E} \left[ e^{T\gamma O} \right]$ at large time. From the CGF, we can extract by simple derivation all the cumulants of our observable. The first and second cumulants are

$$\lim_{T \to +\infty} \mathbf{E}[O] = \frac{\mathrm{d}}{\mathrm{d}\gamma} \phi(\gamma) \Big|_{\gamma=0} \tag{2.13}$$

$$\lim_{T \to +\infty} T \mathrm{Var}(O) = \lim_{T \to +\infty} T \left( \mathbf{E}[O^2] - \mathbf{E}[O]^2 \right) = \frac{\mathrm{d}^2}{\mathrm{d}\gamma^2} \phi(\gamma) \Big|_{\gamma=0}. \tag{2.14}$$

The CGF is also given by the Legendre-Fenchel transform of the LDF. Indeed using the saddle-point approximation, we have

$$\phi(\gamma) = \sup_o \left( \gamma o - I(o) \right). \tag{2.15}$$

**Gärtner-Ellis theorem** The Gärtner-Ellis theorem states that if the CGF exists and is differentiable for all $\gamma$, then $\Pr(O = o)$ respects a large deviation principle and the LDF is given by the Legendre-Fenchel transform of the CGF

$$I(o) = \sup_\gamma \left( \gamma o - \phi(\gamma) \right). \tag{2.16}$$

Therefore the LDF $I(o)$ is a convex function by properties of the Legendre-Fenchel transform. We will study in Ch. 6 the global validity of this property.

**Tilted matrix** Consider now the generating vector, $\mu_x(t) = \mathbf{E}\left[e^{t\gamma O}\right]_x$ where the trajectory average is conditioned on the final state $x$ at time $t$. This generating vector evolves according to the modified master equation [60]

$$\frac{\mathrm{d}}{\mathrm{d}t}\boldsymbol{\mu}_{\mathrm{v}}(t) = \boldsymbol{K}^\gamma \cdot \boldsymbol{\mu}_{\mathrm{v}}(t) \tag{2.17}$$

where the titled matrix is

$$K^\gamma_{x,y} = \begin{cases} \omega_{x,y} e^{\gamma \mathfrak{g}(x,y)} & \text{if } x \neq y \\ -\sum_y \omega_{x,y} + \gamma \mathfrak{f}(x) & \text{if } x = y \end{cases}. \tag{2.18}$$

The CGF is then obtained as the highest eigenvalue of the tilted matrix.

## 2.1.5 Law of large numbers and central limit theorem

The law of large numbers and the central limit theorem are natural consequences of the large deviation principle, as we show in the following.

**Law of large numbers** We assume that the LDF $I(o)$ has a unique global minimum at $o = \bar{o}$. This minimum necessary satisfies $I(\bar{o}) = 0$. Indeed, by definition $\phi(0) = 0$ and we have

$$0 = \phi(0) = \sup_o -I(o) = -I(\bar{o}). \tag{2.19}$$

Furthermore the expected value of $O$ is

$$\mathbf{E}[O] = \int \mathrm{d}o \, o \Pr(O = o) \simeq \int \mathrm{d}o \, o e^{-TI(o)} = \operatorname{argmin} I(o) = \bar{o}. \tag{2.20}$$

From which we conclude that

$$\Pr(O = \bar{o}) \xrightarrow[T \to +\infty]{} 1 \quad \text{and} \quad \Pr(O \neq \bar{o}) \xrightarrow[T \to +\infty]{} 0. \tag{2.21}$$

This is the law of large number. Therefore for LDF with a unique global minimum, expected value and most probable value are equal.

**Ergodic theorem** When the transition matrix (1.20) is irreducible, the jump process is ergodic. The average values of observables are then deducible from the ergodic theorem. In particular we have for the occupation and jump fraction for all state $x, y$ in terms of the steady state probability $\boldsymbol{\pi}_v$

$$\lim_{T \to +\infty} \mathbf{E}\left[R_x\right] = \bar{r}_x = \pi_x \quad \text{and} \quad \lim_{T \to +\infty} \mathbf{E}\left[Q_{x,y}\right] = \bar{q}_{x,y} = \omega_{x,y}\pi_y. \tag{2.22}$$

We derive from the previous expression, the expected empirical current and empirical activity as the stationary current and activity

$$\lim_{T \to +\infty} \mathbf{E}\left[J_{(x,y)}\right] = \bar{j}_{(x,y)} = j^\pi_{(x,y)} \quad \text{and} \quad \lim_{T \to +\infty} \mathbf{E}\left[A_{(x,y)}\right] = \bar{a}_{(x,y)} = a^\pi_{(x,y)}. \tag{2.23}$$

There are the stationary values of the probability current (1.22) and activity (1.24).

**Central limit theorem** When $I(o)$ has a unique global minimum at $\bar{o}$ and is smooth enough, we can expand $I(o)$ about its minimum

$$I(o) \approx \frac{1}{2} \left.\frac{\mathrm{d}^2 I}{\mathrm{d}o^2}\right|_{o=\bar{o}} (o - \bar{o})^2 \tag{2.24}$$

The probability has then a Gaussian shape at large time

$$\Pr\left(O = o\right) \simeq \exp\left[-\frac{T}{2} \left.\frac{\mathrm{d}^2 I}{\mathrm{d}o^2}\right|_{o=\bar{o}} (o - \bar{o})^2\right]. \tag{2.25}$$

Which is a form of central limit theorem, valid for small fluctuations close to the most probable value.

### 2.1.6 Level 2.5 large deviation function

**LDF of occupations times and jump fractions** The LDF $I_{2.5}(\boldsymbol{r}_v, \boldsymbol{q})$ of empirical occupation times (1.76) and of empirical jump fractions (1.77) is known for any ergodic Markov process. We call it the level 2.5 LDF [12] and it writes in terms of the transition rates $\omega_{x,y}$ [38, 45, 100, 122]

$$I_{2.5}(\boldsymbol{r}_v, \boldsymbol{q}) = \sum_{x,y|x \neq y} \left[q_{x,y} \ln \frac{q_{x,y}}{\omega_{x,y}r_y} - q_{x,y} + \omega_{x,y}r_y\right], \tag{2.26}$$

with stationary condition

$$\forall y, \quad \sum_x (q_{x,y} - q_{y,x}) = 0. \tag{2.27}$$

This level 2.5 LDF is derived from the path probability density function (1.72) and the Girsanov formula [38, 122, 30].

**LDF of occupations times, currents and activities**  From the level 2.5 LDF, the LDF $I(\boldsymbol{r}_{\mathrm{v}}, \boldsymbol{a}_{\mathrm{e}}, \boldsymbol{j}_{\mathrm{e}})$ of occupations times (1.76), activities (1.79) and currents (1.80) is obtain by the change of variable $q \to a, j$

$$I_{2.5}(\boldsymbol{r}_{\mathrm{v}}, \boldsymbol{a}_{\mathrm{e}}, \boldsymbol{j}_{\mathrm{e}}) = \sum_{(x,y)} \frac{a_{(x,y)}}{2} \ln \frac{a_{(x,y)}^2 - j_{(x,y)}^2}{4 r_y r_x \omega_{(x,y)} \omega_{(y,x)}} + \frac{j_{(x,y)}}{2} \ln \frac{a_{(x,y)} + j_{(x,y)}}{a_{(x,y)} - j_{(x,y)}} \frac{r_y \omega_{(x,y)}}{r_x \omega_{(y,x)}}$$
$$- a_{(x,y)} + r_x \omega_{(y,x)} + r_y \omega_{(x,y)}. \quad (2.28)$$

The stationary condition (2.27) becomes

$$\forall y, \quad \sum_x j_{(x,y)} = \sum_x j_{(y,x)}, \quad (2.29)$$

that is the sum of current flowing to the state $y$ is equal to the sum of current flowing from the state $y$. Using the probability current and the probability activity, the level 2.5 LDF rewrites using Eqs. (1.27-1.30)

$$I_{2.5}(\boldsymbol{r}_{\mathrm{v}}, \boldsymbol{a}_{\mathrm{e}}, \boldsymbol{j}_{\mathrm{e}}) = \sum_{(x,y)} \left[ \frac{a_{(x,y)}}{2} \ln \frac{a_{(x,y)}^2 - j_{(x,y)}^2}{a_{(x,y)}^r{}^2 - j_{(x,y)}^r{}^2} \right.$$
$$\left. + \frac{j_{(x,y)}}{2} \ln \frac{a_{(x,y)} + j_{(x,y)}}{a_{(x,y)} - j_{(x,y)}} \frac{a_{(x,y)}^r - j_{(x,y)}^r}{a_{(x,y)}^r + j_{(x,y)}^r} - a_{(x,y)} + a_{(x,y)}^r \right]. \quad (2.30)$$

**Stationary condition**  The empirical current (1.80) is an antisymmetric function on edges. Therefore, it undergoes a decomposition on cycles. This decomposition can be thought as follow: let's pick up one state $z$ and consider a particular trajectory. With respect to this state $z$, we can cut the trajectory into three pieces. The first part between the initial time and the first time $t_1$ we arrive at $z$, the part between the first time we arrive at $z$ and the last time $t_n$ we arrive at $z$ and the final part of the trajectory between the last time we arrive at $z$ and the final time. When computing the empirical current on the three pieces, the middle part is the cyclic part of the decomposition, the empirical current being only computed on cyclic trajectory. While the two remaining parts are the vertex part of the decomposition.

The empirical current becomes

$$J_{(x,y)} = \frac{1}{T} \left[ \sum_{0 \leqslant t < t_1 : \Delta X_t \neq 0} \mathbf{1}_x(X_{t^+}) \mathbf{1}_y(X_{t^-}) - \mathbf{1}_y(X_{t^+}) \mathbf{1}_x(X_{t^-}) \right.$$
$$+ \sum_{t_1 \leqslant t < t_n : \Delta X_t \neq 0} \mathbf{1}_x(X_{t^+}) \mathbf{1}_y(X_{t^-}) - \mathbf{1}_y(X_{t^+}) \mathbf{1}_x(X_{t^-})$$
$$\left. + \sum_{t_n \leqslant t \leqslant T : \Delta X_t \neq 0} \mathbf{1}_x(X_{t^+}) \mathbf{1}_y(X_{t^-}) - \mathbf{1}_y(X_{t^+}) \mathbf{1}_x(X_{t^-}) \right]. \quad (2.31)$$

The graph being finite, the initial and final sum have necessary a finite number of elements. When taking the long time limit, they can be ignored, and the empirical edge currents have only a cyclic contribution. This leads to the stationary

condition

$$\boldsymbol{D} \cdot \boldsymbol{j}_{\mathrm{e}} = 0, \tag{2.32}$$

that is another form of the condition (2.29).

**LDF of occupation times and currents** It is possible to realize the contraction of the level 2.5 LDF (2.26) to obtain the level 2.5 LDF of empirical occupations times and currents, that is [122]

$$I_{2.5}(\boldsymbol{r}_{\mathrm{v}}, \boldsymbol{j}_{\mathrm{e}}) = \sum_{(x,y)} j_{(x,y)} \operatorname{arcsinh}\left(\frac{j_{(x,y)}}{\sqrt{4 r_y r_x \omega_{(x,y)} \omega_{(y,x)}}}\right) - \frac{1}{2} j_{(x,y)} \ln \frac{r_x \omega_{(y,x)}}{r_y \omega_{(x,y)}}$$
$$+ \sqrt{(r_y \omega_{(x,y)} - r_x \omega_{(y,x)})^2 + 4 r_y r_x \omega_{(x,y)} \omega_{(y,x)}} - \sqrt{j_{(x,y)}^2 + 4 r_y r_x \omega_{(x,y)} \omega_{(y,x)}}. \tag{2.33}$$

Using the relation (1.27) that connects the probability current, the geometrical activity and the edge affinity, we have [93]

$$\begin{aligned} I_{2.5}(\boldsymbol{r}_{\mathrm{v}}, \boldsymbol{j}_{\mathrm{e}}) &= \sum_{(x,y)} j_{(x,y)} \operatorname{arcsinh}\left(\frac{j_{(x,y)}}{g_{(x,y)}^r}\right) - j_{(x,y)} \operatorname{arcsinh}\left(\frac{j_{(x,y)}^r}{g_{(x,y)}^r}\right) \\ &\quad + \sqrt{j_{(x,y)}^{r\,2} + g_{(x,y)}^{r\,2}} - \sqrt{j_{(x,y)}^2 + g_{(x,y)}^{r\,2}} \qquad (2.34) \\ &= \sum_{(x,y)} j_{(x,y)} \operatorname{arcsinh}\left(\frac{j_{(x,y)}}{j_{(x,y)}^r} \sinh \frac{f_{(x,y)}^r}{2}\right) - j_{(x,y)} \frac{f_{(x,y)}^r}{2} \\ &\quad + \sqrt{j_{(x,y)}^{r\,2} + \frac{j_{(x,y)}^{r\,2}}{\sinh^2 \frac{f_{(x,y)}^r}{2}}} - \sqrt{j_{(x,y)}^2 + \frac{j_{(x,y)}^{r\,2}}{\sinh^2 \frac{f_{(x,y)}^r}{2}}}. \qquad (2.35) \end{aligned}$$

**Contraction of level 2.5 LDF** The LDF of any observable $O$ could be derived from the level 2.5 LDF by contraction using the Eq. (1.78)

$$I(o) = \min_{r, q \,|\, \sum_x \mathfrak{f}(x) r_x + \sum_{x,y} \mathfrak{g}(x,y) q_{x,y} = o} I(\boldsymbol{r}_{\mathrm{v}}, \boldsymbol{q}). \tag{2.36}$$

But this formula is not useful in practice and we usually prefer to compute LDF from the Gärtner-Ellis theorem. Among contractions, the LDF of occupation times is called the level 2 LDF and explicit formula exists when the system respects detailed balance [44, 100].

### 2.1.7 Physical currents

When studying long time behavior of systems, simplifications occur in their description if one focus on physically relevant currents like currents exchanged with the reservoirs.

**Conservation laws** Due to the stationary condition (2.32) on empirical edge currents, the latter are decomposable on cycle. Therefore the empirical reservoir currents write then

$$\boldsymbol{j}_{\mathrm{r}} = \boldsymbol{R} \cdot \boldsymbol{C} \cdot \boldsymbol{j}_{\mathrm{c}}. \qquad (2.37)$$

The cycle-reservoir matrix $\boldsymbol{R} \cdot \boldsymbol{C}$ counts the exchanged quantities with the reservoirs for each cycle of the graph. The entries of the cycle-reservoirs matrix are the influx of state variables along each cycle.

The cycle-reservoir matrix is not in general a full-rank matrix. Let's consider $\boldsymbol{\ell}_{\mathrm{r}}^{\mathrm{T}}$ such that

$$\boldsymbol{\ell}_{\mathrm{r}}^{\mathrm{T}} \cdot \boldsymbol{R} \cdot \boldsymbol{C} = 0. \qquad (2.38)$$

Such vector are named conservation laws since $\boldsymbol{\ell}_{\mathrm{r}}^{\mathrm{T}} \cdot \boldsymbol{j}_{\mathrm{r}} = 0$ [147, 157]. They form quantities that are conserved during the evolution of the system. Indeed $\boldsymbol{\ell}_{\mathrm{r}}^{\mathrm{T}} \cdot \boldsymbol{R}$ is an edge linear form that is decomposable on vertices and there exits $\boldsymbol{\ell}_{\mathrm{v}}^{\mathrm{T}}$ such that

$$\boldsymbol{\ell}_{\mathrm{r}}^{\mathrm{T}} \cdot \boldsymbol{R} = \boldsymbol{\ell}_{\mathrm{v}}^{\mathrm{T}} \cdot \boldsymbol{D}. \qquad (2.39)$$

Then $\boldsymbol{\ell}_{\mathrm{v}}^{\mathrm{T}}$ is a vertex quantity that is constant during the evolution and so a conserved quantity. The number of conservation laws is denoted $Lc$.

We expect to have at least one conservation laws by state variable, as these are conserved quantities, but the topology of the graph embedded into the cycle matrix $\boldsymbol{C}$ can allow for supplementary conserved quantities. We emphasize that if one of the state variable is not conserved by cyclic trajectories, the system cannot reach a stationary-state, as these variable will evolve permanently due to cyclic currents.

If the cycle-reservoirs matrix is zero, then there no permanent flux from the reservoirs to the system and the system reaches an equilibrium state. In particular, this appends when we have at most one reservoirs per state variable $M$.

**Physical currents** The conservation laws induce relations between reservoirs currents. Hence it is not necessary to observe all reservoirs currents to have a good knowledge of the system evolution. It suffices to observe only $Ph = Rev - Lc$ currents, the others currents being obtained from the conservation laws. We call the observed currents the physical currents, there are $Ph$ of them. They are labeled with index $x = 1, \ldots, Ph$ and the vector of physical currents is $\boldsymbol{j}$ without subscript.

**Remark:** In Ref. [147], reservoirs observables are called physicals observables, and physical observables are called fundamental observables.

There exists a well defined procedure to select physical currents that is similar to the one used to decompose edge current between vertex and cycle currents. Let's introduce the $Rev \times Ph$ selection matrix $\boldsymbol{V}$ such that for all conservation laws $\boldsymbol{\ell}_{\mathrm{r}}^{\mathrm{T}}$

$$\boldsymbol{\ell}_{\mathrm{r}}^{\mathrm{T}} \cdot \boldsymbol{V} = 0. \qquad (2.40)$$

Then, we have the relation

$$\boldsymbol{j}_{\mathrm{r}} = \boldsymbol{V} \cdot \boldsymbol{j}, \qquad (2.41)$$

between reservoirs and physical currents. We emphasize that the matrix $\boldsymbol{V}$ is not unique, as one has a choice on the currents to observe.

The matrix $\boldsymbol{V}$ has independent columns, we can then invert Eq. (2.41) to obtain the connection between physical and reservoir currents

$$\boldsymbol{j} = \boldsymbol{V}^+ \cdot \boldsymbol{j}_{\mathrm{r}}. \tag{2.42}$$

As a short notation, we introduce the physical matrix $\boldsymbol{P}$ that connects cycle currents to physical currents

$$\boldsymbol{P} = \boldsymbol{V}^+ \cdot \boldsymbol{R} \cdot \boldsymbol{C}, \tag{2.43}$$

such that

$$\boldsymbol{j} = \boldsymbol{P} \cdot \boldsymbol{j}_{\mathrm{c}}. \tag{2.44}$$

The matrix $\boldsymbol{V}$ selects a independent set of currents. However, one can observe more currents than required by the numbers of reservoirs and conservation laws $Ph = Rev - Lc$. This is done by forgetting some conservation laws in the definition (2.40). In this case, the remaining conservation laws induce relations between currents, as it is the case for tight coupled engines that we describe in sec. 3.1.3.

If we observe not enough currents, we miss a part of the flows between the reservoirs and the system and we cannot accurately describe the dynamics of the system.We study consequences of such missing currents in the sec. 5.2.4.

**Partial entropy production rates**   Once the physical currents are defined, we also defined the physical affinities $\boldsymbol{f}^{\mathrm{T}}$ from the reservoir affinities as

$$\boldsymbol{f}^{\mathrm{T}} = \boldsymbol{f}_{\mathrm{r}}^{\mathrm{T}} \cdot \boldsymbol{V}. \tag{2.45}$$

The entropy production rate $\sigma$ is then simply given by the scalar product

$$\sigma = \boldsymbol{f}^{\mathrm{T}} \cdot \boldsymbol{j} = \sum_X f_X j_X. \tag{2.46}$$

The partial entropy production rates $\sigma_X = f_X j_X$ is the entropy production rates corresponding to the physical current $j_X$.

**Fluctuations relation and large deviation theory**   The fluctuation theorem is a kind of symmetry of the LDF for the entropy production rate and currents. We define the LDF $I(\sigma)$ of the total entropy production as

$$I(\sigma) = \lim_{T \to +\infty} \frac{1}{T} \ln \mathrm{Pr} \left( \frac{\Delta S_{\mathrm{tot}}}{T} = \sigma \right). \tag{2.47}$$

The fluctuation theorem (1.94) writes then

$$I(\sigma) - I(-\sigma) = -\sigma. \tag{2.48}$$

The fluctuation theorem also imposes a symmetry on the CGF $\phi(\gamma)$ of the total entropy production. From the Legendre transform and the Eq. (2.48), we have

$$\phi(\gamma) = \phi(-1-\gamma). \tag{2.49}$$

The CGF, being a convex function, has a unique minimum. This minimum is located at $\gamma = -1/2$ from the symmetry relation (2.49).

When considering instead the LDF for the current, the fluctuation theorem write then

$$I(\boldsymbol{j}) - I(-\boldsymbol{j}) = -\boldsymbol{f}^{\mathrm{T}} \cdot \boldsymbol{j}, \tag{2.50}$$

$\boldsymbol{f}^{\mathrm{T}}$ being the associated affinities such that $\boldsymbol{f}^{\mathrm{T}} \cdot \boldsymbol{j}$ is the entropy production. And the symmetry on the CGF $\phi(\boldsymbol{\gamma})$ for the current becomes

$$\phi(\boldsymbol{\gamma}) = \phi(-\boldsymbol{f} - \boldsymbol{\gamma}). \tag{2.51}$$

## 2.2 Equivalence of dynamical ensembles

A dynamical ensemble is a set of trajectories with a particular path probability density function $d\mathbb{P}[\{X(t)\}_0^T]$. We consider the set of all possibles trajectories on the state space $\Omega$ as the support of all dynamical ensembles. We make the reference on the support of trajectory implicit in the notation and denote a dynamical ensemble by its path probability density function $d\mathbb{P}$.

Few questions arise: Can we connect a particular dynamical ensemble with a well defined stochastic process? Under which conditions two dynamical ensembles lead to the same statistics for some observables. Both questions are related through the notion of ensemble equivalence, as a stochastic process defines a dynamical ensemble through its path probability density (1.72).

To discuss the dynamical ensemble equivalence, one needs to define when two path probabilities $d\mathbb{P}[\{X(t)\}_0^T]$ and $d\mathbb{Q}[\{X(t)\}_0^T]$ are equivalent. They do when [60, 61]

$$\lim_{T \to +\infty} \frac{1}{T} \ln \frac{d\mathbb{P}}{d\mathbb{Q}}[\{X(t)\}_0^T] = 0 \tag{2.52}$$

almost everywhere with respect to $d\mathbb{P}[\{X(t)\}_0^T]$. This means that $d\mathbb{P}[\{X(t)\}_0^T]$ and $d\mathbb{Q}[\{X(t)\}_0^T]$ are equal up to subexponential terms in $T$ for almost all paths. As a consequence, if two path ensembles are equivalent, the mean value (at large time) of any observable will be the same if computed with one or the other path ensemble. We emphasize that the definition of equivalence requires that $d\mathbb{P}[\{X(t)\}_0^T]$ is absolutely continuous with respect to $d\mathbb{Q}[\{X(t)\}_0^T]$ to have the existence of the Randon-Nikodym derivative $d\mathbb{P}/d\mathbb{Q}$. This requires that $d\mathbb{P}[\{X(t)\}_0^T]$ vanishes at least when $d\mathbb{Q}[\{X(t)\}_0^T]$ does. Formally, $d\mathbb{P}[\{X(t)\}_0^T]$ is absolutely continuous with respect to $d\mathbb{Q}$ if for all trajectories $\{x(t)\}_0^T$

$$d\mathbb{Q}[\{x(t)\}_0^T] = 0 \Rightarrow d\mathbb{P}[\{x(t)\}_0^T] = 0. \tag{2.53}$$

**Dynamical ensembles** The *microcanonical ensemble of trajectories* is defined by filtering the trajectory ensemble through a condition on the value of an observable, e.g. $O = o$. We write the path probability of these trajectories

$$d\mathbb{P}_o[\{X(t)\}_0^T] = d\mathbb{P}[\{x(t)\}_0^T | O = o] = \frac{d\mathbb{P}[\{X(t)\}_0^T]}{\text{Pr}\,(O = o)} \mathbf{1}_o(O). \qquad (2.54)$$

In the microcanonical path ensemble, the observable $O$ does not fluctuate and always achieves the same value for all trajectories in the ensemble.

The *canonical ensemble of trajectories* is define by fixing the mean value of the observable $O$ only. The path probability for this ensemble can be computed by tilting (or biasing) the process as follows:

$$d\mathbb{P}^\gamma[\{X(t)\}_0^T] = \frac{e^{T\gamma O} d\mathbb{P}[\{X(t)\}_0^T]}{\mathbf{E}\,[e^{T\gamma O}]}. \qquad (2.55)$$

Notice that this path probability is normalized by construction. The canonical ensemble is also called *s-ensemble* [92], *driven, biased* or *tilted* ensemble [102].

These two dynamical ensembles are analogs of the equilibrium statistical ensembles. For equilibrium statistical ensembles, the constraint is set on the system energy and the counting field $\gamma$ is replaced by the inverse temperature.

**Equivalence condition from LDF convexity** When $O$ respects a large deviation principle with LDF $I(o)$, Chetrite and Touchette proved the equivalence between the microcanonical path ensemble and the canonical path ensemble. Whether $d\mathbb{P}_o$ and $d\mathbb{P}^\gamma$ are equivalent depends on the convexity of $I(o)$. In [60], Touchette and Chetrite distinguished three cases:

- **(Equivalence)** If $I(o)$ is a strictly convex function at $o$, then there exists a unique $\gamma \in \mathbb{R}$ such that $d\mathbb{P}_o$ and $d\mathbb{P}^\gamma$ are equivalent.

- **(Non equivalence)** If $I(o)$ is a non-convex function at $o$, then there are no $\gamma$ such that $d\mathbb{P}_o$ and $d\mathbb{P}^\gamma$ are equivalent.

- **(Partial equivalence)** If $I(o)$ is a convex function but not strictly convex function at $o$, then numerous values of $o$ correspond to the same $\gamma$: It may correspond to linear parts in a convex function or to set of points at which the slope is the same.

We remark that the microcanonical path ensemble $d\mathbb{P}^o$ is absolutely continuous with respect to the canonical path ensemble $d\mathbb{P}^\gamma$, but the converse is not true.

## 2.2.1 Driven process

We ask now the following question, given a dynamical ensemble $d\mathbb{P}$, can we find a jump process, with transition matrix $\boldsymbol{K}$, whose path probability density function $d\mathbb{P}_{\boldsymbol{K}}$ is equivalent to the dynamical ensemble $d\mathbb{P}$?

For canonical path ensemble $d\mathbb{P}^\gamma$, the response is positive. Using the tilted matrix (2.18), its highest eigenvalue the CGF (2.12) and its left eigenvector $\boldsymbol{l}^\gamma$, the Doob's transform of the tilted matrix writes

$$\boldsymbol{K}^{\text{driven}} = \mathbf{Diag}(\boldsymbol{l}^\gamma) \cdot \boldsymbol{K}^\gamma \cdot \mathbf{Diag}(\boldsymbol{l}^\gamma)^{-1} - \phi(\gamma)\mathbf{Id}, \qquad (2.56)$$

where $\mathbf{Diag}(\boldsymbol{l})$ is the diagonal matrix with diagonals elements

$$\text{Diag}(\boldsymbol{l})_{x,y} = \begin{cases} 0 & \text{if } x \neq y \\ l(x) & \text{if } x = y \end{cases}. \qquad (2.57)$$

$\boldsymbol{K}^{\text{driven}}$ is the transition matrix of a jump process, called the driven process. From the results of [60], the dynamical ensemble $d\mathbb{P}_{\boldsymbol{M}^{\text{driven}}}$ generated by this transition matrix is equivalent to the canonical path ensemble. We emphasize that the edge affinity $\boldsymbol{f}^{e,\text{driven}\,\text{T}}$ of the driven process are related to the one $\boldsymbol{f}_{\text{e}}{}^{\text{T}}$ of the original process by the shifting

$$\boldsymbol{f}^{e,\text{driven}\,\text{T}} = \boldsymbol{f}_{\text{e}}{}^{\text{T}} + \boldsymbol{\gamma}\mathfrak{g}_{\text{e}}{}^{\text{T}} + \boldsymbol{f}_{\text{v}}^{\boldsymbol{l}^\gamma\,\text{T}} \cdot \boldsymbol{D} \qquad (2.58)$$

where the edge affinity $\boldsymbol{\gamma}\mathfrak{g}_{\text{e}}{}^{\text{T}}$ is the antisymmetric part of the function $\gamma\mathfrak{g}(x,y)$, it comes from the tilting of Eq. (2.18), and $\boldsymbol{f}_{\text{v}}^{\boldsymbol{l}^\gamma\,\text{T}}$ being a vertex affinity, with components to be the logarithm of the left eigenvector $\boldsymbol{l}^\gamma$.

When the microcanonical ensemble $d\mathbb{P}^o$ is equivalent to the canonical ensemble, it is also equivalent to the ensemble generated by the driven process. In this case, the driven process is the process that realizes as most probable event, the value of the observable $o$ used as a condition to define the microcanonical ensemble $d\mathbb{P}^o$. In other words, it is the process where the affinity and other kinetic parameters has been changed to realized $o$ as most probable event.

### 2.2.2 Equivalence condition from CGF differentiability

The convexity properties of the LDF $I(a)$ are connected to the differentiability properties of the CGF through the Gärtner-Ellis theorem. We define $I^{**}(a)$ as the Legendre-Fenchel transform of the CGF

$$I^{**}(o) = \max_\gamma(\gamma o - \phi(\gamma)) = \gamma(o)o - \phi(\gamma(o)), \qquad (2.59)$$

with $\gamma(o)$ the value of $\gamma$ realizing the minimum. The Gärtner-Ellis theorem states that if $\phi(\gamma)$ is a differentiable function then $I(o) = I^{**}(o)$. The properties of the Legendre-Fenchel transform implies that $I^{**}(o)$ is a convex function. The strict convexity of the LDF and the differentiability of the CGF are then dual conditions. Therefore we have the three following cases:

- **(Equivalence)** If $\phi(\gamma(o))$ is differentiable at $\gamma(o)$, then $I(o) = I^{**}(o)$ from the Gärtner-Ellis theorem, and moreover $o = \partial_\gamma\phi(\gamma)$. $I(o)$ is then a strictly convex function at $o$ and the equivalence holds.

- **(Non equivalence)** If $\phi(\gamma(o))$ is not differentiable at $\gamma(o)$ and $I(o) \neq I^{**}(o)$, then $I(o)$ is non-convex function at $a$ and we have a non equivalence between microcanonical and canonical ensembles.

- **(Partial Equivalence)** If $\phi(\gamma(o))$ is not differentiable at $\gamma(o)$ and $I(o) = I^{**}(o)$, then $I(o)$ is a convex function but not strictly convex function at $o$ and we have a partial equivalence.

Hence, the non-equivalence of ensembles prevents to compute the LDF from the CGF. In this case $I^{**}(o)$ is only the convex hull of $I(o)$.

### 2.2.3   Ensemble equivalence for ergodic systems

Since ensemble equivalence for a stochastic variable relies on the convexity of the corresponding LDF, it is crucial to determine (i) whether the level 2.5 LDF $I_{2.5}(\boldsymbol{r}_{\mathrm{v}}, \boldsymbol{q})$ is convex and (ii) whether the convexity can be inherited upon contraction via Eq. (2.36). The following theorem appearing in Ref. [4] provides an answer to point (ii) when the new variable is additive:

**Theorem.** *Let $f(\boldsymbol{x}, \boldsymbol{z})$ be a convex function and $U(\boldsymbol{z})$ an additive function, i.e. a function verifying*

$$U(\alpha \boldsymbol{z}_1 + (1 - \alpha)\boldsymbol{z}_2) = \alpha U(\boldsymbol{z}_1) + (1 - \alpha)U(\boldsymbol{z}_2), \tag{2.60}$$

*then*

$$g(\boldsymbol{y}) = \min_{\boldsymbol{x} \in \mathcal{C}, \, \boldsymbol{z} \in \mathcal{C}_{\boldsymbol{y}}} f(\boldsymbol{x}, \boldsymbol{z}) \ \text{ with } \mathcal{C} \text{ convex, and } \mathcal{C}_{\boldsymbol{y}} := \{\boldsymbol{z} \,|\, U(\boldsymbol{z}) = \boldsymbol{y}\} \tag{2.61}$$

*is a convex function.*

*Proof.* We consider $(\boldsymbol{x}_1^*, \boldsymbol{z}^*(\boldsymbol{y}_1))$ the couple of variables realizing the minimum in Eq. (2.61) for $\boldsymbol{y}_1$, and similarly $(\boldsymbol{x}_2^*, \boldsymbol{z}^*(\boldsymbol{y}_2))$ for $\boldsymbol{y}_2$. The convexity of $\mathcal{C}$ implies that $\alpha \boldsymbol{x}_1^* + (1 - \alpha)\boldsymbol{x}_2^* \in \mathcal{C}$ when $\alpha \in [0, 1]$. Moreover, the additivity of $U$ implies that $\alpha \boldsymbol{z}^*(\boldsymbol{y}_1) + (1 - \alpha)\boldsymbol{z}^*(\boldsymbol{y}_2) \in \mathcal{C}_{\alpha \boldsymbol{y}_1 + (1-\alpha)\boldsymbol{y}_2}$. Hence, we have

$$
\begin{aligned}
g(\alpha \boldsymbol{y}_1 + (1 - \alpha)\boldsymbol{y}_2) &= \min_{\boldsymbol{x} \in \mathcal{C}, \, \boldsymbol{z} \in \mathcal{C}_{\alpha \boldsymbol{y}_1 + (1-\alpha)\boldsymbol{y}_2}} f(\boldsymbol{x}, \boldsymbol{z}) \\
&\leqslant f(\alpha \boldsymbol{x}_1^* + (1 - \alpha)\boldsymbol{x}_2^*, \alpha \boldsymbol{z}^*(\boldsymbol{y}_1) + (1 - \alpha)\boldsymbol{z}^*(\boldsymbol{y}_2)), \\
&\leqslant \alpha f(\boldsymbol{x}_1^*, \boldsymbol{z}^*(\boldsymbol{y}_1)) + (1 - \alpha)f(\boldsymbol{x}_2^*, \boldsymbol{z}^*(\boldsymbol{y}_2)), \\
&\leqslant \alpha g(\boldsymbol{y}_1) + (1 - \alpha)g(\boldsymbol{y}_2),
\end{aligned}
$$

where we get the third line by using the convexity of $f$, and the fourth line using our knowledge of the minimizers of Eq. (2.61) for both $\boldsymbol{y}_1$ and $\boldsymbol{y}_2$. $\qquad\square$

We now address the point (i) about the convexity of the level 2.5 LDF $I_{2.5}(\boldsymbol{r}_{\mathrm{v}}, \boldsymbol{q})$ (2.26). It is convex since it writes as the sum of a linear part $\sum_{(x,y)} \left[ r_y \omega_{(x,y)} - q_{(x,y)} \right]$ and a KL-divergence between $\boldsymbol{q}$ and $\boldsymbol{r}\boldsymbol{\omega}$

$$D(\boldsymbol{q} \| \boldsymbol{r}\boldsymbol{\omega}) = \sum_{(x,y)} q_{(x,y)} \ln \frac{q_{(x,y)}}{r_y \omega_{(x,y)}}. \tag{2.62}$$

This KL-divergence is convex as a consequence of the log-sum inequality (or Jensen's inequality) [8]

$$D\left(\sum_i \alpha_i q_i \middle\| \sum_i \alpha_i r_i k\right) \le \sum_i D\left(\alpha_i q_i \| \alpha_i r_i k\right) \tag{2.63}$$

for $\sum_i \alpha_i = 1$. Using the previous theorem with $\boldsymbol{z} = (\boldsymbol{r}_{\mathrm{v}}, \boldsymbol{q})$, the additivity of $O$ the convexity of the level 2.5 LDF for both the occupation ratio and the jump fraction, we conclude the contracted LDF $I(o)$ is also convex: The ensemble equivalence holds for ergodic Markov jump processes. In particular, the ensemble equivalence holds for irreducible finite size Markov jump processes since they are always ergodic.

Alternatively, one can prove heuristically the ensemble equivalence using the differentiability of the CGF, that is the dual condition with respect to the LDF convexity. To determine the CGF differentiability, one consider the CGF as the highest eigenvalues of the titled matrix $\boldsymbol{K}^\gamma$ defined in Eq. (2.18). From Perron-Fröbenius theorem for irreducible finite size matrices like $\boldsymbol{K}^\gamma$, the highest (real) eigenvalue is unique: Its multiplicity is always one independently of the value of the counting field and no crossing between the two highest eigenvalues can occur. Moreover, the components of the tilted matrix are differentiable yielding that the CGF is itself differentiable. By duality, the LDF is strictly convex.

From this analysis, we conclude that the non-equivalence between the micro-canonical and canonical ensembles based on observables like $O$ may only happen when the Markov operator is reducible or of infinite dimension. Then, the LDF of the variable $o$ may not be convex. We will study in Chs. 6 and 7 examples of systems associated to non-equivalent ensembles.

## 2.3 Example: a quantum dot

### 2.3.1 Model description

Our example is a simple model of a nanothermoelectric device that have been introduced in Ref. [84]. It consists of a single quantum dot embedded between two leads at different temperatures and chemical potentials. The quantum dot exchanges electrons with the leads, but due to quantum effect we can have at most one electron at a time in the quantum dot. Transitions between the states are possible by exchanging electrons with each of the leads. The sketch of the system is depicted in Fig. 2.2, this is a two state and two edge model. The graph being a multigraph, we denote the edge of the system as $(x, y; \nu)$. We orient all edges toward the state $b$ such that the incidence matrix is

$$\boldsymbol{D} = \begin{pmatrix} -1 & -1 \\ 1 & 1 \end{pmatrix}. \tag{2.64}$$

Therefore its cycle matrix is given by

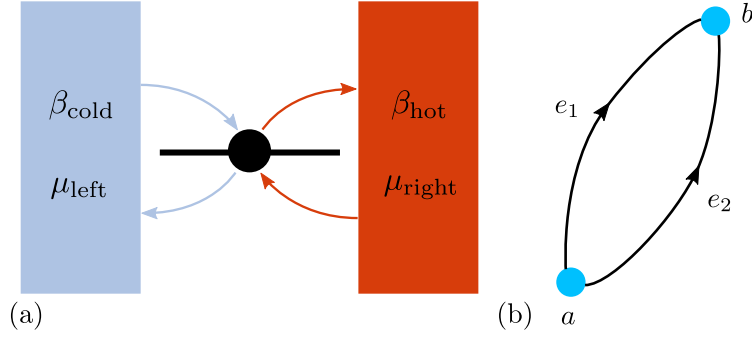$$\boldsymbol{C} = \begin{pmatrix} 1 \\ -1 \end{pmatrix}. \tag{2.65}$$

Figure 2.2: (a) Sketch of the quantum dot connected to two leads. (b) Graph of the model.

**Reservoirs**   The system is connected to four different reservoirs, a cold and hot heat bath at inverse temperature $\beta_{\text{hot}}$ and $\beta_{\text{cold}}$ and two chemical reservoirs of electrons at chemical potential $\mu_{\text{left}}$ and $\mu_{\text{right}}$. The state is characterized by two state variables, the energy $E_x$ and the number of electrons $n_x$, such that $(E_a, n_a) = (0,0)$ correspond to the empty state and $(E_b, n_b) = (\Delta E, 1)$ to the filled state. The reservoirs matrix and the cycle-reservoirs matrix are then

$$\boldsymbol{R} = \begin{pmatrix} 0 & \Delta E \\ \Delta E & 0 \\ 1 & 0 \\ 0 & 1 \end{pmatrix} \begin{matrix} \text{Cold bath} \\ \text{Hot bath} \\ \text{Left lead} \\ \text{Right lead} \end{matrix} \quad \text{and} \quad \boldsymbol{R} \cdot \boldsymbol{C} = \begin{pmatrix} -\Delta E \\ \Delta E \\ 1 \\ -1 \end{pmatrix}. \tag{2.66}$$

The reservoirs affinities are given by $\boldsymbol{f}_{\text{r}}{}^{\text{T}} = (-\beta_{\text{cold}}, -\beta_{\text{hot}}, \beta_{\text{hot}}\mu_{\text{right}}, \beta_{\text{cold}}\mu_{\text{left}})$.

**Local detailed balance**   From the local detailed balance, we have a constraint on the edge affinity that are

$$f_{e_1}^{\omega} = -\beta_{\text{hot}}(\Delta E - \mu_{\text{right}}) \tag{2.67}$$
$$f_{e_2}^{\omega} = -\beta_{\text{cold}}(\Delta E - \mu_{\text{left}}). \tag{2.68}$$

We choose the transition rates to be

$$\omega_{(b,a;1)} = \frac{2e^{-\frac{\beta_{\text{hot}}}{2}(\Delta E - \mu_{\text{right}})}}{\cosh\left(\frac{\beta_{\text{hot}}}{2}(\Delta E - \mu_{\text{right}})\right)}, \quad \omega_{(a,b;1)} = \frac{2e^{\frac{\beta_{\text{hot}}}{2}(\Delta E - \mu_{\text{right}})}}{\cosh\left(\frac{\beta_{\text{hot}}}{2}(\Delta E - \mu_{\text{right}})\right)} \tag{2.69}$$

$$\omega_{(b,a;2)} = \frac{2e^{-\frac{\beta_{\text{cold}}}{2}(\Delta E - \mu_{\text{left}})}}{\cosh\left(\frac{\beta_{\text{cold}}}{2}(\Delta E - \mu_{\text{left}})\right)}, \quad \omega_{(a,b;2)} = \frac{2e^{\frac{\beta_{\text{cold}}}{2}(\Delta E - \mu_{\text{left}})}}{\cosh\left(\frac{\beta_{\text{cold}}}{2}(\Delta E - \mu_{\text{left}})\right)} \tag{2.70}$$

Contrary to previous examples, the symmetric part of the transition rates is not set to a constant to consider the quantum statistics.

**Conservation laws**   We have three conservation laws that correspond respectively to the conservation of the energy $\boldsymbol{\ell}_{\text{r}}^{\boldsymbol{1}} = (1,1,0,0)$ , the conservation of the

number of electrons $\boldsymbol{\ell}_r^2 = (0, 0, 1, 1)$ and a supplementary law due to the unicyclic properties of our system $\boldsymbol{\ell}_r^3 = (1, 0, \Delta E, 0)$. This lead to the selection matrix and its Moore-Penrose pseudo inverse

$$\boldsymbol{V} = \begin{pmatrix} -\Delta E \\ \Delta E \\ 1 \\ -1 \end{pmatrix} \quad \text{and} \quad \boldsymbol{V}^+ = \frac{1}{2((\Delta E)^2 + 1)} \begin{pmatrix} -\Delta E & \Delta E & 1 & -1 \end{pmatrix}. \quad (2.71)$$

As a consequence we have only one physical current that is equal to the cycle current $j_c$. The entropy production rate is then obtain as

$$\sigma = \left[ (\beta_{\text{cold}} - \beta_{\text{hot}})\Delta E + \beta_{\text{hot}}\mu_{\text{right}} - \beta_{\text{cold}}\mu_{\text{left}} \right] j_c = f_c j_c. \quad (2.72)$$

using the cycle affinity $f_c = f_{e_1}^\omega - f_{e_2}^\omega$.

### 2.3.2 Fluctuation of entropy production rate

**Entropy production rate** We look at the statistics of the entropy production rate. For that purpose, we compute the CGF $\phi(\gamma)$. This is the highest eigenvalue of the tilted matrix

$$\boldsymbol{K}^\gamma = \begin{pmatrix} -\omega_{(b,a;1)} - \omega_{(b,a;2)} & \omega_{(a,b;1)}e^{-\gamma f_{e_1}} + \omega_{(a,b;2)}e^{-\gamma f_{e_2}} \\ \omega_{(b,a;1)}e^{\gamma f_{e_1}} + \omega_{(b,a;2)}e^{\gamma f_{e_2}} & -\omega_{(a,b;1)} - \omega_{(a,b;2)} \end{pmatrix}. \quad (2.73)$$

We have

$$\phi(\gamma) = -\frac{\omega}{2} + \sqrt{\left(\frac{\omega}{2}\right)^2 + 2\Gamma\left[\cosh\left(f_c\left(\gamma + \frac{1}{2}\right)\right) - \cosh\left(\frac{f_c}{2}\right)\right]} \quad (2.74)$$

where $\omega = \omega_{(a,b;1)} + \omega_{(a,b;2)} + \omega_{(b,a;1)} + \omega_{(b,a;2)}$ and $\Gamma = \sqrt{\omega_{(a,b;1)}\omega_{(a,b;2)}\omega_{(b,a;1)}\omega_{(b,a;2)}}$. By Legendre-Fenchel transform the LDF of the entropy production rate is

$$I(\sigma) = \frac{|\sigma|}{fc}\text{arccosh}(Y) - \frac{\sigma}{2} + \frac{\omega}{2} - \sqrt{\left(\frac{\omega}{2}\right)^2 + 2\Gamma\left[Y - \cosh\left(\frac{f_c}{2}\right)\right]} \quad (2.75)$$

where

$$Y = \frac{\sigma^2}{\Gamma f_c^2} + \sqrt{1 + \frac{\sigma^2}{\Gamma f_c^2}\left(\frac{\omega^2}{4\Gamma} - 2\cosh\left(\frac{f_c}{2}\right)\right) + \left(\frac{\sigma^2}{\Gamma f_c^2}\right)^2}. \quad (2.76)$$

The last result being also obtained from the level 2.5 LDF (2.33). The CGF and the LDF are plotted on the Fig. 2.3 and present all expected features. Both functions are convex and respect the expected fluctuation symmetry (2.51). The LDF is a positive function with $I(\bar{\sigma}) = 0$.

Here the simplicity of the transition matrix allows for explicit computation of the CGF and the LDF but this is not the case in general . Then, one must rely on numerical computation of the the highest eigenvalues of the titled matrix.
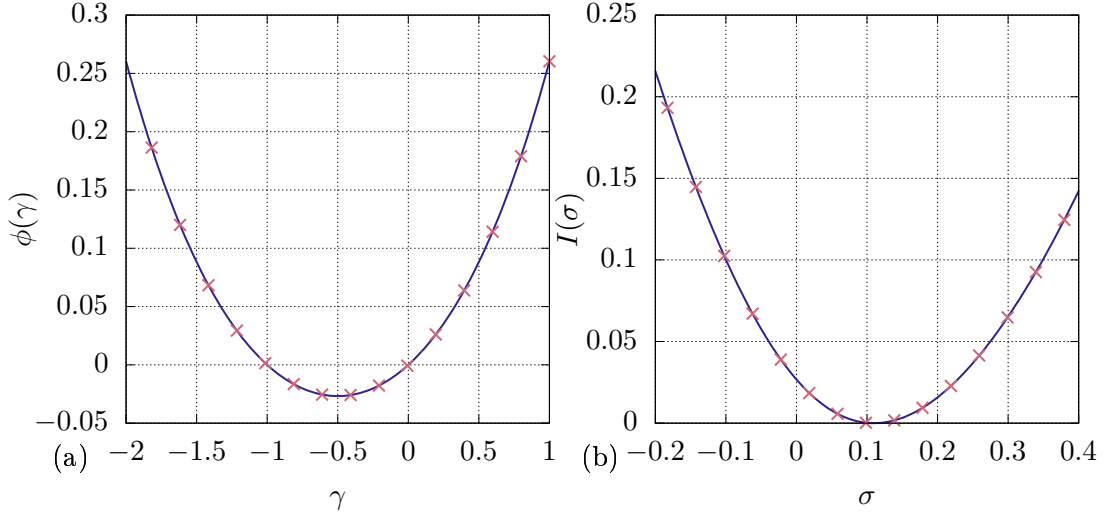
Figure 2.3: (a) CGF $\phi(\gamma)$ of Eq. (2.74) (solid line) compared to $\phi(-1-\gamma)$ (crosses) (b) LDF of the entropy production rate of Eq. (2.75) (solid line) compared to $I(-\sigma) - \sigma$ (crosses). Parameters are $\Delta E = 3$, $\beta_{\text{hot}} = 0.5$, $\beta_{\text{cold}} = 1$, $\mu_{\text{left}} = 1.0$ and $\mu_{\text{right}} = 2.0$.

**Driven process**  As the CGF is always differentiable, we have equivalence of dynamical ensembles. From Eq. (2.56) and the computation of left eigenvectors of the titled matrix (2.73), we can deduce the transition matrix of the driven process

$$\boldsymbol{K}_{\text{driven}} = \begin{pmatrix} -\omega_{(b,a;1)} - \omega_{(b,a;2)} - \phi(\gamma) & +\omega_{(a,b;1)} + \omega_{(a,b;2)} + \phi(\gamma) \\ +\omega_{(b,a;1)} + \omega_{(b,a;2)} + \phi(\gamma) & -\omega_{(a,b;1)} - \omega_{(a,b;2)} - \phi(\gamma) \end{pmatrix}. \qquad (2.77)$$

The driven process is then the jump process whose mean entropy production rate is given by the derivative of the CGF,

$$\bar{\sigma}_{\text{driven}} = \frac{\Gamma f_c \sinh\left(f_c(\gamma + \frac{1}{2})\right)}{\sqrt{\left(\frac{-\omega}{2}\right)^2 + 2\Gamma\left[\cosh\left(f_c(\gamma + \frac{1}{2})\right) - \cosh\left(\frac{f_c}{2}\right)\right]}}. \qquad (2.78)$$

<div align="right">

# 3

</div>

# Thermodynamic machines

A thermodynamics machine is a system that converts energy from one form to another. The study of thermal engines that convert heat to work is at the origin of thermodynamics, in particular the work of Carnot about maximal efficiency [6].

When considering stochastic energy converters, either natural (molecular motor, chloroplast,...) or artificial (quantum dot, colloidal particles,...) we have to take care of their fluctuations and how they matters.

In this chapter, we show how the framework of stochastic thermodynamics is used to describe stochastic energy converters. Then we study the close-to-equilibrium regime that gives first results about the physics of such machines. Finally, we consider the fluctuation of the efficiency that exhibits remarkable generic features.

## 3.1   Stochastic systems as energy converters

From our point of view, we call machine any system that has only two physical currents, one of which is called fueling or input current and the other one useful or output current. Recent experimental realizations have demonstrated the the relevance of considering highly fluctuating machines [49, 125, 169].

We denote in the following the input current by $j_1$ and the output current by $j_2$, the currents being directed towards the machine. To these two currents are associated two thermodynamic forces $f_1$ and $f_2$. We consider here machines whose currents are fluctuating while the thermodynamic forces are fixed.

For machines, the entropy production rate is then

$$\sigma = \sigma_1 + \sigma_2 = j_1 f_1 + j_2 f_2. \tag{3.1}$$

A device operating as a machine (in average) uses a fueling process (the input) flowing in the spontaneous direction of its corresponding forces $\bar{\sigma}_1 \geqslant 0$ (e.g., a heat flowing down a temperature gradient or particle flowing down a chemical potential gradient) in order to power a second process (the output) flowing against the spontaneous direction of its corresponding forces $\bar{\sigma}_2 \leqslant 0$ (e.g., a particles flowing up a chemical potential gradient or a coordinate moving against the direction of a mechanical force).
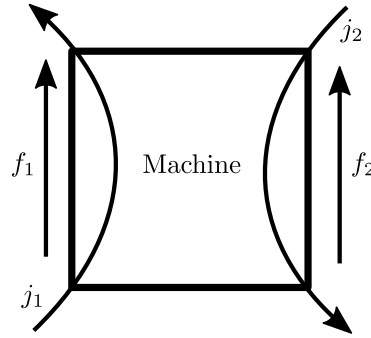
Figure 3.1: Sketch of a typical machine setup with two physical currents and affinities.

### 3.1.1  Characterizing the machine

**Efficiency**   We define the stochastic efficiency of the machine by

$$\eta = \frac{-\sigma_2}{\sigma_1} \tag{3.2}$$

which characterizes the ability of the machine to transform the input current into the output current. Since the two partial entropy production rates are stochastic quantities, efficiency is also a stochastic quantity.

Macroscopic efficiency is defined by

$$\bar{\eta} = \frac{-\bar{\sigma}_2}{\bar{\sigma}_1} \leqslant 1. \tag{3.3}$$

Due to the positivity of the average entropy production rate $\bar{\sigma} \geqslant 0$, the macroscopic efficiency is bounded by the so-called reversible (or Carnot) efficiency $\bar{\eta}_{\text{rev}} = 1$. The macroscopic efficiency does not correspond to the average of the stochastic efficiency, which has no moment, but to its most probable value, see sec. 3.3.

It should be noted that the efficiency is often defined in a slightly different way, for example for a macroscopic thermal machine between two heat sources at temperature $T_h$ and $T_c$ where the work supplied to the machine is denoted $W$ and the heat coming from the hot source $Q_h$, the efficiency is then $\eta_{\text{therm}} = -W/Q_h$ and the Carnot efficiency is $\eta_C = 1 - T_c/T_h$. Our definition of efficiency then amounts to normalizing efficiency as $\eta = \eta_{\text{therm}}/\eta_C$. The traditional definition of efficiency is called type 'I' efficiency while ours is type 'II' efficiency [1].

**Output power**   Whereas the efficiency characterizes the performance of the conversion, we need also to characterize the output power of the machine. In this manuscript we call $-\sigma_2$ the output power. The average output power being then $-\bar{\sigma}_2$.

### 3.1.2 Machines behavior

**Operating modes** As the efficiency is a stochastic variable, the fluctuating machine will not always behave as a machine, but can be running in various modes. We distinguish three different operating modes:

- In the normal operating mode, the machine works as expected, using flow from the fueling process to power the output process. This corresponds to $0 \leqslant \eta \leqslant 1$.

- In the reversed mode, the machine still converts energy but using the flow from the output process to power the fueling process. The role of each process is then exchanged. This corresponds to $\eta \geqslant 1$.

- A useless mode, or dud engine, for which no flow goes against its thermodynamic force. We then have $\eta \leqslant 0$.

The occurrence of these various type of trajectory depends on the noise level of the machine and it disappears completely in the context of large machines for which only the most probable behavior is observed.

When varying the physical affinities of the machines, we also change the macroscopic efficiency and the average operating mode of the device. The diagram that represent the operating mode as a function of the physical affinities is call operation diagram. An example is provided in the sec. 3.4.

**Optimization of the machine** Beyond stochastic aspects, we seek to optimize the average behavior of machines. To this end, we look at the conditions such that the machine works at maximum efficiency or at maximum power [57, 65, 83, 85, 162, 166, 171, 182, 185].

Since these two conditions are generally incompatible, we look at the efficiency at maximum power or the power at maximum efficiency. Another option is to obtain (if possible) the power-efficiency relationship curves.

This optimization can be conceived in several ways, by either optimizing the kinetic parameters of the machine or the affinities of the machine, that means its external conditions. In the latter case, we fix the first affinity $f_1$ and we only vary the affinity $f_2$ linked to the output power.

### 3.1.3 Tight coupled machines

Some machines have a particular property that is call tight coupling [65, 96, 170]. This corresponds to devices where we have an hidden conservation law between input and output fluxes. As a consequence, the efficiency of such machines is fixed by the conservation laws at fluctuating and macroscopic level. The typical examples of tight coupled machines are the unicyclic system as we have only one possible physical current due to the conservation laws.

The fluctuations of the partial entropy production rates are given by a degenerate form of the LDF that only allows fluctuations that respect the conservation

laws. This means that the LDF of the partial entropy production rates is finite only when $\sigma_2 = -\bar\eta\sigma_1$. In this case the LDF of partial entropy production rates and of the total entropy production rate include the same information sine $\sigma = \sigma_1 + \sigma_2 = \sigma_1(1 - \bar\eta)$, and similarly for CGFs.

We will see that tight coupling is an important property for a machine to reach reversible efficiency.

## 3.2   Linear thermodynamics

The connection between the fundamental currents and the fundamental affinities comes from the dynamics that have been described in sec. 1.2 and is in general a non-linear relation. However for small affinities, we can assume a linear relationship between currents and affinities. This approximation is at core of linear thermodynamics and has been a successful direction of research [42].By construction, the system is almost at equilibrium (close to equilibrium) since physical affinities are small.

**Onsager matrix**   The Onsager matrix $\boldsymbol{\mathcal{L}}$ connects linearly mean currents and affinities [131, 132]:

$$\bar{\boldsymbol{j}} = \boldsymbol{\mathcal{L}} \cdot \boldsymbol{f} \tag{3.4}$$

where $\boldsymbol{f}$ is the transpose of the linear form $\boldsymbol{f}^{\mathrm{T}}$. This matrix has few properties. First due to non-negativity of the entropy production, we have

$$\bar\sigma = \boldsymbol{f}^{\mathrm{T}} \cdot \bar{\boldsymbol{j}} = \boldsymbol{f}^{\mathrm{T}} \cdot \boldsymbol{\mathcal{L}} \cdot \boldsymbol{f} \geqslant 0. \tag{3.5}$$

Hence, the Onsager matrix is semi-positive definite (see App. A.1.2). Another important property is the Onsager reciprocal relation

$$\boldsymbol{\mathcal{L}}^{\mathrm{T}} = \boldsymbol{\mathcal{L}} \tag{3.6}$$

that becomes the Onsager-Casimir symmetry when considering time-dependent driving or external magnetic field.

**Remark:** The Onsager matrix could be interpreted as a metric that transform affinities (linear forms) into currents (vectors), the resistance matrix being the inverse metric that transform current (vectors) into affinities (linear forms).

### 3.2.1   Fluctuations in linear regime

**Fluctuation-dissipation theorem**   An important result of the physics of close-to-equilibrium systems is the fluctuation-dissipation theorem, sometimes also called fluctuation-response theorem [113]. With words, this theorem relates the response to a perturbation and spontaneous fluctuations of the system. There are several versions of this theorem, that vary on the detail of the chosen observable or the way the external perturbation is applied on the system. In our case, the fluctuation-dissipation theorem states the equality between the Onsager matrix and half of the equilibrium covariance matrix

$$\boldsymbol{\mathcal{L}} = \frac{\mathbf{Cov}_{\mathrm{eq}}}{2}. \tag{3.7}$$

The covariance matrix is the matrix whose elements are the covariance between currents

$$\text{Cov}_{XY} = \lim_{t \to \infty} t \left[ \mathbf{E} \left[ J_X J_Y \right] - \mathbf{E} \left[ J_X \right] \mathbf{E} \left[ J_Y \right] \right] = \frac{\partial^2 \phi}{\partial \gamma_X \partial \gamma_Y} (0,0). \tag{3.8}$$

This is also the Hessian matrix of the CGF. The equilibrium covariance matrix $\mathbf{Cov}_{\text{eq}}$ is obtained by taken the expectation in the case of the equilibrium system, *i.e.* when physical affinities are zero.

We give here an simple proof of the fluctuation-dissipation theorem, we send for more complete proof and finite-time result to Refs. [34, 114, 23, 29]

Given that physical affinities are small, we can assume that the fluctuations of currents close-to-equilibrium are Gaussian such that the LDF of the current $I_{\text{eq}}(\boldsymbol{j})$ close to equilibrium is given by the following quadratic form

$$I_{\text{LR}}(\boldsymbol{j}) = \frac{1}{2} (\boldsymbol{j} - \bar{\boldsymbol{j}})^{\text{T}} \cdot \mathbf{Cov}_{\text{eq}}^{-1} \cdot (\boldsymbol{j} - \bar{\boldsymbol{j}}). \tag{3.9}$$

From the fluctuation theorem $I_{\text{LR}}(\boldsymbol{j}) - I_{\text{LR}}(-\boldsymbol{j}) = -\boldsymbol{f}^{\text{T}} \cdot \boldsymbol{j}$, we obtain

$$I_{\text{LR}}(\boldsymbol{j}) - I_{\text{LR}}(-\boldsymbol{j}) = -2\bar{\boldsymbol{j}}^{\text{T}} \cdot \mathbf{Cov}_{\text{eq}}^{-1} \cdot \boldsymbol{j} = -\boldsymbol{f}^{\text{T}} \cdot \boldsymbol{j}. \tag{3.10}$$

The last equality being valid for any $\boldsymbol{j}$, this give

$$2\bar{\boldsymbol{j}}^{\text{T}} \cdot \mathbf{Cov}_{\text{eq}}^{-1} = \boldsymbol{f}^{\text{T}} \tag{3.11}$$

to be put in relation with Eq. (3.4) to obtain the fluctuation-dissipation theorem.

**Gaussian fluctuations**  Due to the fluctuation-dissipation theorem, the fluctuations of the currents are obtained from the Onsager matrix. The LDF is given by

$$I_{\text{LR}}(\boldsymbol{j} = \frac{1}{4} (\boldsymbol{j} - \bar{\boldsymbol{j}})^{\text{T}} \cdot \mathcal{L}^{-1} \cdot (\boldsymbol{j} - \bar{\boldsymbol{j}}) \tag{3.12}$$

and the CGF is

$$\phi_{\text{LR}}(\boldsymbol{\gamma}) = \min_{\boldsymbol{j}} \left[ \boldsymbol{\gamma}^{\text{T}} \boldsymbol{j} - I_{\text{LR}}(\boldsymbol{j}) \right] = \boldsymbol{\gamma}^{\text{T}} \cdot \mathcal{L} \cdot \boldsymbol{\gamma} + \boldsymbol{\gamma}^{\text{T}} \cdot \bar{\boldsymbol{j}}. \tag{3.13}$$

## 3.2.2  Machines in linear regime

When studying machines in linear regime, the Onsager framework is particularly powerful [152]. It has been useful in the description of thermoelectric effects [42, 72, 195]. For machines, the Onsager matrix is a $2 \times 2$ matrix

$$\begin{pmatrix} \bar{j}_1 \\ \bar{j}_2 \end{pmatrix} = \begin{pmatrix} \mathcal{L}_{1,1} & \mathcal{L}_{1,2} \\ \mathcal{L}_{2,1} & \mathcal{L}_{2,2} \end{pmatrix} \begin{pmatrix} f_1 \\ f_2 \end{pmatrix}. \tag{3.14}$$

From Onsager reciprocal relation, the Onsager matrix is symmetric $\mathcal{L}_{1,2} = \mathcal{L}_{2,1}$. Being a semi-positive definite matrix, we have $\mathcal{L}_{1,1} > 0$ et $\mathcal{L}_{2,2} > 0$. In order to have a working machine, we need $\mathcal{L}_{1,2} < 0$.

**Degree of coupling** We introduce the linear response degree of coupling [109]

$$\xi_{\mathrm{LR}} = \frac{\mathcal{L}_{1,2}}{\sqrt{\mathcal{L}_{1,1}\mathcal{L}_{2,2}}}. \tag{3.15}$$

The constraints on the Onsager matrix require $\xi_{\mathrm{LR}} \in [-1, 1]$. The degree of coupling characterize the influence of the fueling process on the output process. When $|\xi| = 1$, both fluxes are perfectly coupled and the machine falls into the case of tight coupled machines.

We note also that in the literature on thermoelectricity [42], it is customary to use the figure of merit $ZT$ instead of the degree of coupling. The two notions are simply related by $ZT = \frac{\xi_{\mathrm{LR}}{}^2}{1 - \xi_{\mathrm{LR}}{}^2}$, so that $ZT$ is a real positive number which goes to infinity when $\xi_{\mathrm{LR}}$ tends to $\pm 1$.

**Maximum efficiency** This degree of coupling allows the derivation of useful relations on efficiency and power for machine in linear regime.

Indeed, the efficiency is bounded by a maximum efficiency that solely depends on the degree of coupling

$$\bar{\eta} \leqslant \bar{\eta}_{\mathrm{max,LR}} = \frac{1 - \sqrt{1 - \xi_{\mathrm{LR}}{}^2}}{1 + \sqrt{1 - \xi_{\mathrm{LR}}{}^2}}. \tag{3.16}$$

In particular the reversible efficiency may only be reached by tight coupled machine in linear regime [81].

**Maximum power** The output power

$$- \bar{\sigma}_2 = -f_2(\mathcal{L}_{1,2}f_1 + \mathcal{L}_{2,2}f_2) \tag{3.17}$$

is maximum with respect to $f_2$ when

$$f_2 = -\frac{\mathcal{L}_{1,2}}{2\mathcal{L}_{2,2}}f_1 \tag{3.18}$$

and is given by

$$- \bar{\sigma}_{2,\mathrm{max,LR}} = \frac{\mathcal{L}_{1,2}{}^2}{4\mathcal{L}_{2,2}}f_1{}^2. \tag{3.19}$$

Note that the output power in (3.17) is a quadratic function of $f_2$ and the maximum is obtained for the value corresponding to half of the so-called stalling affinity. The stalling affinity

$$f_{2,\mathrm{stall,LR}} = -\frac{\mathcal{L}_{1,2}}{\mathcal{L}_{2,2}}f_1 \tag{3.20}$$

is the affinity at which the output power vanishes.

**Power-efficiency relations** Not only, we have bounds on the maximum efficiency and power, but we can also derive the relation between efficiency and power as

$$\frac{-\bar{\sigma}_2}{-\bar{\sigma}_{2,\text{max,LR}}} = 2\bar{\eta}\left(\frac{2}{\xi_{\text{LR}}^2} - (1+\bar{\eta}) \pm \sqrt{(1+\bar{\eta})^2 - \frac{4\eta}{\xi_{\text{LR}}^2}}\right). \qquad (3.21)$$

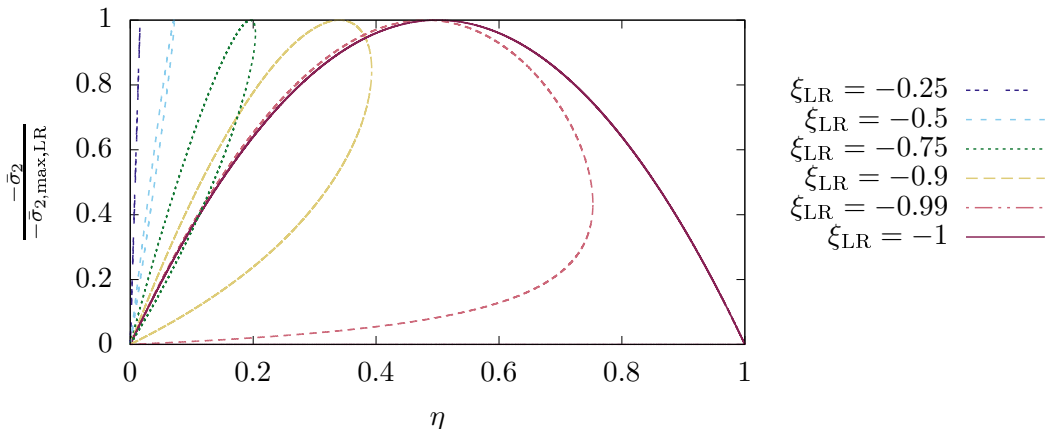This relation is shown on Fig. 3.2. This shows that the relation between power and efficiency is in general bi-valued.



Figure 3.2: Power-efficiency relation for different degrees of coupling.

## 3.3 Efficiency fluctuations

Using the framework of large deviation theory and stochastics thermodynamics, various results have been established about efficiency fluctuations since 2014. Remarkably, the shape of the efficiency LDF is quite generic and displays universal features [95, 186, 189]. These features have been illustrated on different models [150, 155], some of which have gaussian fluctuations [145], an experimental realization has confirmed the results that least likely efficiency is the reversible efficiency and has validated the shape of the efficiency LDF [153].

The efficiency probability $\Pr(\eta)$ is obtained from the probability of entropies productions $\sigma_1, \sigma_2$ as follows

$$\Pr(\eta) = \int d\sigma_1 d\sigma_2 \Pr(\sigma_1, \sigma_2)\, \delta\left(\eta + \frac{\sigma_2}{\sigma_1}\right). \qquad (3.22)$$

Using the change of variable $(\sigma_1, \sigma_2) \rightarrow (\eta, \sigma_2)$, we obtain

$$\Pr(\eta) = \int d\sigma_2 \Pr\left(\frac{\sigma_2}{\eta}, \sigma_2\right) \left|\frac{\sigma_2}{\eta^2}\right|. \qquad (3.23)$$

For large efficiency, the probability of efficiency is a power-law distribution with tails [95, 150]

$$\Pr(\eta \rightarrow \pm\infty) \propto \eta^{-2}. \qquad (3.24)$$

As a consequence, the efficiency has no finite moment. In particular the macroscopic efficiency is not the average efficiency, but its most probable value as we will shown later.

**Efficiency LDF**   The long time limit of the efficiency probability gives the efficiency LDF

$$J(\eta) = \lim_{t \to +\infty} \frac{1}{t} \ln \Pr(\eta). \tag{3.25}$$

We assume that the entropy production probability also respects a large deviation principle, such that the LDF is

$$I(\sigma_1, \sigma_2) = \lim_{t \to +\infty} \frac{1}{t} \ln \Pr(\sigma_1, \sigma_2). \tag{3.26}$$

Using the Lapace approximation on the integral (3.22), we obtain that the efficiency LDF is given by the contraction over the partial entropy productions LDF

$$J(\eta) = \min_{\sigma_1} I(\sigma_1, -\eta\sigma_1). \tag{3.27}$$

This contraction formula is the starting point for the derivation of the main properties of the efficiency LDF $J(\eta)$.

 We assume that the entropy productions LDF satisfies two quite general features:

- The entropies production LDF $I(\sigma_1, \sigma_2)$ is a positive convex function with $I(\bar{\sigma}_1, \bar{\sigma}_2) = 0$. The LDF is defined for all $(\sigma_1, \sigma_2) \in \mathbb{R}^2$. This has been shown to hold for finite size engines in sec. 2.2.3.

- The machine is in a steady state such that the fluctuations relation holds, *i.e.* $I(\sigma_1, \sigma_2) - I(-\sigma_1, -\sigma_2) = -\sigma_1 - \sigma_2$.

 The important case of time-periodic driven machines is not treated in this manuscript as we focus on stationary processes, but has been studied elsewhere [95, 189]

## 3.3.1   Shape of the efficiency LDF

The shape of the efficiency LDF is constrained by the above assumptions.

 First, the efficiency LDF is a bounded function. Indeed from the contraction formula (3.27), we have

$$J(\eta) \leqslant I(0,0), \tag{3.28}$$

where the upper bound follows from the contraction formula (3.27). We used the assumption on the entropy productions LDF that $I(0,0) < +\infty$ to guarantee that the upper bound is finite.

**Most probable efficiency**  The minimum of the efficiency LDF is located at the macroscopic efficiency, since the efficiency LDF vanishes at $\bar{\eta}$

$$J(\bar{\eta}) = \min_{\sigma_1} I(\sigma_1, \sigma_1 \frac{\bar{\sigma}_2}{\bar{\sigma}_1}) = 0 \qquad (3.29)$$

where the minimum is reached for $\sigma = \bar{\sigma}_1$. If the entropy production has an unique minimum, $\bar{\eta}$ is the unique minimum of the efficiency LDF. However if the entropies production LDF has a constant region around its minimum, the efficiency LDF exhibits a plateau at the minimum as well.

**Least likely efficiency**  The location $\eta^\star$ of the maximum can be obtained from the fluctuation theorem. We call $\eta^\star$ the least likely efficiency because it has the highest decay rate $J(\eta^\star)$.

Along a contour line of the entropy productions LDF, the total differential of $I$ vanishes,

$$\mathrm{d}I = \frac{\partial I}{\partial \sigma_1}\mathrm{d}\sigma_1 + \frac{\partial I}{\partial \sigma_2}\mathrm{d}\sigma_2 = \mathrm{d}\sigma_1 \left( \frac{\partial I}{\partial \sigma_1} + \frac{\partial I}{\partial \sigma_2}\frac{\mathrm{d}\sigma_2}{\mathrm{d}\sigma_1} \right) = 0. \qquad (3.30)$$

At the origin, we have $\eta^* = -\mathrm{d}\sigma_2/\mathrm{d}\sigma_1$. So,

$$\eta^* = \left.\frac{\partial I}{\partial \sigma_1}\right|_0 \left( \left.\frac{\partial I}{\partial \sigma_2}\right|_0 \right)^{-1}. \qquad (3.31)$$

We now use the fluctuation theorem for the entropy productions:

$$I(\sigma_1, \sigma_2) - I(-\sigma_1, -\sigma_2) = -\sigma_1 - \sigma_2. \qquad (3.32)$$

Taking the partial derivatives of this equation at origin yields

$$\left.\frac{\partial I}{\partial \sigma_1}\right|_0 = \left.\frac{\partial I}{\partial \sigma_2}\right|_0 = -\frac{1}{2}. \qquad (3.33)$$

Then the least likely efficiency is the reversible efficiency:

$$\eta^* = 1 = \eta_{\mathrm{rev}}, \qquad (3.34)$$

following from Eqs. (3.31) and (3.33).

**Extremas of the LDF**  We are also able to give the general shape of the efficiency LDF from the convexity of the entropies production LDF. Let's study the zeros of the derivative of the efficiency LDF

$$\frac{\mathrm{d}J}{\mathrm{d}\eta}(\eta) = 0. \qquad (3.35)$$

Since the efficiency LDF follows from the contraction formula (3.27), we introduce the fonction $\widetilde{\sigma}_1(\eta)$ as the solution of

$$0 = \frac{\mathrm{d}I}{\mathrm{d}\widetilde{\sigma}_1}\left[I(\widetilde{\sigma}_1, -\eta\widetilde{\sigma}_1)\right] = \frac{\partial I}{\partial \sigma_1}(\widetilde{\sigma}_1, -\eta\widetilde{\sigma}_1) - \eta\frac{\partial I}{\partial \sigma_2}(\widetilde{\sigma}_1, -\eta\widetilde{\sigma}_1). \qquad (3.36)$$

This allows us to write the efficiency LDF as

$$J(\eta) = I(\widetilde{\sigma}_1(\eta), -\eta\widetilde{\sigma}_1(\eta)), \tag{3.37}$$

because $\widetilde{\sigma}_1$ is realizing the maximum in Eq. (3.27). From this equation, the derivative of J may be written as

$$\frac{\mathrm{d}J}{\mathrm{d}\eta}(\eta) = \frac{\partial\widetilde{\sigma}_1}{\partial\eta}(\widetilde{\sigma}_1(\eta), -\eta\widetilde{\sigma}_1(\eta)) - \left(\eta\frac{\partial\widetilde{\sigma}_1}{\partial\eta} + \widetilde{\sigma}_1\right)\frac{\partial I}{\partial\sigma_2}(\widetilde{\sigma}_1(\eta), -\eta\widetilde{\sigma}_1(\eta)). \tag{3.38}$$

Combining this equation with Eq. (3.36), we obtain for the derivative of $J$

$$\frac{\mathrm{d}J}{\mathrm{d}\eta}(\eta) = \widetilde{\sigma}_1(\eta)\frac{\partial I}{\partial\sigma_2}(\widetilde{\sigma}_1(\eta), -\eta\widetilde{\sigma}_1(\eta)) \tag{3.39}$$

which shall vanish at the extremum of $J(\eta)$.

We now distinguish two different cases: either the partial derivative of $I$ vanishes, and we recover the minimum of $J$ previously obtained, or the function $\widetilde{\sigma}_1(\eta)$ vanishes. In the later case, we look for the efficiency such that the function $\widetilde{\sigma}_1(\eta) = 0$. Coming back to the contraction formula (3.27), and assuming the efficiency to be finite, we obtain

$$J(\eta) = I(0,0) \tag{3.40}$$

such that we retrieve the extrema given by the reversible efficiency. At the contrary, at the limite of infinite efficiency, the contraction formula (3.27) becomes

$$\lim_{\eta\to\pm\infty} J(\eta) = \lim_{\eta\to\pm\infty} I(\widetilde{\sigma}_1(\eta), -\eta\widetilde{\sigma}_1(\eta)) \leqslant I(0,0). \tag{3.41}$$

From the last inequality and the convexity of $I$, we conclude that $\eta\widetilde{\sigma}_1(\eta)$ stays finite when $\eta\to\pm\infty$ and necessarily,

$$\lim_{\eta\to\pm\infty} \widetilde{\sigma}_1(\eta) = 0. \tag{3.42}$$

The derivative of J vanishes at infinite efficiency, and the efficiency LDF converges to a finite value $J(\infty)$ at large efficiency since J is bounded.

Therefore the general shape of the efficiency LDF is the one sketched on Fig. 3.3, with one minimum at $\bar{\eta}$, one maximum at $\eta^*$ and a plateau at infinite value.

This shape follows from a geometrical point of view as well, as shown by Verley *et al.* [189].

## 3.3.2 Efficiency LDF from entropy productions CGF

The efficiency LDF can also be derived from the entropies production CGF $\phi(\gamma_1, \gamma_2)$ instead of the LDF. As it is more convenient to derive the CGF of the entropy productions than the LDF, this is very helpful for practical computation of efficiency LDF.
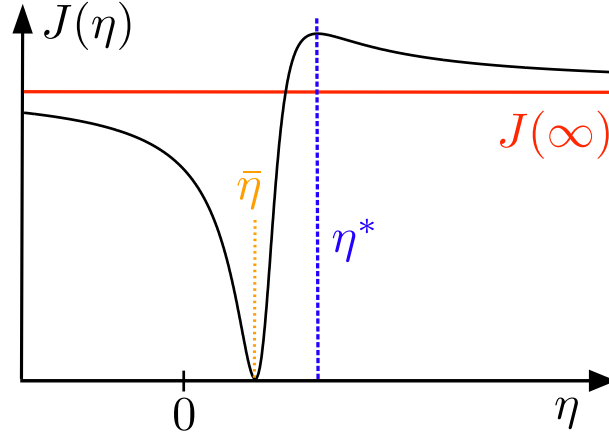
Figure 3.3: Shape of the efficiency LDF

The convexity of the entropy productions LDF assures that the LDF is obtained from the Legendre conjugate of the CGF

$$I(\sigma_1, \sigma_2) = \max_{\gamma_1, \gamma_2} \left[ \gamma_1 \sigma_1 + \gamma_2 \sigma_2 - \phi(\gamma_1, \gamma_2) \right]. \tag{3.43}$$

With the efficiency $\eta = -\sigma_2/\sigma_1$, we can write

$$I(\sigma_1, -\eta\sigma_1) = \max_{\gamma_1, \gamma_2} \left[ (\gamma_1 - \gamma_2\eta)\sigma_1 - \phi(\gamma_1, \gamma_2) \right] \tag{3.44}$$

and the minimization of Eq. (3.27) gives

$$J(\eta) = \min_{\sigma_1} \max_{\gamma_1, \gamma_2} \left[ (\gamma_1 - \gamma_2\eta)\sigma_1 - \phi(\gamma_1, \gamma_2) \right]. \tag{3.45}$$

We set $\gamma = \gamma_1 - \gamma_2\eta$ to obtain

$$J(\eta) = \min_{\sigma_1} \max_{\gamma} \left\{ \gamma\sigma_1 + \max_{\gamma_2} \left[ -\phi(\gamma + \gamma_2\eta, \gamma_2) \right] \right\}. \tag{3.46}$$

We now define the function

$$\begin{aligned} f_\eta(\gamma) &= -\max_{\gamma_2} \left\{ -\phi(\gamma + \gamma_2\eta, \gamma_2) \right\} \\ &= \min_{\gamma_2} \phi(\gamma + \gamma_2\eta, \gamma_2) \end{aligned} \tag{3.47}$$

and its Legendre transform

$$\mathcal{F}_\eta(\sigma_1) = \max_{\gamma} \left\{ \gamma\sigma_1 - f_\eta(\gamma) \right\}. \tag{3.48}$$

Then the efficiency LDF can be rewritten

$$\begin{aligned} J(\eta) &= \min_{\sigma_1} \max_{\gamma} \left\{ \gamma\sigma_1 - f_\eta(\gamma) \right\} \\ &= \min_{\sigma_1} \mathcal{F}_\eta(\sigma_1) \\ &= -\max_{\sigma_1} \left\{ -\mathcal{F}_\eta(\sigma_1) \right\} \\ &= -f_\eta(0), \end{aligned} \tag{3.49}$$

where we used the fact that $\mathcal{F}_\eta$ and $f_\eta$ are Legendre-conjugated in the last step. Using Eq. (3.47), we conclude that

$$J(\eta) = -\min_{\gamma_2} \phi\left(\gamma_2\eta, \gamma_2\right). \tag{3.50}$$

This last formula is interpreted geometrically as follows: We consider the contour line of the CGF in the plane $(\gamma_1, \gamma_2)$. They form closed convex lines encircling the point $(-1/2, -1/2)$ where the CGF reaches its minimal value. For each value of the efficiency, we draw a straight line with slope $1/\eta$ and crossing the origin: $\gamma_2 = \gamma_1/\eta$. The corresponding value of the efficiency LDF $J(\eta)$ is then minus the minimum of the CGF $\phi(\gamma_1, \gamma_2)$ along this line.

### 3.3.3 Various specific cases

There are two specific cases for which the efficiency LDF is explicitly known.

**Efficiency fluctuations for linear engines** For linear regime, the CGF of physical currents is known from the Onsager matrix and the physical affinities, as

$$\phi_{\mathrm{LR}}(\gamma_1, \gamma_2) = \sum_{X,Y=1,2} \gamma_X \gamma_Y f_X f_Y \mathcal{L}_{X,Y} + \sum_{X=1,2} \gamma_X \bar{\sigma}_X. \tag{3.51}$$

The previous formula (3.43) allows us to calculate the efficiency LDF as the ratio of two quadratic form [189]

$$J_{\mathrm{LR}}(\eta) = \frac{1}{4} \frac{(\eta\bar{\sigma}_1 + \bar{\sigma}_2)^2}{\eta^2 f_1{}^2 \mathcal{L}_{1,1} + 2\eta f_1 f_2 \mathcal{L}_{1,2} + f_2{}^2 \mathcal{L}_{2,2}}. \tag{3.52}$$

Assuming Gaussian fluctuations for the currents, we can go a step further and obtain the explicit finite-time probability distribution of the efficiency [145].

**Efficiency fluctuations for tight coupled engines** For tight coupled engines, the fluctuations are degenerate such that the CGF is given by

$$\phi_{\mathrm{TC}}(\gamma_1, \gamma_2) = \phi_{\mathrm{TC}}(\gamma_1 - \bar{\eta}\gamma_2). \tag{3.53}$$

The efficiency LDF is then calculate to be

$$J_{\mathrm{TC}}(\eta) = \begin{cases} 0 & \text{if } \eta = \bar{\eta} \\ \phi_{\mathrm{TC}}(-1/2, -1/2) & \text{else} \end{cases}. \tag{3.54}$$

Due to the fluctuation theorem, $\phi_{\mathrm{TC}}(-1/2, -1/2) = I_{\mathrm{TC}}(0,0)$, we have so only two regimes of fluctuations. For the first regime, the efficiency is equal to his macroscopic values, that corresponds to all non-zero fluctuations of the currents, as they are perfectly proportional. The other regime correspond to a fluctuation for which input current is zero, that gives an undefined value of the efficiency.

The tight coupling condition realizes the collapse between the maximum value of the efficiency LDF with its value at infinite efficiency.
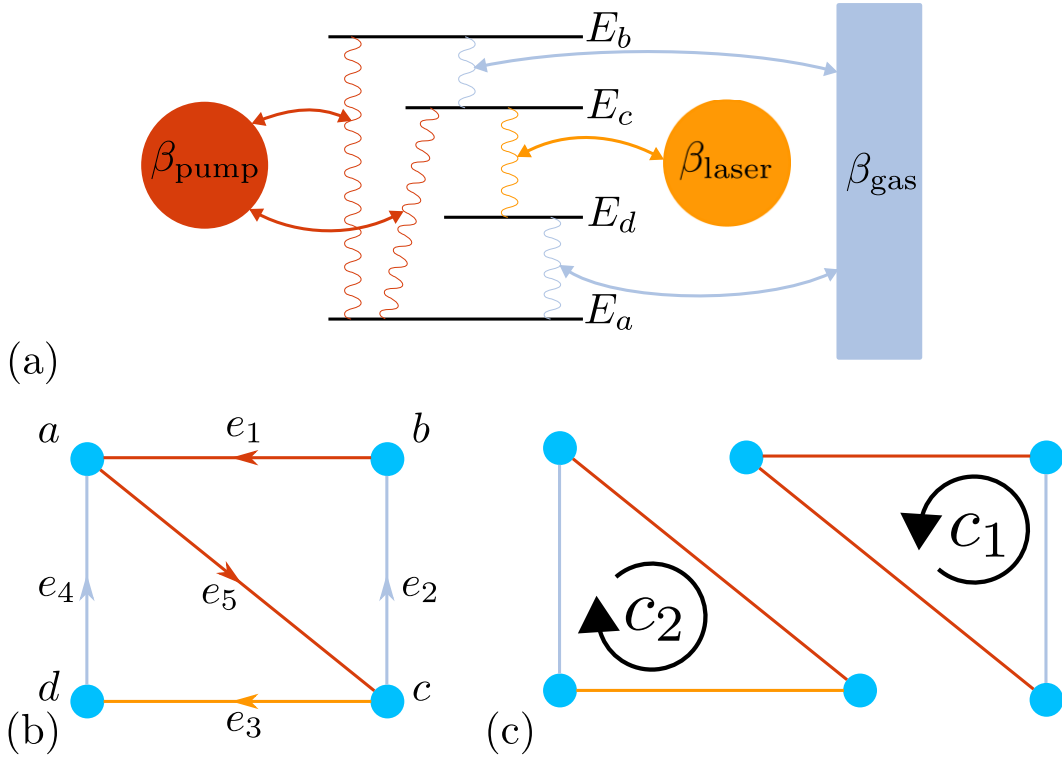
Figure 3.4: (a) Sketch of the four-state atom connected to three external heat baths. (b) Graph of the model with color indicating how reservoirs promote the various transitions (c) Chosen basis of fundamental cycles.

## 3.4 Common example: a simple laser

### 3.4.1 Modeling a laser

We consider a four state atom to model a simple laser. We assume that each state is described by its energy ($E_a$, $E_b$, $E_c$, $E_d$) such that $E_a < E_d < E_c < E_b$. We connect the system to three different external heat baths that represent the environment of our atom. We assume that the atom is surrounded by a gas of particles of inverse temperature $\beta_{\text{gas}}$, the atom is also connected to two other heat baths, the first one of inverse temperature $\beta_{\text{pump}}$ represent the thermal pumping of the atom and the second of inverse temperature $\beta_{\text{pump}}$ is intended to represent the laser radiation [27]. We emphasize that we do not take into account the state of the light field, and model the laser radiation by a thermal bath. The model is sketched on Fig. 3.4a.

We think of the laser as a machine converting the energy flux from the pump to an energy flux of laser radiation.

**Graph** Edge orientation is shown on Fig. 3.4b. The two fundamental cycles are represented on Fig. 3.4c . The incidence matrix and cycle matrix are obtained using the results of sec. 1.1.2.

**Exterior reservoirs** From the connection of the edge transition to the reservoirs the reservoir matrix is

$$\boldsymbol{R} = \begin{pmatrix} E_a - E_b & 0 & 0 & 0 & E_c - E_a \\ 0 & 0 & E_d - E_c & 0 & 0 \\ 0 & E_b - E_c & 0 & E_a - E_d & 0 \end{pmatrix} \begin{matrix} \text{pump} \\ \text{laser} \\ \text{gas} \end{matrix} \qquad (3.55)$$

The product of the reservoir matrix with the cycle matrix gives

$$\boldsymbol{RC} = \begin{pmatrix} E_c - E_b & E_c - E_a \\ 0 & E_d - E_c \\ E_b - E_c & E_a - E_d \end{pmatrix} \qquad (3.56)$$

which has for unique left null eigenvector (1 1 1) such that the total energy of the system is conserved by cyclic trajectories. Hence from Eq. (2.45) relating conservation laws and physical affinities the system has two physical affinities and can be consider as a machine. These two physical affinities are

$$f_1 = (\beta_{\text{gas}} - \beta_{\text{pump}}), \quad f_2 = (\beta_{\text{gas}} - \beta_{\text{laser}}). \qquad (3.57)$$

as expected from Eq. (1.63).

**Transition rates** Using the local detailed balance (1.61), the antisymmetric part of the transition rates follows from the reservoir matrix (3.55) and the reservoir affinity $\boldsymbol{f}_{\text{r}}^{\text{T}} = (\beta_{\text{pump}} \ \beta_{\text{laser}} \ \beta_{\text{gas}})$. The symmetric part is simply set to a constant characterizing the coupling with the reservoirs. The transition rates are then

$$\omega_{e_1} = \Gamma_{\text{pump}} e^{-\frac{\beta_{\text{pump}}}{2}(E_a - E_b)}, \qquad (3.58)$$

$$\omega_{e_2} = \Gamma_{\text{gas}} e^{-\frac{\beta_{\text{gas}}}{2}(E_b - E_c)}, \qquad (3.59)$$

$$\omega_{e_3} = \Gamma_{\text{laser}} e^{-\frac{\beta_{\text{laser}}}{2}(E_d - E_c)}, \qquad (3.60)$$

$$\omega_{e_4} = \Gamma_{\text{gas}} e^{-\frac{\beta_{\text{gas}}}{2}(E_a - E_d)}, \qquad (3.61)$$

$$\omega_{e_5} = \Gamma_{\text{pump}} e^{-\frac{\beta_{\text{pump}}}{2}(E_c - E_a)}. \qquad (3.62)$$

**Remark:** The coupling to the reservoirs is here set to a constant, as we do not consider any quantum effect for simplicity. Taking into account these quantum effects gives to the reservoir couplings $\Gamma$ a dependence in the reservoir affinities.

The transition matrix is then

$$\boldsymbol{M} = \begin{pmatrix} -\omega_{-e_1} - \omega_{e_5} - \omega_{-e_4} & \omega_{e_1} & \omega_{-e_5} & \omega_{e_4} \\ \omega_{-e_1} & -\omega_{e_1} - \omega_{-e_2} & \omega_{e_2} & 0 \\ \omega_{e_5} & \omega_{-e_2} & -\omega_{-e_5} - \omega_{e_2} - \omega_{e_3} & \omega_{-e_3} \\ \omega_{-e_4} & 0 & \omega_{e_3} & -\omega_{e_4} - \omega_{-e_3} \end{pmatrix}. \qquad (3.63)$$

The determination of the cycle affinities from the transition rates and from the cycle-reservoirs matrix is consistent and gives

$$f_{c_1} = (\beta_{\text{gas}} - \beta_{\text{pump}})(E_c - E_b), \qquad (3.64)$$

$$f_{c_2} = (\beta_{\text{gas}} - \beta_{\text{pump}})(E_c - E_a) + (\beta_{\text{gas}} - \beta_{\text{laser}})(E_d - E_c). \qquad (3.65)$$

as expected from Eq. (1.63).

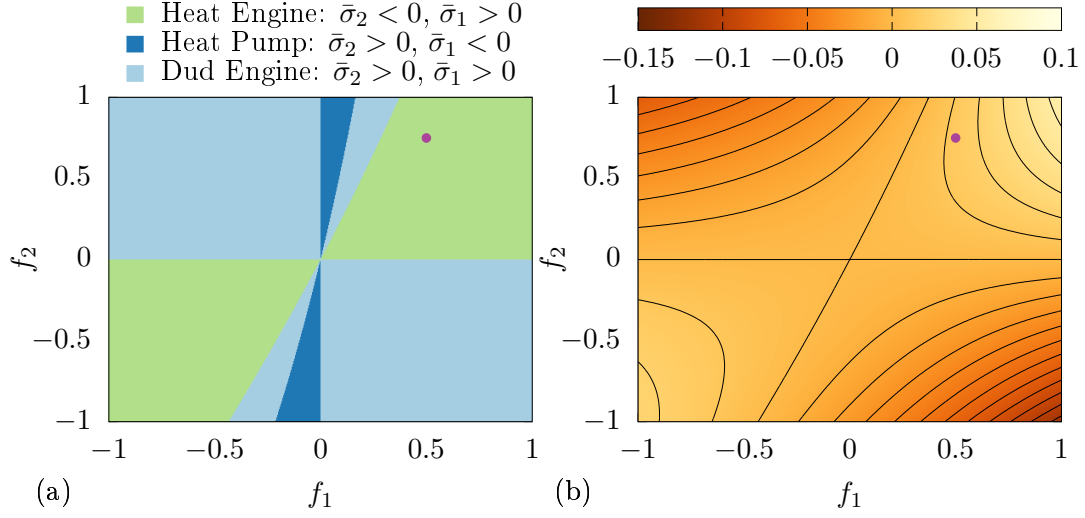## 3.4.2 Machine behavior on average



Figure 3.5: (a) Various operating modes of the machine. (b) Average output power $-\bar{\sigma}_2$ as a function of the affinities Parameters for both figures are $\Gamma_{\text{pump}} = 0.1$, $\Gamma_{\text{laser}} = 10$, $\Gamma_{\text{gas}} = 1$, $E_a = 0.5$, $E_b = 4$, $E_c = 1.5$, $E_d = 1$. The violet point denotes the specific values of affinities taken for other figures.

From the transition matrix (3.63), we compute the stationary probability and the mean currents. The stationary probability is obtained from the spanning tree formula (1.37)

$$\pi_a = \quad (\omega_{-e_2}\omega_{e_3}\omega_{e_4} + \omega_{e_1}\omega_{e_2}\omega_{-e_3} + \omega_{e_1}\omega_{e_2}\omega_{e_4} + \omega_{e_1}\omega_{e_3}\omega_{e_4}$$
$$+\omega_{-e_2}\omega_{-e_3}\omega_{-e_5} + \omega_{e_1}\omega_{e_4}\omega_{-e_5} + \omega_{-e_2}\omega_{e_4}\omega_{-e_5} + \omega_{e_1}\omega_{-e_3}\omega_{-e_5})/Z, \quad (3.66)$$

$$\pi_b = \quad (\omega_{e_2}\omega_{-e_3}\omega_{-e_4} + \omega_{-e_1}\omega_{e_2}\omega_{-e_3} + \omega_{-e_1}\omega_{e_2}\omega_{e_4} + \omega_{-e_1}\omega_{e_3}\omega_{e_4}$$
$$+\omega_{e_2}\omega_{-e_3}\omega_{e_5} + \omega_{-e_1}\omega_{e_4}\omega_{-e_5} + \omega_{e_2}\omega_{e_4}\omega_{e_5} + \omega_{-e_1}\omega_{-e_3}\omega_{-e_5})/Z, \quad (3.67)$$

$$\pi_c = \quad (\omega_{-e_2}\omega_{-e_3}\omega_{-e_4} + \omega_{-e_1}\omega_{-e_2}\omega_{-e_3} + \omega_{-e_1}\omega_{-e_2}\omega_{e_4} + \omega_{e_1}\omega_{-e_3}\omega_{-e_4}$$
$$+\omega_{-e_2}\omega_{-e_3}\omega_{e_5} + \omega_{e_1}\omega_{e_4}\omega_{e_5} + \omega_{-e_2}\omega_{e_4}\omega_{e_5} + \omega_{e_1}\omega_{-e_3}\omega_{e_5})/Z, \quad (3.68)$$

$$\pi_d = \quad (\omega_{-e_2}\omega_{e_3}\omega_{-e_4} + \omega_{-e_1}\omega_{-e_2}\omega_{e_3} + \omega_{e_1}\omega_{e_2}\omega_{-e_4} + \omega_{e_1}\omega_{e_3}\omega_{-e_4}$$
$$+\omega_{-e_2}\omega_{e_3}\omega_{e_5} + \omega_{e_1}\omega_{-e_4}\omega_{-e_5} + \omega_{-e_2}\omega_{-e_4}\omega_{-e_5} + \omega_{e_1}\omega_{e_3}\omega_{e_5})/Z, \quad (3.69)$$

where $Z$ is a normalization factor such that $\pi_a + \pi_b + \pi_c + \pi_d = 1$. The cycle currents are then determined from the stationary current of their associated chord, we have

$$\bar{j}_{c_1} \quad = \quad \bar{j}_{e_1}^{\pi} = \pi_b\,\omega_{e_1} - \pi_a\,\omega_{-e_1}, \quad (3.70)$$
$$\bar{j}_{c_2} \quad = \quad \bar{j}_{e_3}^{\pi} = \pi_c\,\omega_{e_3} - \pi_d\,\omega_{-e_3}. \quad (3.71)$$

Using the mean energy flux from the pump bath $\bar{j}_{\text{pump}}$ and the mean energy flux from the laser bath $\bar{j}_{\text{laser}}$ obtained from the cycle-reservoir matrix $\boldsymbol{RC}$ and from the cycle current (3.70), the mean entropy productions are

$$\bar{\sigma}_1 = f_1\bar{j}_{\text{pump}}, \quad \bar{\sigma}_2 = f_2\bar{j}_{\text{laser}} \quad (3.72)$$

and the macroscopic efficiency

$$\bar{\eta} = \frac{-\bar{\sigma}_2}{\bar{\sigma}_1}. \tag{3.73}$$

Using the previous expression of the mean currents and macroscopic efficiency, we determine the various operating modes of the machine. They are represented on the Fig. 3.5. Depending on the affinities, the machine works in various regime, we choose the affinities such that the machine converts energy from the pump to the laser (heat engine mode).
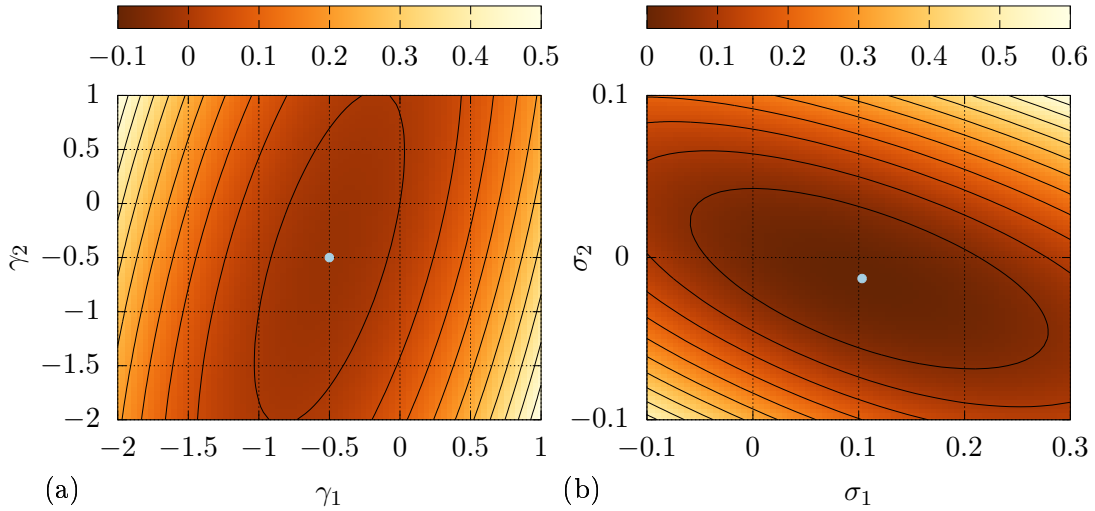
### 3.4.3 Stochastic behavior



Figure 3.6: (a) CGF of the physical currents $J - 1$ and $j_2$ (b) Corresponding LDF. The light blue dots denote the position of the minimum of the CGF and the LDF. Parameters are $f_1 = 0.5$, $f_2 = 0.75$, $\Gamma_{\text{pump}} = 0.1$, $\Gamma_{\text{laser}} = 10$, $\Gamma_{\text{gas}} = 1$, $E_a = 0.5$, $E_b = 4$, $E_c = 1.5$, $E_d = 1$

**Entropy production fluctuations** We obtain the CGF via the highest eigenvalue of the tilted matrix (2.18). The numerical computation of the CGF is shown on Fig. 3.6a . We also plot the numerical Legendre-Fenchel transform of the CGF that give the LDF $I(\sigma_1, \sigma_2)$.

**Efficiency fluctuations** We determine the efficiency LDF $J(\eta)$ from Eq. (3.50). The result is shown in Fig. 3.7. This efficiency LDF reproduces the features described in sec. 3.3.
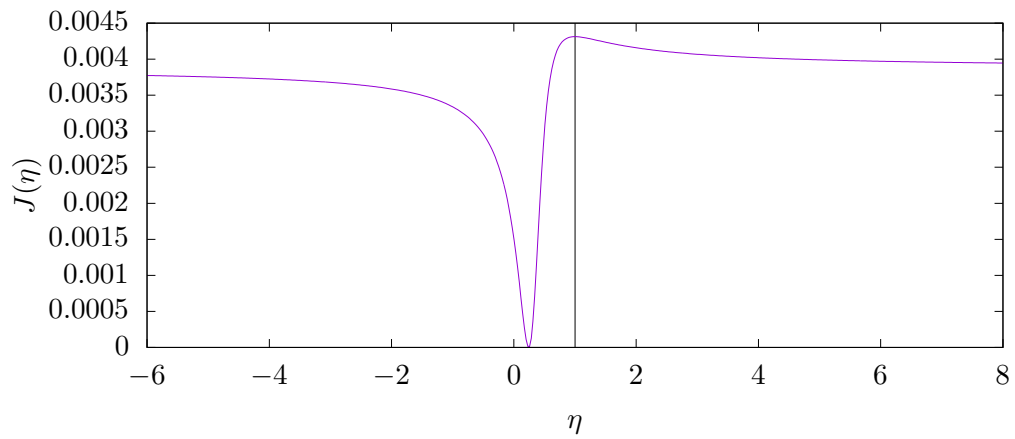
Figure 3.7: Efficiency LDF. The vertical line indicates the location of the reversible efficiency. Parameters are $f_1 = 0.5$, $F_2 = 0.75$, $\Gamma_{\text{pump}} = 0.1$, $\Gamma_{\text{laser}} = 10$, $\Gamma_{\text{gas}} = 1$, $E_a = 0.5$, $E_b = 4$, $E_c = 1.5$, $E_d = 1$

# Non-equilibrium conductance matrix

In the linear response regime near equilibrium, currents become linear function of the affinities, which defines the Onsager response matrix. The framework based on this response matrix has been very successful to describe thermoelectric effects [72, 195], to determine the degree of coupling between influx and outflux [59, 109], or to predict the efficiency at maximum power [85, 182]. A key result of this approach is Onsager's reciprocity relations which can be deduced from a more general symmetry property called fluctuation theorems [34, 35, 23].

Beyond the linear regime, the physical currents become non-linear functions of the affinities but it is not known whether the concept of Onsager matrix can still be used for systems in non-equilibrium stationary state. Previous attempts to generalize the notion of Onsager matrix to non-equilibrium stationary states lead to non-symmetric Onsager matrices, so that many properties were lost for that reason.

In this chapter, building on the work of Bulnes-Cuetara, Esposito, Lazarescu and Polettini [147, 149], we introduce precisely a non-equilibrium conductance matrix that keeps the same symmetry property of the Onsager response matrix, except that its coefficients now become functions of the affinities. Intuitively, such a conductance matrix should exist at the macroscopic scale, because it can be constructed by associating conductances between every pair of states from the microscopic scale up to the macroscopic scale. Naturally, the question whether a symmetric matrix can be constructed in this way even when the system is in a non-equilibrium stationary state requires a more careful analysis.

## 4.1 Construction of the non-equilibrium conductance matrix

We aim to build a matrix $\mathcal{G}$, which we call the non-equilibrium conductance matrix, such that we have the following relation between physical affinities and physical currents

$$\bar{\boldsymbol{j}} = \mathcal{G} \cdot \boldsymbol{f}, \qquad (4.1)$$

with real and symmetric coefficients. An important difference with the close to equilibrium case is that the coefficients of the matrix $\mathcal{G}$ are now necessarily

functions of the affinities $F_1$ and $F_2$ unlike the constant coefficients of the Onsager matrix $\boldsymbol{L}$. Importantly these assumptions together with Eq. (4.1) do not define a unique matrix $\boldsymbol{\mathcal{G}}$, and a more involved procedure must be used.

As a first property, the entropy production is obtained from the conductance matrix as

$$\bar{\sigma} = \boldsymbol{f}^{\mathrm{T}} \cdot \bar{\boldsymbol{j}} = \boldsymbol{f}^{\mathrm{T}} \cdot \boldsymbol{\mathcal{G}} \cdot \boldsymbol{f} \geqslant 0. \tag{4.2}$$

and must be a non-negative quantity. As it should be true whatever the value of the affinities, the conductance matrix should be a semi-positive definite matrix (see App. A.1.2).

When the conductance matrix is positive definite, it has an inverse $\boldsymbol{\mathcal{R}}$ that we name the resistance matrix. The relation between physical currents and affinities becomes

$$\boldsymbol{f}^{\mathrm{T}} = \bar{\boldsymbol{j}}^{\mathrm{T}} \cdot \boldsymbol{\mathcal{R}} = \bar{\boldsymbol{j}}^{\mathrm{T}} \cdot \boldsymbol{\mathcal{G}}^{-1}. \tag{4.3}$$

## 4.1.1 Microscopic framework for the non-equilibrium conductance matrix

In the following, we build $\boldsymbol{\mathcal{G}}$ with emphasis on the physical meaning of $\boldsymbol{\mathcal{G}}$ as a conductance matrix. We intend to show how to switch from the resistance matrix at the edge level to the conductance matrix at the level of physical currents.

**Force-current relation at edge level** Starting at the edge level, we introduce the edge resistance matrix $\boldsymbol{\mathcal{R}}_e$ as the diagonal matrix in the space of edge of elements

$$\mathcal{R}_{(x,y)} = \frac{f_{(x,y)}^{\omega\pi}}{\bar{\bar{j}}_{(x,y)}}. \tag{4.4}$$

It connects the stationary edge current $\bar{j}_{(x,y)} = j_{(x,y)}^{\pi} = \omega_{(x,y)}\pi_y - \omega_{(y,x)}\pi_x$ to the edge affinity $f_{(x,y)}^{\omega\pi} = \ln \dfrac{\omega_{(x,y)}\pi_y}{\omega_{(y,x)}\pi_x}$ as

$$\boldsymbol{f}_{\mathrm{e}}^{\boldsymbol{\omega\pi}} = \boldsymbol{\mathcal{R}}_e \cdot \bar{\boldsymbol{j}}_{\mathrm{e}}. \tag{4.5}$$

The last expression being reminiscent of the Ohm law for electric circuits. The inverse of the edge resistance matrix is the edge conductance matrix $\boldsymbol{\mathcal{G}}_e = \boldsymbol{\mathcal{R}}_e^{-1}$. We remark that the elements of the resistance matrix depend on the physical affinities through transition rates and stationary probability.

**Remark:** We make an abuse of notation to avoid the introduction of a different notation for each level of description, and we use the same notation for resistance and conductance matrix at each level. Matrix subscript or indexation of elements are used to distinguish the levels of description (like for vectors and linear forms).

**Force-current relation at cycle level** We recall that stationary cycle currents and affinities are connected to the stationary edge current using the cycle matrix:

$$\bar{\boldsymbol{j}}_{\mathrm{e}} = \boldsymbol{C} \cdot \bar{\boldsymbol{j}}_{\mathrm{c}} \quad \text{and} \quad \boldsymbol{f}_{\mathrm{c}}^{\mathrm{T}} = \boldsymbol{f}_{\mathrm{e}}^{\boldsymbol{\omega\pi}\,\mathrm{T}} \cdot \boldsymbol{C}. \tag{4.6}$$

At the level of cycles, the matrix $\mathcal{R}_c$ for cycle resistance connects cycle affinities and currents via

$$f_c = \sum_{c'} \mathcal{R}_{c,c'} \bar{j}_{c'}. \tag{4.7}$$

Indeed, using Eq. (4.6) in Eq. (4.4), one may express $\mathcal{R}_c$ as a function of $\mathcal{R}_e$ since

$$f_{(x,y)}^{\omega\pi} = \sum_c \mathcal{R}_{(x,y)} C_{(x,y),c} \bar{j}_c, \tag{4.8}$$

$$f_{c'} = \sum_c \sum_{(x,y)} (C^{\mathrm{T}})_{c',(x,y)} \mathcal{R}_{(x,y)} C_{(x,y),c} \bar{j}_c, \tag{4.9}$$

where we have used Eq. (4.6) in the second step. This leads to the cycle resistance matrix

$$\mathcal{R}_{c',c} = \sum_{(x,y)} (C^{\mathrm{T}})_{c,(x,y)} \mathcal{R}_{(x,y)} C_{(x,y),c}. \tag{4.10}$$

Here the analogy with electric circuits holds: electrical resistances add when connected in series. The cycle conductance matrix $\mathcal{G}_c$ is then

$$\mathcal{G}_c = \mathcal{R}_c^{-1} = (C^{\mathrm{T}} \cdot \mathcal{R}_e \cdot C)^{-1} = C^+ \cdot \mathcal{G}_e \cdot C^{\mathrm{T}+}. \tag{4.11}$$

**Force-current relation at physical level**   At the level of physical observables, the NE conductance connects currents to affinities via

$$\bar{j}_Y = \sum_X \mathcal{G}_{Y,X} f_X. \tag{4.12}$$

Considering that the amount of physical quantity $Y$ exchanged with the environment during cycle $c$ is $P_{Y,c}$ and using Eqs. (4.7), one gets

$$\bar{j}_Y = \sum_c P_{Y,c} \bar{j}_c = \sum_{c,c'} P_{Y,c} \mathcal{G}_{c,c'} f_c = \sum_X \sum_{c,c'} P_{Y,c} \mathcal{G}_{c,c'} P_{c,X}^{\mathrm{T}} f_X. \tag{4.13}$$

Therefore, the physical conductance matrix writes

$$\mathcal{G} = P \cdot (C^{\mathrm{T}} \cdot \mathcal{R}_e \cdot C)^{-1} \cdot P^{\mathrm{T}} = P \cdot C^+ \cdot \mathcal{G}_e \cdot (P \cdot C^+)^{\mathrm{T}}. \tag{4.14}$$

The electrical analogy also holds: cycle conductances add when connected in parallel which makes senses when considering that the current flows from one reservoir to another through sequences of cycles.

**Properties of the non-equilibrium conductance matrix**   From its definition, we have some properties of the conductance matrix. The edge resistances are non negative number. Indeed we have

$$\frac{f_{(x,y)}^{\omega\pi}}{\bar{j}_{(x,y)}} = \frac{\ln \dfrac{\omega_{y,x} \pi_x}{\omega_{x,y} \pi_y}}{\omega_{y,x} \pi_x - \omega_{x,y} \pi_y} \geqslant 0 \tag{4.15}$$

as the function $\ln(a/b)/(a-b)$ is a non-negative function. Therefore, the conductance matrix is a real semi-positive definite matrix as required [16]. Moreover, it is a symmetric matrix, a properties that is reminiscent of the Onsager symmetry.

## 4.1.2 Stochastic construction

In this section, we show that the non-equilibrium conductance matrix appears also when studying LDF of currents.

**Quadratic bound on the edge current LDF**    We start from the occupation-current LDF (2.33-2.34), that is the level 2.5 LDF. We recall its expression

$$
\begin{aligned}
I(\boldsymbol{r}_{\mathrm{v}}, \boldsymbol{j}_{\mathrm{e}}) \;=\; & \sum_{(x,y)} j_{(x,y)} \mathrm{arcsinh}\left(\frac{j_{(x,y)}}{g^r_{(x,y)}}\right) - j_{(x,y)} \mathrm{arcsinh}\left(\frac{j^r_{(x,y)}}{g^r_{(x,y)}}\right) \\
& + \sqrt{j^r_{(x,y)}{}^2 + g^r_{(x,y)}{}^2} - \sqrt{j^2_{(x,y)} + g^r_{(x,y)}{}^2} \qquad (4.16) \\
\;=\; & \sum_{(x,y)} \Psi(j_{(x,y)}, j^r_{(x,y)}, g^r_{(x,y)}) \qquad\qquad\qquad\qquad\quad (4.17)
\end{aligned}
$$

where $\Psi(j, \widetilde{j}, g) = j\,\mathrm{arcsinh}\left(\dfrac{j}{g}\right) - j\,\mathrm{arcsinh}\left(\dfrac{\widetilde{j}}{g}\right) + \sqrt{\widetilde{j}^2 + g^2} - \sqrt{j^2 + g^2}$. The edge current LDF is then given by contraction of the level 2.5 LDF

$$
I(\boldsymbol{j}_{\mathrm{e}}) = \min_{\boldsymbol{r}_{\mathrm{v}}} I(\boldsymbol{r}_{\mathrm{v}}, \boldsymbol{j}_{\mathrm{e}}). \qquad (4.18)
$$

As we cannot realize this minimization explicitly, we bound the currents LDF in two steps. First we bound the minimum in Eq. (4.18) by any normalized probability density. Chosing the stationary probability $\pi$ gives

$$
I(\boldsymbol{j}_{\mathrm{e}}) \leqslant I(\boldsymbol{\pi}_{\mathrm{v}}, \boldsymbol{j}_{\mathrm{e}}) = \sum_{(x,y)} \Psi(j_{(x,y)}, j^\pi_{(x,y)}, g^\pi_{(x,y)}). \qquad (4.19)
$$

Next, we can bound each of the elements of the sum by a quadratic function, as shown in Ref. [93] ,

$$
\Psi(j, \widetilde{j}, g) \leqslant (j - \widetilde{j})^2 \frac{1}{2\widetilde{j}} \mathrm{arcsinh}\frac{\widetilde{j}}{g}. \qquad (4.20)
$$

For stationary probability, we have the relation (1.27) between geometric activity, probability current and edge affinity

$$
\frac{1}{2j^\pi_{(x,y)}} \mathrm{arcsinh}\frac{j^\pi_{(x,y)}}{g^\pi_{(x,y)}} = \frac{f^{\omega\pi}_{(x,y)}}{4j^\pi_{(x,y)}} = \frac{\mathcal{R}_{(x,y)}}{4} \qquad (4.21)
$$

leading to the quadratic bound for the LDF of edge currents in the form

$$
I(\boldsymbol{j}_{\mathrm{e}}) \leqslant \frac{1}{4} \sum_{(x,y)} (j_{(x,y)} - \bar{j}_{(x,y)})^2 \mathcal{R}_{(x,y)}. \qquad (4.22)
$$

We retrieve the edge resistance introduced in sec. 4.1.1. We emphasize that the stationary condition on the current (2.29) is still valid. Hence the currents must be cycle currents.

**Contraction towards cycle currents** Now, the cycle currents $\boldsymbol{j}_c$ are connected to the edge currents $\boldsymbol{j}_e$ by the cycle matrix. When using Eq. (4.6) as a change of variable into Eq. (4.22), we obtain

$$I(\boldsymbol{j}_c) \leqslant \frac{1}{4}(\boldsymbol{j}_c - \bar{\boldsymbol{j}}_c)^{\mathrm{T}} \cdot \boldsymbol{\mathcal{R}}_c \cdot (\boldsymbol{j}_c - \bar{\boldsymbol{j}}_c), \tag{4.23}$$

where $\boldsymbol{\mathcal{R}}_c$ is the cycle resistance matrix of components

$$\mathcal{R}_{c,c'} = \sum_{(x,y)} C_{(x,y),c} \mathcal{R}_{(x,y)} C_{(x,y),c'}. \tag{4.24}$$

**Contraction towards physical currents** By contracting Eq. (4.23) over cycle currents, one obtains an upper bound for the LDF of physical currents $j_1, j_2$. The LDF we are interested in reads

$$I_{\mathrm{quad}}(\boldsymbol{j}) = \frac{1}{4} \min_{\{..\}} (\boldsymbol{j}_c - \bar{\boldsymbol{j}}_c)^{\mathrm{T}} \cdot \boldsymbol{\mathcal{R}}_c \cdot (\boldsymbol{j}_c - \bar{\boldsymbol{j}}_c), \tag{4.25}$$

where $\{..\}$ denotes the minimum over currents $\boldsymbol{j}_c$ such that $\boldsymbol{j} = \boldsymbol{P} \cdot \boldsymbol{j}_c$, with $\boldsymbol{j}$ the vector of physical currents $(j_1, j_2)$. Since the function to be minimized is quadratic and the constraints are linear, this contraction can be achieved exactly as follows: The function to be minimized is

$$f_{\mathrm{quad}} = \frac{1}{4}(\boldsymbol{j}_c - \bar{\boldsymbol{j}}_c)^{\mathrm{T}} \cdot \boldsymbol{\mathcal{R}}_c \cdot (\boldsymbol{j}_c - \bar{\boldsymbol{j}}_c) - \boldsymbol{\Lambda}^{\mathrm{T}} \cdot (\boldsymbol{j} - \boldsymbol{P} \cdot \boldsymbol{j}_c), \tag{4.26}$$

where $\boldsymbol{\Lambda}$ is a Lagrange multiplier. After minimizing $f_{\mathrm{quad}}$ with respect to $\boldsymbol{j}_c$, one obtains an expression of $\boldsymbol{j}$ as a function of $\boldsymbol{\Lambda}$. Then using again the constraint $\boldsymbol{j} = \boldsymbol{P} \cdot \boldsymbol{j}_c$, one finds

$$\boldsymbol{\Lambda} = -\frac{1}{2} \left[ \boldsymbol{P} \cdot \boldsymbol{\mathcal{R}}_c^{-1} \cdot \boldsymbol{P}^{\mathrm{T}} \right]^{-1} \cdot \left( \boldsymbol{j} - \bar{\boldsymbol{j}} \right). \tag{4.27}$$

Inserting this expression into $\boldsymbol{j}_c$ and using it into $I_{\mathrm{quad}}$, one obtains

$$I_{\mathrm{quad}}(\boldsymbol{j}) = \frac{1}{4} \left( \boldsymbol{j} - \bar{\boldsymbol{j}} \right)^{\mathrm{T}} \cdot \boldsymbol{\mathcal{R}} \cdot \left( \boldsymbol{j} - \bar{\boldsymbol{j}} \right). \tag{4.28}$$

where we have $\boldsymbol{\mathcal{R}}$ as the $2 \times 2$ resistance matrix in the basis of physical currents

$$\boldsymbol{\mathcal{R}} = \left( \boldsymbol{P} \cdot \boldsymbol{\mathcal{R}}_c^{-1} \cdot \boldsymbol{P}^{\mathrm{T}} \right)^{-1}. \tag{4.29}$$

The resistance matrix is exactly the inverse of the conductance matrix (4.14). In the end, we obtain the following inequality for the LDF of physical currents:

$$I(\boldsymbol{j}) \leqslant I_{\mathrm{quad}}(\boldsymbol{j}). \tag{4.30}$$

**Fluctuation theorem**  The quadratic bound on the LDF used in Eq. (4.22) has been built to respect the fluctuation theorem [93, 23]. Therefore, at the level of physical observables the quadratic bound obeys the relation

$$I_{\text{quad}}(\boldsymbol{j}) - I_{\text{quad}}(-\boldsymbol{j}) = -\boldsymbol{j}^{\text{T}} \cdot \boldsymbol{f}. \tag{4.31}$$

Once Eq. (4.28) is inserted into this equation, we obtain $\boldsymbol{j}^{\text{T}} \cdot \boldsymbol{\mathcal{R}} \cdot \bar{\boldsymbol{j}} = \boldsymbol{j}^{\text{T}} \cdot \boldsymbol{f}$ for all $\boldsymbol{j}$, or equivalently $\boldsymbol{\mathcal{R}} \cdot \bar{\boldsymbol{j}} = \boldsymbol{f}$ and we recover Eq. (4.1).

To summarize, the property that edge current fluctuations in non-equilibrium stationary states are more likely than those predicted by linear response analysis [93, 141] which is Eq. (4.22), carries out to the level of cycles and from there to the level of physical macroscopic currents. This approach also leads to a relation between affinities and physical macroscopic currents that defines the non-equilibrium conductance matrix.

**When $\boldsymbol{\mathcal{G}}$ is non invertible**  It could happen that $\boldsymbol{\mathcal{G}}$ is not invertible. This happens in particular when two of the physical current are strongly coupled, *i.e.* there exists a strong relation between both currents. In this case, the current LDF is not defined for currents that do not respect this coupling relation, and the resistance matrix should be defined trough the Moore-Penrose pseudo-inverse instead of the regular matrix inverse.

### 4.1.3   Close-to-equilibrium limit and the Onsager matrix

Close to equilibrium, the non equilibrium conductance matrix should be the Onsager matrix. It is easy to show that the limit of vanishing affinity leads to the Onsager matrix. At equilibrium, we have the detailed balance condition with the equilibrium probability distribution $\boldsymbol{\pi}_{\text{v}}^{\text{eq}}$

$$\omega_{y,x} \pi_x^{\text{eq}} = \omega_{x,y} \pi_y^{\text{eq}}. \tag{4.32}$$

We consider steady state $\boldsymbol{\pi}_{\text{v}}$ of our system close to equilibrium such that

$$\forall x, \quad u_x = \frac{\pi_x - \pi_x^{\text{eq}}}{\pi_x^{\text{eq}}} \ll 1 \tag{4.33}$$

Therefore, we have

$$\frac{\bar{j}_{(x,y)}}{f_{(x,y)}^{\omega\pi}} = \frac{\omega_{y,x}(\pi_x^{\text{eq}} u_x + \pi_x^{\text{eq}}) - \omega_{x,y}(\pi_y^{\text{eq}} u_y + \pi_y^{\text{eq}})}{\ln \dfrac{\omega_{y,x}\pi_x^{\text{eq}}}{\omega_{x,y}\pi_y^{\text{eq}}} \dfrac{1+u_x}{1+u_y}} \tag{4.34}$$

Using Eq. (4.32) and developing at first order we obtain

$$\frac{\bar{j}_{(x,y)}}{f_{(x,y)}^{\omega\pi}} = \frac{\omega_{y,x}\pi_x^{\text{eq}}(u_x - u_y)}{\ln \dfrac{1+u_x}{1+u_y}} \simeq \omega_{y,x}\pi_x^{\text{eq}} = \omega_{x,y}\pi_y^{\text{eq}} \tag{4.35}$$

The use of the last result as edge conductance in the Eq. (4.14) gives then the Onsager matrix [163]. The current LDF being quadratic close to equilibrium, the

inequality (4.30) derived in the sec. 4.1.2 is then an equality. We remark also that, due to Eq. (4.32), the edge conductance at equilibrium is given by half of the geometric activity (1.28), which highlights the role of the geometrical activity as a local metric.

## 4.2 Bounds on the conductance matrix

There exists some bounds on the non-equilibrium conductance matrix that allow to derive additional results, *e.g.* thermodynamics uncertainty relations.

### 4.2.1 Degenerate case

We introduce the $Ph \times Ph$ matrix $\boldsymbol{\mathcal{G}}^{\min}$ whose elements are defined from the physical current $\bar{j}$ as

$$\mathcal{G}^{\min}_{X,Y} = \frac{\bar{j}_X \bar{j}_Y}{\bar{\sigma}}. \tag{4.36}$$

As $\bar{\sigma}$ is a positive quantity, the matrix $\boldsymbol{\mathcal{G}}^{\min}$ is semi-definite positive. Indeed for any $\boldsymbol{x} \in \mathbb{R}^{Ph}$, we have

$$\boldsymbol{x}^{\mathrm{T}} \cdot \boldsymbol{\mathcal{G}}^{\min} \cdot \boldsymbol{x} = \frac{\left( \sum_X x_X \bar{j}_X \right)^2}{\bar{\sigma}} \geqslant 0. \tag{4.37}$$

The matrix $\boldsymbol{\mathcal{G}}^{\min}$ is a matrix of rank one. Therefore it has only one non-zero eigenvalue, that is non-negative as proved by Eq. (4.37).

The matrix $\boldsymbol{\mathcal{G}}^{\min}$ is a bound for the conductance matrix, as

$$\boldsymbol{\mathcal{G}} \geqslant \boldsymbol{\mathcal{G}}^{\min}. \tag{4.38}$$

The proof is as follow: let's consider any $\boldsymbol{x} \in \mathbb{R}^{Ph}$, the conductance matrix being positive semi-definite, it defines a semi-inner product and we can apply the Cauchy-Schwartz inequality [16] (Theorem 5.1.8)

$$\boldsymbol{x}^{\mathrm{T}} \cdot \boldsymbol{\mathcal{G}} \cdot \boldsymbol{x} \geqslant \frac{\left( \boldsymbol{x}^{\mathrm{T}} \cdot \boldsymbol{\mathcal{G}} \cdot \boldsymbol{f} \right) \left( \boldsymbol{f}^{\mathrm{T}} \cdot \boldsymbol{\mathcal{G}} \cdot \boldsymbol{x} \right)}{\boldsymbol{f}^{\mathrm{T}} \cdot \boldsymbol{\mathcal{G}} \cdot \boldsymbol{f}} = \boldsymbol{x}^{\mathrm{T}} \cdot \boldsymbol{\mathcal{G}}^{\min} \cdot \boldsymbol{x}. \tag{4.39}$$

The last equality uses the relation (4.1) that convert affinities into currents and the symmetry of the conductance matrix.

The matrix $\boldsymbol{\mathcal{G}}^{\min}$ also connects affinities and currents as

$$\bar{\boldsymbol{j}} = \boldsymbol{\mathcal{G}}^{\min} \cdot \boldsymbol{f}. \tag{4.40}$$

The matrix $\boldsymbol{\mathcal{G}}^{\min}$ being of rank one, it corresponds to the case where all physical currents are strongly coupled. In particular, the inequality Eq. (4.38) becomes an equality for unicyclic systems

### 4.2.2 Fluctuation-dissipation inequality

We now look for an upperbound for $\boldsymbol{\mathcal{G}}$. The Legendre transform of the quadratic LDF is the quadratic CGF

$$\phi_{\text{quad}}(\boldsymbol{\gamma}) = \max_{\boldsymbol{j}}[(\boldsymbol{\gamma}^{\text{T}} \cdot \boldsymbol{j} - I_{\text{quad}}(\boldsymbol{j})]. \tag{4.41}$$

From Eq. (4.30), we have a bounds on the CGF $\phi(\boldsymbol{\gamma})$

$$\phi_{\text{quad}}(\boldsymbol{\gamma}) \leqslant \phi(\boldsymbol{\gamma}), \tag{4.42}$$

where $\phi_{\text{quad}}(\gamma_1, \gamma_2)$ can be explicitly determined using Eq. (4.28) and using the property $\boldsymbol{\mathcal{R}}^{-1} = \boldsymbol{\mathcal{G}}$:

$$\phi_{\text{quad}}(\boldsymbol{\gamma}) = \boldsymbol{\gamma}^{\text{T}} \cdot \boldsymbol{\mathcal{G}} \cdot \boldsymbol{\gamma} + \bar{\boldsymbol{j}} \cdot \boldsymbol{\gamma}. \tag{4.43}$$

Since, the functions $\phi$ and $\phi_{\text{quad}}$ have the same value at origin and the same first derivative with respect to $\boldsymbol{\gamma}$ at the origin, the inequality (4.42) can be carried out to second order derivatives. The result is the following inequality

$$\forall \boldsymbol{\gamma} \in \mathbb{R}^2, \quad \boldsymbol{\gamma}^{\text{T}} \cdot \boldsymbol{\mathcal{G}} \cdot \boldsymbol{\gamma} \leqslant \frac{1}{2} \boldsymbol{\gamma}^{\text{T}} \cdot \mathbf{Cov} \cdot \boldsymbol{\gamma}, \tag{4.44}$$

where the matrix $\mathbf{Cov}$ has been introduced in sec. 3.2 as the currents covariance matrix. In term of matrix partial order we end with $\boldsymbol{\mathcal{G}} \leqslant \mathbf{Cov}/2$.

Choosing $\boldsymbol{\gamma} = (0, \ldots, 0, \gamma_X, 0, \ldots, 0)^{\text{T}}$ in Eq. (4.44) leads to the tight bound derived in Ref. [147] between the variance of the partial entropy production $\Sigma_X = J_X f_x^2$ and the element of the conductance matrix:

$$\mathcal{G}_{X,X} f_X{}^2 \leqslant \frac{\text{Var}(\Sigma_X)}{2}, \tag{4.45}$$

after multiplying the inequalities by $f_X{}^2$. These inequalities are saturated in the linear regime close to equilibrium, where the non-equilibrium conductance matrix becomes the standard Onsager matrix $\boldsymbol{\mathcal{L}}$ and the relation $\boldsymbol{\mathcal{L}} = \mathbf{Cov}/2$ is the well-known fluctuation-dissipation relation.

### 4.2.3 Thermodynamics uncertainty relations

By combining the inequality $\boldsymbol{\mathcal{G}} \leqslant \mathbf{Cov}/2$ obtained in the previous section with Eq. (4.38), one obtains

$$\boldsymbol{\mathcal{G}}^{\text{min}} \leqslant \boldsymbol{\mathcal{G}} \leqslant \frac{\mathbf{Cov}}{2}, \tag{4.46}$$

where the first inequality on the left hand side becomes saturated only if the system has strongly coupled physical currents. The relation $\boldsymbol{\mathcal{G}}^{\text{min}} \leqslant \mathbf{Cov}/2$ implies inequalities by choosing particular values of the vector $\boldsymbol{x}$, namely $(0, \ldots, 0, f_X, 0, \ldots, 0)^{\text{T}}$ and $\boldsymbol{f}$. These are the so-called *thermodynamics uncertainty relations* [40, 93, 94, 141]:

$$\frac{\bar{\sigma}_X^2}{\bar{\sigma}} \leqslant \frac{\text{Var}(\Sigma_X)}{2} \tag{4.47}$$

for the partial entopy production $\Sigma_X$, and

$$\bar{\sigma} \leqslant \frac{\mathrm{Var}(\Sigma)}{2} \tag{4.48}$$

for the total entropy production $\Sigma = \sum_X \Sigma_X$. We emphasize that the first inequality is not saturated close to equilibrium except when the physical currents are strongly coupled, *i.e.* when the inequality (4.38) is an equality.

### 4.2.4 Bound from activity

We start by bounding by below the edgewise resistance matrix as follows

$$\mathcal{R}_{(x,y)} = \frac{f_{(x,y)}^{\omega\pi}}{\bar{j}_{(x,y)}} \geqslant \frac{2}{a_{(x,y)}^{\pi}} \geqslant 0, \tag{4.49}$$

where $a_{(x,y)}^{\pi} = \pi_y \omega_{(x,y)} + \pi_x \omega_{(y,x)}$ is the mean activity along edge $(x,y)$ defined in Eq. (1.24). To prove Eq. (4.49), we remark that [172]

$$
\begin{aligned}
(\pi(x)k(x,y) - \pi(y)k(y,x)) \log \frac{\pi(x)k(x,y)}{\pi(y)k(y,x)} &= \bar{j}_{(x,y)} f_{(x,y)}^{\omega\pi} \\
&\geqslant 2\frac{(\pi(x)k(x,y) - \pi(y)k(y,x))^2}{\pi(x)k(x,y) + \pi(y)k(y,x)} = 2\frac{\bar{j}_{(x,y)}^2}{a_{(x,y)}^{\pi}}.
\end{aligned} \tag{4.50}
$$

Since the mean activity is positive, using the edge diagonal matrix $\mathcal{A}_e$ of elements $\mathcal{A}_{(x,y)} = a_{(x,y)}^{\pi}$, we can build the matrix

$$\mathcal{A} = \boldsymbol{P} \cdot \left(\boldsymbol{C}^{\mathrm{T}} \cdot \mathcal{A}_e^{-1} \cdot \boldsymbol{C}\right)^{-1} \cdot \boldsymbol{P}^{\mathrm{T}} \tag{4.51}$$

which share obvious similarity with the conductance matrix.

Thanks to the properties of semi-positive definite matrices [16] (Corrollary 7.7.4), the inequality (4.49) holds at the level of matrices

$$\mathcal{G} \leqslant \frac{\mathcal{A}}{2} \tag{4.52}$$

This last result allows us to obtain bounds on currents from combination of edge activity, in particular the total entropy production is bounded by

$$\bar{\sigma} = \sum_{X,Y} \mathcal{G}_{X,Y} f_X f_Y \leqslant \sum_{X,Y} \frac{\mathcal{A}_{X,Y}}{2} f_X f_Y. \tag{4.53}$$

We emphasize that the inequality (4.52) becomes an equality in the close-to-equilibrium case. Indeed the matrix $\mathcal{A}/2$ is the Onsager matrix in this case, as seen in sec. 4.1.3.

### 4.2.5 Distance between edgewise and cyclewise conductance matrix

The way non-equilibrium conductance matrix is constructed is complicated, involving matrix inverse and knowledge of a cycle basis. In this section, we look for a simpler matrix built directly from the edge level to the physical level. Starting from Eq. (4.14) and the physical matrix $\boldsymbol{P} = \boldsymbol{V}^+ \cdot \boldsymbol{R} \cdot \boldsymbol{C}$ giving the contribution of cycles to fundamental currents, the non-equilibrium conductance matrix writes

$$\boldsymbol{\mathcal{G}} = \boldsymbol{V}^+ \cdot \boldsymbol{R} \cdot \boldsymbol{C} \cdot \left( \boldsymbol{C}^{\mathrm{T}} \cdot \boldsymbol{\mathcal{G}}_e^{-1} \cdot \boldsymbol{C} \right)^{-1} \cdot (\boldsymbol{V}^+ \cdot \boldsymbol{R} \cdot \boldsymbol{C})^{\mathrm{T}} \tag{4.54}$$

$\boldsymbol{C}$ is a matrix with linearly independent columns: $\boldsymbol{C}^+$ is only a left inverse of $\boldsymbol{C}$ and the product $\boldsymbol{C}\boldsymbol{C}^+$ is not the identity, but is a symmetric matrix.

Let's now consider the conductance matrix $\boldsymbol{\mathcal{G}}^\#$ such that

$$\boldsymbol{\mathcal{G}}^\# = \boldsymbol{V}^+ \cdot \boldsymbol{R} \cdot \boldsymbol{\mathcal{G}}_e \cdot \left( \boldsymbol{V}^+ \cdot \boldsymbol{R} \right)^{\mathrm{T}} \tag{4.55}$$

this is a conductance matrix that respect Eq. (4.1) and a semi-definite positive matrix. We seek for a relation between $\boldsymbol{\mathcal{G}}^\#$ and $\boldsymbol{\mathcal{G}}$. Using the lemma of sec. A.1.4 and the properties of semi-positive definite matrix, we have

$$\boldsymbol{\mathcal{G}}^\# \geqslant \boldsymbol{\mathcal{G}}. \tag{4.56}$$

In particular the bounds on LDF does not hold anymore, and all bounds derived from $\boldsymbol{\mathcal{G}}^\#$ will be weaker than the one derived from $\boldsymbol{\mathcal{G}}$.

The conductance matrix is derived for systems in a stationary state, the currents must be stationary currents, *i.e.* cycle currents. This is why we have contracted on cycle currents in sec. 4.1.2. When using the matrix $\boldsymbol{V}^+ \cdot \boldsymbol{R}$ instead of the matrix $\boldsymbol{P}$, we do not assure that currents are stationary anymore.

## 4.3 Applications to machines

We now specialize to a thermodynamic machine where the number of physical currents is reduced to 2. The first process is the driving process and the second process is the output process. Hence the partial entropy production rate of the first process verifies $\sigma_1 \geqslant 0$ while $\sigma_2 \leqslant 0$ for the second process. We use now the non-equilibrium conductance matrix to deduce constraints on power and efficiency of machines.

Using the properties of the non-equilibrium conductance matrix, we get for the partial entropy production rates

$$\begin{aligned}
\bar{\sigma}_1 &= \bar{j}_1 f_1 = \mathcal{G}_{1,1} {f_1}^2 + \mathcal{G}_{1,2} f_1 f_2, \tag{4.57} \\
\bar{\sigma}_2 &= \bar{j}_2 f_2 = \mathcal{G}_{2,1} f_1 f_2 + \mathcal{G}_{2,2} {f_2}^2. \tag{4.58}
\end{aligned}$$

The conductance matrix is a semi-positive definite matrix. Since $\mathcal{G}_{1,2} = \mathcal{G}_{2,1}$ this means:

$$\mathcal{G}_{1,1} \mathcal{G}_{2,2} \geqslant {\mathcal{G}_{1,2}}^2. \tag{4.59}$$

Using Eqs. (4.57–4.58) combined with the conditions $\sigma_1 \geqslant 0$ and $\sigma_2 \leqslant 0$ leads to the inequalities

$$\mathcal{G}_{1,1}f_1^2 \geqslant -\mathcal{G}_{1,2}f_1f_2 \geqslant \mathcal{G}_{2,2}f_2^2 \geqslant 0, \tag{4.60}$$

which are valid for arbitrary affinities.

## 4.3.1 General parametrization of the efficiency

Thanks to the last two inequalities of the previous section, we can introduce the functions

$$\varphi = \sqrt{\frac{\mathcal{G}_{2,2}f_2^2}{\mathcal{G}_{1,1}f_1^2}}, \quad \text{and} \quad \xi = \frac{\mathcal{G}_{1,2}}{\sqrt{\mathcal{G}_{1,1}\mathcal{G}_{2,2}}} \operatorname{sign}(f_1f_2). \tag{4.61}$$

These functions are direct generalizations of the ones used in the close-to-equilibrium regime [109]. The parameter $\mathcal{G}_{1,1}f_1^2$ determines the dissipation of the driving process when there is no output process coupled to the driving process or when there is one but we choose to ignore it. In the following, we call this quantity the intrinsic dissipation of the driving process. Then $\varphi = \varphi(f_1, f_2)$ is the relative intrinsic dissipation of the output process with respect to the driving process, and finally $\xi = \xi(f_1, f_2)$ quantifies the *degree of coupling* [42, 59, 85, 109, 145]. From the constraints of Eqs. (4.59-4.60), these functions are bounded by

$$\xi \in [-1, 0[, \quad \varphi \in [0, -\xi], \tag{4.62}$$

for the system to operate as a machine. If it does not, the above parametrization could still be used but with a modified range of the parameters, namely $\varphi \geqslant 0$ and $\xi \in [-1, 1]$. Note that we have also excluded the value $\xi = 0$ from our analysis which corresponds to having independent driving and output processes for which $\mathcal{G}_{1,2} = 0$. In this case, the system cannot work as a machine because its efficiency would be negative with $\bar{\eta} = -\varphi^2 \leqslant 0$. Note also that in the literature on thermoelectricity [42, 109], it is customary to use the figure of merit $ZT$ instead of the degree of coupling. The two notions are simply related by $ZT = \xi^2/(1-\xi^2)$, so that $ZT$ is a real positive number which goes to infinity when $\xi$ tends to $-1$.

**Efficiency**   Restricting ourselves to a working machine, we use Eqs. (4.57–4.58) in the definition (3.2) of thermodynamic efficiency to obtain

$$\bar{\eta} = -\frac{\mathcal{G}_{1,2}f_1f_2 + \mathcal{G}_{2,2}f_2^2}{\mathcal{G}_{1,1}f_1^2 + \mathcal{G}_{1,2}f_1f_2}, \tag{4.63}$$

which can be turned into

$$\bar{\eta} = -\frac{\varphi^2 + \xi\varphi}{1 + \xi\varphi}, \tag{4.64}$$

with the aid of Eq. (4.61). We emphasize that with this new parametrization, the machine efficiency does not depend explicitly on the intrinsic dissipation $\mathcal{G}_{1,1}f_1^2$, but only depends on the relative intrinsic dissipation $\varphi$ and on the degree of coupling $\xi$. The specific dependence of the efficiency on the affinities is then completely transferred to $\varphi$ and $\xi$. As we shall see below, this new parametrization of the efficiency provides useful insights into the machine properties. One

important benefit in particular is the ability to bound the machine efficiency and output power.

## 4.3.2   Tight coupling far from equilibrium

In this section, we discuss the notion of tight coupling far-from-equilibrium based on the non-equilibrium conductance matrix and the $(\mathcal{G}_{1,1}f_1^2, \varphi, \xi)$ parametrization. Tight coupling between two entropy fluxes means that the elementary steps must produce entropy in constant proportion. In other words, the physical quantities corresponding to the driving and output processes must be always exchanged in the same proportion in such a way that the two equations in (4.1) are linearly dependent. The latter condition implies that the matrix $\mathcal{G}$ is of rank one, which means that it can be written in the form

$$\mathcal{G} = \begin{pmatrix} \mathcal{G}_{1,1} & \mathcal{G}_{1,2} \\ \mathcal{G}_{2,1} & \mathcal{G}_{2,2} \end{pmatrix} = \mathcal{G}_{1,1} \begin{pmatrix} 1 & \alpha \\ \alpha & \alpha^2 \end{pmatrix}, \qquad (4.65)$$

in terms of a real coefficient $\alpha$. Using Eq. (4.1), one finds $\bar{j}_1 = \alpha \bar{j}_2$, thus $\alpha$ is precisely the proportionality factor between the two currents. Then comparing with Eq. (4.36), one finds $\mathcal{G} = \mathcal{G}^{\min}$. Thus $\mathcal{G}^{\min}$ is the non-equilibrium conductance matrix of the system if it operates in the tight coupling regime. Furthermore, this shows that the inequality of Eq. (4.38) becomes saturated in the tight coupling regime.

Now, from Eqs. (4.61) and (4.64), the coupling parameter reaches the value $\xi = \mathrm{sign}(f_1 f_2 \alpha) = -1$, because $\xi \in [-1, 0[$, and $\bar{\eta} = \varphi = |\alpha f_2 / f_1|$. Thus, in the tight coupling regime, the degree of coupling reaches its minimum value.

Going back to the general case, one deduces from Eq. (4.64) that

$$\left.\frac{\partial \bar{\eta}}{\partial \xi}\right|_{\varphi} = -\frac{\varphi(1 - \varphi^2)}{(1 + \xi\varphi)^2}, \qquad (4.66)$$

which is always negative since $\varphi \in [0, 1]$. Therefore, the efficiency monotonously increases when $\xi$ decreases, and the maximum value of the efficiency at fixed value of $\varphi$ is reached when $\xi = -1$, i.e. at tight coupling.

## 4.3.3   Maximum efficiency as function of the degree of coupling

We now bound the efficiency $\bar{\eta} = \bar{\eta}(\xi, \varphi)$ of Eq. (4.64) by looking at the value of the function $\varphi$ that yields the maximum efficiency in Eq (4.64) at a fixed degree of coupling $\xi$. The condition $\partial \bar{\eta} / \partial \varphi|_{\xi} = 0$ leads to a simple second degree polynomial equation

$$\xi\varphi^2 + 2\varphi + \xi = 0. \qquad (4.67)$$

Multiplying the numerator and denominator of Eq. (4.64) by $2 + \xi\varphi$ and using (4.67), we find that the maximum efficiency becomes $\bar{\eta}_{\max} = -\xi\varphi/(2 + \xi\varphi)$.

Using the solution of Eq. (4.67) in this expression of $\bar{\eta}_{\max}$, we obtain the maximal machine efficiency in terms of the degree of coupling function $\xi$,

$$\bar{\eta}_{\max}(\xi) = \frac{1 - \sqrt{1 - \xi^2}}{1 + \sqrt{1 - \xi^2}}, \qquad (4.68)$$

which is such that

$$\bar{\eta}_{\max}(\xi) \geqslant \bar{\eta}(\xi, \varphi) \qquad (4.69)$$

for all $\xi$ and $\varphi$ in the allowed range. This inequality is illustrated in sect. 4.4. As expected from the previous section, Eq. (4.68) also confirms that the maximum of the curve $\bar{\eta}_{\max}(\xi)$ is reached when the condition of tight coupling holds namely $\xi = -1$ since at this point $\bar{\eta}_{\max} = 1$.

Since the maximum efficiency depends only on the degree of coupling $\xi$, it is possible to bound the efficiency by measuring the degree of coupling. For instance, if it is known that $\xi_{\min} \leqslant \xi$ for all conditions of operation of the machine, then we can deduce from Eq. (4.69) that $\bar{\eta} \leqslant \bar{\eta}_{\max}(\xi_{\min})$.

### 4.3.4 Power-efficiency relations

**Exact relations from the conductance matrix** In this section we derive two upper bounds for the entropy production rate of the output process, a quantity which is the product of the output power of the machine with its affinity. These bounds are functions of the efficiency and hence are called power-efficiency relations, since they represent a constraint for reaching both high power and high efficiency.

To obtain the first bound, we factorize $\mathcal{G}_{1,1} f_1^2$ in Eq. (4.58):

$$- \bar{\sigma}_2 = -\mathcal{G}_{1,1} f_1^2 \left( \frac{\mathcal{G}_{1,2} f_2}{\mathcal{G}_{1,1} f_1} + \frac{\mathcal{G}_{2,2} f_2^2}{\mathcal{G}_{1,1} f_1^2} \right) = -\mathcal{G}_{1,1} f_1^2 \left( \xi \varphi + \varphi^2 \right). \qquad (4.70)$$

From Eq. (4.64) we have $-(\xi\varphi + \varphi^2) = \bar{\eta}(1 + \xi\varphi)$ and therefore

$$- \bar{\sigma}_2 = \mathcal{G}_{1,1} f_1^2 \bar{\eta} \left( 1 + \xi\varphi \right), \qquad (4.71)$$

then using again Eq. (4.64), we can express $\varphi$ in terms of $\bar{\eta}$ and $\xi$ as

$$\varphi^{\pm} = -\frac{\xi \left( \bar{\eta} + 1 \right)}{2} \pm \frac{1}{2} \sqrt{(\bar{\eta} + 1)^2 \xi^2 - 4\bar{\eta}}, \qquad (4.72)$$

where we have used Eq. (4.68-4.69) to guarantee that $\varphi$ is real. Inserting these two solutions in Eq. (4.71), we obtain

$$- \bar{\sigma}_2^{\pm} = \mathcal{G}_{1,1} f_1^2 \bar{\eta} \left( 1 - \xi^2 \frac{1 + \bar{\eta}}{2} \mp \xi \sqrt{\frac{\xi^2}{4} (1 + \bar{\eta})^2 - \bar{\eta}} \right). \qquad (4.73)$$

This equation shows that the relation between the output entropy production rate $-\bar{\sigma}_2$ and the efficiency is in general bi-valued, which means that there are two possible values of the output entropy production rate for the same value of the efficiency. This relation becomes single-valued when $\xi = -1$, i.e. for tight coupling, since in this case $-\bar{\sigma}_2^-$ is equal to zero, and only $-\bar{\sigma}_2^+$ remains.

**Bounds on power from efficiency**    In the general case of arbitrary coupling, it is enough to upper bound $-\bar{\sigma}_2^+$ to obtain a general bound on the output entropy production rate because $-\bar{\sigma}_2^+ \geqslant -\bar{\sigma}_2^-$ for $\xi \in [-1, 0[$. Since one can also show that $-\bar{\sigma}_2^+$ is always a decreasing function of $\xi$ at fixed $\bar{\eta}$, its maximum value is reached at $\xi = -1$, which corresponds to the tight coupling condition. When inserting $\xi = -1$ into the expression of $-\bar{\sigma}_2^+$, we obtain the first inequality:

$$- \bar{\sigma}_2 \leqslant \mathcal{G}_{1,1} f_1^2 \bar{\eta}(1 - \bar{\eta}). \tag{4.74}$$

Alternatively, one can start from Eq. (4.58) and factorize $\mathcal{G}_{2,2} f_2^2$ which leads to $\bar{\sigma}_2 = \mathcal{G}_{2,2} f_2^2 (1 + \xi/\varphi)$. Then, using again the explicit solution of $\varphi$ as a function of $\xi$ and $\bar{\eta}$, one obtains an expression which when evaluated at $\xi = -1$ leads to the second inequality

$$- \bar{\sigma}_2 \leqslant \mathcal{G}_{2,2} f_2^2 \frac{1 - \bar{\eta}}{\bar{\eta}}. \tag{4.75}$$

**Pietzonka-Seifert efficiency-power trade-off**    There are similarities between Eqs. (4.74) and (4.75) with the bounds recently derived in Ref. [143]. We now show how the latter can be derived from the previous bounds. When using the above inequalities (4.45) into (4.74–4.75), one obtains

$$-\bar{\sigma}_2 \;\; \leqslant \;\; \mathcal{G}_{1,1} f_1^2 \bar{\eta}(1 - \bar{\eta}) \leqslant \frac{\mathrm{Var}(\Sigma_1)}{2} \bar{\eta}(1 - \bar{\eta}), \tag{4.76}$$

$$-\bar{\sigma}_2 \;\; \leqslant \;\; \mathcal{G}_{22} f_2^2 \frac{1 - \bar{\eta}}{\bar{\eta}} \leqslant \frac{\mathrm{Var}(\Sigma_2)}{2} \frac{1 - \bar{\eta}}{\bar{\eta}}. \tag{4.77}$$

Thus we retrieve the power-efficiency trade-offs derived by Pietzonka and Seifert [143]

$$-\bar{\sigma}_2 \;\; \leqslant \;\; \frac{\mathrm{Var}(\Sigma_1)}{2} \bar{\eta}(1 - \bar{\eta}), \tag{4.78}$$

$$-\bar{\sigma}_2 \;\; \leqslant \;\; \frac{\mathrm{Var}(\Sigma_2)}{2} \frac{1 - \bar{\eta}}{\bar{\eta}}. \tag{4.79}$$

**Shiraishi *et al.* efficiency-power trade-off**    Shiraishi, Saito and Tasaki have proposed another power efficiency relation involving the machine activity [172], see also Ref. [148] for another derivation of the result. Their result can be retrieved from the conductance matrix framework.

From the power-efficiency relation of Eq. (4.74) and the result of sec. 4.2.4, we derive the power-efficiency trade-off

$$- \bar{\sigma}_2 \leqslant \mathcal{A}_{1,1} \frac{f_1^2}{2} \bar{\eta}(1 - \bar{\eta}). \tag{4.80}$$

We introduce next the matrix

$$\boldsymbol{\mathcal{A}}^{\#} = \boldsymbol{V} \cdot \boldsymbol{R} \cdot \boldsymbol{\mathcal{A}}_e \cdot (\boldsymbol{V} \cdot \boldsymbol{R})^{\mathrm{T}} \tag{4.81}$$

with the matrix $\boldsymbol{\mathcal{A}}_e$ being defined in the sec. 4.2.4. Therefore from the results of the sec. 4.2.5, we have $\mathcal{A}^{\#}{}_{1,1} \geqslant \mathcal{A}_{1,1}$. Hence, we recover the result of Ref. [172], namely

$$- \bar{\sigma}_2 \leqslant \mathcal{A}^{\#}{}_{1,1} \frac{f_1^2}{2} \bar{\eta}(1 - \bar{\eta}). \tag{4.82}$$

where the coefficient is

$$\mathcal{A}^{\#}{}_{1,1} = \left( \sum_{(x,y)} (V^+ \cdot R)_{1,(x,y)} a^{\pi}_{(x,y)} (V \cdot R)^{\mathrm{T}}_{(x,y),1} \right). \tag{4.83}$$

This result indicates that higher activity produces a higher upper bound for NE conductance matrix enabling to reach higher output power. This seems fairly intuitive: whenever the machine undergoes very few transitions per unit time it cannot provide any useful power. The result is here valid only for stationary currents, but it was derived for currents at any time in Ref. [172]. The full case including time-dependent current is left for future work.

## 4.4 Common example: a simple laser

We illustrate the results of this section on our simple model of laser defined in sec. 3.4.

### 4.4.1 Non-equilibrium conductance matrix

Using the formula (4.14) and defining $\mathcal{R}_{e_i}$ as the resistance of the $i^{\text{th}}$ edge, the elements of the non-equilibrium conductance matrix are

$$
\begin{aligned}
\mathcal{G}_{1,1} &= \frac{1}{\mathcal{N}_G}[(E_c - E_b)^2(\mathcal{R}_{e_3} + \mathcal{R}_{e_4}) + (E_a - E_b)^2\mathcal{R}_{e_5} + (E_c - E_a)^2(\mathcal{R}_{e_1} + \mathcal{R}_{e_2})] \\
\mathcal{G}_{1,2} &= \frac{(E_d - E_c)}{\mathcal{N}_G}[(E_c - E_a)(\mathcal{R}_{e_1} + \mathcal{R}_{e_2}) + (E_b - E_a)\mathcal{R}_{e_5}] \\
\mathcal{G}_{2,1} &= \frac{(E_d - E_c)}{\mathcal{N}_G}[(E_c - E_a)(\mathcal{R}_{e_1} + \mathcal{R}_{e_2}) + (E_b - E_a)\mathcal{R}_{e_5}] \\
\mathcal{G}_{2,2} &= \frac{1}{\mathcal{N}_G}[(E_d - E_c)^2(\mathcal{R}_{e_1} + \mathcal{R}_{e_2} + \mathcal{R}_{e_5})]
\end{aligned}
\tag{4.84}
$$

with

$$\mathcal{N}_G = (\mathcal{R}_{e_1} + \mathcal{R}_{e_2} + \mathcal{R}_{e_5})(\mathcal{R}_{e_3} + \mathcal{R}_{e_4} + \mathcal{R}_{e_5}) - \mathcal{R}_{e_5}^2. \tag{4.85}$$

As expected, it is a real symmetric positive definite-matrix.

**Degree of coupling**   The degree of coupling is then deduced from the conductance matrix

$$
\xi = \frac{(E_d - E_c)[(E_c - E_a)(\mathcal{R}_{e_1} + \mathcal{R}_{e_2}) + (E_b - E_a)\mathcal{R}_{e_5}]}{[(E_c - E_b)^2(\mathcal{R}_{e_3} + \mathcal{R}_{e_4}) + (E_a - E_b)^2\mathcal{R}_{e_5} + (E_c - E_a)^2(\mathcal{R}_{e_1} + \mathcal{R}_{e_2})]}
$$
$$
\times \frac{1}{[(E_d - E_c)^2(\mathcal{R}_{e_1} + \mathcal{R}_{e_2} + \mathcal{R}_{e_5})]} \tag{4.86}
$$

**Onsager matrix**   In the close to equilibrium case, the conductance matrix is the Onsager matrix. We plot the Frobenius norm of $\boldsymbol{\mathcal{G}} - \boldsymbol{\mathcal{L}}$ in Fig. 4.1 varying one of the physical affinity when holding the other to zero. We have equality between $\boldsymbol{\mathcal{G}}$ and $\boldsymbol{\mathcal{L}}$ for equilibrium when both physical affinities are zero. We also shown the equality case in Eqs. (4.44) and (4.52) for equilibrium. Unlike the previous matrix, the degenerate matrix $\boldsymbol{\mathcal{G}}^{\min}$ does not collapse with the conductance matrix nor with the Onsager matrix for equilibrium case. In particular, this implies that the thermodynamics uncertainty relation (4.47) are not an equality at equilibrium when considering only partial entropy production.
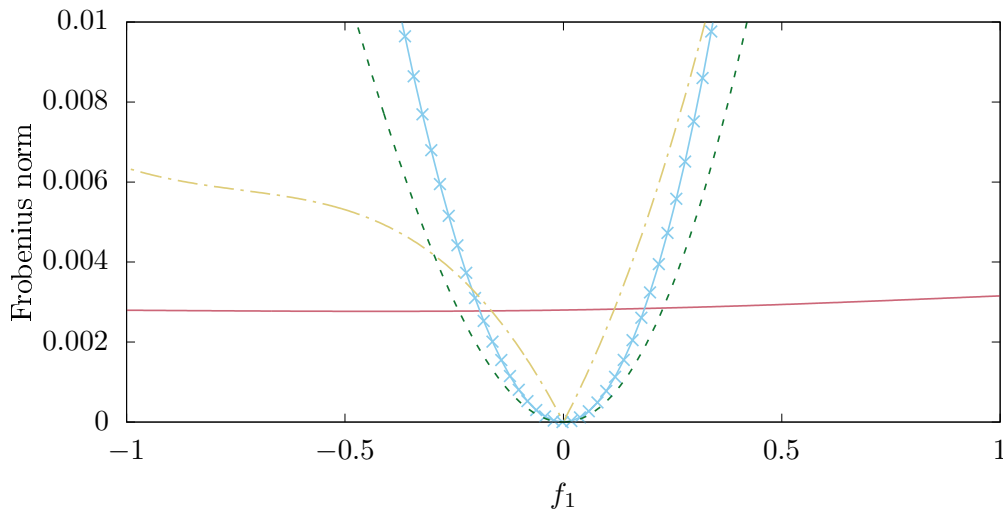


Figure 4.1: Frobenius matrix norm of $\dfrac{\mathbf{Cov}}{2} - \boldsymbol{\mathcal{G}}$ (light blue line with crosses) $\dfrac{\boldsymbol{\mathcal{A}}}{2} - \boldsymbol{\mathcal{G}}$ ( green dashed line), $\boldsymbol{\mathcal{G}}^{\min} - \boldsymbol{\mathcal{G}}$ (red line) and $\boldsymbol{\mathcal{G}} - \boldsymbol{\mathcal{L}}$ (yellow dot-dashed line) as a function of $f_1$ when $f_2 = 0$. The kinetic parameters are $\Gamma_{\mathrm{pump}} = 0.1$, $\Gamma_{\mathrm{laser}} = 10$, $\Gamma_{\mathrm{gas}} = 1$, $E_a = 0.5$, $E_b = 4$, $E_c = 1.5$, $E_d = 1$.

## 4.4.2   Maximum efficiency

The maximal efficiency given by Eq. (4.68) is shown as function of the degree of coupling in Fig. (4.2). This maximal efficiency is compared with the efficiency of the laser model which is analytically solvable. In order to test this bound, we vary either (i) the thermodynamic forces (3.57), via the variation of the heat baths inverse temperature, which together characterize the distance to equilibrium, or (ii) the kinetic parameters of the model (the baths coupling constant and the energy levels). The test (i) is carried out in the main figure in which either the affinity $f_2$ is varied at fixed $f_1$ or vice versa, covering a large regime of conditions far from equilibrium. The test (ii) is carried out in the inset, by scanning over a large panel of kinetic parameters. Both figures confirm that the maximum efficiency only depends on the degree of coupling. These figures also show that this maximum efficiency is physically accessible.
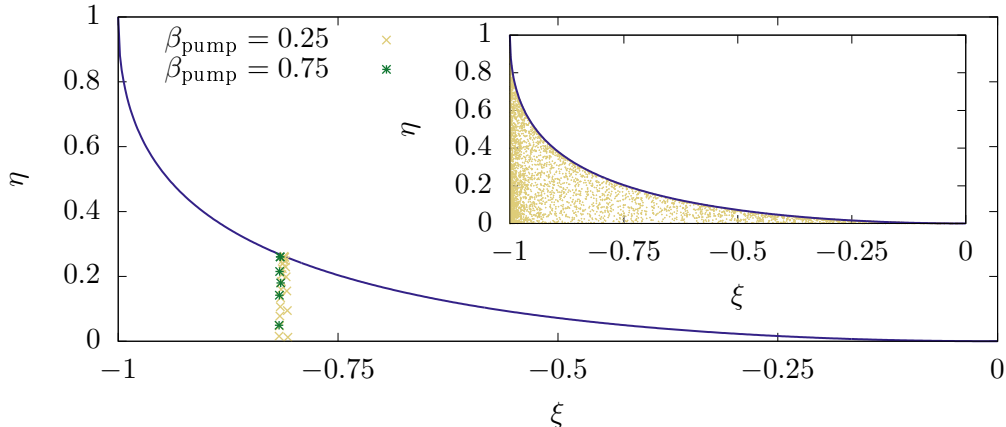
Figure 4.2: Illustration of the bound of Eq. (4.69) on efficiency (blue solid line) for the laser model. For a given $\beta_{\text{pump}}$ the inverse temperature $\beta_{\text{laser}}$ is varied. The kinetic parameters are $\Gamma_{\text{pump}} = 0.1$, $\Gamma_{\text{laser}} = 10$, $\Gamma_{\text{gas}} = 1$, $E_a = 0.5$, $E_b = 4$, $E_c = 1.5$, $E_d = 1$. Inset: Efficiency versus degree of coupling when varying all kinetic parameters at fixed affinities $f_1 = 0.5$ and $f_2 = 0.75$. The kinetic parameters listed above are randomly chosen by multiplying the values used in the main figure by $e^x$ with $x$ drawn uniformly within $[-2, 2]$.

### 4.4.3 Power-efficiency relation

**Power-efficiency from the condutance matrix** Fig. 4.3a and 4.3b illustrate the power-efficiency trade-off, by showing the mean output entropy production rate $-\bar{\sigma}_2$ as function of the efficiency $\eta$. A striking feature in these plots is that the entropy production rate is bi-valued as explained in section 4.3.4. In order to test the inequality of Eqs. (4.74–4.75), we compare $-\langle \sigma_2 \rangle$ (solid line) evaluated using exact expressions of the average currents, with the power-efficiency bounds of Eqs. (4.74–4.75) (empty symbols).

**Pietzonka-Seifert power-efficiency trade-off** The Fig. 4.3a shows a comparison with the power-efficiency inequalities derived by Pietzonka and Seifert [143] (full symbols). The variances appearing in these inequalities have been evaluated from the cumulant generating function of the currents obtained from the highest eigenvalue of tilted matrix. We confirm with this figure that the new bound derived from the present framework is better than the bounds derived in Ref. [143], in agreement with Eqs. (4.76).

**Shiraishi _et al._ power-efficiency trade-off** The Fig. 4.3b shows a comparison with the power-efficiency inequality derived by Shiraishi _et al._ [172] (line with symbols) and the one derived from matrix $\mathcal{A}$ (full circles) As expected, the bounds of Shiraishi _et al._ [172] is less tight due to the difference between edgewise and cyclewise matrix, as explained in sec. 4.2.5.
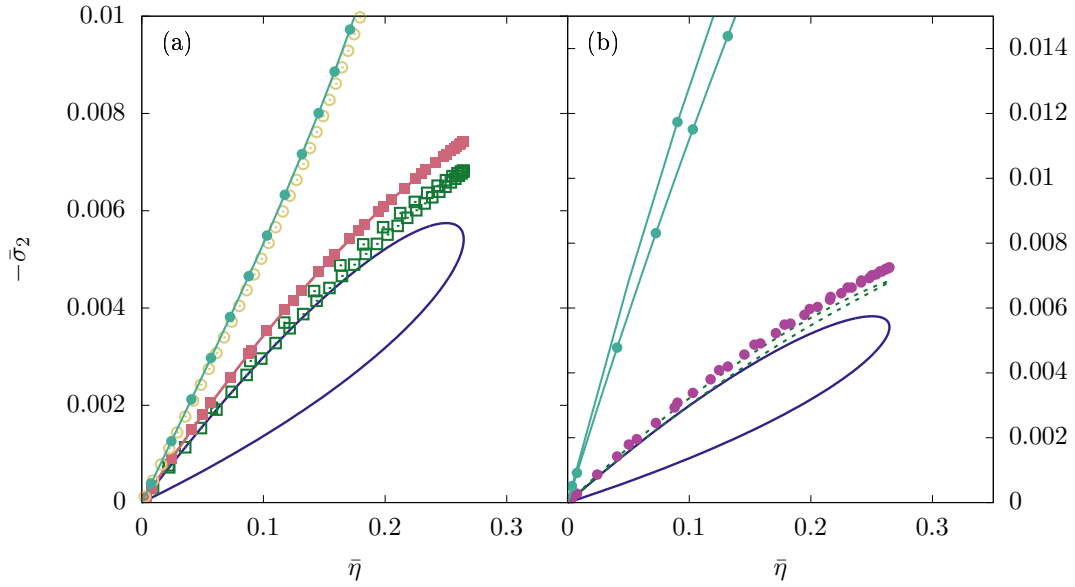
Figure 4.3: Output power as a function of the machine efficiency using exact expression (solid blue line) compared to various power-efficiency bounds. (a) Power-efficiency bounds of Eqs. (4.74) (green open squares) and (4.75) (yellow open circles) compared to Pietzonka-Seifert trade-offs (4.78) (magenta full squares) and (4.79) (blue full circles) (b) Power-efficiency bounds of Eqs. (4.74) (green dashed line) and (4.80) (violet full circles) compared to Shiraishi *et al.* trade-off (4.82) (blue full circles)

# Efficiency fluctuations

In this chapter, we address two different questions about efficiency fluctuations. First, we explore the consequences of the non-equilibrium conductance matrix framework. Using the bound on the currents LDF, we demonstrate the existence of bounds on the efficiency LDF. These bounds are related with the mean value of the entropy production rate or alternatively to the non-equilibrium conductance matrix.

Next we study the efficiency fluctuations for machines with three physical currents. We aim to model machines with losses, when not all currents in the systems are known. We show the consistence with the result of sec. 3.3, namely when the losses are small, we retrieve the previously derived properties of the efficiency LDF.

## 5.1 Bounds on efficiency LDF

Bounds on efficiency fluctuations can be established either from bound on the entropy production LDF $I(\sigma)$ or from the conductance matrix. Both ways offers different insight into efficiency fluctuations.

### 5.1.1 Scale of the LDF

Pietzonka *et al.* [141] have derived numerous bounds on entropy production LDF $I(\sigma)$. We show in this section, that these bounds constrain the scale of the efficiency LDF.

**Bounds from Entropy production LDF** Let's first show that a bound on $I(\sigma)$ give a bound on $J(1)$. As this is the maximum of the efficiency LDF, we obtain the scale of the efficiency LDF.

The total entropy production LDF $I(\sigma)$ is obtained from the partial entropy productions LDF $I(\sigma_1, \sigma_2)$ as

$$I(\sigma) = \min_{\sigma_1} I(\sigma_1, \sigma - \sigma_1). \tag{5.1}$$

Due to the symmetry of the fluctuation theorem $I(\sigma_1, -\sigma_1) = I(-\sigma_1, \sigma_1)$ and the convexity of $I$, the minimum of $I(\sigma_1, -\sigma_1)$ is obtained for $\sigma_1 = 0$ such that $I(0) = I(0,0)$. From the results of sec. 3.3.1, the maximum of the efficiency LDF is $J(1) = I(0,0)$. Hence, any bound on $I(0)$ gives a bound on the scale of the efficiency LDF.

**Parabolic bound**    The first result from Ref. [141] is a parabolic bound on entropy production LDF as

$$I(\sigma) \leqslant I(0) \leqslant \frac{(\sigma - \bar{\sigma})^2}{4\bar{\sigma}} \tag{5.2}$$

Notice that this bound is also a particular case of the quadratic bound derived in the previous chapter. This bound yields

$$J(\eta) \leqslant \frac{\bar{\sigma}}{4}. \tag{5.3}$$

Therefore the efficiency fluctuations have higher probability and accordingly take more time to decay when the system dissipates less. Indeed the time scale on which an efficiency fluctuation disappears is roughly given by the inverse of the maximum value of the efficiency LDF, that is bounded by the mean total entropy production rate. This seems quite intuitive, the more the system dissipates, *e.g.* by taking a macroscopic limit, the less the efficiency fluctuates.

**Exponential bound**    Another interesting bound from Ref. [141] is an exponential bound

$$I(\sigma) \leqslant \begin{cases} \frac{\bar{a}_{\text{tot}}}{\bar{\sigma}} \left( \bar{\sigma} + \sigma - \sigma \ln \left| \frac{\sigma}{\bar{\sigma}} \right| \right) - \sigma & \sigma \leqslant -\bar{\sigma} \exp \left[ -\frac{\bar{\sigma}}{2\bar{a}_{\text{tot}}} \right] \\ \frac{\bar{a}_{\text{tot}}}{\bar{\sigma}} \left( \bar{\sigma} - \sigma + \sigma \ln \left| \frac{\sigma}{\bar{\sigma}} \right| \right) & \sigma \geqslant \bar{\sigma} \exp \left[ -\frac{\bar{\sigma}}{2\bar{a}_{\text{tot}}} \right] \\ a_{\text{tot}} \left( 1 - \exp \left[ -\frac{\bar{\sigma}}{2\bar{a}_{\text{tot}}} \right] \right) - \frac{\sigma}{2} & \text{otherwise} \end{cases} , \tag{5.4}$$

in terms of the mean total activity $\bar{a}_{\text{tot}} = \sum_{(x,y)} a_{(x,y)}^\pi$. That yields

$$J(\eta) \leqslant \bar{a}_{\text{tot}} \left( 1 - \exp \left[ -\frac{\bar{\sigma}}{2\bar{a}_{\text{tot}}} \right] \right) \leqslant \frac{\bar{\sigma}}{2} \tag{5.5}$$

The second inequality is obtained from $1 - e^{-x} \leqslant x$. These bounds are plotted in Fig. 5.1a for the laser model introduced in sec. 3.4 with random parameters. We observe that the parabolic bound is quite close to $J(1)$ and gives in general better bounds than the exponential bounds but not always.

**Others bounds**    Others bounds have been derived on entropy production LDF [140, 141, 149]. They require more information on the system in general, but give more precise bounds on the entropy production fluctuations. Evaluating these alternative bounds at zero entropy production will produce new bounds on efficiency LDF.

## 5.1.2 Bounds from conductance matrix

However to obtain bounds not only on the maximum of the efficiency LDF but on the whole efficiency LDF, we need a bound on the entropy productions LDF $I(\sigma_1, \sigma_2)$. We use now the result of sec. 4.1.2 to construct a bound on the efficiency LDF derived from the non-equilibrium conductance matrix.

**Quadratic bound** A quadratic bound on entropy production LDF is easily derived from the quadratic bound (4.30) on currents LDF as

$$I_{\text{quad}}(\sigma_1, \sigma_2) = (\sigma_1, \sigma_2) \begin{pmatrix} G_{1,1}f_1^2 & G_{1,2}f_1f_2 \\ G_{1,2}f_1f_2 & G_{2,2}f_2^2 \end{pmatrix}^{-1} \begin{pmatrix} \sigma_1 \\ \sigma_2 \end{pmatrix}. \tag{5.6}$$

The quadratic bound on efficiency LDF is obtained by contraction of Eq. (5.6)

$$J_{\text{quad}}(\eta) = \frac{\bar{\sigma}_1^2}{4} \frac{(\eta - \bar{\eta})^2}{G_{1,1}f_1^2\eta^2 + 2G_{1,2}f_1f_2\eta + G_{2,2}f_2^2} \tag{5.7}$$

$$= \frac{\bar{\sigma}_1^2}{4G_{1,1}f_1^2} \frac{(\eta - \bar{\eta})^2}{\eta^2 + 2\xi\varphi\eta + \varphi^2}, \tag{5.8}$$

using the parametrization of the efficiency of sec. 4.3.1. Not only the conductance matrix is connected to the macroscopic efficiency, but it also constrains the efficiency fluctuations. We also connect the functional form of Eq. (5.7) with the one of the efficiency LDF in linear response case (3.52), given in both case by the ratio of two quadratic forms.
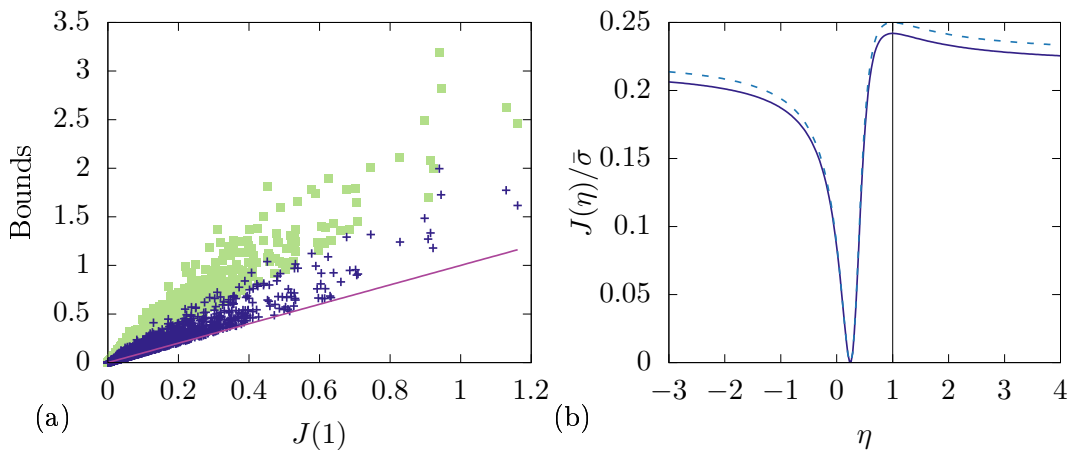


Figure 5.1: (a) Comparison of bounds (5.3) (blue crosses) and (5.5) (green squares). The red solid line is the line of equation $y = x$. (b) Quadratic bound of Eq. (5.7) (greem dashed line) compared to the efficiency LDF $J(\eta)$ (blue solid line). Figures are drawn using the laser model defined in sec. 3.4. The kinetic parameters are $\Gamma_{\text{pump}} = 0.1$, $\Gamma_{\text{laser}} = 10$, $\Gamma_{\text{gas}} = 1$, $E_a = 0.5$, $E_b = 4$, $E_c = 1.5$, $E_d = 1$ for right figure. For left figure they are randomly chosen by multiplying the previous values $e^x$ with $x$ drawn uniformly within $[-2, 2]$. Affinities are set to $f_1 = 0.5$ and $f_2 = 0.75$ for both figures.

**Connection with parabolic bound** The maximum of the quadratic bounds (5.7) is

$$J_{\text{quad}}(1) = \frac{\bar{\sigma}}{4}. \tag{5.9}$$

To connect with Eq. (5.3). When the degree of coupling in Eq. (5.8) is $-1$, the bounds becomes

$$J(\eta) \leqslant \begin{cases} 0 & \text{if } \eta = \bar{\eta} \\ \dfrac{\bar{\sigma}}{4} & \text{otherwise} \end{cases}. \tag{5.10}$$

The parabolic bound (5.3) then assumes the tight coupling of entropy production.

The bounds of Eqs. (5.7) and (5.9) are plotted on Fig. 5.1b for the simple model of machine already defined in sec. 3.4. As expected, the maximum of the quadratic bound $J_{\text{quad}}(1)$ is obtained for $\bar{\sigma}/4$ given by the parabolic bound.

## 5.2 Efficiency fluctuations of small machines in presence of losses

Beyond bounds on efficiency LDF, we also study the case of efficiency fluctuations in presence of losses.

### 5.2.1 Modeling the losses

As defined in sec. 3.1, a machine is a system with two physical fluxes. We consider now system with three fluxes. The first and second fluxes still represent input and output process. Our third process will either flow spontaneously $\bar{\sigma}_3 > 0$, and the machine will have two input processes, the third process helping with the machine objective; or in the opposite direction when $\bar{\sigma}_3 < 0$, and the machine will have two output processes, in this case the third process models losses, *i.e.* energy that goes somewhere else.

We define the stochastic efficiencies $\eta_1$, $\eta_2$, and $\eta_3$ by

$$\eta_1 = -\frac{\sigma_1}{\sigma_1} = -1, \quad \eta_2 = -\frac{\sigma_2}{\sigma_1} \quad \text{and} \quad \eta_3 = -\frac{\sigma_3}{\sigma_1}, \tag{5.11}$$

where $\eta_1$ has been introduced by convention. The most probable values of $\eta_2$ and $\eta_3$ converge in the long time limit to the macroscopic values $\bar{\eta}_2$ and $\bar{\eta}_3$ defined by

$$\bar{\eta}_2 = -\frac{\bar{\sigma}_2}{\bar{\sigma}_1} \qquad \text{and} \qquad \bar{\eta}_3 = -\frac{\bar{\sigma}_3}{\bar{\sigma}_1}, \tag{5.12}$$

which are the conventional thermodynamic efficiencies. Since the second law imposes $\bar{\sigma} \geqslant 0$, we have the following constraint on the macroscopic efficiencies

$$\bar{\eta}_2 + \bar{\eta}_3 \leqslant 1, \tag{5.13}$$

that is reminiscent of the Carnot Bound for machines with two physical currents and a unique efficiency. We remark here that the third process may model losses since it decreases the upper bound of the efficiency $\bar{\eta}_2 \leqslant 1 - \bar{\eta}_3$.

Below, we study the fluctuations of the efficiencies $(\eta_2, \eta_3)$ considering that the statistics of all the entropy productions $(\sigma_1, \sigma_2, \sigma_3)$ is accessible. We will next consider the case where the statistics of the third entropy production is unknown, that is presumably a more common situation.

## 5.2.2 Definition of the large deviation function of the efficiencies

We denote by $P_t(\sigma_1, \sigma_2, \sigma_3)$ the probability density of the entropy production rates $\sigma_1, \sigma_2, \sigma_3$ after a time $t$. Assuming that a large deviation principle holds, this probability density is asymptotically given at large time by

$$P_t(\sigma_1, \sigma_2, \sigma_3) \asymp \exp\{-tI(\sigma_1, \sigma_2, \sigma_3)\}. \tag{5.14}$$

Following Ref. [189], we obtain the LDF of the efficiencies from the LDF of the entropy productions. The joint probability density at time $t$ to observe efficiencies $\eta_2$ and $\eta_3$ is given by

$$P_t(\eta_2, \eta_3) = \int d\sigma_1 d\sigma_2 d\sigma_3 P_t(\sigma_1, \sigma_2, \sigma_3) \times \delta\left(\eta_2 + \frac{\sigma_2}{\sigma_1}\right) \delta\left(\eta_3 + \frac{\sigma_3}{\sigma_1}\right). \tag{5.15}$$

Using Eq. (5.14) in Eq. (5.15) and the saddle point method to compute the integral, we find for large time

$$P_t(\eta_2, \eta_3) \asymp \exp\{-tJ(\eta_2, \eta_3)\}, \tag{5.16}$$

where

$$J(\eta_2, \eta_3) = \min_{\sigma_1} I(\sigma_1, -\eta_2\sigma_1, -\eta_3\sigma_1)\}. \tag{5.17}$$

From this, we deduce that $J$ is a non-negative and bounded function, with for all $\eta_2, \eta_3$

$$0 \leqslant J(\eta_2, \eta_3) \leqslant I(0, 0, 0), \tag{5.18}$$

**Efficiency LDF from CGF** The efficiency LDF also follows from the cumulant generating function (CGF) $\phi(\gamma_1, \gamma_2, \gamma_3)$ of the entropy productions [189]. Indeed, when $I$ is convex, $\phi$ and $I$ are conjugated by Legendre transform

$$I(\sigma_1, \sigma_2, \sigma_3) = \max_{\gamma_1, \gamma_2, \gamma_3} \left\{ \sum_{i=1}^{3} \gamma_i \sigma_i - \phi(\gamma_1, \gamma_2, \gamma_3) \right\}. \tag{5.19}$$

We can write

$$I(\sigma_1, -\eta_2\sigma_1, -\eta_3\sigma_1) = \max_{\gamma_1, \gamma_2, \gamma_3} \left[ (\gamma_1 - \gamma_2\eta_2 - \gamma_3\eta_3)\sigma_1 - \phi(\gamma_1, \gamma_2, \gamma_3) \right] \tag{5.20}$$

and the minimization of Eq. (5.17) gives

$$J(\eta_2, \eta_3) = \min_{\sigma_1} \max_{\gamma_1, \gamma_2, \gamma_3} \left[ (\gamma_1 - \gamma_2\eta_2 - \gamma_3\eta_3)\sigma_1 - \phi(\gamma_1, \gamma_2, \gamma_3) \right]. \tag{5.21}$$

We set $\gamma = \gamma_1 - \gamma_2\eta_2 - \gamma_3\eta_3$ to obtain

$$J(\eta_2, \eta_3) = \min_{\sigma_1} \max_{\gamma} \left\{ \gamma\sigma_1 + \max_{\gamma_2,\gamma_3} \left[ -\phi(\gamma + \gamma_2\eta_2 + \gamma_3\eta_3, \gamma_2, \gamma_3) \right] \right\}. \qquad (5.22)$$

We now define the function

$$\begin{aligned}
f_{\eta_2,\eta_3}(\gamma) &= -\max_{\gamma_2,\gamma_3} \left\{ -\phi(\gamma + \gamma_2\eta_2 + \gamma_3\eta_3, \gamma_2, \gamma_3) \right\} \\
&= \min_{\gamma_2,,\gamma_3} \phi(\gamma + \gamma_2\eta_2 + \gamma_3\eta_3, \gamma_2, \gamma_3) \qquad (5.23)
\end{aligned}$$

and its Legendre transform

$$\mathcal{F}_{\eta_2,\eta_3}(\sigma_1) = \max_{\gamma} \left\{ \gamma\sigma_1 - f_{\eta_2,\eta_3}(\gamma) \right\}. \qquad (5.24)$$

Then the efficiency LDF can be rewritten

$$\begin{aligned}
J(\eta_2, \eta_3) &= \min_{\sigma_1} \max_{\gamma} \left\{ \gamma\sigma_1 - f_{\eta_2,\eta_3}(\gamma) \right\} \\
&= \min_{\sigma_1} \mathcal{F}_{\eta_2,\eta_3}(\sigma_1) \\
&= -\max_{\sigma_1} \left\{ -\mathcal{F}_{\eta_2,\eta_3}(\sigma_1) \right\} \\
&= -f_{\eta_2,\eta_3}(0). \qquad (5.25)
\end{aligned}$$

Using Eq. (5.23), we conclude that

$$J(\eta_2, \eta_3) = -\min_{\gamma_2,\gamma_3} \phi(\gamma_2\eta_2 + \gamma_3\eta_3, \gamma_2, \gamma_3). \qquad (5.26)$$

This formula is of particular interest since CGF are more convenient to compute in practice.

### 5.2.3 Shape of the efficiencies LDF

In this section we look for the specific features of the various extrema of the efficiency LDF $J$. We first show that the location of the maxima follows from a linear constraint on the efficiencies, second that $J$ has a unique global minimum, and third that no other extremum exists at finite values of the efficiency. All these features are illustrated in Sec. 5.2.6.

**Maximum of the efficiency LDF**   We look for the location of the maxima of $J$. Since we have $J(\eta_2, \eta_3) \leqslant I(0,0,0)$, if there exists at least one couple $(\eta_2^*, \eta_3^*)$ satisfying

$$J(\eta_2^*, \eta_3^*) = I(0,0,0), \qquad (5.27)$$

then $(\eta_2^*, \eta_3^*)$ is the position of a maximum. Along a contour line of the entropy productions LDF, the total differential of $I$ vanishes,

$$\mathrm{d}I = \sum_{i=1}^{3} \frac{\partial I}{\partial \sigma_i} \mathrm{d}\sigma_i = \mathrm{d}\sigma_1 \left( \frac{\partial I}{\partial \sigma_1} + \frac{\partial I}{\partial \sigma_2} \frac{\mathrm{d}\sigma_2}{\mathrm{d}\sigma_1} + \frac{\partial I}{\partial \sigma_3} \frac{\mathrm{d}\sigma_3}{\mathrm{d}\sigma_1} \right) = 0. \qquad (5.28)$$

At the origin, we have $\eta_i^* = -\mathrm{d}\sigma_i/\mathrm{d}\sigma_1$ with $i = 2, 3$ where the $\eta_i^*$ are defined by $J(\eta_2^*, \eta_3^*) = I(0, 0, 0)$. So,

$$\left.\frac{\partial I}{\partial \sigma_2}\right|_0 \left(\left.\frac{\partial I}{\partial \sigma_1}\right|_0\right)^{-1} \eta_2^* + \left.\frac{\partial I}{\partial \sigma_3}\right|_0 \left(\left.\frac{\partial I}{\partial \sigma_1}\right|_0\right)^{-1} \eta_3^* = 1 \tag{5.29}$$

where the subscript $0$ indicates evaluation in the origin. All efficiencies respecting Eq. (5.29) also verify Eq. (5.27). This ensemble is a straight line in the plane $(\eta_2, \eta_3)$ .

We now use the fluctuation theorem for the entropy productions:

$$I(\sigma_1, \sigma_2, \sigma_3) - I(-\sigma_1, -\sigma_2, -\sigma_3) = -\sigma_1 - \sigma_2 - \sigma_3. \tag{5.30}$$

Taking the partial derivatives of this equation at origin yields

$$\left.\frac{\partial I}{\partial \sigma_i}\right|_0 + \left.\frac{\partial I}{\partial \sigma_i}\right|_0 = -1 \quad \text{with} \quad i \in \{1, \ldots, 3\}. \tag{5.31}$$

This allow to simplify Eq. (5.29) into

$$\eta_2^* + \eta_3^* = 1. \tag{5.32}$$

From Eq. (5.13) we see that the efficiencies satisfying Eq. (5.32) correspond to efficiencies obtained along the reversible trajectories (even though the system is out of equilibrium). The unique, reversible, and least likely efficiency of an engine with two processes is replaced, for an engine with three processes, by a couple of reversible efficiencies, one of arbitrary value and the other one following from Eq. (5.32).

**Global minimum of the efficiency LDF** Assuming the convexity and no constant region, $I$ has a unique minimum at $(\bar{\sigma}_1, \bar{\sigma}_2, \bar{\sigma}_3)$. The efficiency LDF $J$ vanishes at the macroscopic efficiencies $(\bar{\eta}_2, \bar{\eta}_3)$ given by Eq. (5.12),

$$J(\bar{\eta}_2, \bar{\eta}_3) = \min_{\sigma_1} I\left(\sigma_1, \sigma_1 \frac{\bar{\sigma}_2}{\bar{\sigma}_1}, \sigma_1 \frac{\bar{\sigma}_3}{\bar{\sigma}_1}\right) = 0, \tag{5.33}$$

where the minimum is reached for $\sigma_1 = \bar{\sigma}_1$. Since $J$ is a non-negative function, $(\bar{\eta}_2, \bar{\eta}_3)$ is a global minimum.

If $I$ has a constant region, due to its convexity, it is necessarily a region around $(\bar{\sigma}_1, \bar{\sigma}_2, \bar{\sigma}_3)$ where the LDF of entropy production vanishes. In this case, the minimum of $J$ is not unique, but is a domain including $(\bar{\eta}_2, \bar{\eta}_3)$.

**Asymptotic behavior of the efficiency LDF** Let us now verify that $J$ has no other extremum than $(\bar{\eta}_2, \bar{\eta}_3)$ and $(\eta_2^*, \eta_3^*)$. To do so, we look for the zeros of the partial derivatives of $J$ with respect to $\eta_2$ and $\eta_3$,

$$\frac{\partial J}{\partial \eta_2}(\eta_2, \eta_3) = 0 \quad \text{and} \quad \frac{\partial J}{\partial \eta_3}(\eta_2, \eta_3) = 0. \tag{5.34}$$

Since $J$ follows from a minimization on $\sigma_1$, see Eq. (5.17), we introduce the function $\widetilde{\sigma}_1(\eta_2, \eta_3)$ as the solution of

$$0 = \frac{\mathrm{d}}{\mathrm{d}\widetilde{\sigma}_1}\left[I(\widetilde{\sigma}_1, -\eta_2\widetilde{\sigma}_1, -\eta_3\widetilde{\sigma}_1)\right] = \frac{\partial I}{\partial \sigma_1} - \eta_2 \frac{\partial I}{\partial \sigma_2} - \eta_3 \frac{\partial I}{\partial \sigma_3}, \qquad (5.35)$$

with all partial derivatives evaluated in $(\widetilde{\sigma}_1, -\eta_2\widetilde{\sigma}_1, -\eta_3\widetilde{\sigma}_1)$. This allows us to write the efficiency LDF as

$$J(\eta_2, \eta_3) = I(\widetilde{\sigma}_1(\eta_2, \eta_3), -\eta_2\widetilde{\sigma}_1(\eta_2, \eta_3), -\eta_3\widetilde{\sigma}_1(\eta_2, \eta_3)). \qquad (5.36)$$

From this equation, the partial derivative of $J$ may be written as

$$\frac{\partial J}{\partial \eta_2}(\eta_2, \eta_3) = \frac{\partial \widetilde{\sigma}_1}{\partial \eta_2} \frac{\partial I}{\partial \sigma_1} - \left(\eta_2 \frac{\partial \widetilde{\sigma}_1}{\partial \eta_2} + \widetilde{\sigma}_1\right) \frac{\partial I}{\partial \sigma_2} - \eta_3 \frac{\partial \widetilde{\sigma}_1}{\partial \eta_2} \frac{\partial I}{\partial \sigma_3}, \qquad (5.37)$$

where partial derivatives are still taken at $(\widetilde{\sigma}_1, -\eta_2\widetilde{\sigma}_1, -\eta_3\widetilde{\sigma}_1)$, with $\widetilde{\sigma}_1 = \widetilde{\sigma}_1(\eta_2, \eta_3)$. From Eqs. (5.35) and (5.37), it is possible to rewrite Eq. (5.34) as

$$\widetilde{\sigma}_1 \frac{\partial I}{\partial \sigma_2}(\widetilde{\sigma}_1, -\eta_2\widetilde{\sigma}_1, -\eta_3\widetilde{\sigma}_1) = 0, \qquad (5.38)$$

$$\widetilde{\sigma}_1 \frac{\partial I}{\partial \sigma_3}(\widetilde{\sigma}_1, -\eta_2\widetilde{\sigma}_1, -\eta_3\widetilde{\sigma}_1) = 0. \qquad (5.39)$$

We distinguish now two different cases: first, the partial derivatives of $I$ may vanish and we recover the minimum of $J$ studied in Sec. 5.2.3; secondly, the function $\widetilde{\sigma}_1(\eta_2, \eta_3)$ vanishes. In the latter case, we look for $(\widetilde{\eta}_2, \widetilde{\eta}_3)$ such that $\widetilde{\sigma}_1(\widetilde{\eta}_2, \widetilde{\eta}_3) = 0$. In this view, we evaluate Eq.(5.36) at $(\widetilde{\eta}_2, \widetilde{\eta}_3)$ yielding, if $\widetilde{\eta}_2$ and $\widetilde{\eta}_3$ are finite,

$$J(\widetilde{\eta}_2, \widetilde{\eta}_3) = I(0, 0, 0), \qquad (5.40)$$

such that we retrieve the extrema $(\widetilde{\eta}_2, \widetilde{\eta}_3) \in (\eta_2^*, \eta_3^*)$ of Sec. 5.2.3. Alternatively, if one of the efficiencies, for instance $\eta_2$, is infinite, Eq. (5.36) becomes

$$\lim_{\eta_2 \to \pm\infty} J(\eta_2, \eta_3) = \lim_{\eta_2 \to \pm\infty} I\left(\widetilde{\sigma}_1(\eta_2, \eta_3), -\eta_2\widetilde{\sigma}_1(\eta_2, \eta_3), -\eta_3\widetilde{\sigma}_1(\eta_2, \eta_3)\right) \qquad (5.41)$$

$$\leqslant I(0, 0, 0). \qquad (5.42)$$

From the last inequality and the convexity of $I$ we conclude that $\eta_2\widetilde{\sigma}_1(\eta_2, \eta_3)$ stays finite when $\eta_2 \to \pm\infty$, and necessarily

$$\lim_{\eta_2 \to \pm\infty} \widetilde{\sigma}_1(\eta_2, \eta_3) = 0. \qquad (5.43)$$

The derivative of $J$ vanishes at infinite efficiencies and the efficiency LDF converges to a finite value at large efficiencies since $J$ is bounded. Moreover the limit $\lim_{\eta_2 \to \pm\infty} \eta_2\widetilde{\sigma}_1(\eta_2, \eta_3)$ is a constant independent of $\eta_3$, it follows that the limit $\lim_{\eta_2 \to \pm\infty} J(\eta_2, \eta_3)$ is also independent of $\eta_3$, if $\eta_3$ remains finite. The same arguments hold when taking the limit $\eta_3 \to \pm\infty$ keeping $\eta_2$ finite. In the end, we have recovered all the extrema at finite values of the efficiencies and shown that the two partial derivatives of $J$ vanish at large efficiencies.

## 5.2.4 Efficiency statistics of a machine with three processes: Forgetting the third process

We now study the fluctuations of the efficiency $\eta_2$ without taking into account the statistics on the third process. This may correspond to an experimental set-up for which the third current exists, but cannot be measured. In this case, we consider that $\eta_3$ (or equivalently $\sigma_3$) always takes the typical value associated with some given efficiency $\eta_2$: this leads to contracting the LDF $J(\eta_2, \eta_3)$ on $\eta_3$. We analyze in this section the general shape of the contracted LDF and study its extrema.

The contracted LDF is by definition

$$J_{\mathrm{ct}}(\eta_2) = \min_{\eta_3} J(\eta_2, \eta_3) = \min_{\sigma_1} I_{\mathrm{ct}}(\sigma_1, -\eta_2 \sigma_1), \tag{5.44}$$

with

$$I_{\mathrm{ct}}(\sigma_1, \sigma_2) = \min_{\eta_3} I(\sigma_1, \sigma_2, -\eta_3 \sigma_1) = \min_{\sigma_3} I(\sigma_1, \sigma_2, \sigma_3). \tag{5.45}$$

As in the previous case, we can express the contracted efficiency LDF in terms of the CGF:

$$J_{\mathrm{ct}}(\eta_2) = -\min_{\gamma_2} \phi(\gamma_2 \eta_2, \gamma_2, 0). \tag{5.46}$$

We now determine some properties of this contracted LDF. From (5.44), we have for all $\eta_2$

$$0 \leqslant J_{\mathrm{ct}}(\eta_2) \leqslant I_{\mathrm{ct}}(0, 0), \tag{5.47}$$

so $J_{\mathrm{ct}}$ is a non-negative, bounded function. In particular, we are interested in the extrema of $J_{\mathrm{ct}}$.

First, looking for the minimum, we have

$$J_{\mathrm{ct}}(\bar{\eta}_2) \leqslant J(\bar{\eta}_2, \bar{\eta}_3) = 0, \tag{5.48}$$

so, due to the positivity of $J_{\mathrm{ct}}$, the efficiency $\bar{\eta}_2$ is a global minimum of $J_{\mathrm{ct}}$, and corresponds to the macroscopic efficiency.

Second, we look for the maximum of $J_{\mathrm{ct}}(\eta_2)$. We call $\eta_{2,\mathrm{ct}}^*$ the efficiency such that $J_{\mathrm{ct}}(\eta_{2,\mathrm{ct}}^*) = I_{\mathrm{ct}}(0, 0)$, and, reasoning as sec. 5.2.3, we have

$$\eta_{2,\mathrm{ct}}^* = \left( \left. \frac{\partial I_{\mathrm{ct}}}{\partial \sigma_1} \right|_0 \right) \left( \left. \frac{\partial I_{\mathrm{ct}}}{\partial \sigma_2} \right|_0 \right)^{-1}, \tag{5.49}$$

Since $I_{\mathrm{ct}}$ follows from the minimization of Eq. (5.45) over $\sigma_3$, we introduce $\widetilde{\sigma}_3(\sigma_1, \sigma_2)$ the solution of this minimization, yielding,

$$I_{\mathrm{ct}}(\sigma_1, \sigma_2) = I(\sigma_1, \sigma_2, \widetilde{\sigma}_3(\sigma_1, \sigma_2)). \tag{5.50}$$

And next, we find

$$\left. \frac{\partial I_{\mathrm{ct}}}{\partial \sigma_2} \right|_0 = \frac{\partial I}{\partial \sigma_2}(0, 0, \widetilde{\sigma}_3(0, 0)), \tag{5.51}$$

$$\left. \frac{\partial I_{\mathrm{ct}}}{\partial \sigma_1} \right|_0 = \frac{\partial I}{\partial \sigma_1}(0, 0, \widetilde{\sigma}_3(0, 0)). \tag{5.52}$$

After contraction on $\sigma_3$, Eq. (5.49) yields the least likely efficiency

$$\eta_{2,\text{ct}}^* = \left( \frac{\partial I}{\partial \sigma_1}(0, 0, \widetilde{\sigma}_3(0, 0)) \right) \left( \frac{\partial I}{\partial \sigma_2}(0, 0, \widetilde{\sigma}_3(0, 0)) \right)^{-1}. \tag{5.53}$$

In this equation we see that the least likely efficiency is achieved when processes 1 and 2 evolve reversibly while the third process evolves typically (with the condition that the first two processes are reversible). In other words, at the least likely efficiency, the system chooses the most probable trajectories compatible with the reversibility of the first two processes. Since in the general case $I_{\text{ct}}$ will not satisfy a fluctuation theorem, we have no constraint on the location of the maximum of $J_{\text{ct}}(\eta_2)$. If $\widetilde{\sigma}_3(0, 0)$ is small, a Taylor expansion of Eq. (5.53) around $(0, 0, 0)$ shows that the maximum is slightly moved away from $\eta_2^*$ given by Eq. (5.32) taken at $\eta_3^* = 0$. But for arbitrary value of $\widetilde{\sigma}_3(0, 0)$, the maximum of $J_{\text{ct}}$ can be anywhere, even below $\bar{\eta}_2$. This does not contradict the second law of thermodynamics since the third process (that is ignored here) may fuel the machine as much as waste its power.

Finally, we verify the absence of another extremum of $J_{\text{ct}}$ at finite efficiency. To do so, we seek as earlier the zeros of the derivative of $J_{\text{ct}}$

$$\frac{\mathrm{d}J_{\text{ct}}}{\mathrm{d}\eta_2} = 0. \tag{5.54}$$

To find an expression for this derivative, we introduce the function $\widetilde{\sigma}_1'(\eta_2)$ realizing the minimum in Eq. (5.44), such that

$$\begin{aligned} J_{\text{ct}}(\eta_2) &= I_{\text{ct}}(\widetilde{\sigma}_1'(\eta_2), -\eta_2\widetilde{\sigma}_1'(\eta_2)) \\ &= I(\widetilde{\sigma}_1'(\eta_2), -\eta_2\widetilde{\sigma}_1'(\eta_2), -\widetilde{\sigma}_3(\widetilde{\sigma}_1'(\eta_2), -\eta_2\widetilde{\sigma}_1'(\eta_2))). \end{aligned} \tag{5.55}$$

The total derivative of $J_{\text{ct}}(\eta_2)$ yields

$$\frac{\mathrm{d}J_{\text{ct}}}{\mathrm{d}\eta_2}(\eta_2) = -\widetilde{\sigma}_1'(\eta_2)\frac{\partial I}{\partial \sigma_2}. \tag{5.56}$$

With arguments similar to those of Sec. 5.2.3, the above derivative vanishes only at the previously obtained extrema and for infinite values of efficiency. Since $J_{\text{ct}}$ is bounded, it converges to finite values when $\eta_2 \to \pm\infty$.

Therefore, $J_{\text{ct}}$ has the typical shape of the efficiency LDF for two external processes [189] but with a displaced maximum. An example is provided in Fig. 5.5.

## 5.2.5  Close-to-equilibrium machine

Close to equilibrium, the cumulant generating function of entropy productions is a quadratic function. From the Onsager matrix (3.4), it is written as

$$\phi(\gamma_1, \gamma_2, \gamma_3) = \sum_{i,j=1}^{3} \mathcal{L}_{i,j}^f \gamma_i\gamma_j + \sum_{i=1}^{3} \gamma_i\bar{\sigma}_i, \tag{5.57}$$

where $\mathcal{L}_{i,j}^f$ is a short notation for the product of Onsager coefficient and physical affinities $\mathcal{L}_{i,j}f_i f_j$. From Eqs. (5.26) and (5.57) we calculate the efficiency LDF

$$J(\eta_2, \eta_3) = \frac{\sum\limits_{i,j=2}^{3} (\bar{\sigma}_i + \eta_i \bar{\sigma}_1)\, M_{5-i,5-j}\, (\bar{\sigma}_j + \eta_j \bar{\sigma}_1)}{\sum\limits_{s,s'} \epsilon(s)\epsilon(s')\eta_{s(1)}\eta_{s'(1)}\mathcal{L}_{s(2),s'(2)}^f \mathcal{L}_{s(3),s'(3)}^f} \qquad (5.58)$$

where $s$ denote a permutation of three elements and $\epsilon(s)$ its parity and

$$M_{i,j} = (-1)^{i+j} \left( \mathcal{L}_{i,j}^f + \mathcal{L}_{1,i}^f \bar{\eta}_j + \mathcal{L}_{1,j}^f \bar{\eta}_i + \mathcal{L}_{1,1}^f \bar{\eta}_i \bar{\eta}_j \right) \qquad (5.59)$$

for $i,j = 2,3$. We can also rewrite $J(\eta_2, \eta_3)$ in a form that is convenient for generalization

$$J(\eta_2, \eta_3) = \frac{\sum\limits_{s,s'} \epsilon(s)\epsilon(s')\eta_{s(1)}\eta_{s'(1)}\mathcal{L}_{s(2),s'(2)}^f \bar{\sigma}_{s(3)}\bar{\sigma}_{s'(3)}}{\sum\limits_{s,s'} \epsilon(s)\epsilon(s')\eta_{s(1)}\eta_{s'(1)}\mathcal{L}_{s(2),s'(2)}^f \mathcal{L}_{s(3),s'(3)}^f}. \qquad (5.60)$$

As in ref. [189], the close-to-equilibrium efficiency LDF is the ratio of two quadratic forms. It vanishes as expected at the macroscopic efficiencies $(\bar{\eta}_2, \bar{\eta}_3)$. A comparison between the close-to-equilibrium case and a general calculation on efficiency LDF is provided in Sec. 5.2.6 for a specific model.

Furthermore, from linear response theory, the mean entropy production rates are connected to the asymptotic covariances of entropy production as follows

$$\bar{\sigma}_i = \frac{1}{2}\sum_{j=1}^{3} \mathcal{L}_{i,j}^f \qquad (5.61)$$

Then, Eq. (5.60) may be rewritten using only the coefficient $\mathcal{L}_{i,j}^f$

$$J(\eta_2, \eta_3) = \frac{\sum\limits_{s,s'}\sum\limits_{i,j=1}^{3} \epsilon(s)\epsilon(s')\eta_{s(1)}\eta_{s'(1)}\mathcal{L}_{s(2),s'(2)}^f \mathcal{L}_{i,s(3)}^f \mathcal{L}_{j,s'(3)}^f}{2\sum\limits_{s,s'} \epsilon(s)\epsilon(s')\eta_{s(1)}\eta_{s'(1)}\mathcal{L}_{s(2),s'(2)}^f \mathcal{L}_{s(3),s'(3)}^f}. \qquad (5.62)$$

Since the asymptotic covariances are proportional to the response coefficient of the machine, the close-to-equilibrium efficiency LDF is completely known from the response property of the machine.

From this LDF for the two efficiencies we now explicitly compute $J_{\text{ct}}$. After the contraction on the efficiency $\eta_3$, we retrieve the functional form of the efficiency LDF for a machine with two processes [189],

$$J_{\text{ct}}(\eta_2) = \frac{1}{2}\frac{(\eta_2 \bar{\sigma}_1 + \bar{\sigma}_2)^2}{(\eta_2)^2 \mathcal{L}_{1,1}^f + 2\eta_2 \mathcal{L}_{1,2}^f + \mathcal{L}_{2,2}^f}, \qquad (5.63)$$

keeping in mind that we have now $\bar{\sigma}_i = \sum_{j=1}^{3} \mathcal{L}_{i,j}^f / 2$ and not $\bar{\sigma}_i = \sum_{j=1}^{2} \mathcal{L}_{i,j}^f / 2$ as in Ref. [189]. The maximum is no longer at $\eta_2 = 1$ but at $\eta_2 = \eta_{2,\text{ct}}^*$, with

$$\eta_{2,\text{ct}}^* = \frac{\mathcal{L}_{2,2}^f \mathcal{L}_{1,1}^f + \mathcal{L}_{1,3}^f \mathcal{L}_{2,2}^f - {\mathcal{L}_{1,2}^f}^2 - \mathcal{L}_{1,2}^f \mathcal{L}_{2,3}^f}{\mathcal{L}_{2,2}^f \mathcal{L}_{1,1}^f + \mathcal{L}_{2,3}^f \mathcal{L}_{1,1}^f - {\mathcal{L}_{1,2}^f}^2 - \mathcal{L}_{1,2}^f \mathcal{L}_{1,3}^f}. \tag{5.64}$$

As expected, when $\mathcal{L}_{1,3}^f$ and $\mathcal{L}_{2,3}^f$ vanish, $\eta_{2,\text{ct}}^* = 1$: when the third process decouples from the others, we retrieve the least likely efficiency of a machine with only two processes.

We emphasize that bounds similar to Eq. (5.7) can be derived for machines with three physical fluxes. They take the same functional form that the close-to-equilibrium efficiency LDFs (5.62) and (5.63) with the Onsager matrix substituted by the non-equilibrium conductance matrix.

### 5.2.6 Example: Photoelectric device with losses

**Model** We use as an example a simple model of photoelectric device first studied in Ref. [64, 160]. The device is composed of two quantum dots each with a single energy level $E_l$ and $E_r$ ($E_r > E_l$), cf. Fig. 5.2. It is powered by two black-body sources at inverse temperature $\beta_\text{h}$ and $\beta_\text{m}$, and a cold heat reservoir at inverse temperature $\beta_\text{c}$. Each quantum dot can exchange electrons with an electronic lead at inverse temperature $\beta_\text{c}$, the left (right) dot being connected to the left (right) lead. Each lead is at a different voltage and is modeled by an electron reservoir at chemical potential $\mu_\text{r} > \mu_\text{l}$. The three different states of the machine are indexed by $j = 0, l, r$, corresponding respectively to no electron in the device, one electron in the left quantum dot, and one in the right dot. The three different heat reservoirs are labeled by $\nu = \text{c}, \text{m}, \text{h}$. Sketch and graph of the model are represented on Fig. 5.2. The cycle and reservoirs matrices are given by

$$\boldsymbol{C} = \begin{pmatrix} 1 & 0 & 0 \\ 0 & 1 & 0 \\ 1 & 1 & 1 \\ 0 & 0 & 1 \\ 0 & 0 & 1 \end{pmatrix}, \quad \boldsymbol{R} = \begin{pmatrix} E_r - E_l & 0 & 0 & 0 & 0 \\ 0 & E_r - E_l & 0 & 0 & 0 \\ 0 & 0 & E_l - E_r & E_r & -E_l \\ 0 & 0 & 0 & 0 & -1 \\ 0 & 0 & 0 & 1 & 0 \end{pmatrix} \tag{5.65}$$

with the reservoirs affinities $\boldsymbol{f}_\text{r}^\text{T} = (\beta_\text{h}, \beta_\text{m}, \beta_\text{c}, -\beta_\text{c}\mu_r, -\beta_\text{c}\mu_l)$. Using local detailed balance, the transition rates are written [160, 190]

$$\omega_{(0,l)} = \Gamma_l \frac{2e^{-\frac{\beta_\text{c}}{2}(E_l - \mu_l)}}{\cosh\left(\beta_\text{c}(E_l - \mu_l)/2\right)}, \qquad \omega_{(l,0)} = \Gamma_l \frac{2e^{\frac{\beta_\text{c}}{2}(E_l - \mu_l)}}{\cosh\left(\beta_\text{c}(E_l - \mu_l)/2\right)}; \tag{5.66}$$

$$\omega_{(0,r)} = \Gamma_r \frac{2e^{-\frac{\beta_\text{c}}{2}(E_r - \mu_r)}}{\cosh\left(\beta_\text{c}(E_r - \mu_r)/2\right)}, \qquad \omega_{(r,0)} = \Gamma_r \frac{2e^{\frac{\beta_\text{c}}{2}(E_r - \mu_r)}}{\cosh\left(\beta_\text{c}(E_r - \mu_r)/2\right)}; \tag{5.67}$$

$$\omega_{(r,l;\nu)} = \Gamma_\nu \frac{2e^{-\frac{\beta_\nu}{2}(E_r - E_l)}}{\sinh\left(\beta_\nu(E_r - E_l)/2\right)}, \qquad \omega_{(l,r;\nu)} = \Gamma_\nu \frac{2e^{\frac{\beta_\nu}{2}(E_r - E_l)}}{\sinh\left(\beta_\nu(E_r - E_l)/2\right)}. \tag{5.68}$$
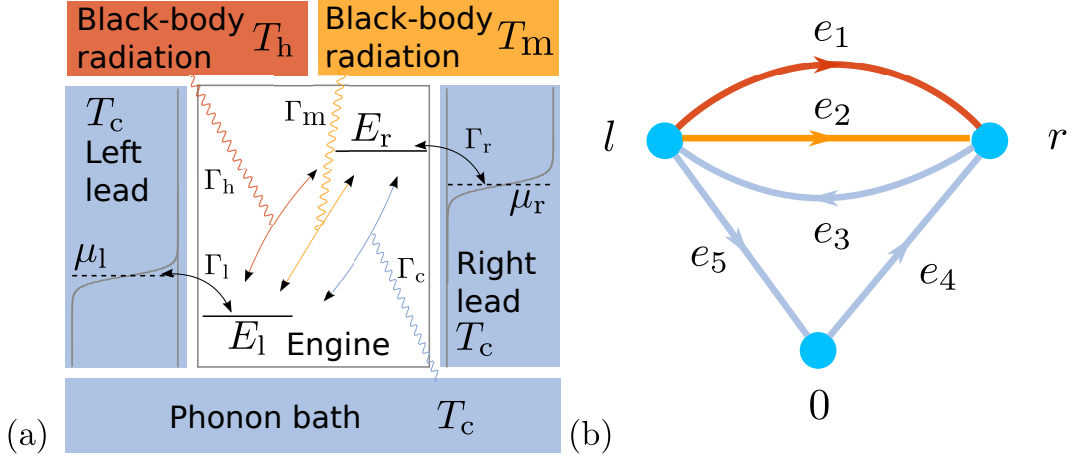
Figure 5.2: (a) Sketch of the photoelectric device. The device is made of two single-level quantum dots (in white) connected to two leads (in blue) at inverse temperature $\beta_c$ and at different chemical potentials $\mu_r$ and $\mu_l$. The electron transitions between left and right quantum dots are induced either by photons from black-body radiation at inverse temperature $\beta_h$ (in red) or $\beta_m$ (in orange), or by phonons at temperature $\beta_c$ (in blue). The arrows indicate possible electronic transitions between different energy levels and the $\Gamma$'s represent the coupling strengths with the reservoirs. (b) Graph of the model with labeled edges.

The total rate for the left to right transition is $\omega_{(r,l)} = \sum_\nu \omega_{(r,l;\nu)}$ and similarly for the right to left transition. The $\Gamma$'s are the different coupling strengths with the reservoirs, see Fig. (5.2), and the symmetric part of the rates is intented to consider quantum statistics, as in the example of sec. 2.3.

**Physical currents** Using the cycle and reservoirs matrices (5.65), we determine two conservation laws

$$\boldsymbol{\ell}_r^{\mathbf{1}\,\mathrm{T}} = (1, 1, 1, 0, 0) \quad \boldsymbol{\ell}_r^{\mathbf{2}\,\mathrm{T}} = (0, 0, 0, 1, 1). \tag{5.69}$$

Such that the selection and physical matrices are obtained as

$$\boldsymbol{V} = \begin{pmatrix} -1 & 0 & 0 \\ 0 & 0 & -1 \\ 1 & 0 & 1 \\ 0 & 1 & 0 \\ 0 & -1 & 0 \end{pmatrix}, \quad \boldsymbol{P} = \begin{pmatrix} E_r - E_l & 0 & 0 \\ 0 & 0 & E_r - E_l \\ 0 & 1 & 0 \end{pmatrix}. \tag{5.70}$$

We have now three physical fluxes that are associated with physical affinities

$$f_1 = \beta_c - \beta_h, \qquad f_2 = \beta_c(\mu_r - \mu_l) \qquad f_3 = \beta_c - \beta_m. \tag{5.71}$$

With all these elements, the mean entropy production rates $\bar{\sigma}_i$, $i = 1, 2, 3$ are determined leading to the operation diagram of Fig. 5.3.
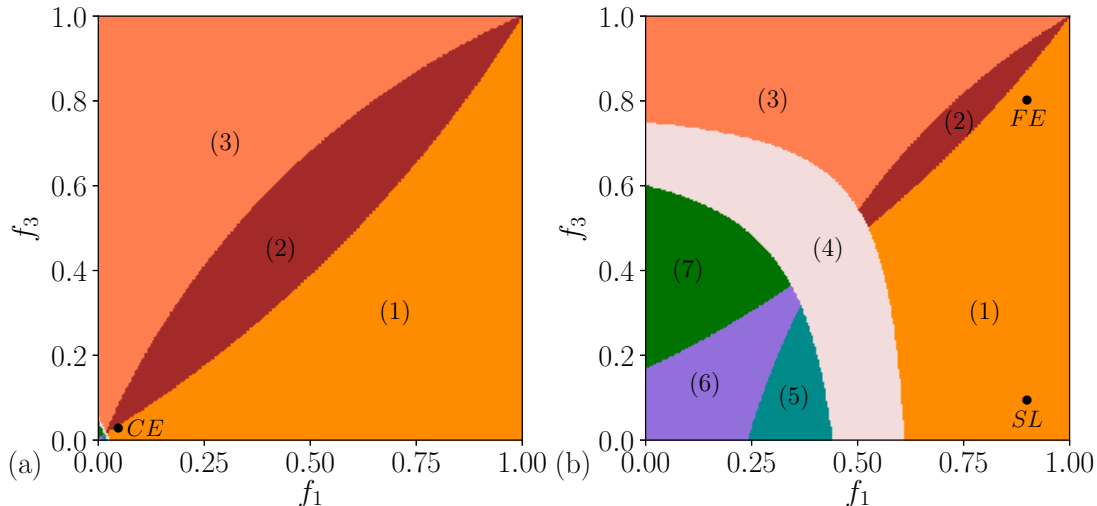
Figure 5.3: Diagram representing the various operating modes of the photoelectric cell as a function of the affinities $f_1$ and $f_3$ for (a) a small chemical potential difference $\Delta\mu = 0.035$, (b) a large chemical potential difference $\Delta\mu = 1$. Black dots correspond to the three studied cases: the close-to-equilibrium case "CE", the small loss case "SL", and the far from equilibrium case "FE". (1) to (3): Heat Engine, for each label $\bar{\sigma}_2 < 0$, and more specifically (1) $\bar{\sigma}_1 > 0 > \bar{\sigma}_3$, (2) $\bar{\sigma}_1 > 0$, $\bar{\sigma}_3 > 0$, (3) $\bar{\sigma}_1 < 0 < \bar{\sigma}_3$, (4): Dud Engine, $\bar{\sigma}_1 > 0$, $\bar{\sigma}_2 > 0$, $\bar{\sigma}_3 > 0$. (5) to (7): Refrigerator and Heat Pump, for each label $\bar{\sigma}_2 > 0$, and more specifically (5) $\bar{\sigma}_1 > 0 > \bar{\sigma}_3$, (6) $\bar{\sigma}_1 < 0$, $\bar{\sigma}_3 < 0$, (7) $\bar{\sigma}_1 < 0 < \bar{\sigma}_3$. Parameters for the machine are $E_r = 2.5$, $E_l = 0.5$, $\Gamma_c = 1$, $\Gamma_m = 5$, and $\Gamma_h = \Gamma_l = \Gamma_r = 10$, and more specifically in the CE case: $T_c = 1$, $\mu_l = 1$, $\mu_r = 1.035$, $T_m = 1.025$, and $T_h = 1.05$ ; in the FE case: $\mu_l = 1$, $\mu_r = 2$, $T_c = 1$, $T_m = 5$, and $T_h = 10$ ; and in the SL case: $\mu_l = 1$, $\mu_r = 2$, $T_c = 1$, $T_m = 1.1$, and $T_h = 10$.

**Efficiency fluctuations** We now turn to the study of the efficiencies fluctuations. Below, the fluctuations of the efficiencies $(\eta_2, \eta_3)$ are quantitatively analyzed in three different cases: a close-to-equilibrium (CE) case, a far-from-equilibrium (FE) case, and a small loss (SL) case. The parameter values in each case are summarized in the caption of Fig. 5.3. The efficiencies statistics has been obtained first by computing numerically the highest eigenvalue of the tilted matrix yielding the CGF $\phi(\gamma_1, \gamma_2, \gamma_3)$ of the various entropy production rates, and in a second step, by using Eq. (5.26) to get the efficiency LDF from $\phi(\gamma_1, \gamma_2, \gamma_3)$.

In Fig. 5.4(a) and 5.4(b) we show the efficiency LDF $J(\eta_2, \eta_3)$ in the CE and FE cases respectively. As expected, the maximum of $J$ is located on the line $\eta_2 + \eta_3 = 1$ corresponding to the reversible efficiencies. The minimum corresponds to the macroscopic efficiencies $(\bar{\eta}_2, \bar{\eta}_3) = (0.19, 0.14)$ in the CE case, and to $(\bar{\eta}_2, \bar{\eta}_3) = (0.24, 0.33)$ in the FE case.

In Fig. 5.4(c) we verify the validity of the CE limit developed in Sec. 5.2.5. The cross-sections of the efficiency LDF $J$ obtained by direct numerical computation are in perfect agreement with the same cross-sections, but obtained from Eq. (5.62). In Fig. 5.4(d), we also show the cross-sections of $J$, but in the FE case illustrating that all the fluctuations associated to a large efficiency becomes
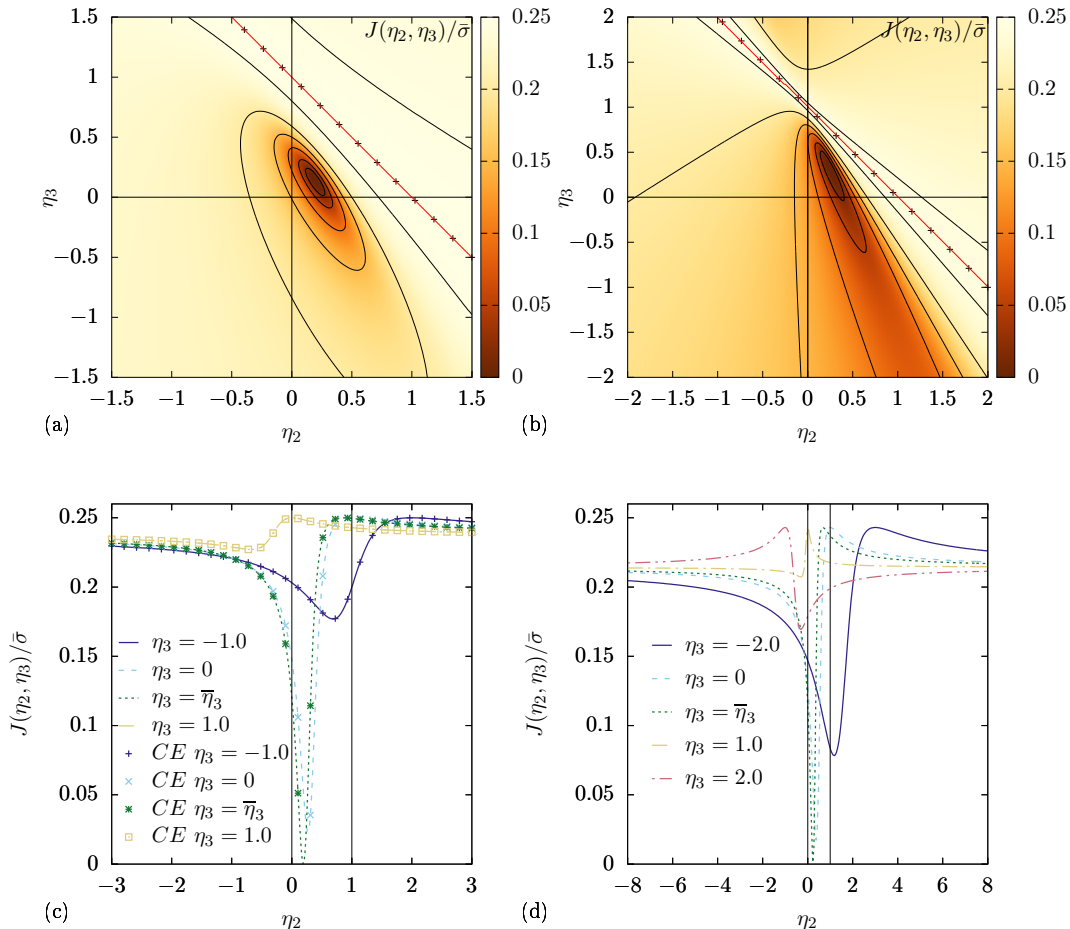
Figure 5.4: Efficiency LDF $J(\eta_2, \eta_3)$ for the photoelectric device of Fig. 5.2 operating on average as a heat engine. (a) and (b) Color map of the efficiency LDF $J(\eta_2, \eta_3)$ The maximum of $J$ is achieved on the red contour line while black solid lines are contour lines for smaller $J$. The straight line of equation $\eta_2 + \eta_3 = 1$ is shown with cross marks. (c) and (d) Cross-sections of $J(\eta_2, \eta_3)$ for various $\eta_3$. Symbols in (c) are obtained from Eq. (5.62). The efficiency LDF are normalized by the mean total entropy production rate with $\bar{\sigma} = 0.00187$ for CE case and $\bar{\sigma} = 1.056$ for FE case. The figures on the left and on the right are for the CE and the FE cases respectively, see the parameters of Fig. 5.3.

generically equally likely independently of the value of the other efficiency: the LDF flattens and converges to the same limit at infinity for the different cross-sections. Comparing Fig. 5.4(c) and 5.4(d), we remark that the time scale on which an efficiency fluctuation disappears is much longer close to equilibrium than far from equilibrium. Indeed the order of magnitude of this time scale is roughly the inverse of the maximum value of the efficiency LDF, and this maximum is connected to the mean total entropy production.

Finally, we comment the effect of the contraction in Eq. (5.44) on the statistics of the remaining efficiency. This situation corresponds to ignoring the third process even though it is still influencing the machine dynamics. In Fig. 5.5 we provide the contracted LDF $J_{\mathrm{ct}}(\eta_2)$. It displays the generic shape of an efficiency
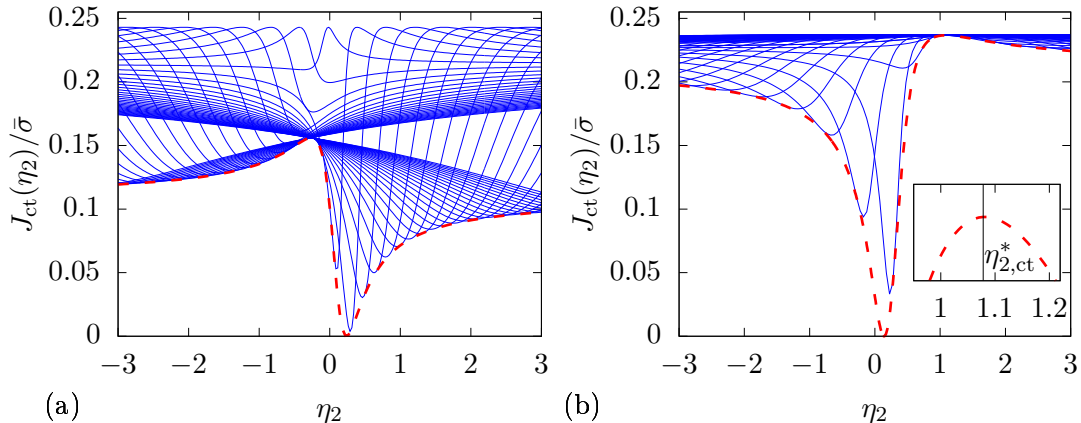
Figure 5.5: Contracted LDF $J_{\mathrm{ct}}(\eta_2)$ (thick dashed red line) and various cross-sections of $J(\eta_2, \eta_3)$ (thin blue lines) for $\eta_3 \in [-10; 10]$. The LDF are normalized by the mean total entropy production rate $\bar{\sigma}$. (a) Far-from-equilibrium contracted LDF $J_{\mathrm{ct}}(\eta_2)$. The minimum is for $\bar{\eta}_2 = 0.24$. The mean total entropy production rate is $\bar{\sigma} = 1.056$. (b) Contracted LDF $J_{\mathrm{ct}}(\eta_2)$ for small losses. The minimum is for $\bar{\eta}_2 = 0.14$ and the maximum for $\eta_{2,\mathrm{ct}}^* = 1.08$. The mean total entropy production rate is $\bar{\sigma} = 3.027$. Insert: zoom on the maximum.

LDF excepted that no constraint exists on the position of the maximum, e.g. it is below $\bar{\eta}_2$ in the FE case. This would be forbidden by the laws of thermodynamics in a machine with only two processes, but it is allowed whenever an additional process has been ignored in the description of the machine. Logically, when the ignored process is weakly irreversible as in the SL case of Fig. 5.5(b), the maximum of the efficiency LDF must be located close to the reversible efficiency: in the limit of a vanishing affinity for the ignored process, we retrieve the usual efficiency fluctuations of a stationary machine with only two processes for which the reversible efficiency is the least likely.

# Non equivalence of dynamical ensembles

The microcanonical and canonical ensembles are equivalent when the same computations done within one or the other ensemble leads to the same result. Computations are in general more difficult within the microcanonical ensemble and easier within the canonical ensemble. Hence, the ensemble equivalence is of particular importance, and its validity conditions are essential for practical use. Beyond the case of equivalent ensembles, we aim at obtaining relevant informations within one ensemble from computations done in the other ensemble.

For dynamical ensembles, we saw in previous chapters that equivalence holds for ergodic systems. In this chapter, we are interested in the case where equivalence for dynamical ensembles breaks down, due to the existence of several metastable states. Adapting a method developed by Touchette [177, 178] to compute non concave entropy within the equilibrium ensembles, we are able to obtain the non-convex LDF of dynamical observables for systems in or out of equilibrium.

We apply this method on a dynamical version of the fully connected Ising model to determine the asymptotic probability of activity and magnetization. For this model, the non-equivalence emerges in the thermodynamic limit, making crucial the order of large size and long time limit, that we discuss in the last section of this chapter.

## 6.1 Explicit calculation of a LDF for non-ergodic systems

First, we adapt the method developed in Ref. [177] for equilibrium ensembles to compute non-convex LDF from their corresponding generating function. We start with a simple example of non-ergodic system to explain how to compute a non-convex LDF from the propagator of the generating function.

### 6.1.1   A four state model with non-convex LDF of activity

**LDF from explicit probability**   Let's consider a four state system made of two subsystems with two states $(1, 2)$ and $(3, 4)$. The four state system evolves according to the master equation

$$
\frac{\mathrm{d}}{\mathrm{d}t}
\begin{pmatrix} \rho_1 \\ \rho_2 \\ \rho_3 \\ \rho_4 \end{pmatrix}
=
\begin{pmatrix}
-1 & 1 & 0 & 0 \\
1 & -1 & 0 & 0 \\
0 & 0 & -2 & 2 \\
0 & 0 & 2 & -2
\end{pmatrix}
\cdot
\begin{pmatrix} \rho_1 \\ \rho_2 \\ \rho_3 \\ \rho_4 \end{pmatrix}.
\tag{6.1}
$$

The Markov operator is reducible yielding to a non ergodic process. We aim at computing the system activity assuming that one cannot distinguish in which subsystem a transition occurs. The activity rate $A_{\mathrm{tot}}$ is the total number of jumps per unit time: It is given by Eq. (1.73) when $\mathfrak{f}(x) = 0$ and $\mathfrak{g}(x, y) = 1$ for all $(x, y)$. By definition of the Markov operator in the right hand side of Eq. (6.1), the activity probability distribution of each subsystem is a Poisson distribution of mean value $T$ for the subsystem $(1, 2)$ and $2T$ for the subsystem $(3, 4)$. Indeed there is respectively 1 and 2 jumps per unit time in each subsystem respectively. The probability distribution of the total number of jumps is the sum of Poisson distributions weighted by the respective initial probability $\rho_n^{\mathrm{i}}$ to start in state $n$. The probability of having $aT$ jumps after a time $T$ is

$$
\mathrm{Pr}\left(A_{\mathrm{tot}}T = aT\right) = (\rho_1^{\mathrm{i}} + \rho_2^{\mathrm{i}})\frac{(T)^{aT}e^{-T}}{(aT)!} + (\rho_3^{\mathrm{i}} + \rho_4^{\mathrm{i}})\frac{(2T)^{aT}e^{-2T}}{(aT)!}
\tag{6.2}
$$

For $T$ large enough, $\mathrm{Pr}\left(A_{\mathrm{tot}}T = aT\right)$ will be bimodal, and the LDF within the microcanonical ensemble reads

$$
I_{\mathrm{mca}}(a) = -\lim_{T \to +\infty}\frac{1}{T}\ln \mathrm{Pr}\left(A_{\mathrm{tot}} = a\right) =
\begin{cases}
a\ln a - a + 1 & \text{if } a < 1/\ln 2 \\
a\ln\dfrac{a}{2} - a + 2 & \text{if } a \geqslant 1/\ln 2
\end{cases},
\tag{6.3}
$$

where we have used Stirling formula and chosen the minimum of the two LDF corresponding to each Poisson distribution. The above non-convex LDF of activity is shown in Fig. 6.1b. It is crucial to note that the initial condition plays a fundamental role here: if the system never starts in states 1 or 2, i.e. $\rho_1^{\mathrm{i}} = \rho_2^{\mathrm{i}} = 0$, the LDF will include the branch corresponding to the second line of Eq. (6.3) only. The non-ergodicity impacts the long time statistics of the dynamical observables through the choice of initial conditions.

**Propagator of the generating function**   For the four state model, it is straightforward to determine the probability of the activity, but for other systems or observables this task may be more challenging: one must often compute the CGF instead. Let's derive the result of Eq. (6.3) in this way using the propagator for the generating function of the activity defined by $G(x^{\mathrm{f}}, x^{\mathrm{i}}, \gamma) = \mathbf{E}\left[e^{T\gamma A_{\mathrm{tot}}}\right]_{x^{\mathrm{f}}, x^{\mathrm{i}}}$, where the subscripts $x^{\mathrm{i}}$ and $x^{\mathrm{f}}$ provide respectively the initial and final states of

the trajectories appearing in the average. Using standard approach [25, 28], the propagator is obtained from the tilted matrix

$$
\boldsymbol{K}^\gamma = \begin{pmatrix} -1 & e^\gamma & 0 & 0 \\ e^\gamma & -1 & 0 & 0 \\ 0 & 0 & -2 & 2e^\gamma \\ 0 & 0 & 2e^\gamma & -2 \end{pmatrix}
\tag{6.4}
$$

as the components of its matrix exponential $[\exp(T\boldsymbol{K}^\gamma)](x^{\mathrm{f}}, x^{\mathrm{i}}) = G(x^{\mathrm{f}}, x^{\mathrm{i}}, \gamma)$. Using eigenvalues and eigenvectors decomposition of $\boldsymbol{K}^\gamma$, we explicit the matrix exponential as

$$
\exp[T\boldsymbol{K}^\gamma] = e^{T(-1+e^\gamma)} \begin{pmatrix} 1/2 \\ 1/2 \\ 0 \\ 0 \end{pmatrix} \cdot \begin{pmatrix} 1 & 1 & 0 & 0 \end{pmatrix} + e^{2T(-1+e^\gamma)} \begin{pmatrix} 0 \\ 0 \\ 1/2 \\ 1/2 \end{pmatrix} \cdot \begin{pmatrix} 0 & 0 & 1 & 1 \end{pmatrix}
$$

$$
+ e^{-T(1+e^\gamma)} \begin{pmatrix} 1/2 \\ -1/2 \\ 0 \\ 0 \end{pmatrix} \cdot \begin{pmatrix} 1 & -1 & 0 & 0 \end{pmatrix} + e^{-2T(1+e^\gamma)} \begin{pmatrix} 0 \\ 0 \\ 1/2 \\ -1/2 \end{pmatrix} \cdot \begin{pmatrix} 0 & 0 & 1 & -1 \end{pmatrix}.
\tag{6.5}
$$

The orthogonal basis of eigenvectors has normalized right eigenvectors, and the scalar products of the left and right eigenvectors associated to the same eigenvalue are all equal to 1. We notice that the eigenvectors separate in two sets whose supports are disjoint and correspond to each subsystem respectively. We remark also that the above propagator should be norm conserving when $\gamma = 0$, but the two terms in the second line of Eq. (6.5) do not fulfill this requirement. We do not consider them as physical and keep only the first two terms in Eq. (6.5). Then, the activity LDF is recovered from this propagator by summing first over the initial and final states

$$
\mathbf{E}\left[e^{T\gamma A_{\mathrm{tot}}}\right] = \sum_{x^{\mathrm{f}}, x^{\mathrm{i}}} G(x^{\mathrm{f}}, x^{\mathrm{i}}, \gamma)\rho^{\mathrm{i}}_{x^{\mathrm{i}}},
\tag{6.6}
$$

second, by applying an inverse Laplace transform, and finally by taking the limit $T \to \infty$. For ergodic systems, this procedure leads to the same LDF whatever the order of these operations. On the contrary, the order matters for non-ergodic systems.

**LDF from CGF**  For our 4 state model, the generating function writes

$$
\mathbf{E}\left[e^{T\gamma A_{\mathrm{tot}}}\right] = (\rho^{\mathrm{i}}_1 + \rho^{\mathrm{i}}_2)e^{T(-1+e^\gamma)} + (\rho^{\mathrm{i}}_3 + \rho^{\mathrm{i}}_4)e^{2T(-1+e^\gamma)}.
\tag{6.7}
$$

Its inverse Laplace transform yields the probability density function of activity given in Eq. (6.2). However, first computing the long time limit of the generating function leads to the CGF

$$
\phi(\gamma) = \lim_{T \to +\infty} \frac{1}{T} \ln \sum_{x^{\mathrm{f}}, x^{\mathrm{i}}} G(x^{\mathrm{f}}, x^{\mathrm{i}}, \gamma)\rho^{\mathrm{i}}_{x^{\mathrm{i}}} = \begin{cases} e^\gamma - 1 & \text{if } \gamma < 0, \\ 2(e^\gamma - 1) & \text{if } \gamma \geqslant 0 \end{cases},
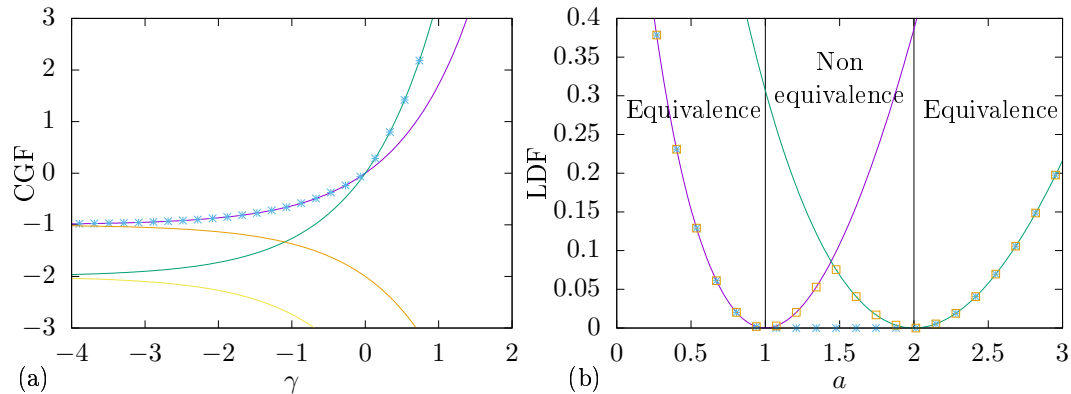\tag{6.8}
$$

Figure 6.1: (a) Four eigenvalues of the tilted matrix (6.4) (solid line) and corresponding CGF (cross). (b) Partial LDFs (solid lines) corresponding to the Legendre transform of the two highest eigenvalues, canonical LDF (cross) and microcanonical LDF (squares).

as long as $\rho_x^{\mathrm{i}} > 0$ for all $x$. Noticing that the limit $T \to +\infty$ enables to use a saddle-point method to approximate the inverse Laplace transform into a Legendre-Fenchel transform, the asymptotic probability of activity follows from its corresponding LDF

$$I_{\mathrm{ca}}(a) = \max_{\gamma} \left[ a\gamma - \phi(\gamma) \right] = \begin{cases} a \ln a - a + 1 & \text{if } a < 1 \\ 0 & \text{if } a \in [1, 2] \\ a \ln \dfrac{a}{2} - a + 2 & \text{if } a > 2 \end{cases}, \qquad (6.9)$$

that is not the one of Eq. (6.3). It corresponds to the LDF computed within the canonical ensemble. The former LDF is convex because a Legendre-Fenchel transform only yields convex functions by definition, while the latter is not convex.

**LDF from the propagator of the generating function** Alternatively, one may obtain the microcanonical LDF by taking the long time limit on the propagator of the generating function of Eq. (6.5), and not on the generating function itself, yielding

$$\phi_{x^{\mathrm{i}}}(\gamma) = \lim_{T \to +\infty} \frac{1}{T} \ln G(x^{\mathrm{f}}, x^{\mathrm{i}}, \gamma) = \begin{cases} (e^{\gamma} - 1) & \text{if } x^{\mathrm{i}} = 1, 2 \\ 2(e^{\gamma} - 1) & \text{if } x^{\mathrm{i}} = 3, 4 \end{cases}. \qquad (6.10)$$

The Legendre-Fenchel conjugates of these two branches associated to different initial states are precisely the two branches of the microcanonical LDF in Eq. (6.3):

$$I_{x^{\mathrm{i}}}(a) = \max_{\gamma} \left[ a\gamma - \phi_{x^{\mathrm{i}}}(\gamma) \right] = \begin{cases} a \ln a - a + 1 & \text{if } x^{\mathrm{i}} = 1, 2 \\ a \ln \dfrac{a}{2} - a + 2 & \text{if } x^{\mathrm{i}} = 3, 4 \end{cases} \qquad (6.11)$$

The summation over initial and final conditions is now carried out using an asymptotic approximation, which can be written heuristically as

$$e^{-TI_{\mathrm{mca}}(a)} \simeq \sum_{x^{\mathrm{i}}} \rho_{x^{\mathrm{i}}}^{\mathrm{i}} e^{-TI_{x^{\mathrm{i}}}(a)} \simeq \exp\left( -T \min_{x^{\mathrm{i}}} I_{x^{\mathrm{i}}}(a) \right) \qquad (6.12)$$

explaining why a minimum on the branches of Eq. (6.11) appears in the final non convex LDF of Eq. (6.3). To summarize, from the Legendre-Fenchel conjugate of all the eigenvalues appearing in the tilted matrix of Eq. (6.4), we determined the partial LDFs. The minimum among these partial LDFs produces the microcanonical LDF. We illustrate this procedure in Fig. 6.1. From this figure, we conclude on the ensemble equivalence for this model: it holds for $a \in [0, 1[\bigcup]2, +\infty[$, but the equivalence is partial at $a = 1, 2$ and there is no equivalence for $a \in ]1, 2[$.

## 6.1.2 General framework

In the above example, we have seen that one can determine the asymptotic fluctuations of a physical observable by switching from one dynamical ensemble to another as long as the LDFs are piecewise-convex. In this section, we develop this approach for the more general framework of sec. 2.2. In practice, this amount to express the inverse Laplace transform as a Legendre-Fenchel transform, using the saddle point method and taking care of the initial condition appropriately.

**Microcanonical LDF**   By definition, the microcanonical LDF for the observable $O$ (1.73) writes

$$I_{\text{mca}}(o) = \lim_{T \to +\infty} \frac{-1}{T} \ln \int_{b-i\infty}^{b+i\infty} \mathrm{d}\gamma \, e^{-T\gamma o} \sum_{x^{\text{f}}, x^{\text{i}}} G(x^{\text{f}}, x^{\text{i}}, \gamma) \rho_{x^{\text{i}}}^{\text{i}}, \qquad (6.13)$$

in term of the propagator

$$G(x^{\text{f}}, x^{\text{i}}, \gamma) = \mathbf{E} \left[ e^{T\gamma O} \right]_{x^{\text{f}}, x^{\text{i}}} \qquad (6.14)$$

that generates the cumulants of $O$ under given initial and final conditions. Indeed, the argument of the logarithm is exactly the probability distribution function of $O$. Since solely the most probable events contribute to the LDF, we can focus on the initial conditions leading to the minimal value of the LDF (as seen in section 6.1.1):

$$I_{\text{mca}}(o) = \min_{x^{\text{f}}, x^{\text{i}}} \lim_{T \to +\infty} \frac{-1}{T} \ln \int_{b-i\infty}^{b+i\infty} \mathrm{d}\gamma \, e^{-T\gamma o} G(x^{\text{f}}, x^{\text{i}}, \gamma) \rho_{x^{\text{i}}}^{\text{i}}. \qquad (6.15)$$

Finally, the complex integral for the inverse Laplace conjugate follows from the saddle point method:

$$I_{\text{mca}}(o) = \min_{x^{\text{f}}, x^{\text{i}}} \max_{\gamma} \left( \gamma o - \lim_{T \to +\infty} \frac{1}{T} \ln G(x^{\text{f}}, x^{\text{i}}, \gamma) \rho_{x^{\text{i}}}^{\text{i}} \right). \qquad (6.16)$$

**Convex hull of the LDF**   Alternatively, the convex hull of $I_{\text{mca}}(o)$ is the Legendre-Fenchel conjugate of the CGF for the observable $O$, namely

$$I_{\text{ca}}(o) = \max_{\gamma} \left( \gamma o - \lim_{T \to +\infty} \frac{1}{T} \ln \sum_{x^{\text{f}}, x^{\text{i}}} G(x^{\text{f}}, x^{\text{i}}, \gamma) \rho_{x^{\text{i}}}^{\text{i}} \right), \qquad (6.17)$$

That is also the LDF computed within the canonical ensemble. As seen in section 6.1.1, the propagator $G$ may have an eigendecomposition for which the terms contributing to the CGF in the limit $T \to \infty$ depend on the initial or final conditions. Hence, a maximum on $x^{\mathrm{f}}$ and $x^{\mathrm{i}}$ must appear

$$I_{\mathrm{ca}}(o) = \max_{\gamma} \left( \gamma o - \max_{x^{\mathrm{f}}, x^{\mathrm{i}}} \lim_{T \to +\infty} \frac{1}{T} \ln G(x^{\mathrm{f}}, x^{\mathrm{i}}, \gamma) \rho_{x^{\mathrm{i}}}^{\mathrm{i}} \right), \qquad (6.18)$$

to select the dominant asymptotic behavior in the limit $T \to \infty$. In view of comparing with Eq. (6.16), the maximization can be modified into a minimization through the commutation with the minus sign:

$$I_{\mathrm{ca}}(o) = \max_{\gamma} \min_{x^{\mathrm{f}}, x^{\mathrm{i}}} \left( \gamma o - \lim_{T \to +\infty} \frac{1}{T} \ln G(x^{\mathrm{f}}, x^{\mathrm{i}}, \gamma) \rho_{x^{\mathrm{i}}}^{\mathrm{i}} \right). \qquad (6.19)$$

In the end, the difference between the LDF $I_{\mathrm{mca}}(o)$ and its convex hull $I_{\mathrm{ca}}(o)$ comes from the non commutation of $\max_{\gamma}$ and $\min_{x^{\mathrm{f}}, x^{\mathrm{i}}}$ as a consequence of the dependence on the initial conditions, i.e. of the non-ergodicity. Of course, if both microcanonical and microcanonical LDF are convex, the ordering of these extremizations would not matter.

**Eigenvalues of the propagator** The eigendecomposition of the propagator $G$ involves the eigenvalues of the tilted matrix of Eq. (2.18). For a non ergodic systems or when the state space is infinite, the assumption of the Perron-Fröbenius theorem does not hold and several eigenvalues may cross each other. To compute exactly the microcanonical LDF, one needs all the branches corresponding to each eigenvalue that becomes the highest eigenvalue for at least one $\gamma$. Only those branches matters, and other eigenvalues will not contribute, so as can be understood from the following argument: Be two eigenvalues $\phi_1(\gamma)$ and $\phi_2(\gamma)$ such that $\phi_1(\gamma) > \phi_2(\gamma)$. Since $\gamma o - \phi_1(\gamma) < \gamma o - \phi_2(\gamma)$, we have

$$I_1(o) = \max_{\gamma} \left\{ \gamma o - \phi_1(\gamma) \right\} < I_2(o) = \max_{\gamma} \left\{ \gamma o - \phi_2(\gamma) \right\}. \qquad (6.20)$$

The last minimization in Eq. (6.16) on the partial LDFs withdraws the contribution coming from the eigenvalue $\phi_2(\gamma)$ if it is smaller that $\phi_1(\gamma)$ for all $\gamma$.

**Systems with several subparts** Physically speaking, we study a rare event in a system that has several independent subparts. We assume that the initial probability cannot be zero in all states of a subsystem, otherwise this subsystem shall be ignored. Each subpart of the system has its own probability to realize the rare event at stake. The subpart for which the event is the most likely will determine the event probability. This will be so if the rare event corresponds to a fluctuation of a time average quantity over a sufficiently long time so as to neglect the role of the initial state probability.

Mathematically speaking, when dealing with reducible tilted matrices whose highest eigenvalue is the CGF of interest, we must divide the matrix into irreducible sub-matrices for which holds the ensemble equivalence. For every sub-matrices we proceed normally using the ensemble equivalence to determine the

partial LDFs of the chosen observable from the Legendre-Fenchel transform of the highest eigenvalue of the sub-matrix. The final LDF for the total system is then given by the minimum over all partial LDFs. This explains why the final LDF is piecewise convex.

**Connection with driven processes** The non-equivalence arises, due to the crossing of two eigenvalues. At this point, the highest eigenvalue is associated with two different eigenvectors. This leads to the definition of two different driven processes, that are connected with the various subparts of the system.

We emphasize that there is another possibility to have a non-equivalence of dynamical ensemble when the driven process cannot be defined. This appends for non-compact state spaces where the left eigenvector cannot be normalized [118, 127, 175].

## 6.2 Mean field Ising model

Using the results of sec. 6.1.2, we study the activity and magnetization of an infinite range Ising model. This model is ergodic when considering a finite number of spins, but breaks ergodicity in the thermodynamics limit. In the following, we first introduce the model and its mean field (MF) treatment. Second, we provide the propagator of the generating function for magnetization and activity, and next use it to determine the CGF and both the canonical and microcanonical LDFs.

### 6.2.1 Model description and thermodynamics limit

**Model** We consider the fully connected Ising model made of $N$ interacting spins $\{s\} = (s_1, \ldots, s_N)$. Each spin $s_i$ can hop between states $+1$ and $-1$ by exchanging heat with a thermostat at inverse temperature $\beta$. The interaction energy between two spins is $V/N$ when the spins are not aligned and vanishes for parallel spins. The interaction energy is independent of the distance between spins. Beside the spin-spin interaction, each spin has a potential energy $-s_i H$ due to the presence of an external magnetic field. We introduce the free energy $\mathcal{F}_n = E_n - S_n/\beta$ of the mesostate $n = \sum_{i=1}^{N} s_i$ in term of the total energy given (up to a constant) by

$$E_n = -\frac{V}{N} \sum_{1 \leqslant i \leqslant j \leqslant N} s_i s_j - H \sum_{1 \leqslant i \leqslant N} s_i = -n^2 \frac{V}{2N} - nH \qquad (6.21)$$

and of the internal entropy

$$S_n = \ln N! / [\left(\frac{N+n}{2}\right)! \left(\frac{N-n}{2}\right)!]. \qquad (6.22)$$

The stationary probability $\pi_n$ is the equilibrium probability

$$\pi_n = \frac{e^{-\mathcal{F}_n}}{Z_{\text{eq}}} \quad \text{with} \quad Z_{\text{eq}} = \sum_{n=0}^{N} e^{-\mathcal{F}_n}. \qquad (6.23)$$

The system is in thermal equilibrium and the transition rates satisfy the detail balance equation

$$\ln \frac{\omega_{n+2\epsilon,n}}{\omega_{n,n+2\epsilon}} = -\beta(\mathcal{F}_{n+2\epsilon} - \mathcal{F}_n), \tag{6.24}$$

We chose the transition rate from $n$ to $n + 2\epsilon$ (with $\epsilon = \pm 1$) to be

$$\omega_{n+2\epsilon,n} = \Gamma\left(N - \epsilon n\right) e^{\frac{\beta}{2}((2\epsilon n + 2)V/N + 2\epsilon H)}. \tag{6.25}$$

In the following we take $\Gamma = 1$ and $\beta = 1$ to set the time and energy scales respectively. The probability $\boldsymbol{\rho}_v(t)$ evolves according to the master equation

$$\dot{\boldsymbol{\rho}}_v(t) = \boldsymbol{K} \cdot \boldsymbol{\rho}_v(t), \tag{6.26}$$

with the transition matrix $\boldsymbol{K}$ of elements

$$\begin{aligned} K_{n,n} &= -\sum_{\epsilon=\pm1} \omega_{n+2\epsilon,n}; \\ K_{n,n+2} &= \omega_{n,n+2\epsilon}; \\ K_{n,n-2} &= \omega_{n,n-2}. \end{aligned} \tag{6.27}$$

**Observables**  The time-averaged stochastic magnetization is obtained from Eq. (1.73) by choosing the state dependent function $\mathfrak{f}(n) = n/N$ and a vanishing function $\mathfrak{g}(n, n') = 0$ for all $(n, n')$:

$$M = \frac{1}{NT} \int_0^T \mathrm{d}t\, X(t), \tag{6.28}$$

where $X(t)$ is the mesostate at time $t$. We denote by $m$ some real value that can be achieved by the stochastic variable $M$. The mean magnetization in the stationary state writes

$$\mathbf{E}\left[M\right] = \frac{1}{N} \sum_{n=0}^{N} n\pi_n. \tag{6.29}$$

The activity rate is obtained from Eq. (1.73) by choosing $\mathfrak{g}(n, n') = 1/N$ and $\mathfrak{f}(n) = 0$ for all $(n, n')$:

$$A = \frac{1}{NT} \sum_{0 \leqslant t \leqslant T : \Delta n_t \neq 0} 1 \tag{6.30}$$

The activity rate is thus a time-symmetric observable : the number of spin flips (per unit time and per spin) are identical in a trajectory and its time reversal. We denote by $a$ some real value that can be achieved by the stochastic variable $A$. The mean activity in the stationary state writes

$$\mathbf{E}\left[A\right] = \frac{1}{N} \sum_{n=0}^{N} \sum_{\epsilon=\pm1} \pi_n \omega_{n+2\epsilon,n}. \tag{6.31}$$
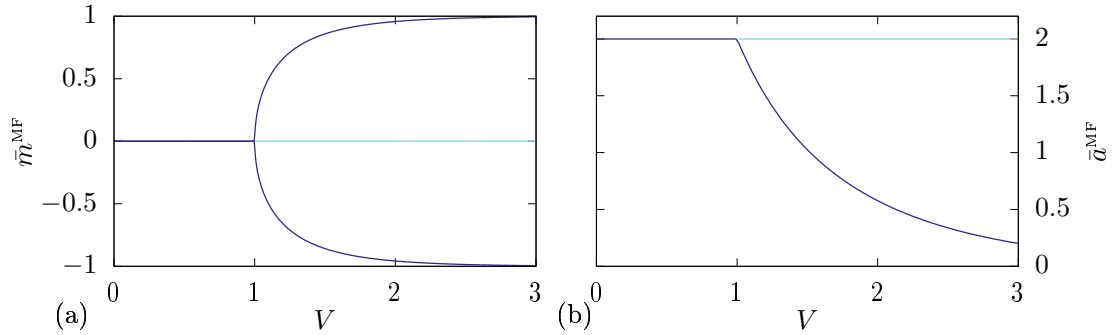
Figure 6.2: (a) Stable (dark blue) and unstable (light blue) mean field steady state densities $\bar{m}^{\mathrm{MF}}$ versus interaction energy $V$. (b) Stable (dark blue) and unstable (light blue) mean field steady state activity $\bar{a}^{\mathrm{MF}}$ versus interaction energy $V$. For both figures, $H = 0$.

**Thermodynamic limit** In the thermodynamic limit, when taking the continuous limit for the mesostate $x = n/N \in [-1, 1]$, the system energy changes by

$$\lim_{N \to \infty} [E_{n+2\epsilon} - E_n] = 2\epsilon(Vx + H) \tag{6.32}$$

for a transition from $n$ to $n+2\epsilon$. Accordingly, the transition rates are in the same limit

$$J_\epsilon(x) = \lim_{N \to +\infty} \frac{\omega_{xN+2\epsilon, xN}}{N} = (1 - \epsilon x)\, e^{\epsilon[Vx + H]}. \tag{6.33}$$

In this case, the master equation Eq. (6.26) can be transformed into an evolution equation for $x$ in the mean field (MF) approximation

$$\bar{\dot{x}} = \sum_{\epsilon = \pm 1} \epsilon J_\epsilon(\bar{x}). \tag{6.34}$$

The steady state solution of this equation is the mean field magnetization $\bar{x} = \bar{m}^{\mathrm{MF}}$ verifying

$$J_-\left(\bar{m}^{\mathrm{MF}}\right) = J_+\left(\bar{m}^{\mathrm{MF}}\right). \tag{6.35}$$

Using Eq. (6.33), the previous equation is equivalent to the transcendental equation

$$\bar{m}^{\mathrm{MF}} = \tanh\left(V\bar{m}^{\mathrm{MF}} + H\right). \tag{6.36}$$

The MF activity follows from the mean-field magnetization:

$$\bar{a}^{\mathrm{MF}} = J_-\left(\bar{m}^{\mathrm{MF}}\right) + J_+\left(\bar{m}^{\mathrm{MF}}\right) = \left[1 - \bar{m}^{\mathrm{MF}}\right] e^{V\bar{m}^{\mathrm{MF}} + H} + \left[1 + \bar{m}^{\mathrm{MF}}\right] e^{-V\bar{m}^{\mathrm{MF}} - H}. \tag{6.37}$$

The MF magnetization and activity are shown in the bifurcation diagram of Fig.6.2. At a critical value of the interaction energy, three MF magnetizations appear instead of a unique one, due to the well studied ferromagnetic transition in the Ising model. This bifurcation also affects the system activity as shown on the Fig.6.2b and as expected from Eq. (6.37) since $\bar{a}^{\mathrm{MF}}$ is a function of $\bar{m}^{\mathrm{MF}}$. We remark that the system activity is an even function of the magnetization and hence the bifurcation diagram for activity has two branches only. We also notice that the MF activity is higher for the branch that does not break the system symmetry.

## 6.2.2 Propagator of the generating function for magnetization and activity

Like in the four state model of sec. 6.1.1, we look for the propagator of the generating function for the activity and magnetization:

$$G(x^{\mathrm{f}}, x^{\mathrm{i}}, \kappa, \gamma) = \mathbf{E}\left[e^{NT(\kappa m + \gamma a)}\right]_{x^{\mathrm{f}}, x^{\mathrm{i}}}, \tag{6.38}$$

where as before the subscripts indicate a conditioning on the initial and final states, respectively $x^{\mathrm{i}} = n^{\mathrm{i}}/N$ and $x^{\mathrm{f}} = n_{\mathrm{f}}/N$. From a path integral approach [33, 107, 22], an asymptotic expression of the propagator reads

$$G(x^{\mathrm{f}}, x^{\mathrm{i}}, \kappa, \gamma) \simeq_{N \to +\infty} \exp\left(N \int_0^T \mathrm{d}t \mathscr{L}(x_t, \dot{x}_t, \kappa, \gamma)\right), \tag{6.39}$$

where $\mathscr{L}$ is the Lagrangian

$$\mathscr{L}(x, \dot{x}, \kappa, \gamma) = \frac{\dot{x}}{2} \ln\left(\frac{-\dot{x} + \sqrt{\dot{x}^2 + \varphi(x, \gamma)}}{2J_-(x)e^\gamma}\right) - \sum_{\epsilon = \pm 1} J_\epsilon(x) + \sqrt{\dot{x}^2 + \varphi(x, \gamma)} + \kappa x, \tag{6.40}$$

with

$$\varphi(x, \gamma) = 4 \prod_{\epsilon = \pm 1} J_\epsilon(x)e^\gamma = 4(1 + x)(1 - x)e^{2\gamma}. \tag{6.41}$$

The propagator of Eq. (6.39) is almost explicit: the path $x_t$ starting in $x^{\mathrm{i}}$ and ending in $x^{\mathrm{f}}$ must be determined using the Euler-Lagrange equation

$$\frac{\partial \mathscr{L}}{\partial x} = \frac{\mathrm{d}}{\mathrm{d}t}\left(\frac{\partial \mathscr{L}}{\partial \dot{x}}\right). \tag{6.42}$$

Hence, the propagator of the generating function is fully determined by the initial and final conditions.

As explained in sec. 6.1.2, we now vary initial and final conditions to obtain the dominant contributions to the generating function. As the large size and long time limit of the propagator is evaluated with large size limit first and then long time limit, the system is non-ergodic. Due to this non-ergodicity, the dominant contributions are obtained from stationary trajectories, *i.e.* element of the propagator $G(x^*, x^*, \kappa, \gamma)$ such that

$$\frac{\partial \mathscr{L}}{\partial x}(x^*, 0, \kappa, \gamma) = 0. \tag{6.43}$$

and we denote $x^*(\kappa, \gamma)$ the various solution of this equation. These constant trajectories are the only ones that will dominate for at least one value of $(\kappa, \gamma)$. Following sec. 6.1.2, we can restrain the extremization over initial and final conditions to these stationary trajectories.

We provide an heuristic argument for the choice of stationary trajectories: Dominant trajectories correspond to long-time behavior of the tilted system. We expect the tilted system to be in a stationary state at long-time, as we study

an equilibrium system. Neglecting the boundary terms due to long time limit, we restrain to trajectories starting and ending into a stationary state. The system being non-ergodic, we forbid trajectories that start and end into different stationary states. This approach is confirmed by numerical computation of the CGF that we will see in the next section.

In the next section, we use the propagator of Eq. (6.39) to derive the CGF of magnetization and activity. For taking advantage of the left/right symmetry, we set $H$ to zero.

### 6.2.3  CGF of magnetization and activity
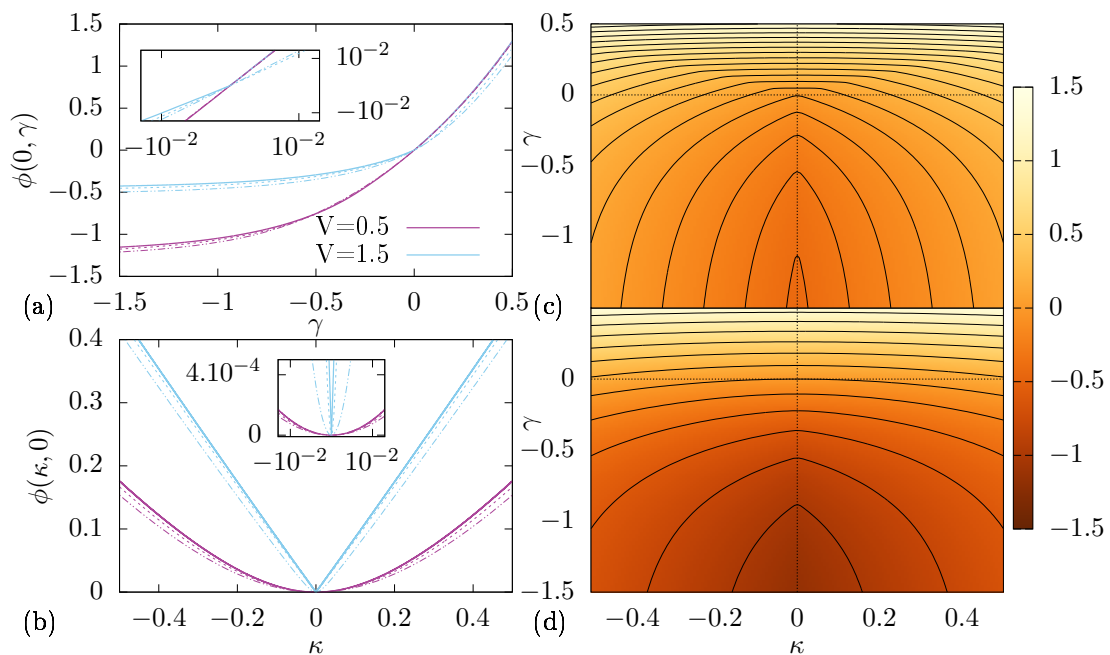


Figure 6.3:   Cross-sections of the CGF $\phi(\kappa, \gamma)$ along (a) $\kappa = 0$ and (b) $\gamma = 0$ (solid lines), and corresponding CGFs for the finite size system with $N = 10$ (dot-dashed lines) and $N = 25$ particles (dashed lines). Inserts: Zoom on the non-differentiable point of the light blue line for which $V = 1.5$. (c) CGF $\phi(\kappa, \gamma)$ and level lines for $V = 1.5$ (d) CGF $\phi(\kappa, \gamma)$ and level lines for $V = 0.5$. For all figures $H = 0$.

The CGF proceeds from the leading elements of the propagator of the generating function

$$\phi(\kappa, \gamma) = \lim_{N,T \to \infty} \frac{1}{NT} \ln \mathbf{E} \left[ e^{NT\gamma A + Nt\kappa M} \right]$$

$$= \max_{x^{\mathrm{f}}, x^{\mathrm{i}}} \lim_{N,T \to \infty} \frac{1}{NT} \ln G(x^{\mathrm{f}}, x^{\mathrm{i}}, \kappa, \gamma) \rho^{\mathrm{i}}(x^{\mathrm{i}}). \quad (6.44)$$

As explained above, we can focus on stationary trajectories that solve Eq. (6.43). Then, solving for $x$ amounts to find the extrema of $\mathscr{L}(x, 0, \kappa, \gamma)$. Assuming that

$\rho^{\mathrm{i}}(x) > 0$ for all $x$, one can safely drop the initial probability $\rho^{\mathrm{i}}$ in Eq. (6.44) ending with

$$\phi(\kappa, \gamma) = \max_x \mathscr{L}(x, 0, \kappa, \gamma) = \sqrt{\varphi(x^*(\kappa, \gamma), \gamma)} - \sum_{\epsilon = \pm 1} J_\epsilon(x^*(\kappa, \gamma)) + \kappa x^*(\kappa, \gamma),$$

(6.45)

Unfortunately, the determination of $x^*(\kappa, \gamma)$ involves a transcendental equation. We solved this equation numerically to provide the CGFs before and after the bifurcation in Fig 6.3d and 6.3c respectively. Cross-sections of the CGF in the plane $\kappa = 0$ and $\gamma = 0$ are shown in Fig 6.3a-b. After the bifurcation for $V = 1.5$, the CGF is clearly not differentiable. The left and right partial derivatives at $(\kappa, \gamma) = (0, 0)$ leads to different mean magnetization and activity in agreement with the bifurcation diagram of Fig 6.2 of the mean-field framework. We notice on Fig 6.3d that before the transition the CGF has a non differentiability not located at the origin of the $(\gamma, \kappa)$ plane. Hence the mean magnetization and activity are unique but their fluctuations are impacted by the phase transition. We confirm our results by computing numerically the CGF as the highest eigenvalue of the tilted matrix

$$K_{x,y}^{\gamma, \kappa} = \begin{cases} \omega_{(x,y)} e^{\gamma/N} & \text{if } x \neq y \\ \sum_y \omega_{(x,y)} + \kappa x/N & \text{if } x = y \end{cases},$$

(6.46)

for systems with $N = 10$ and $N = 25$ spins. As explained in sec. 2.2.3, the CGFs of finite size systems are everywhere differentiable and only approach gradually the non-differentiable CGF in the thermodynamic limit.

## 6.2.4 Canonical LDF of magnetization and activity

The canonical LDF $I_{\mathrm{ca}}(m, a)$ shown in Fig. 6.4c-d is the Legendre-Fenchel conjugate of the CGF

$$I_{\mathrm{ca}}(m, a) = \max_{\kappa, \gamma} \{\kappa m + \gamma a - \phi(\kappa, \gamma)\}.$$

(6.47)

At low interaction energy $V$, we observe a smooth function whose unique minimum is given by the mean-field solution of Eqs. (6.36-6.37). However at higher interaction energy, a plateau appears in the LDF between the MF solutions. This plateau, in association with the non-differentiability of the CGF, indicates a phase transition. As emphasized before, we always have ergodicity within the canonical ensemble, and this plateau is the result of a "temporal coexistence" of MF states: the system spends most of its time into the various MF states leading to a time averaged magnetization and activity belonging to the convex area defined by the MF solutions, here a triangle.

The contracted LDF for activity $I_{\mathrm{ca}}(a)$ and magnetization $I_{\mathrm{ca}}(m)$ defined by

$$I_{\mathrm{ca}}(m) = \min_a I_{\mathrm{ca}}(m, a) = \max_\kappa \{\kappa m - \phi(\kappa, 0)\}$$

(6.48)

$$I_{\mathrm{ca}}(a) = \min_m I_{\mathrm{ca}}(m, a) = \max_\gamma \{\gamma a - \phi(0, \gamma)\},$$

(6.49)

are shown in Fig. 6.4a-b, together with the LDFs for the finite size systems obtained from the Legendre transform of their corresponding CGFs in Fig. 6.3a-b. The latter LDFs converge towards the plateau with a speed that is lower for

the activity LDF than for the magnetization LDF in agreement with the fact that the plateau for the LDF of activity lies between a stable MF solution and an unstable MF solution, while the plateau for the magnetization lies between two stable solutions.
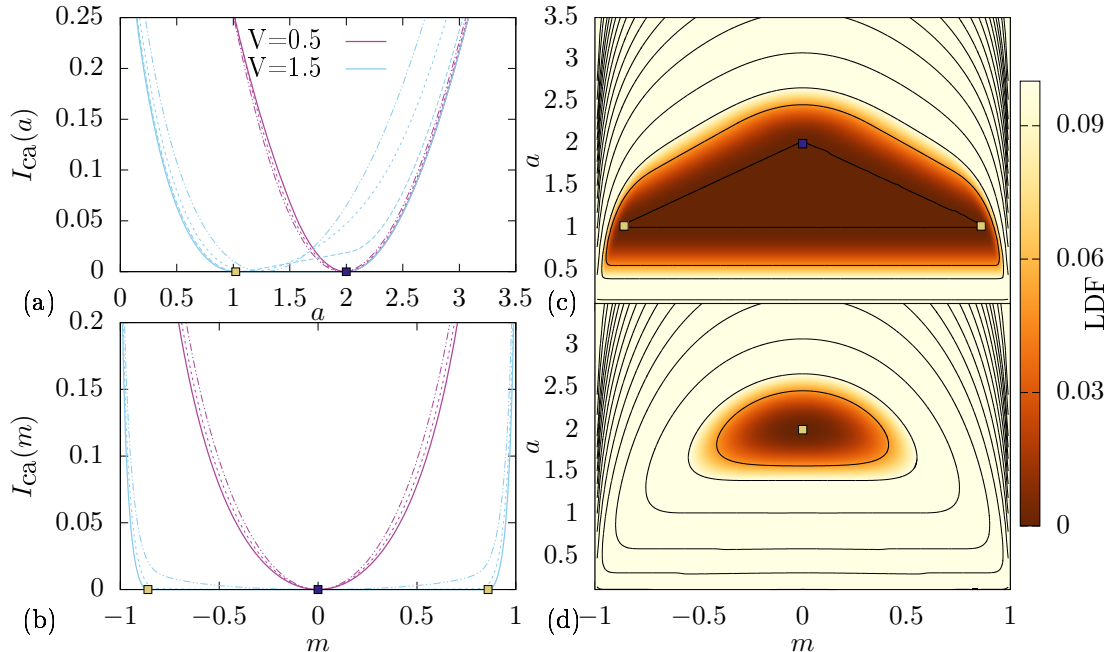


Figure 6.4: Canonical LDF $I_{\mathrm{ca}}(m,a)$ of activity and magnetization. (a) Canonical LDF $I_{\mathrm{ca}}(a)$ (solid lines) and finite size LDF for $N = 10$ (dot-dashed lines), $N = 25$ (dashed lines) and N=100 (long-dashed lines). (b) Canonical LDF $I_{\mathrm{ca}}(m)$ (solid lines) and finite size LDF for $N = 10$ (dot-dashed lines) and $N = 25$ (dashed lines). Parameters are for (a-b): $V = 0.5$ (magenta lines) and $V = 1.5$ (light blue lines). (c) Canonical LDF and level lines for $V = 1.5$. (d) Canonical LDF and level lines for $V = 0.5$. Beige squares indicate the location of the stable solutions of Eqs. (6.36-6.37) whereas dark-blue squares are for unstable solutions. For all figures $H = 0$. For figure (c-d), the color map replaces the level lines for low values of the LDFs.

## 6.2.5 Microcanonical LDF of magnetization and activity

As explained in the sec. 6.1.2, the microcanonical LDF follows from the Legendre-Fenchel transform of the elements of the propagator of the generating function. Therefore Eq. (6.16) yields

$$I_{\mathrm{mca}}(m,a) = \min_{x^{\mathrm{f}},x^{\mathrm{i}}} \max_{\kappa,\gamma} \left[ \kappa m + \gamma a - \lim_{N,T \to \infty} \frac{1}{NT} \ln G(x^{\mathrm{f}}, x^{\mathrm{i}}, \kappa, \gamma)\rho^{\mathrm{i}}(x^{\mathrm{i}}) \right] \quad (6.50)$$

Each stationary solution of Eq. (6.43) denoted $x^*$ defines a partial LDF

$$I_{x^*}(m,a) = \max_{\kappa,\gamma} \left\{ \kappa m + \gamma a - \mathscr{L}(x^*(\kappa,\gamma), 0, \kappa, \gamma) \right\}. \quad (6.51)$$

If the initial magnetization is in the attraction basin of the solution $x^*$, the system's fluctuations are best described by $I_{x^*}(m, a)$. When ensemble averaging on the initial condition, we look for the minimum on the stationary trajectories to obtain the microcanonical LDF

$$I_{\text{mca}}(m, a) = \min_{x \in \{x^*\}} I_x(m, a).$$  (6.52)

From the fact that $I_{\text{ca}}$ is the convex hull of $I_{\text{mca}}$, we get the following inequality between the two LDFs:

$$I_{\text{mca}}(m, a) \geqslant I_{\text{ca}}(m, a).$$  (6.53)

The microcanonical LDF $I_{\text{mca}}(m, a)$ is shown after the bifurcation on Fig. 6.5c, We also provide in Fig. 6.5a-b the partial LDF for activity and magnetization (after contraction) and their convex hulls. As expected, the microcanonical LDF is not convex: the ensemble equivalence does not hold (in a specific interval of magnetization and activity) for our model in the thermodynamics limit, due to non-ergodicity.

Comparing the canonical LDF obtained from Eq. (6.48) and the microcanonical LDF, we notice that the former is as expected the convex hull of the latter.

## 6.3 Non convex LDF and divergent mixing time

In the previous sections, we have obtained the two LDF of activity and magnetization for two different ensembles at thermodynamic limit. In this limit, the ensemble equivalence is broken. However at finite size, we have equivalence of the ensemble. We now explore the transition from equivalence to non-equivalence when increasing the size of the system, putting the emphasis on the order of the large size and long time limits in the computation of the statistics of magnetization and activity.

In this section, we point out the existence of a mixing time $t_{\text{mix}}$ that depends on the system size. For systems of finite size, the mixing time governs the fluctuation regime. First, we define the mixing time from the spectral gap of the finite size transition matrix $\boldsymbol{K}$. Second, we give an estimate of the mixing time for the Ising model and prove that it diverges when $N \to \infty$. This means that for large systems, it is impossible to fully relax from the initial condition, this leads to an ergodicity breaking. Finally, we explore the different regimes of fluctuations at finite size and time with numerical simulations, enlightening the coherence of our previous results.

For our numerical simulations in this section, the magnetic field is non zero ($H = 0.2$) in order to break the up-down symmetry of the Ising model. Without the magnetic field, one would see bi-modality of the activity probability density function at large $N$ only, in such a way that the unstable MF activity matters. This is beyond numerical reach. The use of a magnetic field simply overcome this difficulty, leading to two different stable MF activities and thus to a bi-modality in the activity fluctuations.
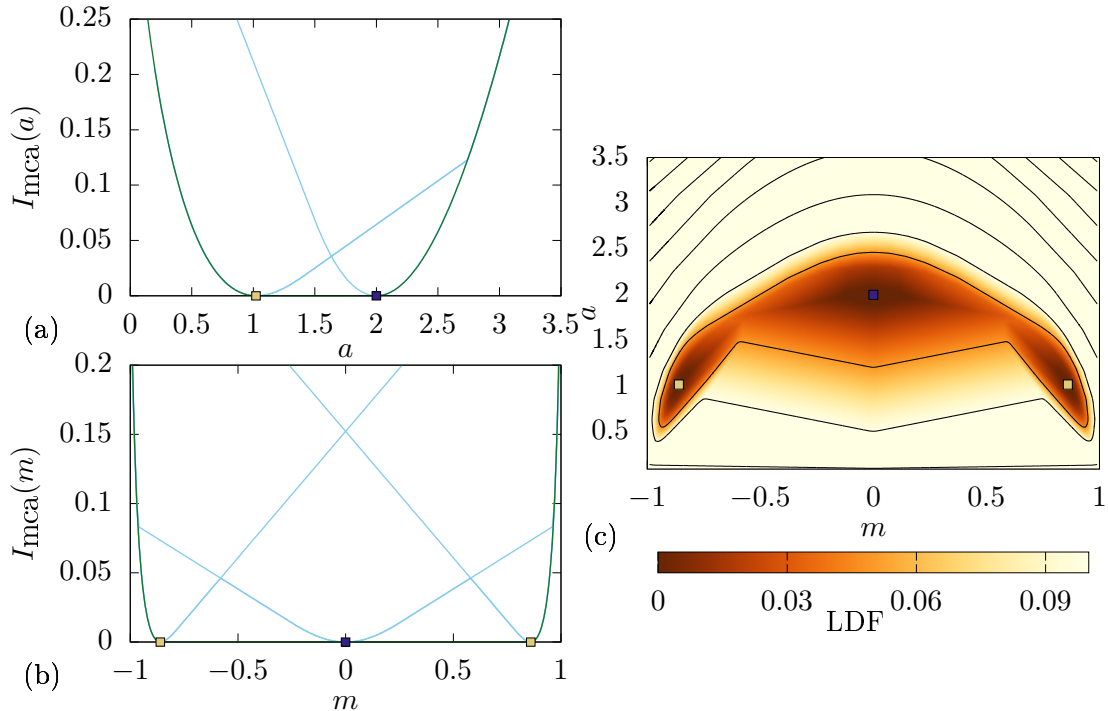
Figure 6.5: Branches of the microcanonical LDF of (a) activity and (b) magnetization, the microcanonical LDF being the minimum over those branches. Solid line represents the canonical LDF and dashed line the microcanonical LDF. (c) Level lines of the microcanonical LDF of activity and magnetization (color plot informs on the small values of the LDF only). For all figures, parameters are: $H = 0$ and $V = 1.5$. For figure (c), the color map replaces the level lines for low values of the LDF.

## 6.3.1 Decay of fluctuations for stationary finite size systems

**Definition of the mixing time** We come back to a finite size process with a transition matrix $\boldsymbol{K}$. We assume that this Markov operator is diagonalizable. The eigenvalues are $\lambda_n$, $n = 0 \ldots, N$, where $\lambda_0 = 0$ and all other eigenvalues are negative. The eigenvectors are $\boldsymbol{l}_v^n$, $\boldsymbol{r}_v^n$ with $n = 0 \ldots, N$ where $\boldsymbol{l}_v^0 = \boldsymbol{1}_v$ is a uniform vector and $\boldsymbol{r}_v^0 = \boldsymbol{\pi}_v$ the stationary probability. The spectral gap $\Delta\lambda$ of the matrix $\boldsymbol{K}$ is the difference between the largest eigenvalue $\lambda_0$ and the real part of its second eigenvalues $\lambda_1$. Considering the initial probability $\boldsymbol{\rho}_v^i$, the probability

$$\boldsymbol{\rho}_v(t) = e^{\boldsymbol{K}t} \cdot \boldsymbol{\rho}_v^i = \boldsymbol{\pi}_v + \sum_{n=1}^{N} e^{\lambda_n t} \boldsymbol{r}_v^n \boldsymbol{l}_v^{n\mathrm{T}} \cdot \boldsymbol{\rho}_v^i \tag{6.54}$$

is a formal solution to the master equation (1.19). Since the spectral gap $\Delta\lambda$ of the operator $\boldsymbol{K}$ is positive, the probability $\boldsymbol{\rho}_v(t)$ converges towards $\boldsymbol{\pi}_v$. The mixing time $t_{\mathrm{mix}}(\varepsilon)$ is used to quantify the time that the system takes to relax to the stationary probability [9]. By definition, the mixing time $t_{\mathrm{mix}}(\varepsilon)$ is the minimal time for which starting from any initial probability the system is at

most at a distance $\varepsilon$ of the stationary probability. Formally, the mixing time is

$$t_{\mathrm{mix}}(\varepsilon) = \inf \left\{ t \geqslant 0 \; : \; \max_{\rho^{\mathrm{i}}} \| e^{t\boldsymbol{K}} \cdot \boldsymbol{\rho}_{\mathrm{v}}^{\mathrm{i}} - \boldsymbol{\pi}_{\mathrm{v}} \|_{TV} \leqslant \varepsilon \right\}, \tag{6.55}$$

where the total variation distance is defined as $\|u\|_{TV} = \sup_A u(A)$. A common choice for $\varepsilon$ is $e^{-1}$, such that $t_{\mathrm{mix}} = t_{\mathrm{mix}}(e^{-1})$. The mixing time quantifies the time needed to reach stationary probability whatever the initial probability. In particular, an infinite mixing time is a feature of non-ergodic systems. When considering large deviation statistics, we must formally take long time limit. We emphasize that if we are at time long with respect to the mixing time, the large deviation statistics are approximately valid.

**Estimation of the mixing time from the spectral gap**   The mixing time of Eq. (6.55) is a maximization over all initial probability, therefore looking at $\|e^{t\boldsymbol{K}} \rho^{\mathrm{i}} - \boldsymbol{\pi}_{\mathrm{v}}\|_{TV}$ for a uniform initial probability $\boldsymbol{\rho}_{\mathrm{v}}^{\mathrm{i}} = \mathbf{1}_{\mathrm{v}}$ underestimates the mixing time. We plot on Fig. 6.6c, the evolution of this distance for various sizes.

First, we observe an exponential scaling of the total variation distance with time. When comparing with Eq. (6.54), we expect the mixing time to be connected with the spectral gap. Indeed we have for Markov processes [9]

$$\frac{1}{\Delta\lambda} \leqslant t_{\mathrm{mix}} \leqslant -\frac{\log \rho^{\mathrm{i}}{}_{\mathrm{min}}}{\Delta\lambda} \tag{6.56}$$

where $\rho^{\mathrm{i}}{}_{\mathrm{min}} = \min_n \rho_n^{\mathrm{i}}$ and $\Delta\lambda$ is the spectral gap.

Second, at very short times, the evolution of total variation distance have a different scaling. This short time behavior is the manifestation of the other eigenvalues whose influence over the probability $\boldsymbol{\rho}_{\mathrm{v}}(t)$ disappears quickly.

Finally, the evolution of the total variation distance with system size reveals the strong dependencies of the mixing time on the system size allowing for longer and longer transient behavior.

**Structure of fluctuations around the mixing time**   At finite time, the fluctuations critically differ if $T \ll t_{\mathrm{mix}}$ or if $T \gg t_{\mathrm{mix}}$. On Fig. 6.6a and 6.6b we show the empirical density probability of activity and magnetization for a system of $N = 60$ spins and trajectories of duration $T$, with $t_{\mathrm{mix}} \simeq 100$. And on Fig. 6.6d, we plot the empirical probability density of activity for a system size $N = 200$ where $t_{\mathrm{mix}} \simeq 10^5$.

For $T \gg t_{\mathrm{mix}}$, the long time probabilities of magnetization and activity, are the ones of an ergodic systems and are then linked with the convex LDFs of the sec. 6.2.4. As we add a small magnetic field, they are unimodal probability density functions, see Fig. 6.6a and 6.6b at $T = 300$.

Otherwise when the second eigenvalue is well separated from the others eigenvalues, *i.e.* when $\Delta\lambda \ll |\lambda_0 - \lambda_3|$, the probability $\boldsymbol{\rho}_{\mathrm{v}}(t)$ is well approximated for $0 \ll T \ll t_{\mathrm{mix}}$ by

$$\boldsymbol{\rho}_{\mathrm{v}}(t) \simeq \boldsymbol{\pi}_{\mathrm{v}} + e^{-t\Delta\lambda} \boldsymbol{r}_{\mathrm{v}}^1 \boldsymbol{l}_{\mathrm{v}}^{1\mathrm{T}} \cdot \boldsymbol{\rho}_{\mathrm{v}}^{\mathrm{i}}. \tag{6.57}$$
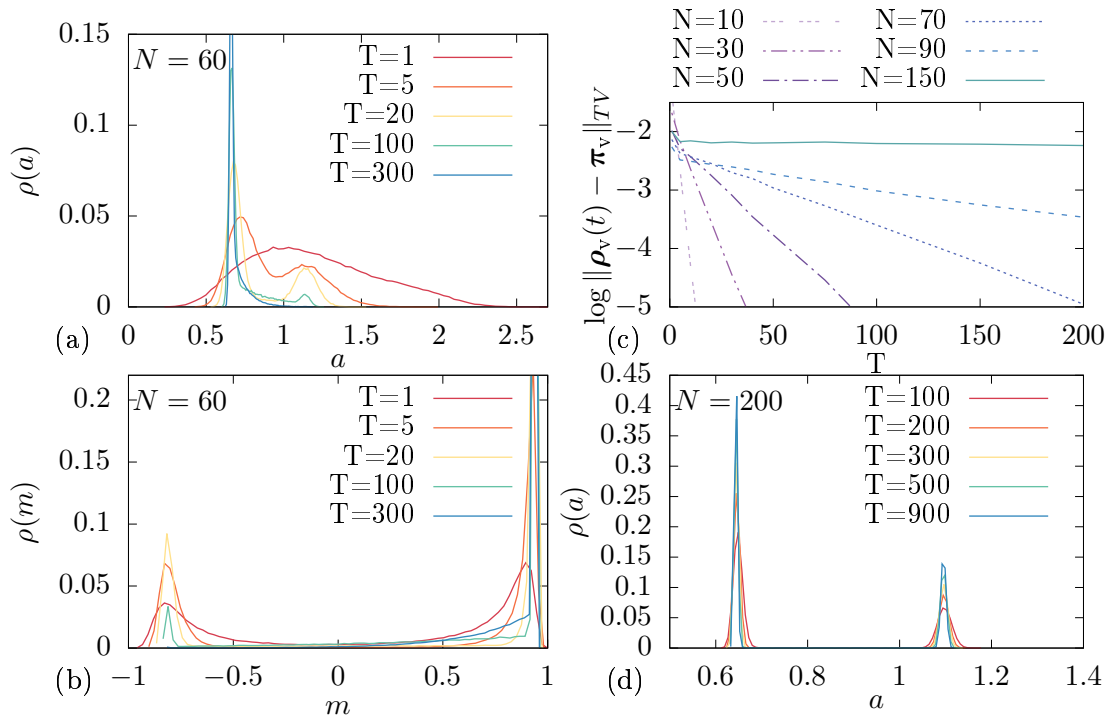
Figure 6.6: (a) Activity and (b) magnetization probability density functions obtained from numerical simulations of various duration $T$ for $N = 60$. (c) Logarithm of the total variation distance between $e^{TK} \cdot \rho_v^i$ and $\pi_v$ as a function of the duration of the evolution for various system size $N$. We simulate the evolution of $N$ spins using the Gillespie algorithm. For each size and time, a total of $15.10^4$ trajectories are drawn. The initial condition of the trajectory is draw from uniform distribution $\mathbf{1}_v$. The probability density functions are computed from a histogram of 75 bins between the minimum and maximum values. The total variation distance is the maximum of the difference between an histogram of the final value of the trajectory and an histogram of $15.10^4$ points drawn from probability of Eq. (6.23). (d) Activity probability density functions obtained from numerical simulations of various duration $T$ for $N = 200$. The parameters are: $V = 1.7$, $H = 0.2$.

It contains a term coming from the second eigenvalue. This second term induces the secondary peak on the probability density function. Therefore, for intermediate times before the mixing time, the system behaves as an effective non-ergodic system with fluctuations around each MF states (the system lacks of time to switch between states). We have a transient behavior where the probabilities of magnetization and activity are then bimodal, see Fig. 6.6d, and are linked with the microcanonical LDF of sec. 6.2.5.
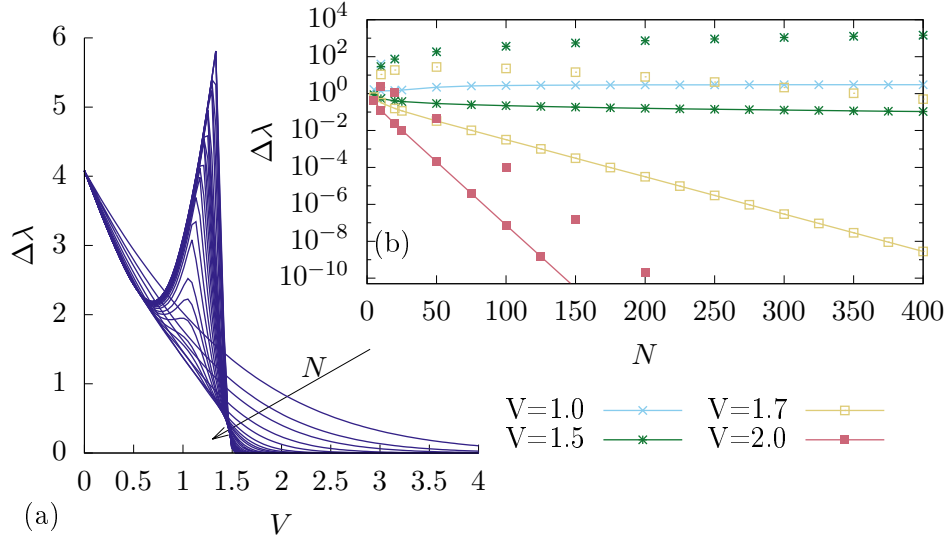
Figure 6.7: (a) Spectral gap as a function of the interaction energy $V$ for various system size between $N = 1$ and $N = 1000$. (b) Spectral Gap (lines with symbols) and bound of Eq. (6.66) (symbols) as a function of the system size for various interaction energy $V$. Parameter: $H = 0.2$.

## 6.3.2   Estimation of the spectral gap for equilibrium system

In order to determine how the mixing time scales with the system size, we now look for an upper bound on the spectral gap of equilibrium systems. Then, we can estimate using Eq. (6.56) the scaling of the mixing time with the system size from this bound.

**Cheeger constant**   For equilibrium Markov processes, we can estimate the spectral gap from the Cheeger bound. Indeed, transition matrices for equilibrium systems are similar to symmetric matrices for which exact result on the gap exist. We introduce the matrix $\mathbf{Diag}(\sqrt{\pi})$ as the diagonal matrix with elements $\mathrm{Diag}(\sqrt{\pi})_{n,n} = \sqrt{\pi_n}$. If the transition matrix $\boldsymbol{K}$ respects detailed balance, then the matrix

$$\mathbf{Diag}(\sqrt{\pi}) \cdot \boldsymbol{K} \cdot \mathbf{Diag}(\sqrt{\pi})^{-1} \tag{6.58}$$

is symmetric, and we can use the Cheeger constant as a bound for the spectral gap. We introduce the Cheeger constant as

$$\Phi = \inf_{\Xi \subset \Omega,\, 0 < \pi(\Xi) \leqslant 1/2} \frac{Q(\Xi^c, \Xi)}{\pi(\Xi)} \tag{6.59}$$

where $\Xi$ is any subset of the set of state of our system $\Omega$ such that $\pi(\Xi) = \sum_{x \in \Xi} \pi_x < 1/2$ and,

$$Q(\Xi^c, \Xi) = \sum_{x,y\,|\,x \in \Xi,\, y \in \Xi^c} \pi_x \omega_{y,x} \tag{6.60}$$

is the sum of probability flow from the subset $\Xi$ to the complementary of $\Xi$, denoted $\Xi^c$. From Ref. [116], we have

$$\Delta\lambda \leqslant 2\Phi. \tag{6.61}$$

**Upper bound for the Cheeger constant**   Computing the Cheeger constant is not easy in general, but it is quite easy to bound it from above. For a subset $\Xi$, the probability flow from $\Xi$ to $\Xi^c$, is simply bounded by

$$Q(\Xi^c, \Xi) \leqslant N_b \pi_{\acute{x}} \omega_{\acute{y}, \acute{x}} \tag{6.62}$$

where $N_b$ is the number of edge connecting $\Xi$ and $\Xi^c$ and

$$(\acute{x}, \acute{y}) = \operatorname*{argmax}_{x \in \Xi, \, y \in \Xi^c} \pi_x \omega_{y,x}, \tag{6.63}$$

the edge supporting the biggest probability flow from $\Xi$ to $\Xi^c$. Denoting then $\widetilde{x}$ the most probable state in $\Xi$, we have

$$\Phi \leqslant \frac{N_b \pi_{\acute{x}} \omega_{\acute{y}, \acute{x}}}{\pi_{\widetilde{x}}}. \tag{6.64}$$

As we are mainly interested in the large size limit of the mixing time, let's now assume that the stationary probability respects a large deviation principle

$$\pi_x \simeq_{N \to +\infty} e^{-N\mathscr{I}(x)}. \tag{6.65}$$

We consider a connected subset of states $\Xi$ such that the state $\bar{x}$ with $\mathscr{I}(\bar{x}) = 0$ is not in $\Xi$. For large enough $N$, the probability of $\Xi$ is surely less than $1/2$. Using the bound (6.64) on the Cheeger constant, we have a large deviation estimate as

$$\Phi \leqslant \frac{N_b \pi_{\acute{x}} \omega_{\acute{y}, \acute{x}}}{\pi_{\widetilde{x}}} \simeq N_b \omega_{\acute{y}, \acute{x}} e^{N(\mathscr{I}(\widetilde{x}) - \mathscr{I}(\acute{x}))}. \tag{6.66}$$

Therefore if it exists $\Xi$ such that the LDF $\mathscr{I}(x)$ has a local minimum on $\Xi$ that is not a global minimum, we will have $\mathscr{I}(\widetilde{x}) - \mathscr{I}(\acute{x}) < 0$. Then if the product $N_b \omega_{\acute{y}, \acute{x}}$ is not diverging exponentially, we have bounded the spectral gap by something going to 0 as $N \to +\infty$. Therefore the mixing time diverges with the system size, and the divergence is even exponential.

**Application to the Ising model**   In our case. we consider the subset of state $\Xi^- = \{x | x \leqslant 0\}$, if $H \geqslant 0$ it has a stationary probability less than $1/2$, otherwise if $H < 0$, we consider the subset $\Xi^+ = \{x | x \geqslant 0\}$. We have then $N_b = 1$, $\acute{x} = 0^-$ and $\acute{y} = 0^+$, the lower and upper closest states to 0. The stationary probability respects a large deviation principle, with a local minimum appearing after the phase transition. Therefore, we have a diverging mixing time after the phase transition, but not before.

These results are confirmed by numerical computation of the spectral gap. On Fig. 6.7a, we plot the spectral gap as a function of the system size $N$ and of the interaction energy $V$. Before the phase transition, the spectral gap remains finite

and so does the mixing time. After the phase transition, the spectral gap goes to zero when increasing $N$. The speed of convergence of the spectral gap is well caught by the bounds (6.66) as indicates the exponential decay with increasing $N$ shown on Fig. 6.7b. The mixing time is so at least diverging exponentially with the system size.

### 6.3.3   Non convexity and ergodicity

**Fluctuations and mixing time**   From the previous results, we are now able to explain the transition between equivalence and non-equivalence of ensembles. As emphasized, the fluctuations are different before and after the mixing time, and the mixing time is diverging with the system size. Therefore if we take long time limit before large size limit, we overcome the mixing time, the system stays ergodic. As the equivalence remains valid, the correct behavior of the fluctuations is given by the canonical LDF. However if we take large size limit first, the mixing time is infinite such that we stay in the regime of fluctuations before the mixing time, i.e. the LDF is non convex.

**Metastability in equilibrium systems**   We also emphasize that from the sec. 6.3.2, the presence of equilibrium metastable states leads to non-ergodicity and then to the non-equivalence of dynamical ensembles. The existence of such metastable states originates in the breaking of equivalence for equilibrium ensembles.

When considering the equilibrium ensembles, the question of the equivalence have been studied in detail [179], the non-equivalence is connected with either long-range interactions [41, 50, 56] or phase transitions [69, 80]. In particular, the fully connected Ising model that we studied in the sec. 6.2 exhibits both infinite range interactions and phase transitions.

Hence, we reveal a connection between the equivalence of equilibrium ensembles and the equivalence of dynamical ensembles when studying systems in equilibrium.

**Zeros of the LDF**   The most probable states are determined from the zeros of the LDF. When the system is non-ergodic and the LDF is non-convex, we observe separate zeros of the LDF. As the ergodicity is broken, they correspond to the most probable value of the observable generated by each metastable state, for the fully connected Ising model this is the various mean-field value of the observables. Theirs relative probability is determined from the initial probability to start within each subpart of the state space.

On the contrary, when the system is ergodic and the LDF convex, we observe a whole continuous set of observables values for which the LDF is zero, *e.g.* the triangle region in Fig. 6.4c. These values corresponds to trajectories that will spend a fraction of time around one metastable state and another fraction around another metastable state, the final value of the observables being the time average on the trajectory. The move between metastable states is allowed due to the ergodicity. These trajectories are connected with the instantons of

the Lagrangian, *i.e.* trajectories going from a stationary solution to another stationary solution of the Euler-Lagrange equation [14, 97, 130]. We did not take them in account in the minimization of Eq. (6.44). However, taking them into account does not modify the canonical LDF, but gives instead another LDF at a different scaling of large deviation [128].

# A complex model of machine: the Brownian Donkey

We introduce in this chapter a more complex model of machine, the Brownian Donkey, which is a non-equilibrium version of the model studied in the previous chapter [67]. This model is used to study the effects of interaction between several nanomachines on efficiency and power. The chosen interaction is here simple enough to allow (almost) analytical computations, as a coarse-grained representation of the model is available. We observe on this model emergent features in the thermodynamic limit, such as an emergent tight coupling and a phase transition. We study their consequences on the average efficiency and power. At fluctuating level, we obtain efficiency LDF with singular properties that we examine and explain.

## 7.1 Model definition and first properties

### 7.1.1 Association of simple machines

**Simple unicyclic machines** We start by considering a single noninteracting unicyclic nanomachine $i$, sketched in Fig. 7.1(a). It can be thought as a particle which can hop in two ways between a lower state $s_i = 0$ of energy zero and an upper state $s_i = 1$ of energy $H$. One way involves crossing an energy barrier of height $E_\mathrm{a}$ by exchanging energy with the cold reservoir $\nu = \mathrm{c}$ while another way involves crossing another energy barrier of the same height but by exchanging energy with the hot reservoir $\nu = \mathrm{h}$. Furthermore, hopping from $s_i = 1$ to $s_i = 0$ via cold channel requires to do work against the external nonconservative force $F$, while doing the same via hot channel gains work from $F$. The transition rates

$$\omega_{\epsilon;\mathrm{c}} = \Gamma e^{-\frac{\beta_\mathrm{c}}{2}[E_\mathrm{a} + \epsilon H - \epsilon F]} \tag{7.1}$$

$$\omega_{\epsilon;\mathrm{h}} = \Gamma e^{-\frac{\beta_\mathrm{h}}{2}[E_\mathrm{a} + \epsilon H + \epsilon F]} \tag{7.2}$$

therefore describes the probability per unit time for hopping upward ($\epsilon = +1$) or downward ($\epsilon = -1$) via channel $\nu = \mathrm{c}, \mathrm{h}$. We set the transitions rates to zero if the transition is not allowed. $\Gamma = 1$ sets the time scale unit.
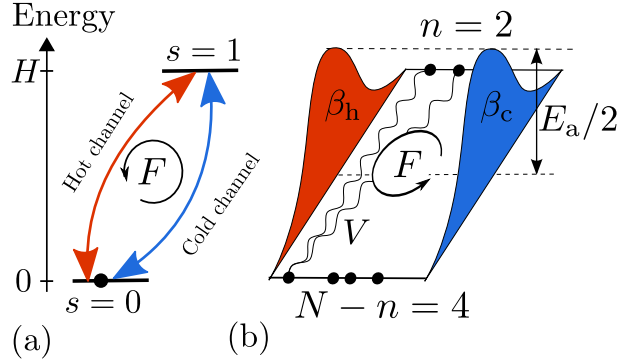
Figure 7.1: (a) Single two state machine subjected to a nonconservative force $F$ and which can change state due to two reservoirs. (b) Ensemble of $N = 6$ interacting machines in state $n = 2$.

In absence of force, the particle will in average move clockwise (i.e. go up via the hot reservoir and down via the cold one). When doing the same in presence of force, the machine operates as a heat engine which produces work by rotating against the force. When rotating on average counterclockwise (i.e. up via cold and down via hot reservoir), the machine operates as a heat pump since work is spent to bring energy from the cold to the hot reservoir.

This is one of the simplest model of thermal machines. However, being an unicyclic model, the machine is tight coupled.

**Interaction** We now turn to a collection of $N$ such unicyclic nanomachines as shown in Fig.7.1(b) interacting via an infinite range pairwise repulsive interaction of value $V/N$ between the particles with opposite states. The internal energy is thus

$$E_{\{s\}} = H \sum_{i=0}^{N} s_i + \frac{V}{N} \sum_{i=0}^{N} \sum_{j=0}^{N} s_i(1 - s_j), \tag{7.3}$$

where $\{s\}$ denotes a many-body state of the collective machine.

Via the mapping of state $s_i$ on the spin value $2s_i - 1$, the internal energy of Eq. 7.3 is that of the infinite range Ising model with coupling constant $V/4$ and magnetic field $H/2$. We thus recover the Ising model when $\beta_c = \beta_h$ and $F = 0$.

This collection of machines have been introduced in Ref [67, 183] as the Brownian Donkey, in order to study how negative mobility originates from fluctuations, explaining the origin of the name.

**Coarse-graining of the dynamics** The exact dynamics in term of microscopic states (i.e. many-body states), $\{s\}$, introduced in Eq. (7.1), can be exactly mapped into a dynamics on mesostates $n(\{s\}) = \sum_{i=0}^{N} s_i$ denoting the number of nanomachines in state $s_i = 1$. The mesostate probability $\rho_n(t) = \sum_{\{s\}} \rho_{\{s\}}(t)\delta_{n(\{s\}),n}$ evolves according to the master equation

$$\frac{\partial}{\partial t}\rho_n(t) = \sum_{\epsilon=\pm 1} \rho_{n+\epsilon}(t)\omega_{(n+\epsilon,n)} - \rho_n(t) \sum_{\epsilon=\pm 1} \omega_{(n,n+\epsilon)}, \tag{7.4}$$

where the transition rates for jumping from $n \to n + \epsilon$ due to reservoir $\nu$ are given by

$$\omega_{(n+\epsilon,n;\nu)} = \sum_i \omega_{\epsilon;\nu} \delta_{n,n(\{s\})} \delta_{s_i,(1-\epsilon)/2}. \tag{7.5}$$

We have for the cold and hot channel

$$\omega_{(n+\epsilon,n;c)} = N \left( \frac{1+\epsilon}{2} - \epsilon\frac{n}{N} \right) e^{-\frac{\beta_c}{2}(E_a + E_{n+\epsilon} - E_n - \epsilon F)} \tag{7.6}$$

$$\omega_{(n+\epsilon,n;h)} = N \left( \frac{1+\epsilon}{2} - \epsilon\frac{n}{N} \right) e^{-\frac{\beta_h}{2}(E_a + E_{n+\epsilon} - E_n + \epsilon F)} \tag{7.7}$$

with $E_n = Vn(N-n)/N + Hn$ the energy of the mesostate $n$. This result is due to the fact that the microscopic rates in Eq. (7.1) are the same for all microstates $\{s\}$ associated to the same mesostate $n$. We also define the total rates $\omega_{(n+\epsilon,n)} = \sum_\nu \omega_{(n+\epsilon,n;\nu)}$.

**Cycle and reservoirs matrix**   The graph of the coarse-grained system is represented on Fig. 7.2. It has $N+1$ states, $2N$ edges and $N$ cycles. The edges are labeled as $e_{2n-1}$, $n = 1,\ldots,N$ for edges connected to the cold bath and $e_{2n}$, $n = 1,\ldots,N$ for edges connected to the hot bath. The cycles $c_1,\ldots,c_N$ are obtained from the cycle matrix

$$\boldsymbol{C} = \begin{pmatrix} 1 & 0 & 0 & \cdots \\ -1 & 0 & 0 & \cdots \\ 0 & 1 & 0 & \cdots \\ 0 & -1 & 0 & \cdots \\ \vdots & & 0 & \ddots \end{pmatrix}. \tag{7.8}$$

The nonconservative force $F$ is applied on all transition, , see sec. 1.2.6, such that the reservoirs matrix is a $4 \times 2N$ matrix (the two columns represented correspond to edge $e_{2n-1}$ and $e_{2n}$)

$$\boldsymbol{R} = \begin{pmatrix} & E_n - E_{n-1} & 0 & \\ \cdots & 0 & E_n - E_{n-1} & \cdots \\ & -1 & 0 & \\ & 0 & 1 & \end{pmatrix}, \tag{7.9}$$

with reservoir affinities

$$\boldsymbol{f}_{\mathrm{r}}^{\mathrm{T}} = (-\beta_c, -\beta_h, \beta_c F, \beta_h F). \tag{7.10}$$

Using the reservoirs matrix, the mesoscopic rates satisfy the local detailed balance

$$\ln \frac{\omega_{(n+\epsilon,n;c)}}{\omega_{(n,n+\epsilon;c)}} = -\beta_c(E_{n+\epsilon} - E_n - \epsilon F) + S_{n+\epsilon} - S_n, \tag{7.11}$$

$$\ln \frac{\omega_{(n+\epsilon,n;h)}}{\omega_{(n,n+\epsilon;h)}} = -\beta_h(E_{n+\epsilon} - E_n + \epsilon F) + S_{n+\epsilon} - S_n \tag{7.12}$$

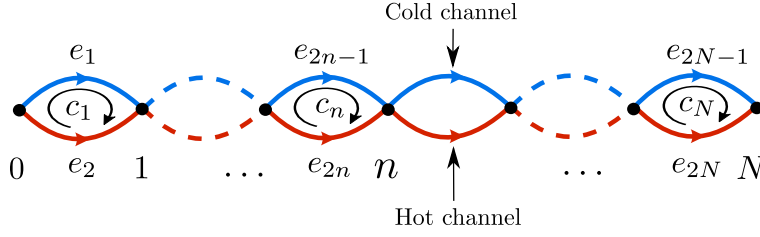where each state has now an associated internal entropy $S_n = \ln N!/[n!(N-n)!]$.

Figure 7.2: Graph representation of an ensemble of $N$ interacting machines with identification of the edges and cycles; the two types of edges correspond to the hot (red) and cold (blue) heat reservoirs.

**Stationary probability**   We derive the explicit stationary probability enabling to compute currents of the collective machine with a finite number of particles. The stationary probability is given by the spanning tree formula [163]:

$$\pi_n \propto \sum_{T_\alpha(n)} \prod_{(n,\epsilon)\in T_\alpha(n)} \sum_\nu \omega_{(n+\epsilon,n;\nu)}. \tag{7.13}$$

The sum runs on all spanning trees $T_\alpha(n)$ rooted in $n$. The product spans all possible edges (oriented to the root) in a tree: $(n,\epsilon)$ is the edge associated to the transition $n \to n+\epsilon$. For the graph displayed in Fig. 7.2, the sum on spanning trees can be factorized into the more explicit expression

$$\pi_n = \frac{1}{Z} \left[ \prod_{m=0}^{n-1} \sum_\nu \omega_{(m+1,m;\nu)} \right] \left[ \prod_{m=n+1}^{N} \sum_\nu \omega_{(m-1,m;\nu)} \right], \tag{7.14}$$

where $Z$ is a normalization constant scaling like $N^N$. Using this stationary probability, the steady state cycle current per machine $j_{c_n}$ of the cycle $c_n$ reads

$$N j_{c_n} = \omega_{(n+1,n;2)}\pi_n - \omega_{(n,n+1;2)}\pi_{n+1} = \omega_{(n,n+1;1)}\pi_{n+1} - \omega_{(n+1,n;1)}\pi_n. \tag{7.15}$$

**Tree-like system**   Even if the system is set out of equilibrium by its external reservoirs, the total rates $\omega_{(n+\epsilon,n)}$ respect detailed balance with respect to the stationary probability (7.14). Indeed if we join togheter the two edges linking each pair of states, the graph of the system of Fig. 7.2 becomes a linear tree and do not have cycles.

## 7.1.2   The Brownian Donkey as a machine

We study the assembly of machines as a single machine, let's see how to obtain the physical currents of the coarse-grained system.

**Physical currents and partial entropy rate**   From the cycle and reservoirs matrix, we have two conservations laws

$$\boldsymbol{\ell_r^{1T}} = (1,1,0,0) \quad \text{and} \quad \boldsymbol{\ell_r^{2T}} = (0,0,1,-1). \tag{7.16}$$

We set the selection matrix and physical matrix (the represented column corresponds to cycle $c_n$) as

$$\mathbf{V} = \begin{pmatrix} 1 & -F/2 \\ -1 & F/2 \\ 0 & 1/2 \\ 0 & 1/2 \end{pmatrix} \quad \mathbf{P} = \begin{pmatrix} \cdots & E_n - E_{n-1} + F & \cdots \\ \cdots & -2 & \cdots \end{pmatrix} \tag{7.17}$$

such that the two physical affinities are given by

$$f_1 = \beta_c - \beta_h \tag{7.18}$$
$$f_2 = \beta_c F. \tag{7.19}$$

**Power and efficiency** From the physical matrix, the partial entropy production rates are the input entropy production rate

$$\sigma_1 = (\beta_c - \beta_h) \sum_{n=1}^{N} [E_n - E_{n-1} + F] \, j_{c_n}, \tag{7.20}$$

this is the entropy production rate associated with the heat coming from the hot reservoir, and the output entropy production rate

$$\sigma_2 = -2\beta_c F \sum_{n=1}^{N} j_{c_n}, \tag{7.21}$$

this is the entropy production rate associated with the work done by the external non-conservative force.

From Eqs. (7.20–7.21), we see that in absence of interactions, $V = 0$, the property of tight coupling is satisfied. Indeed both the input and the output entropy production rates are in this case proportional to the same current $\sum_{n=1}^{N} j_{c_n}$. However, this property is lost in presence of interaction since the input entropy production rate looses this proportionality while the input does not.

Based on the entropy production decomposition (7.20–7.21), the efficiency of the machine operating as a heat engine ensues

$$\eta = \frac{-\sigma_2}{\sigma_1} \quad \text{and} \quad \bar{\eta} = \frac{-\bar{\sigma}_2}{\bar{\sigma}_1}. \tag{7.22}$$

Indeed, in average work is extracted, $\bar{\sigma}_2 < 0$, heat is absorbed from the hot reservoir, $\bar{\sigma}_1 > 0$, particles rotate on average in the clockwise direction. When $\bar{\sigma}_2 > 0$ and $\bar{\sigma}_1 < 0$, the machine operates as a heat pump, particles rotate in the counter clockwise direction on average, and the macroscopic efficiency of the heat pump, $1/\eta$, is bounded by $1 \geq 1/\bar{\eta} > 0$. The dud engine regime occurs when $\bar{\eta} < 0$.

**Remark:** The coarse-graining does not affect the entropy production rates. In the absence of transition between microstates inside the same mesostate, the determination of the entropy production rates from the coarse-grained transition rates is the same than the one determined from the microstate transition rates [82].

### 7.1.3 Thermodynamics limit

In the following, we set $H$ to zero for simplicity.

**Mean-field density** In the thermodynamic limit, i.e. when $N \gg 1$, the energy change for the transition $n \to n + \epsilon$ becomes

$$\lim_{N \to \infty} E_{n+\epsilon} - E_n = \epsilon \Delta E(x) = \epsilon V(1 - 2x) \qquad (7.23)$$

where the state of the system is now a density of particle $x = n/N$. In the same idea, the transition rates are

$$
\begin{aligned}
J_{\epsilon;\nu}(x) &= \lim_{N \to +\infty} \frac{\omega(xN+\epsilon, xN; \nu)}{N} \\
&= \begin{cases}
\left(\dfrac{1+\epsilon}{2} - \epsilon x\right) e^{-\frac{\beta_c}{2}[E_a + \epsilon \Delta E(x) - \epsilon F]} & \nu = c; \\
\left(\dfrac{1+\epsilon}{2} - \epsilon x\right) e^{-\frac{\beta_h}{2}[E_a + \epsilon \Delta E(x) + \epsilon F]} & \nu = h.
\end{cases}
\end{aligned} \qquad (7.24)
$$

In the continuous limit, the master equation Eq. (7.4) can be transformed into an evolution equation for the density

$$\langle \dot{x} \rangle = \sum_{\epsilon = \pm 1} \epsilon \langle J_\epsilon(x) \rangle, \qquad (7.25)$$

with $J_\epsilon(x) = J_{\epsilon;c}(x) + J_{\epsilon;h}(x)$. The serie expansion of Eq. (7.25) shows that momenta $\langle x^m \rangle$ of order $m \geq 1$ appear in the right hand side: the equation is not closed. Upon mean field approximation, whose validity is studied in the next paragraph, we close this equation into the following non linear equation

$$\langle \dot{x} \rangle = \sum_{\epsilon = \pm 1} \epsilon J_\epsilon(\langle x \rangle). \qquad (7.26)$$

Its steady state solutions are the mean field densities $x^{\mathrm{MF}}$ verifying

$$J_-(x^{\mathrm{MF}}) = J_+(x^{\mathrm{MF}}). \qquad (7.27)$$

These densities are represented in the branching diagram of Fig.7.3a. At a critical value of the interaction energy $V_{\mathrm{cr}}^{\mathrm{MF}}$ of the interaction, three MF densities appear instead of a unique density. The complete phase diagram of the model is provided in the next section.

**Fokker-Planck equation** We confirm the validity of the mean-field approximation by expanding (up to second order) the master equation (7.4) leading to the Fokker-Planck equation:

$$\dot{\rho}_x(t) = -\frac{\partial}{\partial x}\left\{[J_+(x) - J_-(x)]\rho_x(t)\right\} + \frac{1}{2N}\frac{\partial^2}{\partial x^2}\left\{[J_+(x) + J_-(x)]\rho_x(t)\right\}. \quad (7.28)$$

The last term disappears when $N \to +\infty$ and the mean field approximation is exact: the state $x^{\mathrm{MF}}$ will be the state of maximum probability in the stationary state.
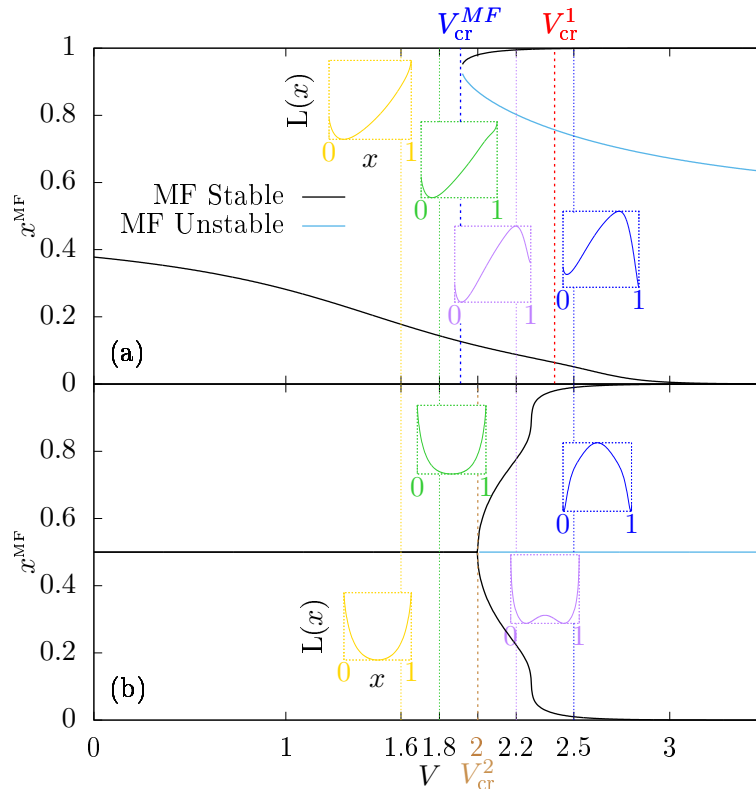
Figure 7.3: Stable (black) and unstable (light blue) mean field steady state densities $x^{\mathrm{MF}}$ versus interaction (a) In a presence of a first order phase transition, $F = 0.5$. energy $V$. Insets: density LDFs versus the density $x$ for four values of $V$ indicated by vertical dashed lines. The value of the minimum of the density LDF changes abruptly across the phase transition denoted by the thick dashed line (red). (b) In a presence of second order phase transition, $F = 0$. The value of the minimum of the density LDF changes smoothly at $V^2_{\mathrm{cr}}$. The other parameters are: $E_{\mathrm{a}} = 2$, $\beta_{\mathrm{c}} = 10$, $\beta_{\mathrm{h}} = 1$.

**LDF of density** We can go a step further and compute the large size limit of the stationary probability $\boldsymbol{\pi}_{\mathrm{v}}$ (7.14). We use the following convention for the continuous limit

$$\sum_{m=0}^{n-1} \frac{1}{N} \longrightarrow \int_0^x \mathrm{d}x', \tag{7.29}$$

to obtain

$$\pi_x = \frac{1}{Z} \exp\left[N \int_0^x \mathrm{d}x' \ln J_+(x') + N \int_x^1 \mathrm{d}x' \ln J_-(x')\right] \tag{7.30}$$

$$Z = \int_0^1 \mathrm{d}x \exp\left[N \int_0^x \mathrm{d}x' \ln J_+(x') + N \int_x^1 \mathrm{d}x' \ln J_-(x')\right]. \tag{7.31}$$

We use the Laplace's method to compute the non-equilibrium partition function $Z$ for large $N$. The exponent is maximum for each densities $x_i^{\mathrm{MF}}$ corresponding to the $i$th mean field solutions (ordered in growing order by convention) of the

master equation $J^-\left(x^{\text{MF}}\right) = J^+\left(x^{\text{MF}}\right)$. Let's denote $\kappa$ the total number of mean field solutions $x^{\text{MF}}$ for which the exponent in Eq. (7.31) has the same global maximum value. In this case, we have

$$Z \simeq \kappa \exp\left[N \int_0^{x^{\text{MF}}} \mathrm{d}x' \ln J_+(x') + N \int_{x^{\text{MF}}}^1 \mathrm{d}x' \ln J_-(x')\right]. \qquad (7.32)$$

Remark that the other solutions $x_i^{\text{MF}}$ for which the exponent has a smaller local maximum do not contribute in the large $N$ limit. Thanks to this expression of the non-equilibrium partition function, we can obtain the large deviation function of density for this model defined by

$$\mathscr{I}(x) = \lim_{n\to\infty} \frac{-1}{N} \ln \pi_{\left(x=\frac{n}{N}\right)} \qquad (7.33)$$

Using Eqs. (7.30) and (7.32), we get

$$\mathscr{I}(x) = \int_x^{x^{\text{MF}}} \mathrm{d}x' \ln \frac{J_+(x')}{J_-(x')}, \qquad (7.34)$$

whose vanishing minimum is at the mean field density $x^{\text{MF}}$ with highest probability. The stationary probability for density writes asymptotically

$$\pi_x \asymp e^{-N\mathscr{I}(x)}. \qquad (7.35)$$

This density LDF is shown in the inset of Fig. 7.3a for different values of the interaction energy $V$.

**Phase diagram** Eq. (7.27) exhibits one or several solutions, indicating a critical behavior. This phase transition has been studied by Cleuren and Van den Broeck to show that it was associated with negative response phenomena when applying the external nonconservative force [67]. Noticing that a negative response is equivalent to a work production, we aim at describing the thermodynamic behavior of the machine in the presence of the phase transition.

At the mean-field level, the transition (at the critical interaction energy $V_{\text{cr}}^{\text{MF}}$) from one to three MF densities is the signature of a phase transition. The analytical value of $V_{\text{cr}}^{\text{MF}}$ can be computed for $F = 0$ [67]

$$V_{\text{cr}}^{\text{MF}} = 2 \frac{e^{-\beta_\text{c} E_\text{a}/2} + e^{-\beta_\text{h} E_\text{a}/2}}{\beta_\text{c} e^{-\beta_\text{c} E_\text{a}/2} + \beta_\text{h} e^{-\beta_\text{h} E_\text{a}/2}}. \qquad (7.36)$$

The new MF densities may not be reached right after crossing the critical value $V_{\text{cr}}^{\text{MF}}$. This is illustrated by the inset of Fig.7.3a representing the large deviation function of density whose extrema are located at the MF densities. We observe that the minimum of the LDF, corresponds to the most likely density and changes abruptly for $V_{\text{cr}}^1 \simeq 2.4 > V_{\text{cr}}^{\text{MF}}$. Therefore, the system undergoes a first order phase transition on the critical line $V_{\text{cr}}^1$ at higher energy than the mean field critical line $V_{\text{cr}}^{\text{MF}}$. The corresponding phase diagram is provided in Fig.7.4. This phase transition is of significant relevance since the discontinuity of the density produces
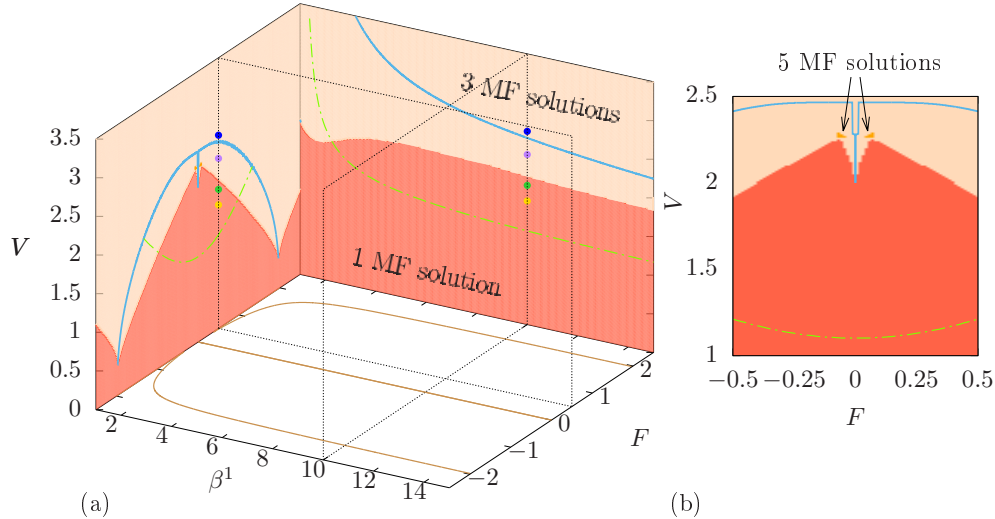
Figure 7.4: (a) Non-equilibrium phase diagram of the machine. A cross-section for $\beta_c = 10$ is projected on the back left face, and for $F = 0.5$ on the back right face. The solid blue line represents the locus of the transition $V_{cr}^1$, and the dot-dashed green line, the locus of $\bar{\eta} = 1$. The frontier between the red and salmon area is the line $V_{cr}^{MF}$. The yellow ($V = 1.6$), green ($V = 1.8$), violet ($V = 2.2$) and blue ($V = 2.5$) points indicate the location in the phase diagram corresponding to the parameters taken for other figures. The critical line $V_{cr}^2$ is projected on the bottom face (solid brown line): this line is the intersection of the locus of the transition $V_{cr}^1$ with the red area (b) Zoom over the cross-section for $F = 0.5$ to emphasize the possibility of 5 MF solutions. The parameters are: $E_a = 2$, $\beta_h = 1$.

a discontinuity of other thermodynamic variables, like for instance the entropy production rates or the efficiency due to the dependence of these variables on the MF density.

The system undergoes also a second order phase transition on the critical line $V_{cr}^2$, as show on Fig. 7.3b. In this case, the phase transition coincides with the appearance of the new MF densities. Outside of the zone delimited by this critical line, the system no longer has a phase transition, and is supercritical. In particular, we retrieve the classical order-disorder phase transition of the Ising model for the system under equilibrium conditions, i.e. $F = 0$ and $\beta_c = \beta_h$. We emphasize also the possibility to have five different MF solutions to Eq. (7.27), as shown on Fig. 7.4b.

## 7.2 Emerging tight coupling

### 7.2.1 Efficiency and power in the thermodynamic limit

We now turn to the mean field approximation for the input and output parts of the entropy production rate per machine that become

$$
\begin{aligned}
\bar{\sigma}_1^{\mathrm{MF}} &= (\beta_{\mathrm{c}} - \beta_{\mathrm{h}}) \left[\Delta E(x^{\mathrm{MF}}) + F\right] j_{c_{Nx^{\mathrm{MF}}}} && (7.37) \\
\bar{\sigma}_2^{\mathrm{MF}} &= -2\beta_{\mathrm{c}} F j_{c_{Nx^{\mathrm{MF}}}}, && (7.38)
\end{aligned}
$$

because the number of particles in the upper state converges to $Nx^{\mathrm{MF}}$ in the macroscopic limit. Note that the mean field approximation restores the tight coupling property in presence of interaction as both the input and output entropy production rates become proportional to $j_{c_{Nx^{\mathrm{MF}}}}$ in the macroscopic limit and hence proportional to each other. The macroscopic efficiency becomes in the mean field description

$$
\bar{\eta}^{\mathrm{MF}} = -\frac{\bar{\sigma}_2^{\mathrm{MF}}}{\bar{\sigma}_1^{\mathrm{MF}}} = \frac{2\beta_{\mathrm{c}} F}{(\beta_{\mathrm{c}} - \beta_{\mathrm{h}}) \left[\Delta E(x^{\mathrm{MF}}) + F\right]}. \tag{7.39}
$$

Due to the tight coupling property one expects this efficiency to be higher than the efficiency of a finite ensemble of interacting machines.

The emergent tight coupling originates in a local coupling between output and input entropy production rates. Indeed for each cycle, we can define a local efficiency as

$$
\eta_{c_n}^{\mathrm{l}} = \frac{2\beta_{\mathrm{c}} F}{(\beta_{\mathrm{c}} - \beta_{\mathrm{h}})[(E_{n+1} - E_n) + F]}, \tag{7.40}
$$

which is the ratio between input and output entropy production rates for each cycle. In the thermodynamic limit, only few cycles around $c_{Nx^{\mathrm{MF}}}$ contribute to the total entropy production rate. As a consequence, the local efficiency (7.40) for cycle $c_{Nx^{\mathrm{MF}}}$ becomes the macroscopic efficiency (7.39). The existence of a local efficiency function of the state $n$ will significantly influence the efficiency fluctuations in connection with the critical behavior of the particle density.

### 7.2.2 Non-equilibrium conductance matrix

Previous results can be confirmed by looking at the non-equilibrium matrix. From the cycle and physical matrix (7.8) and (7.17), we can compute the non-equilibrium matrix. The corresponding degree of coupling is given by

$$
\xi = -\frac{\sum_{n=1}^{N}(E_n - E_{n-1} + F)\frac{j_{c_n}}{f_{c_n}}}{\sqrt{\left(\sum_{n=1}^{N}(E_n - E_{n-1} + F)^2\frac{j_{c_n}}{f_{c_n}}\right)\left(\sum_{n=1}^{N}\frac{j_{c_n}}{f_{c_n}}\right)}}, \tag{7.41}
$$

with $f_{c_n} = (\beta_{\mathrm{c}} - \beta_{\mathrm{h}})(E_n - E_{n-1}) - (\beta_{\mathrm{c}} + \beta_{\mathrm{h}})F$ the affinity of the cycle $c_n$. The degree of coupling is plotted as a function the system size $N$ in Fig. 7.6. When the system is composed of only one nanomachine we have tight coupling. This property is lost as soon as two nanomachines are coupled together, but reappears in the infinite size limit. We emphasize that the sign of the degree of coupling is in accordance with the efficiency of Fig. 7.5b.
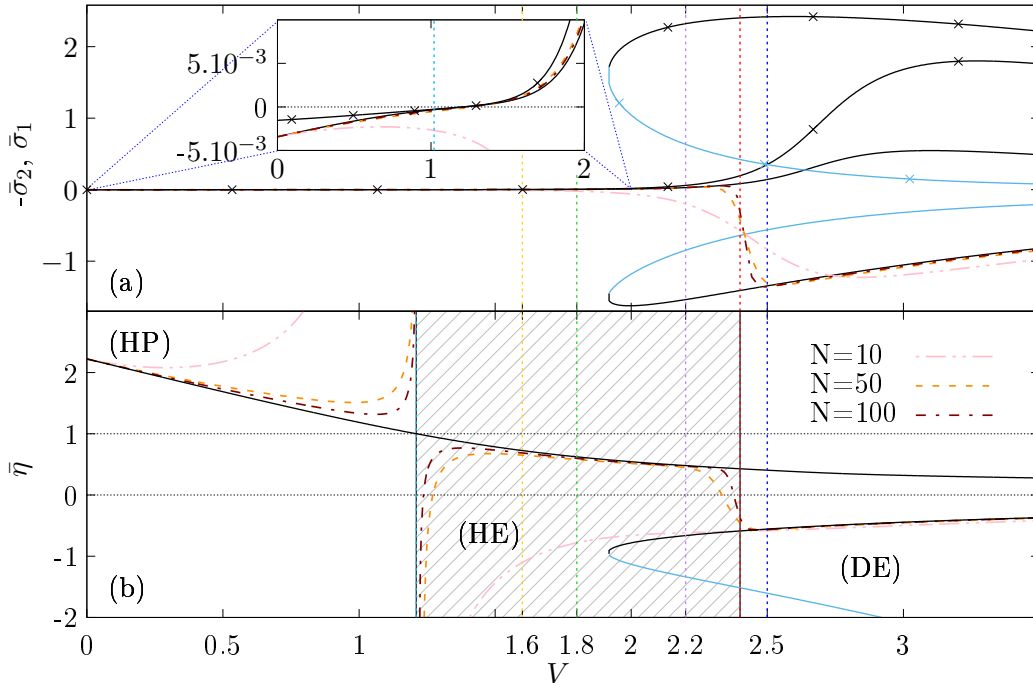
Figure 7.5: (a) Input (resp. output) entropy production rate $\bar{\sigma}_1$ (resp. $-\bar{\sigma}_2$) per machine received (resp. delivered to the outside) by the ensemble of $N$ interacting machines, as a function of the interaction energy $V$. Black (and light blue) crossed lines for $\bar{\sigma}_1$, and black (and light blue) solid lines for $-\bar{\sigma}_2$. The color indicates the stability of the mean field solutions ($N \to \infty$): stable for black lines and unstable for light blue lines. Vertical dashed lines correspond to our four value of $V$. Dot-dashed lines (pink, orange and brown) correspond to input entropy production rate for various values of $N$. Inset: Zoom of the input and output entropy production rates for $V \in [0, 2]$. (b) Macroscopic efficiency for finite $N$ (dot-dashed lines) and in the mean field limit (solid lines). HE, HP and DE denotes respectively the Heat Engine, the Heat Pump and the Dud Engine regimes. The heat engine regime is hatched by gray lines. The parameters are: $E_a = 2$, $\beta_c = 10$, $\beta_h = 1$, $F = 0.5$.

## 7.3 Currents and efficiency fluctuations

We now turn to the study of the currents and efficiency fluctuations in the large size and long time limit. Based on the results of Ch. 6, we compute the propagator of the generating function and obtain the efficiency LDF within microcanonical and canonical ensemble.
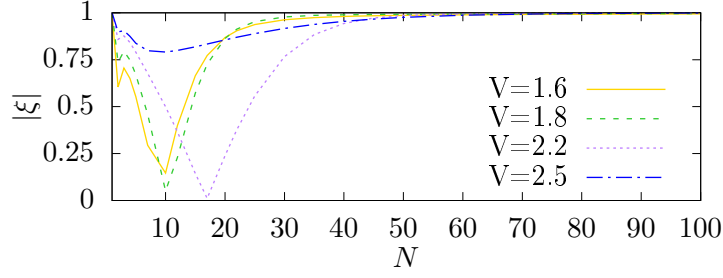
Figure 7.6: Absolute value of the degree of coupling (7.41) as a function of the system size $N$ for various interaction strength $V$. The degree of coupling for $V = 2.5$ is positive wheras all others have negative value. We used the same parameters as in Fig. 7.5.

### 7.3.1 Propagator of the generating function

**Tilted matrix**   For a finite number of machines, the fluctuations are obtained from the tridiagonal tilted matrix $\boldsymbol{K}^{\gamma_1,\gamma_2}$ of elements

$$
\begin{aligned}
K^{\gamma_1,\gamma_2}{}_{n,n} &= -\sum_{\epsilon=\pm 1,\,\nu=\text{c,h}} \omega_{(n,n+\epsilon;\nu)} \\
K^{\gamma_1,\gamma_2}{}_{n+1,n} &= \omega_{(n+1,n;\text{c})} + \omega_{(n+1,n;\text{h})} e^{\gamma_1(\beta_\text{c}-\beta_\text{h})(E_{n+1}-E_n+F)-2\gamma_2\beta_\text{c}F} \\
K^{\gamma_1,\gamma_2}{}_{n-1,n} &= \omega_{(n-1,n;\text{c})} + \omega_{(n-1,n;\text{h})} e^{-\gamma_1(\beta_\text{c}-\beta_\text{h})(E_{n-1}-E_n+F)+2\gamma_2\beta_\text{c}F}
\end{aligned}
\tag{7.42}
$$

We remark that the tilted matrix is similar to the symmetric tridiagonal matrix $\boldsymbol{K}^{\gamma_1,\gamma_2}_\text{sym}$ of elements [16]

$$
\begin{aligned}
K^{\gamma_1,\gamma_2}_\text{sym}{}_{n,n} &= K^{\gamma_1,\gamma_2}{}_{n,n}; \tag{7.43} \\
K^{\gamma_1,\gamma_2}_\text{sym}{}_{n+1,n} &= K^{\gamma_1,\gamma_2}_\text{sym}{}_{n-1,n} = \sqrt{K^{\gamma_1,\gamma_2}{}_{n+1,n} K^{\gamma_1,\gamma_2}{}_{n-1,n}}. \tag{7.44}
\end{aligned}
$$

Then all the eigenvalues of the tilted matrix are real, and we can use results of Ch. 6. This is in accordance with the tree-like structure of graph 7.2 when considering total transition rates.

**Large size propagator**   From standard methods [33, 107, 22], we obtain the propagator of the generating function of the entropy production rates as

$$
G(x^\text{f}, x^\text{i}, \gamma_1, \gamma_2) = \mathbf{E}\left[ e^{NT(\gamma_1+\gamma a_2)} \right]_{x^\text{f},x^\text{i}} \tag{7.45}
$$

$$
\simeq_{N\to+\infty} \exp\left( N \int_0^T \mathrm{d}t\, \mathscr{L}(x_t, \dot{x}_t, \gamma_1, \gamma_2) \right) \tag{7.46}
$$

where $\mathscr{L}$ is the Lagrangian

$$
\mathscr{L}(x, \dot{x}, \gamma_1, \gamma_2) = \dot{x} \ln\left( \frac{-\dot{x} + \sqrt{\dot{x}^2 + \varphi(x, \gamma_1, \gamma_2)}}{2 \sum_{\nu=1,2} J_{-1;\nu}(x) e^{-f_\nu(x,\gamma_1,\gamma_2)}} \right)
$$

$$
- \sum_{\epsilon=\pm 1,\nu=\text{c,h}} J_{\epsilon;\nu}(x) + \sqrt{\dot{x}^2 + \varphi(x, \gamma_1, \gamma_2)} \tag{7.47}
$$

with

$$\varphi(x, \gamma_1, \gamma_2) = 4 \prod_{\epsilon = \pm 1} \sum_{\nu = \mathrm{c,h}} J_{\epsilon;\nu}(x) e^{\epsilon f_\nu(x,\gamma_1,\gamma_2)}, \qquad (7.48)$$

and

$$\begin{aligned} f_\mathrm{c}(x, \gamma_1, \gamma_2) &= 1; && (7.49)\\ f_\mathrm{h}(x, \gamma_1, \gamma_2) &= \gamma_1(\beta_\mathrm{c} - \beta_\mathrm{h})(\Delta E(x) + F) - 2\gamma_2 \beta_\mathrm{c} F \\ &= (\beta_\mathrm{c} - \beta_\mathrm{h})(\Delta E(x) + F)(\gamma_1 - \eta^\mathrm{l}(x)\gamma_2). && (7.50) \end{aligned}$$

where $\eta^\mathrm{l}(x)$ is equivalent to $\eta^\mathrm{l}_{c_n}$ introduced in the Eq. (7.40) with $x = n/N$. Notice the similarity with the Lagrangian (6.40) for the fully connected Ising model. The propagator of Eq. (7.45) is almost explicit: the path $x_t$ starting in $x^\mathrm{i}$ and ending in $x^\mathrm{f}$ must be determined using the Euler-Lagrange equation

$$\frac{\partial \mathscr{L}}{\partial x} = \frac{\mathrm{d}}{\mathrm{d}t}\left(\frac{\partial \mathscr{L}}{\partial \dot{x}}\right). \qquad (7.51)$$

Due to the large size limit and as explained in the previous chapters, the model is non-ergodic. At large time, the dominants contribution are obtained from stationary solutions of Euler-Lagrange equation that we denote $x^*$.

## 7.3.2 CGF of the currents

The CGF proceeds from the leading elements of the propagator of the generating function

$$\phi(\gamma_1, \gamma_2) = \max_{x^\mathrm{f},x^\mathrm{i}} \lim_{N,T\to\infty} \frac{1}{NT} \ln G(x^\mathrm{f}, x^\mathrm{i}, \gamma_1, \gamma_2)\rho^\mathrm{i}(x^\mathrm{i}) = \max_x \mathscr{L}(x, 0, \gamma_1, \gamma_2). \quad (7.52)$$

The CGF is plotted on Fig. 7.7 for various values of the interaction strength. It reveals interesting features in connection with the properties of the Brownian Donkey studied in sec. 7.1.3 and 7.2.

**Metastability** For certain values of $(\gamma_1, \gamma_2)$, the CGF is non differentiable, the locus of this non differentiability is represented on Fig. 7.7 by a gray dashed line. In particular the point $(\gamma_1, \gamma_2) = (0,0)$ becomes a point of non differentiability when three MF solutions appear (this is the case for $V = 2.2$). This is in accordance with results of Ch. 6.

**Emergent tight coupling** The property of local proportionality of cycle entropy production rates leads to a particular symmetry of the Lagrangian. We introduce the function

$$\widetilde{\gamma}(\gamma, x) = -1/2 + (\gamma + 1/2)\eta^\mathrm{l}(x), \qquad (7.53)$$

Accordingly, the Lagrangian verifies the symmetry

$$\forall\, x \in \mathbb{R} \quad \mathscr{L}(x, 0, \widetilde{\gamma}(\gamma_2, x), \gamma_2) = \mathscr{L}(x, 0, -\frac{1}{2}, -\frac{1}{2}) \qquad (7.54)$$
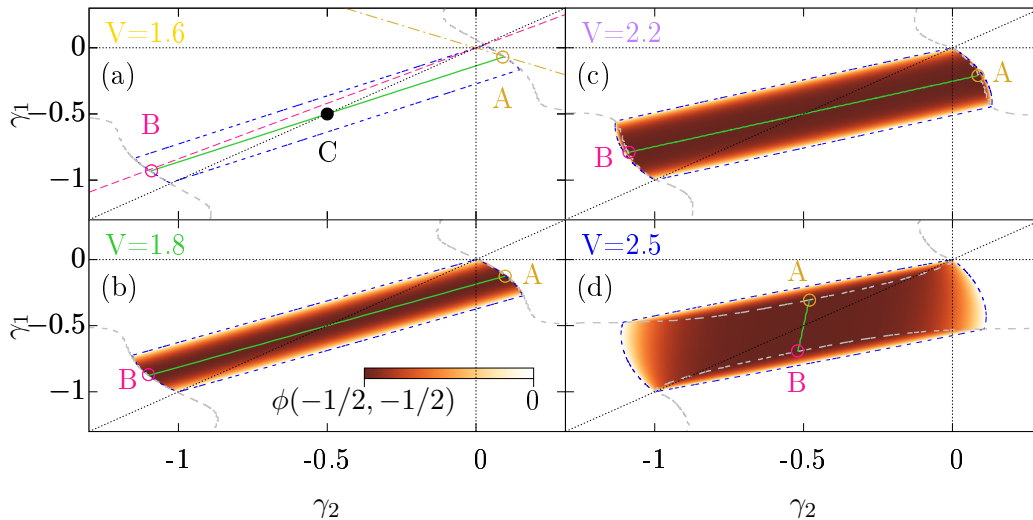
Figure 7.7: (a–d): CGFs (7.52) as a function of $\gamma_1$ and $\gamma_2$ for four different values of the interaction energy $V$. The green solid line denotes the location of the minimum of the CGF. The blue dashed line is the contour line of the CGF for $\phi = 0$. The gray dashed line separates the regions with different dominant trajectories. We used the same parameters as in Fig. 7.5.

The same symmetry holds for the partial derivatives with respect to $x$ at constant $\gamma_1, \gamma_2$ of $\mathscr{L}(x, 0, \gamma_1, \gamma_2)$. As a consequence, these partial derivative evaluated in $(x^*)$ and $(\widetilde{\gamma}(\gamma_2, x^*), \gamma_2)$ vanishes. Hence if a stationnary trajectory $x^*$ is a solution for $(\gamma_1, \gamma_2) = (-1/2, -1/2)$ it is also a stationary solution of the Euler-Lagrange equation along the line $\widetilde{\gamma}(\gamma_2, x^*)$ of Eq. (7.53) in the $\gamma_1, \gamma_2$ space. As such, it is at least a local extremum of the action and may be a global maximum. The fact that the same maximizing trajectory, here $x^*$, exists for different values of $\gamma_1, \gamma_2$ implies that the classical action stays constant leading to a degeneracy of $\phi(\gamma_1, \gamma_2)$ in the $\gamma$ space.

There are now three possible cases:

(i) $x^*$ is the maximizing trajectory along the whole line of Eq. (7.53) and the machine displays tight coupling in the large size limit.

(ii) $x^*$ is a maximizing trajectory on a segment of the line of Eq. (7.53) due to the apparition of (at least) one new maximizing trajectory when changing $\gamma_1, \gamma_2$. This is related to the presence of a dynamical phase transition in the system between a null entropy production phase and higher entropy production phase.

(iii) $x^*$ is never a maximizing trajectory, excepted at $(\gamma_1, \gamma_2) = (-1/2, -1/2)$: another maximizing trajectory immediately appears when deviating from this point.

This symmetry leads to a degeneracy of the minimum of the CGF, that is illustrated in Fig. 7.7 by a green solid line. For the Brownian Donkey, we are in the case (ii) the degeneracy is interrupted by the presence of the dynamical phase transition.
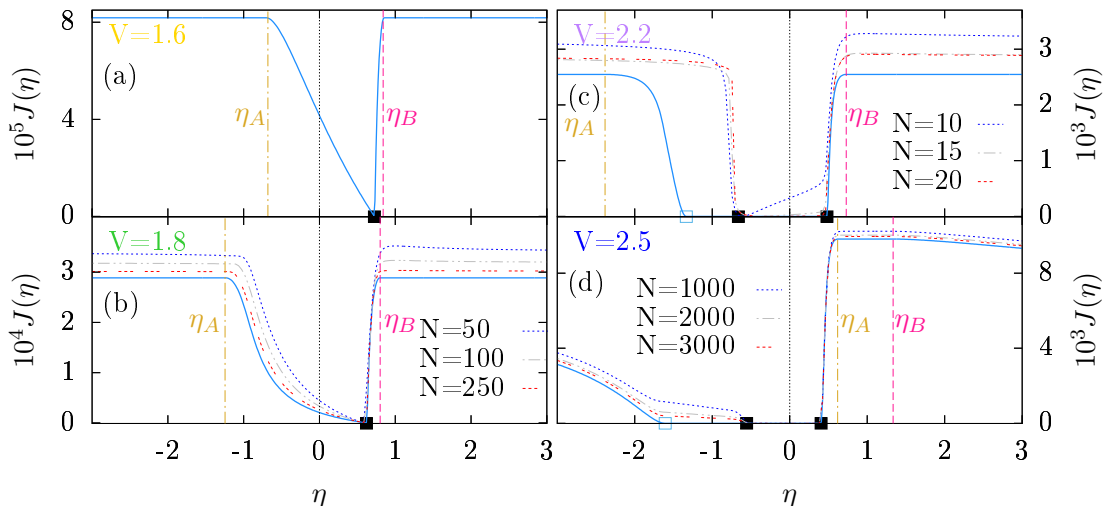
Figure 7.8: (a–d): Long time efficiency LDF at finite $N$ (dashed lines) and $N \to \infty$ (solid line) for our four values of $V$. The solid black squares mark the position of the stable MF efficiencies while the empty blue squares mark the position of the unstable MF efficiency. The dashed vertical lines are located at the efficiency values $\eta_A$ and $\eta_B$ corresponding to slopes of the lines crossing the boundaries of the plateaus on Fig. 7.7(a–d) We used the same parameters as in Fig. 7.5.

### 7.3.3 Efficiency fluctuations

**Ergodic case** First, we compute the efficiency LDF within the canonical ensemble. The efficiency LDF is obtained directly from the Eq. (3.50)

$$J_{\mathrm{ca}}(\eta) = -\min_{\gamma_2} \phi(\gamma_2 \eta, \gamma_2). \qquad (7.55)$$

The results are presented on the Fig. 7.8 for different values of the interaction energy $V$ smaller and higher than the critical value $V_{\mathrm{cr}}^1$. We remark two particular features of these curves regarding its maximum and minimum.

First, we notice that the maximum is a plateau at any interaction energy $V$. The height of this plateau is given by the opposite of the degenerated minimum of the CGF $\phi(\gamma_1, \gamma_2)$ of Fig. 7.7 (green solid line). Hence, the plateau is associated with the degeneracy of the minimum of the entropy production CGF that we discussed earlier. Using a geometrical interpretation of Eq. (7.55), a straight line crossing the origin in Fig.7.7 can be associated with an efficiency $\eta$ given by its slope; then the minimum of $\phi(\gamma_1, \gamma_2)$ along this line yields $-J_{\mathrm{ca}}(\eta)$. Hence, the boundaries $\eta_A$ and $\eta_B$ of the higher plateaus of the efficiency LDF are the slopes of the lines crossing A and B in Fig.7.7. These points are at the intersection of the line of Eq. (7.53) with the critical line (gray dashed line) at which the classical trajectory changes abruptly. Therefore, even though the interaction energy is far below the critical value $V = 2.4$, the phase transition impacts the rare efficiency fluctuations producing the higher plateau of $J_{\mathrm{ca}}(\eta)$.

Second, the minimum of the efficiency LDF is given by another plateau connecting MF values of the efficiencies. Since the partial derivatives of $\phi(\gamma_1, \gamma_2)$ at
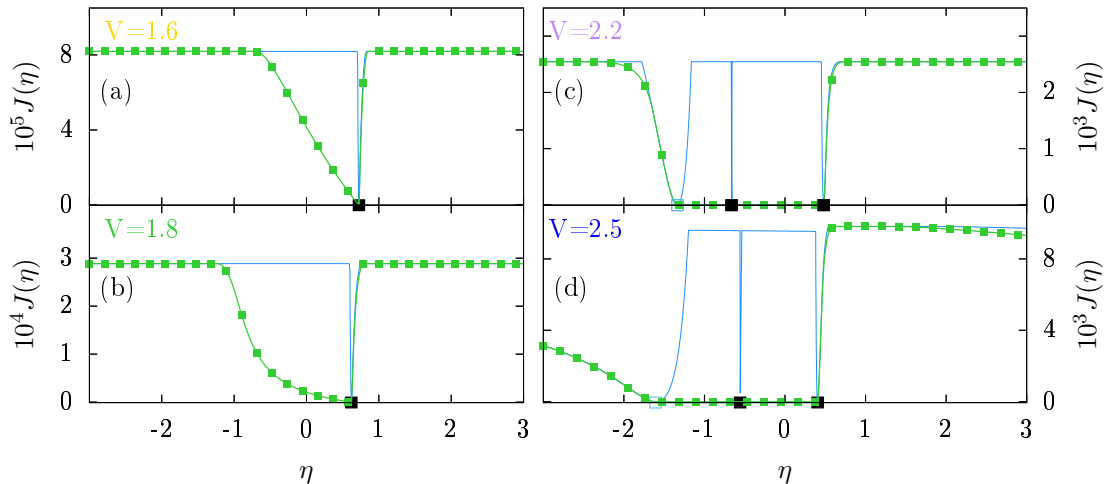
Figure 7.9: (a–d): Long time efficiency LDF for $N \to \infty$ for our four values of $V$. The solid black squares mark the position of the stable MF efficiencies while the empty blue squares mark the position of the unstable MF efficiency. Solid lines are for the microcanonical LDF and lines with squares are for the canonical LDF. We used the same parameters as in Fig. 7.5.

the origin $(\gamma_1, \gamma_2) = (0, 0)$ gives the mean entropy production rate, the efficiency line tangent to the contour $\phi(\gamma_1, \gamma_2) = 0$ at the origin corresponds to the macroscopic efficiency. On Fig.7.7a, this macroscopic efficiency is well defined. On Fig.7.7b as well, but the critical line (gray dashed line) is approaching the origin. On Fig.7.7c–d a cusp has appeared at the origin for the critical line meaning that the tangent may take two different values. This means that a subdominant trajectory (soon to become dominant) starts to play a role as a local extremum of the action. This subdominant trajectory first flattens $J_{\mathrm{ca}}(\eta)$ on Fig.7.8b and produces the plateau connecting the MF efficiencies in Fig.7.8c–d when becoming a dominant trajectory.

We note that the numerical results at finite size show a faster convergence on the right side of this plateau as compared to the left side. Indeed, the left part of the plateau is due to the unstable MF efficiency. In the large size limit, i.e. when the system undergoes no fluctuations, this efficiency is a correct solution at long time, however at smaller size, the fluctuations exponentially reduce the probability of the unstable MF efficiency.

However this lower plateau is a result of the non equivalence of the canonical and microcanonical ensembles because the efficiency LDF is computed from the convex hull of the LDF for the entropy production rates. As a consequence, a number of entropy production rates are equally probable, just as the corresponding efficiencies. As explained in sec. 6.3.3, another LDF with a different large deviation scaling appears on this plateau and gives a finer analysis of the efficiency relative probability [128]

**Non-ergodic case**  Next, we compute the efficiency LDF within the microcanonical ensemble. The microcanonical efficiency LDF comes from

$$
\begin{aligned}
J_{\mathrm{mca}}(\eta) &= -\max_{x^{\mathrm{f}},x^{\mathrm{i}}} \min_{\gamma_2} \lim_{N,T\to\infty} \frac{1}{NT} \ln G(x^{\mathrm{f}}, x^{\mathrm{i}}, \gamma_2\eta, \gamma_2)\rho^{\mathrm{i}}(x^{\mathrm{i}}) \qquad &(7.56) \\
&= -\max_{x^*} \min_{\gamma_2} \mathscr{L}(x^*, 0, \gamma_2\eta, \gamma_2). &(7.57)
\end{aligned}
$$

Denoting $J_{x^*}(\eta) = -\min_{\gamma_2} \mathscr{L}(x^*, 0, \gamma_2\eta, \gamma_2)$ the various branches of the efficiency LDF deriving from each stationary solutions of the Euler-Lagrange equation, we have

$$
J_{\mathrm{mca}}(\eta) = \min_{x^*} J_{x^*}(\eta). \qquad (7.58)
$$

When comparing both efficiency LDF, we have

$$
\forall \eta, \quad J_{\mathrm{mca}}(\eta) \geqslant J_{\mathrm{ca}}(\eta). \qquad (7.59)
$$

The microcanonical LDF of efficiency is provided in Fig. 7.9 and compared with the canonical LDF.

We first note the persistence of the higher plateau, even if it can be of different size (see Fiq. 7.9a and b for example). As the symmetry of the Eq. (7.53) is still valid for all branches having a solution for $(\gamma_1, \gamma_2) = (-1/2, -1/2)$, they have also the plateau. In particular, for $\eta = 1$ the solution is found for both cases at $\gamma_2 = -1/2$ and therefore the canonical and the microcanonical efficiency LDF have the same value for $\eta = 1$.

Second, we comment the behavior of the minimum of the LDF in the microcanonical case. There is now a finite number of zeros given by the MF values of the efficiency. Due to the ergodicity breaking, they correspond to the most probable efficiencies associated to each subpart of the state space, as explained in sec. 6.3.3. Their relative probabilities are then given by the initial probability to start within each subspace according to Eq. (7.56).

# Conclusion

Our journey across the world of small machines in stationary state stops here. We have investigated various aspects of the thermodynamics and fluctuations of machines.

Small machines with a discrete state space are described by Markov processes on graphs. The relation between Markov processes and the graph theory gives first insights into the behavior of small machines: the evolution of probability, ruled by the master equation, depends on the edge currents and impact the physics of the system at various levels of description. The thermodynamics structure is set by the connection with the environment, through the reservoir matrix. This setup provides an efficient description of stochastic machines.

**Mean operation**   We have introduced the non-equilibrium conductance matrix as a generalization of the close-to-equilibrium Onsager matrix. It connects affinities and mean currents. The extension of close-to-equilibrium concepts to far-from-equilibrium gives an effective parametrization of the efficiency of machines.

The degree of coupling constrains the maximum efficiency, specifying that Carnot efficiency is only reachable by tight coupled machines. The tight coupling is generally a properties of unicyclic systems but we have seen a model where the tight coupling emerges in the thermodynamics limit.

Beyond maximum efficiency, the conductance matrix also constrains the relation between power and efficiency and we have unified the various available power-efficiency trade-offs into a common structure.

**Fluctuations**   We have studied the fluctuations in the framework of large deviation theory. Efficiency LDF can be derived and reveals surprising features, *e.g.* the maximum of efficiency LDF is connected to the reversible efficiency, and the shape of the efficiency LDF is universal. We have shown that these features are conserved for machines with more than two physical fluxes, with the extra fluxes modeling machines losses. When the losses are unknown and small, the efficiency LDF is almost the one without losses.

We have also considered mean-field interacting models. They feature an ergodicity breaking in the thermodynamics limit, that can be related to the presence

of metastable states. This affects the equivalence of dynamical ensembles that is widely used to compute LDFs. We have demonstrated how one can overcome this difficulty by taking care of the metastable branches of the CGF. The efficiency LDF for the Brownian Donkey have been then computed and compared with efficiency LDF obtained from a convex entropy production rates LDF.

**Connection between mean and fluctuating level**   Fluctuations and mean values of currents are not independent. The non-equilibrium conductance matrix not only set the mean values of the currents but also bounds the currents and efficiency LDF. Through this connection, we have derived generalized fluctuation-dissipation relations. Therefore the determination of the non-equilibrium conductance matrix gives insights into the behavior of small machines.

# Open problems

Even if this manuscript answers a few questions about the thermodynamics and fluctuations of small machines, there are still questions to be answered. We list here some of the directions that can be explored:

**Diffusive system** Diffusive systems have a continuous state space and are not covered by this manuscript. However, we expect that most of the results could be extended. The quadratic structure of the fluctuations should even simplify the description by a non-equilibrium conductance matrix [126, 149]. For ergodic continuous state space, there is a possibility of non-equivalence of ensembles when the left eigenvectors of the tilted matrix cannot be normalized [127, 129, 175], and this impacts efficiency fluctuations [98].

**Time-periodic machines** This manuscript concentrates on time-independent machines. However, we can also drive machines by considering time-periodic driving. Standard engine protocols, including the Carnot and Stirling cycles, feature such time-periodic driving and generally lack time-reversal symmetry in both macroscopic and microscopic realizations [49]. This broken time-reversal symmetry affects many of the results derived in this manuscript, *e.g.* we have modified versions of the detailed fluctuation theorem [86, 173] or of the Onsager matrix [151, 154]. For efficiency fluctuations, the maximum of the efficiency LDF is no longer the Carnot efficiency [95, 189]. Being an active direction of research, there is a growing number of results about time-periodic driven systems, but questions about generalization of non-equilibrium conductance matrix and associated relations (thermodynamics uncertainty relations, efficiency-power trade-offs, bounds on efficiency LDF,...) are still open.

**Finite time fluctuations** The results derived in this manuscript are focused on large time fluctuations. We could seek for the extension of our results to finite-time systems or at least the derivation of finite-time corrections to large deviation regime. There has been a recent derivation of finite-time thermodynamics uncertainty relations [101, 142] that represents a good

starting point for the extension of the non-equilibrium conductance matrix and subsequent relations. About efficiency fluctuations, it exists results for all time fluctuations of close-to-equilibrium machines [145], and the generalization of these results to machines with several fluxes seems straightforwards. We expect that the finite-time conductance matrix could provide a useful framework for approximating efficiency fluctuations at all time for far-from-equilibrium machines.

**Mixing time** The mixing time gives an approximate time scale upon which large deviations begin to be valuable. The Cheeger bound of sec. 6.3.2 is only valid for equilibrium systems [116], but its generalization to out-of-equilibrium systems could give new insights to the mixing time and the different time scales at play in non-equilibrium systems.

**Dynamical phase transition** For systems with a dynamical phase transition but ergodic [181], the LDF can feature a plateau for the minimum (zero) values. We emphasize in sec. 6.3.3 that another LDF with a different scaling has to be considered [25]. The study of fluctuations at this different scaling is a fully open question [128].

**Experiments** This manuscript stays at a rather theoretical level, but this is the hope of the author that the tools and results developed here will find useful applications for modeling real physical systems. The question remains open to known whether the non-equilibrium conductance matrix can itself be determined experimentally or used to design efficient machines. The results about non-equivalence of dynamical ensembles could be used in the description of glassy systems that features large mixing time [48, 92, 110].

# Appendix

## A.1 Matrix glossary

Matrices are often used in this manuscript. For this reason, we recall in this section few useful definitions and properties of matrices.

### A.1.1 Positive matrix

A matrix is a positive when its components are all positive. A matrix $\boldsymbol{A}$ is a Metzler matrix if there exists a constant $c$ such that $\boldsymbol{A} + c\,\mathbf{Id}$ is a positive matrix. Hence, this is a matrix with positive off-diagonals elements.

A nonnegative matrix $\boldsymbol{A} \in \mathbb{R}^{n \times n}$ is a matrix whose all components are nonnegative, morever it is a irreductible matrix if and only of $(\mathbf{Id} + A)^{n-1}$ is a positive matrix.

For nonnegative matrices the Perron-Fröbenius theorem is [16]

**Theorem: Perron-Fröbenius.** *Let $\boldsymbol{A} \in \mathbb{R}^{n \times n}$ be a irreducible and nonnegative matrix, and suppose that $n \geqslant 2$. Then*

a) *There is a positive real number $\lambda_0$, called the Perron–Frobenius eigenvalue (also called the leading eigenvalue or dominant eigenvalue), such that $\lambda_0$ is an eigenvalue of $\boldsymbol{A}$ and any other eigenvalue $\lambda$ is stricly smaller than $\lambda_0$ in absolute value.*

b) *$\lambda_0$ is an algebraically simple eigenvalue of $\boldsymbol{A}$*

c) *$\boldsymbol{A}$ has a unique right eigenvector $\boldsymbol{r}$ with eigenvalue $\lambda_0$ whose components are all positive.*

d) *$\boldsymbol{A}$ has a unique left eigenvector $\boldsymbol{l}$ with eigenvalue $\lambda_0$ whose components are all positive.*

### A.1.2 Positive-definite matrix

A matrix $\boldsymbol{A} \in \mathbb{R}^{n \times n}$ is positive-definite if

$$\forall \boldsymbol{x} \in \mathbb{R}^n, \quad \boldsymbol{x}^{\mathrm{T}} \cdot \boldsymbol{A} \cdot \boldsymbol{x} > 0 \tag{A.1}$$

and it is positive semi-definite if the equality case is allowed in the previous equation.

We introduce a matrix order for symmetric matrices, called Loewner partial order [16]. It is defined in such a way that $\boldsymbol{A} \geqslant \boldsymbol{B}$ means that $\boldsymbol{A} - \boldsymbol{B}$ is a positive semi-definite matrix. This implies that for two symmetric $n \times n$ matrices $\boldsymbol{A}$ and $\boldsymbol{B}$:

$$\boldsymbol{A} \geqslant \boldsymbol{B} \Leftrightarrow \forall \boldsymbol{x} \in \mathbb{R}^n, \quad \boldsymbol{x}^{\mathrm{T}} \cdot \boldsymbol{A} \cdot \boldsymbol{x} \geqslant \boldsymbol{x}^{\mathrm{T}} \cdot \boldsymbol{B} \cdot \boldsymbol{x}. \tag{A.2}$$

### A.1.3   Moore-Penrose pseudo inverse

**Definition**   The Moore-Penrose pseudo inverse is a generalization of the inverse matrix. Lets' $\boldsymbol{A}$ be a $n \times m$ real matrix, the Moore-Penrose pseudo inverse $\boldsymbol{A}^+$ is the unique matrix satisfying the following four conditions

- $\boldsymbol{A} \cdot \boldsymbol{A}^+ \cdot \boldsymbol{A} = \boldsymbol{A}$

- $\boldsymbol{A}^+ \cdot \boldsymbol{A} \cdot \boldsymbol{A}^+ = \boldsymbol{A}^+$

- $(\boldsymbol{A} \cdot \boldsymbol{A}^+)^{\mathrm{T}} = \boldsymbol{A} \cdot \boldsymbol{A}^+$

- $(\boldsymbol{A}^+ \cdot \boldsymbol{A})^{\mathrm{T}} = \boldsymbol{A}^+ \cdot \boldsymbol{A}$

**Properties**   We have some properties

- As $\boldsymbol{A}$ is a real matrix, $\boldsymbol{A}^+$ is also a real matrix.

- If $\boldsymbol{A}$ is invertible, the pseudo-inverse is just the inverse $\boldsymbol{A}^+ = \boldsymbol{A}^{-1}$.

- The pseudoinverse of the pseudoinverse is the original matrix: $(\boldsymbol{A}^+)^+ = \boldsymbol{A}$.

- The pseudoinversion commutes with transposition $(\boldsymbol{A}^{\mathrm{T}})^+ = (\boldsymbol{A}^+)^{\mathrm{T}}$.

- The kernel and image of $\boldsymbol{A}^+$ are given by those of $\boldsymbol{A}^{\mathrm{T}}$: $\ker(\boldsymbol{A}^+) = \ker(\boldsymbol{A}^{\mathrm{T}})$ and $\mathrm{im}(\boldsymbol{A}^+) = \mathrm{im}(\boldsymbol{A}^{\mathrm{T}})$.

**Solutions of linear systems**   We consider the linear system

$$\boldsymbol{A} \cdot \boldsymbol{x} = \boldsymbol{b} \tag{A.3}$$

The Moore-Penrose pseudo-inverse provides a least squares solution, as $\boldsymbol{x} = \boldsymbol{A}^+ \cdot \boldsymbol{b}$, but is not the unique solution to this equation. The whole set of solution is given by

$$x = \boldsymbol{A}^+ \cdot \boldsymbol{b} + \left[ \mathbf{Id} - \boldsymbol{A}^+ \cdot \boldsymbol{A} \right] \cdot \boldsymbol{w}, \tag{A.4}$$

where $\mathbf{Id}$ is the identity matrix and $\boldsymbol{w}$ an arbitrary vector. The solution requires that $\boldsymbol{A}^+ \cdot \boldsymbol{A} \cdot \boldsymbol{b} = \boldsymbol{b}$, otherwise the system does not have solutions.

**Some particular cases**

- When $\boldsymbol{A}$ is a non zero-vector, then $\boldsymbol{A}^+ = \dfrac{\boldsymbol{A}^{\mathrm{T}}}{\boldsymbol{A}^{\mathrm{T}} \cdot \boldsymbol{A}}$

- When $\boldsymbol{A}$ have linearly independent columns, then $\boldsymbol{A}^+ = (\boldsymbol{A}^{\mathrm{T}} \cdot \boldsymbol{A})^{-1} \cdot \boldsymbol{A}^{\mathrm{T}}$

- When $\boldsymbol{A}$ have linearly independent rows, then $\boldsymbol{A}^+ = \boldsymbol{A}^{\mathrm{T}} \cdot (\boldsymbol{A}^{\mathrm{T}} \cdot \boldsymbol{A})^{-1}$.

## A.1.4 A useful lemma

Let's proove the following lemma:

**Lemma.** *If $\boldsymbol{A}$ is a $n \times n$ positive-definite diagonalizable matrix and $\boldsymbol{B}$ a $n \times m$ full rank matrix with $m \leqslant n$ then we have*

$$\boldsymbol{B} \cdot \left(\boldsymbol{B}^{\mathrm{T}} \cdot \boldsymbol{A}^{-1} \cdot \boldsymbol{B}\right)^{-1} \cdot \boldsymbol{B}^{\mathrm{T}} \leqslant \boldsymbol{A} \tag{A.5}$$

*Proof.* As $\boldsymbol{A}$ and $\boldsymbol{B}$ are full-rank, we can decompose the inversion using Moore-Penrose pseudo-inverse,

$$\boldsymbol{B} \cdot \left(\boldsymbol{B}^{\mathrm{T}} \cdot \boldsymbol{A}^{-1} \cdot \boldsymbol{B}\right)^{-1} \cdot \boldsymbol{B}^{\mathrm{T}} = \boldsymbol{B} \cdot \boldsymbol{B}^+ \cdot \boldsymbol{A} \cdot \left(\boldsymbol{B} \cdot \boldsymbol{B}^+\right)^{\mathrm{T}}. \tag{A.6}$$

Now, $\boldsymbol{B} \cdot \boldsymbol{B}^+$ is an orthogonal projector whose eigenvalue are either 0 or 1. Therefore, $\boldsymbol{B} \cdot \left(\boldsymbol{B}^{\mathrm{T}} \cdot \boldsymbol{A}^{-1} \cdot \boldsymbol{B}\right)^{-1} \cdot \boldsymbol{B}^{\mathrm{T}}$ shares $m$ eigenvalues with $\boldsymbol{A}$ while the $n - m$ other eigenvalues are 0. Hence the result on the ordering from eigenvalues comparaison. $\square$

# Résumé du manuscrit

Le développement de la machine à vapeur, brevetée en 1769 par James Watt, est une des causes de la révolution industrielle. Son usage croissant a apporté de nouvelles questions sur la description physique de ces machines, en particulier sur la conversion de la chaleur en travail. Pour y répondre, une nouvelle branche de la physique, la thermodynamique, se développe progressivement au cours du XIX$^e$ siècle. La formulation des lois de la thermodynamique a permis d'apporter des réponses sur le fonctionnement et l'amélioration des machines à vapeur. Le lien entre la thermodynamique et le comportement au niveau microscopique des systèmes a ensuite été explicité par l'émergence de la physique statistique d'équilibre.

Ces deux théories étudient spécifiquement des systèmes macroscopiques qui peuvent alors être caractérisés par un petit nombre de degré de liberté.

A l'inverse quand on se concentre sur des petits systèmes, les fluctuations dues à l'environnement vont influer fortement sur leur comportement. Le mouvement de colloïdes dans l'eau, ou mouvement Brownien, est un exemple typique de petits systèmes. Quand leur taille augmente, les systèmes ne sont plus sensibles à ces fluctuations et on retrouve le cadre de la thermodynamique. On appelle ainsi petit système un système pour lequel les fluctuations de l'environnement sont perceptibles.

La thermodynamique stochastique s'est développée ces vingt dernières années pour fournir un cadre conceptuel à la description des petits systèmes en contact avec un environnement fluctuant. Parmi les résultats majeurs de la thermodynamique stochastique, on peut citer :

- La définition des quantités thermodynamiques à l'échelle des trajectoires, par exemple l'énergie ou l'entropie. Ce qui a par la suite facilité l'usage de la théorie des grandes déviations.

- Le théorème de fluctuations, qui impose une symétrie sur la distribution de probabilité de la production d'entropie. Cette symétrie a d'abord été observée dans des simulations numérique de fluides cisaillés puis généralisée à de nombreux cas.

- La validation expérimentale de la thermodynamique stochastique à travers de nombreuses expériences sur la manipulation de molécules uniques, le

confinement optique de colloïdes ou le comptage d'électrons uniques sur des systèmes électroniques mésoscopiques. Par exemple, la mesure de différences d'énergie libre pour des petits systèmes allant du pendule de torsion à la molécule d'ADN, la détermination de la distribution de probabilité de la production d'entropie pour un électron unique ou bien diverses réalisations connectant information et thermodynamique stochastique.

Parmis les problématiques initiales de la thermodynamique, la conversion d'énergie est toujours intensivement étudiée dans le cadre de la thermodynamique stochastique. Dans ce manuscrit, nous étudions les petites machines, en utilisant la théorie des grandes déviations, pour répondre aux questions suivantes :

- Comment décrire les petites machines dans le cadre de la thermodynamique stochastique?

- Est-t-il possible de généraliser, en se basant sur les relations d'incertitude thermodynamique, la description linéaire proche équilibre aux machines loin de l'équilibre?

- L'étude des fluctuations d'efficacité a révélé les propriétés générales de la fonction de grande déviations de l'efficacité. Que se passe-t-il dans les cas plus généraux non encore étudiés, en particulier le cas de systèmes avec pertes ou non-ergodique?

Pour les petites machines, il est généralement possible d'adopter une description discrète de leur espace des états. Dans ce cas, l'espace des états est souvent de taille fini et peut être décrit via la théorie des graphes. Celle-ci est décrite dans la section 1.1 via l'introduction des cycles qui permettent la description de la topologie du graphe.

Au delà de la géométrie de l'espace des états, la dynamique de l'évolution est décrit par la théorie des processus markoviens, dans la section 1.2. En particulier, l'évolution des probabilités est donnée par l'équation maîtresse. La relation entre les processus markoviens et la théorie des graphes donne une première approche du comportement des petites machines : l'évolution des probabilités dépend fortement des courants d'arêtes et de cycles. Cette description introduit les deux premiers niveaux de description des systèmes qui sont complétés ensuite par l'introduction des réservoirs. La structure thermodynamique est établie par la connection avec l'environnement. Ce formalisme fournit une description efficace des petites machines.

L'étude des fluctuations des petites machines se fait dans le cadre de la théorie des grandes déviations, décrite dans le chapitre 2. L'objectif de la théorie des grandes déviations est de fournir une estimation à temps long des probabilités d'une observable, via la fonction de grande déviation. Cette observable est calculée le long d'une trajectoire unique du système, comme expliqué dans la section 1.3. Dans le cadre de la théorie des grandes déviations, de nombreux résultats sont disponibles, notamment la possibilité de calculer la fonction de grande déviation via le calcul, souvent plus simple dans notre cas d'un espace

d'états discrets, de la fonction génératrice des cumulants. Lorsque que ce calcul est possible on parle alors d'équivalence d'ensembles dynamiques.

La définition formelle des petites machines est faite dans le chapitre 3. A l'aide de la matrice d'échange avec les réservoirs, et en utilisant les lois de conservations, on construit la matrice physique qui quantifie les échanges avec l'environnement. Une machine est alors un système avec deux courants physiques associés à deux affinités physiques. La relation entre affinités et courants physiques caractérise alors le comportement des petites machines. La thermodynamique linéaire, propose une relation linéaire entre courants et affinités en introduisant la matrice d'Onsager. Les propriétés de cette matrice, développées dans la section 3.2, donnent des contraintes fortes sur le fonctionnement des machines dans le régime proche de l'équilibre.

Au delà des courants moyens, les fluctuations induites par l'environnement influent le comportement des petites machines, en particulier leurs efficacités. La section 3.3 expose la forme générale de la fonction de grande déviation de l'efficacité, dont la forme possède des propriétés surprenantes et universelles. Par exemple la fonction de grande déviation de l'efficacité est borné et son maximum est relié à l'efficacité de Carnot.

Dans le chapitre 4, on introduit la notion de matrice de conductance comme une généralisation de la matrice d'Onsager proche de l'équilibre. Elle relie les affinités et les courants moyens arbitrairement loin de l'équilibre au prix d'une dépendance dans les affinités. Toutefois, cela permet l'extension des concepts introduit en thermodynamique linéaire, comme le degré de couplage. Le degré de couplage contraint l'efficacité maximum, spécifiant que l'efficacité de Carnot peut être atteinte pour les machines en régime stationnaire uniquement pour les machines en couplage fort. Au delà de cette contrainte sur l'efficacité maximum, la matrice de conductance contraint également la relation entre l'efficacité et la puissance et fournit une vision unifiée des différentes relations efficacité-puissance précédemment dérivées par d'autres auteurs. La matrice de conductance a également un lien avec les fluctuations, puisqu'elle fournit une borne quadratique sur la fonction de grande déviation des courants physiques.

L'étude des fluctuations d'efficacité est traitée dans le chapitre 5. D'une part par l'introduction de bornes sur la fonction de grande déviation de l'efficacité. Ces bornes issues de l'étude de la matrice de conductance relient la dissipation aux fluctuations d'efficacité. D'autre part, l'étude d'une machine avec trois courants physiques dans la section 5.2 montre la convervation des propriétés de la fonction de grande déviation de l'efficacité dans ce cadre plus général. De plus, quand le troisième courant physique est inconnu et petit, on retrouve la fonction de grande déviation de l'efficacité avec deux courants physiques ce qui démontre la robustesse des propriétés des grandes déviations de l'efficacité.

Le chapitre 6 s'intéresse aux effets d'une brisure d'ergodicité sur les propriétés des fonctions de grandes déviations. Cette brisure d'ergodicité a, entre autres, pour origine l'existence d'une interaction à longue portée dont l'exemple le plus simple est une interaction de champ moyen et est reliée à l'existence d'états métastables. Cela affecte la possibilité de calculer les fonctions de grande déviations à partir des fonctions génératrices des cumulants, brisant alors l'équiva-

lence des ensembles dynamiques. On regarde alors comment passer outre cette difficulté via le calcul des branches métastables de la fonction génératrice des cumulants pourobtenir les non-convexités des fonctions de grande déviation.

Dans le chapitre 7, l'accent est mis sur l'étude d'un modèle plus complexe de machines en interaction. Au niveaux des courants est montré l'émergence, quand le nombre de machines augmente, d'un couplage fort. En relation avec l'interaction de champ moyen entre les machines, les techniques développées au chapitre 6 sont utilisées pour étudier les fluctuations à la fois des courants et de l'efficacité. L'effet à la fois du couplage fort et de la brisure d'ergodicité est alors visible sur les courbes de fluctuations d'efficacité.

En conclusion, cette thèse apporte une étude précise du comportement des machines stationnaires loin de l'équilibre à la fois au niveau des courants moyens et des fluctuations. Il reste néanmoins plusieurs questions qui mériterait d'être débattues, dont la généralisation de ces résultats aux machines conduites périodiquement.

# Books, thesis and review articles

[1] A. Bejan, *Advanced engineering thermodynamics* (Wiley, New York, 2006).

[2] L. Bertini, A. De Sole, D. Gabrielli, G. Jona-Lasinio, and C. Landim, *Macroscopic fluctuation theory*, Rev. Mod. Phys. Vol. 87, pp. 593–636 (2015).

[3] N. Biggs, *Algebraic graph theory*, 2nd ed., Cambridge Mathematical Library (Cambridge University Press, 1974).

[4] S. Boyd and L. Vandenberghe, *Convex optimization* (Cambridge University Press, 2004).

[5] H. B. Callen, *Thermodynamics and an introduction to thermostatistics* (Wiley, 1985).

[6] S. Carnot, *Réflexions sur la puissance motrice du feu et sur les machines propres à développer cette puissance* (Bachelier, Paris, 1824).

[7] R. Chetrite, "Grandes déviations et relations de fluctuation dans certains modèles de systèmes hors d'équilibre", PhD thesis (ENS Lyon, 2008).

[8] I. Csiszár and P. C. Shields, *Information theory and statistics: a tutorial* (Now Foundations and Trends, 2004).

[9] E. L. W. David A. Levin Yuval Peres, *Markov chains and mixing times*, Vol. 58 (American Mathematical Society, 2008).

[10] S. de Groot and P. Mazur, *Non-equilibrium thermodynamics* (North-Holland Publishing Company, Amsterdam, 1962).

[11] B. Derrida, *Non-equilibrium steady states: fluctuations and large deviations of the density and of the current*, Journal of Statistical Mechanics: Theory and Experiment Vol. 2007, P07023–P07023 (2007).

[12] R. Ellis, *Entropy, large deviations, and statistical mechanics*, 2006th ed., Classics in Mathematics (Springer, 2006).

[13] W. Feller, *An introduction to probability theory and its applications*, Vol. 2 (John Wiley & Sons, 2008).

[14] M. I. Freidlin and A. D. Wentzell, *Random perturbations of dynamical systems*, Grundlehren der mathematischen Wissenschaften (Springer-Verlag, New-York, 1984).

[15] C. Herbert, "An introduction to large deviations and equilibrium statistical mechanics for turbulent flows", in *Stochastic equations for complex systems: theoretical and computational topics*, edited by S. Heinz and H. Bessaih (Springer International Publishing, Cham, 2015), pp. 53–84.

[16] R. A. Horn and C. R. Johnson, *Matrix analysis*, 2nd ed. (Cambridge University Press, 2012).

[17] W. Kelvin, J. Larmor, and J. Joule, *Mathematical and physical papers*, Mathematical and Physical Papers vol. 1 (Cambridge University Press, Cambridge, 1882).

[18] A. Lazarescu, *The physicist's companion to current fluctuations: one-dimensional bulk-driven lattice gases version 1*, The Self Journal Science (2015).

[19] M. Polettini, "Geometric and combinatorial aspects of nonequilibrium statistical mechanics", PhD thesis (Alma Mater. Università di Bologna, 2012).

[20] I. Prigogine, *Introduction to thermodynamics of irreversible processes* (Wiley, New-York, 1967).

[21] M.-P. Q. Da-Quan Jiang Min Qian, *Mathematical theory of nonequilibrium steady states* (Springer, 2004).

[22] J. Ross, *Thermodynamics and fluctuations far from equilibrium* (Springer-Verlag Berlin Heidelberg, 2008).

[23] U. Seifert, *Stochastic thermodynamics, fluctuation theorems and molecular machines*, Reports on Progress in Physics Vol. 75, p. 126001 (2012).

[24] K. Sekimoto, *Stochastic energetics*, Vol. 799, Lecture Notes in Physics (Springer, New York, 2010).

[25] H. Touchette, *The large deviation approach to statistical mechanics*, Physics Reports Vol. 478, pp. 1–69 (2009).

[26] H. Touchette and R. J. Harris, "Large deviation approach to nonequilibrium systems", in *Nonequilibrium statistical physics of small systems* (Wiley-Blackwell, 2013) Chap. 11, pp. 335–360.

[27] N. Treps and F. Bretenaker, *Le laser* (EDP Sciences, Les Ulis, 2010).

[28] N. Van Kampen, *Stochastic processes in physics and chemistry (third edition)*, Third Edition (Elsevier, Amsterdam, 2007).

[29] G. Verley, "Fluctuations et réponse des systèmes hors d'équilibre", Theses (Université Pierre et Marie Curie - Paris VI, Sept. 2012).

[30] B. Wynants, "Structures of nonequilibrium fluctuations: dissipation and activity", PhD thesis (Universiteit K.U. Leuven, 2010).

# Research articles

[31] A. Alemany, M. Ribezzi-Crivellari, and F. Ritort, "From free energy measurements to thermodynamic inference in nonequilibrium small systems", New Journal of Physics **17**, 075009 (2015).

[32] A. Alemany, A. Mossa, I. Junier, and F. Ritort, "Experimental free-energy measurements of kinetic molecular states using fluctuation theorems", Nature Physics **8**, 688 (2012).

[33] M. Alexander, R. D. R. Michiel, and A. Peletier Mark, "A generalization of onsager's reciprocity relations to gradient flows with nonlinear mobility", Journal of Non-Equilibrium Thermodynamics **41**, 141 (2016).

[34] D. Andrieux and P. Gaspard, "Fluctuation theorem and onsager reciprocity relations", The Journal of Chemical Physics **121**, 6167–6174 (2004).

[35] D. Andrieux and P. Gaspard, "Fluctuation theorem for currents and schnakenberg network theory", English, Journal of Statistical Physics **127**, 107–131 (2007).

[36] Y. Baek, Y. Kafri, and V. Lecomte, "Dynamical symmetry breaking and phase transitions in driven diffusive systems", Phys. Rev. Lett. **118**, 030604 (2017).

[37] A. C. Barato and U. Seifert, "Unifying three perspectives on information processing in stochastic thermodynamics", Phys. Rev. Lett. **112**, 090601 (2014).

[38] A. C. Barato and R. Chetrite, "A formal view on level 2.5 large deviations and fluctuation relations", Journal of Statistical Physics **160**, 1154–1172 (2015).

[39] A. C. Barato and U. Seifert, "Cost and precision of brownian clocks", Phys. Rev. X **6**, 041053 (2016).

[40] A. C. Barato and U. Seifert, "Thermodynamic uncertainty relation for biomolecular processes", Phys. Rev. Lett. **114**, 158101 (2015).

[41] J. Barré, D. Mukamel, and S. Ruffo, "Inequivalence of ensembles in a system with long-range interactions", Phys. Rev. Lett. **87**, 030601 (2001).

[42] G. Benenti, G. Casati, K. Saito, and R. S. Whitney, "Fundamental aspects of steady-state conversion of heat to work at the nanoscale", Physics Reports **694**, Fundamental aspects of steady-state conversion of heat to work at the nanoscale, 1–124 (2017).

[43] L. Bertini, A. De Sole, D. Gabrielli, G. Jona-Lasinio, and C. Landim, "Macroscopic fluctuation theory for stationary non-equilibrium states", English, Journal of Statistical Physics **107**, 635–675 (2002).

[44] L. Bertini, A. Faggionato, and D. Gabrielli, "From level 2.5 to level 2 large deviations for continuous time markov chains", Markov Processes and Related Fields **20** (2012).

[45] L. Bertini, A. Faggionato, and D. Gabrielli, "Flows, currents, and cycles for markov chains: large deviation asymptotics", Stochastic Processes and their Applications **125**, 2786–2819 (2015).

[46] A. Bérut, A. Petrosyan, and S. Ciliberto, "Detailed jarzynski equality applied to a logically irreversible procedure", EPL (Europhysics Letters) **103**, 60002 (2013).

[47] A. Bérut, A. Arakelyan, A. Petrosyan, S. Ciliberto, R. Dillenschneider, and E. Lutz, "Experimental verification of landauer's principle linking information and thermodynamics", Nature **483**, 187 (2012).

[48] G. Biroli and J. P. Garrahan, "Perspective: the glass transition", The Journal of Chemical Physics **138**, 12A301 (2013).

[49] V. Blickle and C. Bechinger, "Realization of a micrometre-sized stochastic heat engine", Nat Phys **8**, 143–146 (2012).

[50] F. Bouchet, S. Gupta, and D. Mukamel, "Thermodynamics and dynamics of systems with long-range interactions", Physica A: Statistical Mechanics and its Applications **389**, Proceedings of the 12th International Summer School on Fundamental Problems in Statistical Physics, 4389–4405 (2010).

[51] K. Brandner, K. Saito, and U. Seifert, "Strong bounds on onsager coefficients and efficiency for three-terminal thermoelectric transport in a magnetic field", Phys. Rev. Lett. **110**, 070603 (2013).

[52] K. Brandner, K. Saito, and U. Seifert, "Thermodynamics of micro- and nano-systems driven by periodic temperature variations", Phys. Rev. X **5**, 031019 (2015).

[53] K. Brandner and U. Seifert, "Multi-terminal thermoelectric transport in a magnetic field: bounds on onsager coefficients and efficiency", New Journal of Physics **15**, 105003 (2013).

[54] G. Bulnes Cuetara, M. Esposito, and A. Imparato, "Exact fluctuation theorem without ensemble quantities", Phys. Rev. E **89**, 052119 (2014).

[55] C. Bustamante, Y. R. Chemla, N. R. Forde, and D. Izhaky, "Mechanical processes in biochemistry", Annual Review of Biochemistry **73**, PMID: 15189157, 705–748 (2004).

[56] A. Campa, T. Dauxois, and S. Ruffo, "Statistical mechanics and dynamics of solvable models with long-range interactions", Physics Reports **480**, 57–159 (2009).

[57] M. Campisi and R. Fazio, "The power of a critical heat engine", Nature Communications **7**, 11895– (2016).

[58] M. Campisi, J. Pekola, and R. Fazio, "Nonequilibrium fluctuations in quantum heat engines: theory, example, and possible solid state experiments", New Journal of Physics **17**, 035012 (2015).

[59] S. Caplan, "The degree of coupling and its relation to efficiency of energy conversion in multiple-flow systems", Journal of Theoretical Biology **10**, 209–235 (1966).

[60] R. Chetrite and H. Touchette, "Nonequilibrium markov processes conditioned on large deviations", Annales Henri Poincaré **16**, 2005–2057 (2015).

[61] R. Chetrite and H. Touchette, "Nonequilibrium microcanonical and canonical ensembles and their equivalence", Phys. Rev. Lett. **111**, 120601 (2013).

[62] S. Ciliberto, "Experiments in stochastic thermodynamics: short history and perspectives", Phys. Rev. X **7**, 021051 (2017).

[63] S. Ciliberto, S. Joubaud, and A. Petrosyan, "Fluctuations in out-of-equilibrium systems: from theory to experiment", Journal of Statistical Mechanics: Theory and Experiment **2010**, P12003 (2010).

[64] B. Cleuren, B. Rutten, and C. Van den Broeck, "Cooling by heating: refrigeration powered by photons", Phys. Rev. Lett. **108**, 120603 (2012).

[65] B. Cleuren, B. Rutten, and C. Van den Broeck, "Universality of efficiency at maximum power", The European Physical Journal Special Topics **224**, 879–889 (2015).

[66] B. Cleuren and C. Van den Broeck, "Brownian motion with absolute negative mobility", Phys. Rev. E **67**, 055101 (2003).

[67] B. Cleuren and C. Van den Broeck, "Ising model for a brownian donkey", EPL (Europhysics Letters) **54**, 1 (2001).

[68] D. Collin, F. Ritort, C. Jarzynski, S. B. Smith, I. Tinoco Jr, and C. Bustamante, "Verification of the crooks fluctuation theorem and recovery of rna folding free energies", Nature **437**, 231 (2005).

[69] M. Costeniuc, R. S. Ellis, and H. Touchette, "Complete analysis of phase transitions and ensemble equivalence for the curie-weiss-potts model", J. Math. Phys. **46,** 063301, 2005. (2005).

[70] G. E. Crooks, "Entropy production fluctuation theorem and the nonequilibrium work relation for free energy differences", Phys. Rev. E **60**, 2721–2726 (1999).

[71] G. E. Crooks, "Nonequilibrium measurements of free energy differences for microscopically reversible markovian systems", Journal of Statistical Physics **90**, 1481–1487 (1998).

[72] C. A. Domenicali, "Irreversible thermodynamics of thermoelectricity", Rev. Mod. Phys. **26**, 237–275 (1954).

[73] M. D. Donsker and S. R. S. Varadhan, "Asymptotic evaluation of certain markov process expectations for large time, i", Communications on Pure and Applied Mathematics **28**, 1–47 (1975).

[74] M. D. Donsker and S. R. S. Varadhan, "Asymptotic evaluation of certain markov process expectations for large time, ii", Communications on Pure and Applied Mathematics **28**, 279–301 (1975).

[75] M. D. Donsker and S. R. S. Varadhan, "Asymptotic evaluation of certain markov process expectations for large time. iv", Communications on Pure and Applied Mathematics **36**, 183–212 (1983).

[76] M. D. Donsker and S. R. S. Varadhan, "Asymptotic evaluation of certain markov process expectations for large time—iii", Communications on Pure and Applied Mathematics **29**, 389–461 (1976).

[77] F. Douarche, S. Ciliberto, and A. Petrosyan, "Estimate of the free energy difference in mechanical systems from work fluctuations: experiments and models", Journal of Statistical Mechanics: Theory and Experiment **2005**, P09011 (2005).

[78] R. S. Ellis, "An overview of the theory of large deviations and applications to statistical mechanics", Scandinavian Actuarial Journal **1995**, 97–142 (1995).

[79] R. S. Ellis, "The theory of large deviations: from boltzmann's 1877 calculation to equilibrium macrostates in 2d turbulence", Physica D: Nonlinear Phenomena **133**, 106–136 (1999).

[80] R. S. Ellis, H. Touchette, and B. Turkington, "Thermodynamic versus statistical nonequivalence of ensembles for the mean-field blume–emery–griffiths model", Physica A: Statistical Mechanics and its Applications **335**, 518–538 (2004).

[81] O. Entin-Wohlman, J.-H. Jiang, and Y. Imry, "Efficiency and dissipation in a two-terminal thermoelectric junction, emphasizing small dissipation", Phys. Rev. E **89**, 012123 (2014).

[82] M. Esposito, "Stochastic thermodynamics under coarse graining", Phys. Rev. E **85**, 041125 (2012).

[83] M. Esposito, R. Kawai, K. Lindenberg, and C. Van den Broeck, "Efficiency at maximum power of low-dissipation carnot engines", Phys. Rev. Lett. **105**, 150603 (2010).

[84] M. Esposito, K. Lindenberg, and C. Van den Broeck, "Thermoelectric efficiency at maximum power in a quantum dot", EPL (Europhysics Letters) **85**, 60010 (2009).

[85] M. Esposito, K. Lindenberg, and C. Van den Broeck, "Universality of efficiency at maximum power", Phys. Rev. Lett. **102**, 130602 (2009).

[86] M. Esposito and C. Van den Broeck, "Three detailed fluctuation theorems", Phys. Rev. Lett. **104**, 090601 (2010).

[87] M. Esposito and C. Van den Broeck, "Three faces of the second law. i. master equation formulation", Phys. Rev. E **82**, 011143 (2010).

[88] D. J. Evans, E. G. D. Cohen, and G. P. Morriss, "Probability of second law violations in shearing steady states", Phys. Rev. Lett. **71**, 2401–2404 (1993).

[89] D. J. Evans and D. J. Searles, "The fluctuation theorem", Advances in Physics **51**, 1529–1585 (2002).

[90] D. J. Evans, D. J. Searles, and S. R. Williams, "On the fluctuation theorem for the dissipation function and its connection with response theory", The Journal of Chemical Physics **128**, 014504 (2008).

[91] G. Gallavotti and E. G. D. Cohen, "Dynamical ensembles in nonequilibrium statistical mechanics", Phys. Rev. Lett. **74**, 2694–2697 (1995).

[92] J. P. Garrahan, R. L. Jack, V. Lecomte, E. Pitard, K. van Duijvendijk, and F. van Wijland, "First-order dynamical phase transition in models of glasses: an approach based on ensembles of histories", Journal of Physics A: Mathematical and Theoretical **42**, 075007 (2009).

[93] T. R. Gingrich, J. M. Horowitz, N. Perunov, and J. L. England, "Dissipation bounds all steady-state current fluctuations", Phys. Rev. Lett. **116**, 120601 (2016).

[94] T. R. Gingrich, G. M. Rotskoff, and J. M. Horowitz, "Inferring dissipation from current fluctuations", Journal of Physics A: Mathematical and Theoretical **50**, 184004 (2017).

[95] T. R. Gingrich, G. M. Rotskoff, S. Vaikuntanathan, and P. L. Geissler, "Efficiency and large deviations in time-asymmetric stochastic heat engines", New Journal of Physics **16**, 102003 (2014).

[96] A. Gomez-Marin and J. M. Sancho, "Tight coupling in thermal brownian motors", Phys. Rev. E **74**, 062102 (2006).

[97] T. Grafke, R. Grauer, and T. Schäfer, "The instanton method and its numerical implementation in fluid mechanics", Journal of Physics A: Mathematical and Theoretical **48**, 333001 (2015).

[98] D. Gupta and S. Sabhapandit, "Stochastic efficiency of an isothermal work-to-work converter engine", Phys. Rev. E **96**, 042130 (2017).

[99] D. Hartich, A. C. Barato, and U. Seifert, "Stochastic thermodynamics of bipartite systems: transfer entropy inequalities and a maxwell's demon interpretation", Journal of Statistical Mechanics: Theory and Experiment **2014**, P02016 (2014).

[100] J. Hoppenau, D. Nickelsen, and A. Engel, "Level 2 and level 2.5 large deviation functionals for systems with and without detailed balance", New Journal of Physics **18**, 083010 (2016).

## Research articles

[101]   J. M. Horowitz and T. R. Gingrich, "Proof of the finite-time thermodynamic uncertainty relation for steady-state currents", Phys. Rev. E **96**, 020103 (2017).

[102]   R. L. Jack and P. Sollich, "Large deviations and ensembles of trajectories in stochastic models", Progress of Theoretical Physics Supplement **184**, 304–317 (2010).

[103]   C. Jarzynski, "Equilibrium free-energy differences from nonequilibrium measurements: a master-equation approach", Phys. Rev. E **56**, 5018–5035 (1997).

[104]   C. Jarzynski, "Nonequilibrium equality for free energy differences", Phys. Rev. Lett. **78**, 2690–2693 (1997).

[105]   C. Jarzynski, "Equalities and inequalities: irreversibility and the second law of thermodynamics at the nanoscale", Annual Review of Condensed Matter Physics **2**, 329–351 (2011).

[106]   F. Jülicher, A. Ajdari, and J. Prost, "Modeling molecular motors", Rev. Mod. Phys. **69**, 1269–1282 (1997).

[107]   M. Kaiser, R. L. Jack, and J. Zimmer, "Canonical structure and orthogonality of forces and currents in irreversible markov chains", Journal of Statistical Physics (2018) `10.1007/s10955-018-1986-0`.

[108]   S. Katz, J. L. Lebowitz, and H. Spohn, "Phase transitions in stationary nonequilibrium states of model lattice systems", Phys. Rev. B **28**, 1655–1658 (1983).

[109]   O. Kedem and S. R. Caplan, "Degree of coupling and its relation to efficiency of energy conversion", Trans. Faraday Soc. **61**, 1897–1911 (1965).

[110]   A. S. Keys, D. Chandler, and J. P. Garrahan, "Using the $s$ ensemble to probe glasses formed by cooling and aging", Phys. Rev. E **92**, 022304 (2015).

[111]   J. V. Koski, T. Sagawa, O.-P. Saira, Y. Yoon, A. Kutvonen, P. Solinas, M. Möttönen, T. Ala-Nissila, and J. P. Pekola, "Distribution of entropy production in a single-electron box", Nature Physics **9**, 644 (2013).

[112]   R. Kraaij, A. Lazarescu, C. Maes, and M. Peletier, "Deriving generic from a generalized fluctuation symmetry", Journal of Statistical Physics (2017) `10.1007/s10955-017-1941-5`.

[113]   R. Kubo, "The fluctuation-dissipation theorem", Reports on Progress in Physics **29**, 255 (1966).

[114]   J. Kurchan, "Fluctuation theorem for stochastic dynamics", Journal of Physics A: Mathematical and General **31**, 3719 (1998).

[115]   A. W. C. Lau, D. Lacoste, and K. Mallick, "Nonequilibrium fluctuations and mechanochemical couplings of a molecular motor", Phys. Rev. Lett. **99**, 158102 (2007).

[116] G. F. Lawler and A. D. Sokal, "Bounds on the $l^2$ spectrum for markov chains and markov processes: a generalization of cheeger's inequality", Transactions of the American Mathematical Society **309**, 557–580 (1988).

[117] J. L. Lebowitz and H. Spohn, "A gallavotti–cohen-type symmetry in the large deviation functional for stochastic dynamics", Journal of Statistical Physics **95**, 333–365 (1999).

[118] J. S. Lee, C. Kwon, and H. Park, "Modified saddle-point integral near a singularity for the large deviation function", Journal of Statistical Mechanics: Theory and Experiment **2013**, P11002 (2013).

[119] L.-H. Lim, "Hodge laplacians on graphs", (2015).

[120] J. Liphardt, S. Dumont, S. B. Smith, I. Tinoco, and C. Bustamante, "Equilibrium information from nonequilibrium measurements in an experimental test of jarzynski's equality", Science **296**, 1832–1835 (2002).

[121] E. Lutz and S. Ciliberto, "Information: from maxwell's demon to landauer's eraser", Physics Today **68**, 30–35 (2015).

[122] C. Maes and K. Netočný, "Canonical structure of dynamical fluctuations in mesoscopic nonequilibrium steady states", EPL (Europhysics Letters) **82**, 30003 (2008).

[123] C. Maes and K. Netočný, "Time-reversal and entropy", Journal of Statistical Physics **110**, 269–310 (2003).

[124] C. Maes, F. Redig, and A. V. Moffaert, "On the definition of entropy production, via examples", Journal of Mathematical Physics **41**, 1528–1554 (2000).

[125] I. A. Martinez, E. Roldan, L. Dinis, D. Petrov, J. M. R. Parrondo, and R. A. Rica, "Brownian carnot engine", Nat Phys **12**, 67–70 (2016).

[126] C. Nardini and H. Touchette, "Process interpretation of current entropic bounds", The European Physical Journal B **91**, 16 (2018).

[127] T. Nemoto, "Zon-cohen singularity and negative inverse temperature in a trapped-particle limit", Phys. Rev. E **85**, 061124 (2012).

[128] D. Nickelsen and H. Touchette, "Anomalous scaling of dynamical large deviations", Phys. Rev. Lett. **121**, 090602 (2018).

[129] J. D. Noh and J.-M. Park, "Fluctuation relation for heat", Phys. Rev. Lett. **108**, 240603 (2012).

[130] L. Onsager and S. Machlup, "Fluctuations and irreversible processes", Phys. Rev. **91**, 1505–1512 (1953).

[131] L. Onsager, "Reciprocal relations in irreversible processes. i.", Phys. Rev. **37**, 405–426 (1931).

[132] L. Onsager, "Reciprocal relations in irreversible processes. ii.", Phys. Rev. **38**, 2265–2279 (1931).

[133] Y. Oono and M. Paniconi, "Steady state thermodynamics", Progress of Theoretical Physics Supplement **130**, 29–44 (1998).

[134] T. E. Ouldridge, C. C. Govern, and P. R. ten Wolde, "Thermodynamics of computational copying in biochemical systems", Phys. Rev. X **7**, 021004 (2017).

[135] G. W. Paltridge, "Climate and thermodynamic systems of maximum dissipation", Nature **279**, 630 (1979).

[136] M. Paniconi and Y. Oono, "Phenomenological framework for fluctuations around steady state", Phys. Rev. E **55**, 176–188 (1997).

[137] J. M. R. Parrondo and P. Español, "Criticism of feynman's analysis of the ratchet as an engine", American Journal of Physics **64**, 1125–1130 (1996).

[138] J. M. R. Parrondo, J. M. Horowitz, and T. Sagawa, "Thermodynamics of information", Nature Physics **11**, 131 (2015).

[139] E. A. J. F. Peters, "Detailed fluctuation theorem for mesoscopic modeling", Phys. Rev. E **70**, 066114 (2004).

[140] P. Pietzonka, A. C. Barato, and U. Seifert, "Affinity- and topology-dependent bound on current fluctuations", Journal of Physics A: Mathematical and Theoretical **49**, 34LT01 (2016).

[141] P. Pietzonka, A. C. Barato, and U. Seifert, "Universal bounds on current fluctuations", Phys. Rev. E **93**, 052145 (2016).

[142] P. Pietzonka, F. Ritort, and U. Seifert, "Finite-time generalization of the thermodynamic uncertainty relation", Phys. Rev. E **96**, 012101 (2017).

[143] P. Pietzonka and U. Seifert, "Universal trade-off between power, efficiency, and constancy in steady-state heat engines", Phys. Rev. Lett. **120**, 190602 (2018).

[144] M. Polettini, "Nonequilibrium thermodynamics as a gauge theory", EPL (Europhysics Letters) **97**, 30003 (2012).

[145] M. Polettini, G. Verley, and M. Esposito, "Efficiency statistics at all times: carnot limit at finite power", Phys. Rev. Lett. **114**, 050601 (2015).

[146] M. Polettini, "Best statistics of markovian fluxes: a tale of eulerian tours and fermionic ghosts", J. Phys. A: Math. Theor. **48**, 365005 (2015).

[147] M. Polettini, G. Bulnes Cuetara, and M. Esposito, "Conservation laws and symmetries in stochastic thermodynamics", Phys. Rev. E **94**, 052117 (2016).

[148] M. Polettini and M. Esposito, "Carnot efficiency at divergent power output", EPL (Europhysics Letters) **118**, 40003 (2017).

[149] M. Polettini, A. Lazarescu, and M. Esposito, "Tightening the uncertainty principle for stochastic currents", Phys. Rev. E **94**, 052104 (2016).

[150] K. Proesmans, B. Cleuren, and C. Van den Broeck, "Stochastic efficiency for effusion as a thermal engine", EPL (Europhysics Letters) **109**, 20004 (2015).

[151] K. Proesmans, B. Cleuren, and C. Van den Broeck, "Linear stochastic thermodynamics for periodically driven systems", Journal of Statistical Mechanics: Theory and Experiment **2016**, 023202 (2016).

[152] K. Proesmans, B. Cleuren, and C. Van den Broeck, "Power-efficiency-dissipation relations in linear thermodynamics", Phys. Rev. Lett. **116**, 220601 (2016).

[153] K. Proesmans, Y. Dreher, M. Gavrilov, J. Bechhoefer, and C. Van den Broeck, "Brownian duet: a novel tale of thermodynamic efficiency", Phys. Rev. X **6**, 041010 (2016).

[154] K. Proesmans and C. Van den Broeck, "Onsager coefficients in periodically driven systems", Phys. Rev. Lett. **115**, 090601 (2015).

[155] K. Proesmans and C. Van den Broeck, "Stochastic efficiency: five case studies", New Journal of Physics **17**, 065004 (2015).

[156] H. Qian, "Cycle kinetics, steady state thermodynamics and motors—a paradigm for living matter physics", Journal of Physics: Condensed Matter **17**, S3783 (2005).

[157] R. Rao and M. Esposito, "Conservation laws shape dissipation", New Journal of Physics **20**, 023007 (2018).

[158] R. Rao and M. Esposito, "Nonequilibrium thermodynamics of chemical reaction networks: wisdom from stochastic thermodynamics", Phys. Rev. X **6**, 041064 (2016).

[159] J. Roßnagel, S. T. Dawkins, K. N. Tolazzi, O. Abah, E. Lutz, F. Schmidt-Kaler, and K. Singer, "A single-atom heat engine", Science **352**, 325–329 (2016).

[160] B. Rutten, M. Esposito, and B. Cleuren, "Reaching optimal efficiencies using nanosized photoelectric devices", Phys. Rev. B **80**, 235122 (2009).

[161] A. Ryabov, V. Holubec, M. H. Yaghoubi, M. Varga, M. E. Foulaadvand, and P. Chvosta, "Transport coefficients for a confined brownian ratchet operating between two heat reservoirs", Journal of Statistical Mechanics: Theory and Experiment **2016**, 093202 (2016).

[162] T. Schmiedl and U. Seifert, "Efficiency at maximum power: an analytically solvable model for stochastic heat engines", EPL (Europhysics Letters) **81**, 20003 (2008).

[163] J. Schnakenberg, "Network theory of microscopic and macroscopic behavior of master equation systems", Rev. Mod. Phys. **48**, 571–585 (1976).

[164] D. J. Searles, L. Rondoni, and D. J. Evans, "The steady state fluctuation relation for the dissipation function", Journal of Statistical Physics **128**, 1337–1363 (2007).

[165] U. Seifert, "Stochastic thermodynamics of single enzymes and molecular motors", The European Physical Journal E **34**, 26 (2011).

[166] U. Seifert, "Efficiency of autonomous soft nanomachines at maximum power", Phys. Rev. Lett. **106**, 020601 (2011).

[167] U. Seifert, "Entropy production along a stochastic trajectory and an integral fluctuation theorem", Phys. Rev. Lett. **95**, 040602 (2005).

[168] K. Sekimoto, "Langevin equation and thermodynamics", Progress of Theoretical Physics Supplement **130**, 17–27 (1998).

[169] M. Serra-Garcia, A. Foehr, M. Molerón, J. Lydon, C. Chong, and C. Daraio, "Mechanical autonomous stochastic heat engine", Phys. Rev. Lett. **117**, 010602 (2016).

[170] S. Q. Sheng and Z. C. Tu, "Hidden symmetries and nonlinear constitutive relations for tight-coupling heat engines", New Journal of Physics **17**, 045013 (2015).

[171] N. Shiraishi, "Attainability of carnot efficiency with autonomous engines", Phys. Rev. E **92**, 050101 (2015).

[172] N. Shiraishi, K. Saito, and H. Tasaki, "Universal trade-off relation between power and efficiency for heat engines", Phys. Rev. Lett. **117**, 190601 (2016).

[173] N. Singh and B. Wynants, "Dynamical fluctuations for periodically driven diffusions", Journal of Statistical Mechanics: Theory and Experiment **2010**, P03007 (2010).

[174] P. Strasberg, G. Schaller, T. Brandes, and M. Esposito, "Quantum and information thermodynamics: a unifying framework based on repeated interactions", Phys. Rev. X **7**, 021003 (2017).

[175] J. Szavits-Nossan and M. R. Evans, "Inequivalence of nonequilibrium path ensembles: the example of stochastic bridges", Journal of Statistical Mechanics: Theory and Experiment **2015**, P12008 (2015).

[176] O. Tange, "Gnu parallel - the command-line power tool", ;login: The USENIX Magazine **36**, 42–47 (2011).

[177] H. Touchette, "Methods for calculating nonconcave entropies", J. Stat. Mech. P **05008** (2010).

[178] H. Touchette, "Simple spin models with non-concave entropies", Am. J. Phys. **76,** 26–30, 2008 (2008).

[179] H. Touchette, R. S. Ellis, and B. Turkington, "An introduction to the thermodynamic and macrostate levels of nonequivalent ensembles", Physica A: Statistical Mechanics and its Applications **340**, News and Expectations in Thermostatistics, 138–146 (2004).

[180] S. Toyabe, T. Sagawa, M. Ueda, E. Muneyuki, and M. Sano, "Experimental demonstration of information-to-energy conversion and validation of the generalized jarzynski equality", Nature Physics **6**, 988 (2010).

[181] S. Vaikuntanathan, T. R. Gingrich, and P. L. Geissler, "Dynamic phase transitions in simple driven kinetic networks", Phys. Rev. E **89**, 062108 (2014).

[182] C. Van den Broeck, "Thermodynamic efficiency at maximum power", Phys. Rev. Lett. **95**, 190602 (2005).

[183] C. Van den Broeck, B. Cleuren, R. Kawai, and M. Kambon, "A trio of brownian donkeys", International Journal of Modern Physics C **13**, 1195–1200 (2002).

[184] C. Van den Broeck and M. Esposito, "Ensemble and trajectory thermodynamics: a brief introduction", Physica A: Statistical Mechanics and its Applications **418**, Proceedings of the 13th International Summer School on Fundamental Problems in Statistical Physics, 6–16 (2015).

[185] C. Van den Broeck, N. Kumar, and K. Lindenberg, "Efficiency of isothermal molecular machines at maximum power", Phys. Rev. Lett. **108**, 210602 (2012).

[186] G. Verley, M. Esposito, T. Willaert, and C. Van den Broeck, "The unlikely carnot efficiency", Nat Comms **5**, 4721 (2014).

[187] G. Verley, C. Van den Broeck, and M. Esposito, "Modulated two-level system: exact work statistics", Phys. Rev. E **88**, 032137 (2013).

[188] G. Verley, C. Van den Broeck, and M. Esposito, "Work statistics in stochastically driven systems", New Journal of Physics **16**, 095001 (2014).

[189] G. Verley, T. Willaert, C. Van den Broeck, and M. Esposito, "Universal theory of efficiency fluctuations", Phys. Rev. E **90**, 052145 (2014).

[190] H. Vroylandt, A. Bonfils, and G. Verley, "Efficiency fluctuations of small machines with unknown losses", Phys. Rev. E **93**, 052123 (2016).

[191] H. Vroylandt, M. Esposito, and G. Verley, "Collective effects enhancing power and efficiency", EPL (Europhysics Letters) **120**, 30009 (2017).

[192] H. Vroylandt, D. Lacoste, and G. Verley, "Degree of coupling and efficiency of energy converters far-from-equilibrium", Journal of Statistical Mechanics: Theory and Experiment **2018**, 023205 (2018).

[193] H. Vroylandt and G. Verley, "Non equivalence of dynamical ensembles and emergent non ergodicity", Journal of Statistical Physics (2018) 10.1007/s10955-018-2186-7.

[194] M. P. Wojtkowski, "Abstract fluctuation theorem", Ergodic Theory and Dynamical Systems **29**, 273–279 (2009).

[195] C. Wood, "Materials for thermoelectric energy conversion", Reports on Progress in Physics **51**, 459 (1988).

**Titre :** Thermodynamique et fluctuations des petites machines

**Mots clés :** Thermodynamique Stochastique, Théorie des grandes déviations, Efficacité, Machines thermodynamique, Fluctuations

**Résumé :** Les petites machines, comme les moteurs moléculaires ou les particules actives, fonctionnent dans un environnement fortement fluctuant qui affecte leur efficacité ou leur puissance. L'objectif de cette thèse est de décrire les petites machines à l'aide de la thermodynamique stochastique et de la théorie des grandes déviations. En reliant localement puis globalement les courants aux forces thermodynamiques, on introduit une matrice de conductance hors d'équilibre, qui généralise la matrice d'Onsager pour un système stationnaire hors d'équilibre. Cela permet de majorer l'efficacité des machines par une fonction universelle qui ne dépend que du degré de couplage entre les courants d'entrée et de sortie. On obtient aussi de nouvelles relations générales entre puissance et efficacité.

Du point de vue des fluctuations, la matrice de conductance hors d'équilibre est reliée à une borne quadratique pour les fonctions de grande déviation des courants. Cette borne permet d'obtenir des bornes pour les fonctions de grande déviation de l'efficacité, mais aussi de revisiter le théorème de fluctuation-dissipation comme une inégalité dans le cas des systèmes loin de l'équilibre. Pour terminer, on étudie l'effet d'une brisure d'ergodicité sur les fluctuations d'observables comme l'activité, les courants ou l'efficacité. En particulier, on calcule la fonction de grande déviation de l'efficacité pour un ensemble de nanomachines en interaction pour lesquelles un couplage fort et une brisure d'ergodicité apparaissent à la limite thermodynamique.

**Title :** Thermodynamics and fluctuations of small machines

**Keywords :** Stochastic thermodynamics, Large deviations theory, Efficiency, Thermodynamic machines, Fluctuations

**Abstract :** Small machines -- like molecular motors or active particles -- operate in highly fluctuating environments that affect their efficiency and power. This thesis aims at describing small machines using stochastic thermodynamics and large deviation theory. By relating mean currents to thermodynamic forces, locally first and then at the global level, we introduce the non-equilibrium conductance matrix that generalizes the Onsager matrix for stationary non-equilibrium systems. We use it to bound machine efficiency by a universal function depending only on the degree of coupling between input and output currents and to find new general power-efficiency trade-offs.

On the fluctuations side, the non-equilibrium conductance matrix can be used to find a quadratic bound on the large deviation function of currents. This enables to revisit the fluctuation-dissipation theorem as an inequality when dealing with far-from-equilibrium systems, but also to derive bounds on the efficiency large deviation function. Finally, we study the effects of ergodicity breaking on the fluctuations of observables like activity, currents or efficiency. In particular, we derive the efficiency large deviation function for a model of interacting nanomachines, for which tight coupling and ergodicity breaking emerge in the thermodynamic limit.